THERMAL CONDUCTANCE OF METALLIC CONTACTS

BY

HENRY H. Y. WONG

THESIS SUBMITTED FOR THE DEGREE
OF DOCTOR OF PHILOSOPHY
TO THE FACULTY OF ENGINEERING
THE UNIVERSITY OF GLASGOW

Department of Aeronautics
and Fluid Mechanics,
The University of Glasgow.

November,
1967.

THERMAL CONDUCTANCE OF METALLIC CONTACTS

List of errata

Page	Line	Errata	Corrected to
2	5	assist	exist
10	12	are --- equal	m
16	9	junction	function
33	18	$\int_o^a$	$\int_o^\infty$
33	20	$(\frac{T}{Z})$	$(\frac{\partial T}{\partial Z})$
48	1	$\frac{\delta}{R^2 k_s} I_t$	$\frac{\delta}{\pi R^2 k_s} I_t$
52	13	parameter --- a	and
77	Fig. 4.10a	punging	plunging
83	10	determined with	determined. With
84	26	Fibrefrox	Fibrefrax
90	12	volts	μ volts
95	12	warm	worm
95	22	tope	top
104	12	cup	cap
173	1	d	dz
175	1	$y_1 = \frac{1}{R}$	$y_1 = \frac{\delta_1}{R}$
180	6	radius --- and	z
189	8	$Z = -Z$	$Z = -Z_2$
45	12	( )	[ ]

ProQuest LLC.
789 East Eisenhower Parkway
P.O. Box 1346
Ann Arbor, MI 48106 – 1346

SUMMARY

Across a contact joint, different modes of heat transfer take place, namely, by conduction through the metallic junctions, by conduction of the fluid through the interstitial space and by radiation. They are in reality interrelated so that any solution to the problem must take into account the inter-dependent nature of these three modes. The greatest obstacle to the seeking of a satisfactory solution lies in the uncertainty of the size and distribution of metallic junctions engaged in contact and of the exact dimensions of the interstitial space which is usually filled with a fluid of a lower thermal conductivity than that of the metal. Under these circumstances, it is necessary to introduce an idealised contact model for the convenience of obtaining a mathematical solution. In this model the contact members are represented by two circular cylindrical blocks while the irregularities on the surfaces which are engaged in contact are represented by two protuberant junctions of cylindrical shape with a diameter smaller than that of the main blocks. The thermal resistance of these junctions, however small it may be, is considered to have a governing effect on the heat transfer characteristics of a contact joint and it is included in the formulation of the theory. The theory thus obtained can be conveniently extended to cover contact models other than the idealised one with cylindrical junctions. Since the shape of the asperities on a surface resembles a cone more than a circular cylinder, it is suggested that a more realistic contact model could be one having its contact junctions represented by a pair of conic frusta. By taking an appropriate equivalent thermal conductivity of the junctions, the theory derived from the idealised contact model can be applied without any modification A simplified method for the solution of a contact problem is also suggested.

This method under certain conditions yields results very close to those obtained by the analytical method. The merit of this method lies in its comparative ease of formulation.

Experiments were carried out for the study of the fundamental phenomena of heat transfer across a metallic contact. In order to achieve this object it was necessary to eliminate some of the governing factors for others to be observed. To overcome the obscurity of the matching condition at a contact interface an artificial contact joint was introduced. This was done by inserting small steel balls and small aluminium discs between the contact surfaces for different experiments. The contact thermal conductance was measured under conditions in vacuum and with argon and helium gases, while the inserted objects were subjected to an applied load of various magnitudes. The test results agree favourably with the calculated values. They also confirm that the thermal conductance of a contact cannot be reliably determined from electrical measurements. The hysteresis phenomenon observed by a number of investigators was found to be due to the seizure of the contact junctions as well as due to the irreversible deformation of the material. The primary governing factors of heat transferred through the fluid path and through the solid path are the fluid contact parameter K_f, the solid contact parameter K_s and the contact area parameter X. By specifying the magnitudes of these parameters, it is possible to estimate the heat transfer rate through each path. By altering their values, it may also be possible to control the thermal contact conductance for a given purpose.

ACKNOWLEDGEMENT

The author wishes to express his profound gratitude to Professor T.R.F. Nonweiler for his interest in and advice on the work he has undertaken, the result of which is presented in this thesis. He would also like to extend his sincere thanks to Professor A.J. Ede, University of Aston, Birmingham and to Dr. R.W. Powell, Purdue University, West Lafayette for their most constructive discussions during the initial stages of this research. Thanks are due also to Mr. John Kinnear for his care in constructing the apparatus.

Financial support for this work was provided by the Ministry of Technology whose generosity is gratefully acknowledged.

CONTENTS

Page No.

LIST OF FIGURES

LIST OF TABLES

NOMENCLATURE

a	radius of contact area
a_o	radius of contact end of a conic frustum
b	a constant defined by equation (2-23)
c	a constant defined by equation (2-22)
c_p	specific heat for constant pressure
c_v	specific heat for constant volume
d	a radius used in Appendix B.
d_1, d_2	distances measured along specimens
$\Delta d_1, \Delta d_2$	distances between two thermocouple positions
f	a fraction
h	height of asperity
k	thermal conductivity
k_a	thermal conductivity of aluminium disc
k_m	equivalent solid thermal conductivity
k'_m	harmonic mean value of thermal conductivity
k_b	thermal conductivity of steel ball
k_i	thermal conductivity of insulating powder
k_r	equivalent thermal conductivity for radiation
l	temperature jump distance; a variable length
Δl	length between two adjacent thermocouple positions
m	number of contact spot per unit area
n	number of contact spots
p	gas pressure
q	heat flux per unit area
q_r	heat flux per unit area by radiation

Δq	radial heat gain or loss
r	radial coordinate; radius
r_d	radius of flow dividing surface
r'	a variable radius as defined in Appendix D
r_s	radius of specimen
r_q	radius of guard tube
s	a variable distance as defined in Appendix D
t	surface film thickness
w	a parameter
x	dimensionless parameter a/R
y	dimensionless parameter $\delta/2R$
Z	axial coordinate
A	actual total area of contact
A_a	apparent area of contact
B	$= \frac{C_t \delta}{\pi R^2 k_f}$ in equation (3-48) or $\frac{C_t \delta}{\pi (R^2 - a^2) k_f}$ in equation (3-51);
	a constant
C	thermal conductance; a constant
C_f	fluid contact conductance
C_s	solid contact conductance
D	a constant
E	Young's modulus
$F(x)$	a function of x
G_1, G_2	functions of x as defined in equations (A-17) and (A-18)
H	yield pressure; Meyer hardness value
H_1, H_2	constants defined in section 3.1

I magnification factor of contact gap distance

K_f fluid contact parameter $= \dfrac{k_f}{y\, k_s}$

K_s solid contact parameter $= \dfrac{k_m}{y\, k_s}$

M molecular weight

N a dimensionless parameter $= \dfrac{a}{R_b}$

P mean applied pressure

Pr Prandtl number

Q heat flux

R radius of contact model

R_a total resistance of a pair of conic frusta

R_b radius of steel ball; lateral heat transfer resistance

R_e electrical resistance

R_c constriction resistance

R_s solid contact resistance

R_f fluid contact resistance

R_o surface film resistance

R_g universal gas constant

R_{cb} constriction resistance of a sphere

R_{mb} material resistance of a sphere

R_{cf} constriction resistance of a conic frustum

R_{mf} material resistance of a conic frustum

R_{ts} total contact resistance by the simplified method

T temperature

T_o temperature of contact plane; temperature as defined in Appendix C

T' temperature in regions extended from the solid spot; temperature as defined in Appendix C

ΔT temperature between contact surface and contact plane

T_s specimen temperature

T_g guard tube temperature

W applied load

W_{op} load for onset of plasticity

Y yield stress

L $= R_b/R$

Greek letter symbols:

α accommodation coefficient; constant defined in section 3.1

β constant defined in section 3.1; a parameter equal to $\frac{a-a_o}{h}$

γ ratio of specific heats

λ mean free path of gas; constant defined in section 3.1

η percentage of discrepancy

ϵ emissivity

ψ a variable angle as defined in Appendix D

θ a variable angle as defined in Appendix B.

θ_o half subtended angle of a conic frustum

ω applied contact pressure

ω_o maximum pressure at centre of contact

σ electric resistivity of surface film; Stefan-Boltzmann's constant

ν Poisson's ratio

μ coefficient of viscosity

ρ density of gas; electric resistivity

δ contact gap distance

δ_r total separation between two planes at location r

δ_e	effective contact gap distance
Δ_r	local deformation

Subscripts:

1	solid 1
2	solid 2
b	ball
c	constriction
e	electric
o	film
f	fluid
m	material
s	solid; simplified method
t	total

SUMMARY

Across a contact joint, different modes of heat transfer take place, namely, by conduction through the metallic junctions, by conduction of the fluid through the interstitial space and by radiation. They are in reality interrelated so that any solution to the problem must take into account the inter-dependent nature of these three modes. The greatest obstacle to the seeking of a satisfactory solution lies in the uncertainty of the size and distribution of metallic junctions engaged in contact and of the exact dimensions of the interstitial space which is usually filled with a fluid of a lower thermal conductivity than that of the metal. Under these circumstances, it is necessary to introduce an idealised contact model for the convenience of obtaining a mathematical solution. In this model the contact members are represented by two circular cylindrical blocks while the irregularities on the surfaces which are engaged in contact are represented by two protuberant junctions of cylindrical shape with a diameter smaller than that of the main blocks. The thermal resistance of these junctions, however small it may be, is considered to have a governing effect on the heat transfer characteristics of a contact joint and it is included in the formulation of the theory. The theory thus obtained can be conveniently extended to cover contact models other than the idealised one with cylindrical junctions. Since the shape of the asperities on a surface resembles a cone more than a circular cylinder, it is suggested that a more realistic contact model could be one having its contact junctions represented by a pair of conic frusta. By taking an appropriate equivalent thermal conductivity of the junctions, the theory derived from the idealised contact model can be applied without any modification. A simplified method for the solution of a contact problem is also suggested.

This method under certain conditions yields results very close to those obtained by the analytical method. The merit of this method lies in its comparative ease of formulation.

Experiments were carried out for the study of the fundamental phenomena of heat transfer across a metallic contact. In order to achieve this object it was necessary to eliminate some of the governing factors for others to be observed. To overcome the obscurity of the matching condition at a contact interface an artificial contact joint was introduced. This was done by inserting small steel balls and small aluminium discs between the contact surfaces for different experiments. The contact thermal conductance was measured under conditions in vacuum and with argon and helium gases, while the inserted objects were subjected to an applied load of various magnitudes. The test results agree favourably with the calculated values. They also confirm that the thermal conductance of a contact cannot be reliably determined from electrical measurements. The hysteresis phenomenon observed by a number of investigators was found to be due to the seizure of the contact junctions as well as due to the irreversible deformation of the material. The primary governing factors of heat transferred through the fluid path and through the solid path are the fluid contact parameter K_f, the solid contact parameter K_s and the contact area parameter X. By specifying the magnitudes of these parameters, it is possible to estimate the heat transfer rate through each path. By altering their values, it may also be possible to control the thermal contact conductance for a given purpose.

CHAPTER I

INTRODUCTION.

When two surfaces are brought into contact they do so only at discrete points no matter how carefully the surfaces have been prepared. Under the influence of external loads, the size and number of these points may increase but the actual area of intimate metallic contact will still be very small compared with the apparent size of the contact members. The reason for this is that surfaces are never perfectly flat and smooth, and irregularities whether they be macroscopic or microscopic in size are an inherent part of a surface. This being so, the flow of heat from one member to another across a contact can never be in the same manner as it would be in a continuous solid. Furthermore, it has to encounter whatever substances may occupy the void space vacated by the solid members. The behaviour of these foreign materials in transmitting heat may not be similar to that of the main bodies. It is equally possible that their reactions towards the change of temperature may be different. The effects they may have on the heat transfer characteristics of the contact as a whole must depend on their properties as well as on their quantities, which latter depend in turn on the space left unoccupied by the surface irregularities. Therefore we see that the condition of heat flow across a contact must depend primarily on the irregularities, their size, shape and distribution and on how well they establish themselves in real contact. If this information is available, the quantities of heat transfer across the contact whether through the solid junctions or the void space (which is usually filled with a fluid)

can then be judged according to the resistance of various paths which exist between the two surfaces. The contact conductance of the whole system can be divided into solid contact conductance and fluid contact conductance according to their ability of transmiting heat so that it may be possible to examine whatever governing factors may assist and to control them if necessary for any specific purpose.

In order to make a prediction it is necessary first to know the texture of the contact surfaces and then to estimate the actual areas of contact and the fluid gap distance when the two surfaces are engaged in contact. We also require to know the properties of both the solid and the fluid and their degree of sensitivity to temperature. If the surfaces are covered with some tarnish films, we need to know their effects on the heat transfer condition at the interface. We then realise that the thermal conductance of a contact is a complex function of some contact parameters as well as the mechanical and physical properties of the materials in and surrounding the contact. We further realise that all governing factors are inter-related and any success in finding a solution must necessitate some degree of simplification of the problem. How this should be approached will require a knowledge of the various problems involved. A comprehensive survey of the subject and the work carried out by other investigators was given in reference (1). and will not be repeated. It is sufficient to say that the thermal conductance of metallic contacts has become increasingly a problem of considerable significance in many practices of engineering and applied science and has received a great deal of attention in recent years.

CHAPTER II

FUNDAMENTAL CONCEPTS AND ACTUAL PHYSICAL PROBLEMS

2.1 Mechanism of heat transfer

In a solid body the condition of heat flow follows the law of conduction. When one body is brought into contact with another, no matter how carefully their surfaces are prepared they can never form one perfect body and the heat flow will experience a discontinuity at the contact where there is a sudden temperature drop. Perfect contact is hampered because surfaces are covered with irregularities so that at the interface actual metallic contacts are established over a very small area and the rest of the space is occupied by a fluid. By virtue of the fact that metal surfaces are usually covered with a layer of tarnish film, further complication arises. There not only is the solid-fluid interface separated by this film but also some of the irregularities which would otherwise engage in contact are separated by it. Hence the flow of heat at the contact will be forced to take up different modes of transfer dictated by the conditions at the interface. The following diagram represents approximately the various paths through which heat may be transmitted.

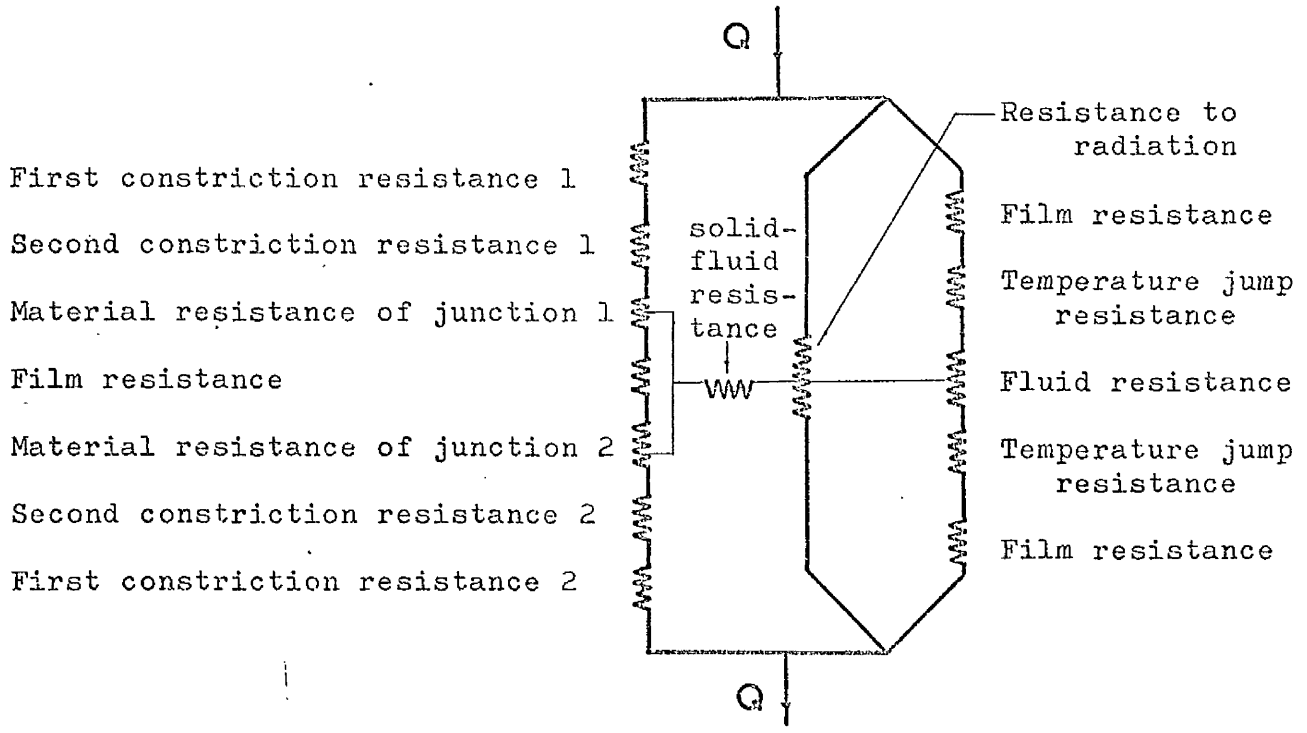

Fig. 1.1 Resistances exist along different paths of heat transfer across the contact.

The detail of each resistance in the circuit will be considered in this chapter and in chapter 3. In broad terms, there are three modes of heat transfer.

1. Heat transfer by conduction through metallic junctions.

Owing to the thermal conductivities of metals being much higher than those of fluids, the lines of heat flow will converge towards the contact spots giving rise to the constriction resistance. From the base to the tip of an asperity, secondary constriction of flow will take place. In the event of the actual contact of two asperities being prevented by the presence of a tarnish film, additional resistance will arise. The total solid resistance is denoted by R_s.

2. Heat transfer through the interstitial gas (normally the fluid is a gas).

If the distance between the two surfaces in contact is small, convective heat transfer becomes insignificant and heat transfer can be considered as by means of conduction. At the solid-gas interface there is a temperature drop the effect of which is specified in terms of the accommodation coefficient. When the surfaces are covered with tarnish films, the fluid resistance will consist of the resistance due to the temperature jump, the conduction resistance of the film and the conduction resistance of the fluid. The total resistance is denoted by R_f.

3. Heat transfer by direct radiation.

Through the interface, energy is transported by the molecules of the fluid and also by photons since both processes often occur simultaneously. The analysis of such a case is usually performed by calculating each process separately and adding up the results, although in reality they are interrelated. The amount of heat transferred by radiation depends on the absolute temperatures of the two surfaces and on the surface emissivities. If the interstitial gas is hot, it may also emit radiant energy, but this is really of no great significance. For simplicity of calculation we let the resistance due to radiation be included in the fluid resistance.

Besides these three modes of heat transfer, heat can also be transferred laterally between the solid asperities and the fluid. Thus the situation can be represented by the following diagram

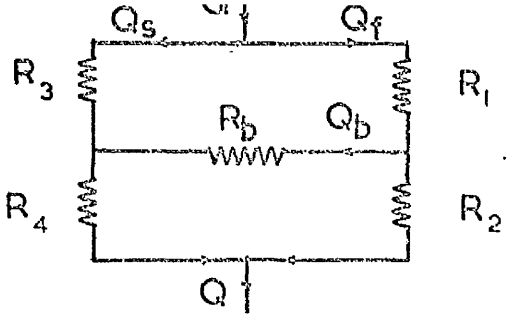

Fig. 1.2 Main paths of heat transfer across the contact

where the sum of the resistances R_1 and R_2 is equal to R_f and that of R_3 and R_4 is equal to R_s. R_b represents the lateral heat transfer resistance. Q is the total heat flux and Q_s and Q_f are the heat fluxes through the solid and the fluid respectively. Thus we find

$$Q_f = \frac{Q\left(R_s + R_3\frac{R_2+R_4}{R_b}\right)}{R_f+R_s+\frac{(R_1+R_3)(R_2+R_4)}{R_b}} \qquad (2\text{-}1)$$

$$Q_s = \frac{Q\left(R_f + R_1\frac{R_2+R_4}{R_b}\right)}{R_f+R_s+\frac{(R_1+R_3)(R_2+R_4)}{R_b}} \qquad (2\text{-}2)$$

If the contact gap distance is small (as it usually is) compared with the size of the contact, it is possible to assume negligible lateral heat transfer between the solid and the fluid (i.e. $Q_b \to 0$). This is equivalent to saying that $R_b \to \infty$. Hence equations (2-1) and (2-2) reduce to

$$Q_f = Q\frac{R_s}{R_f + R_s} \qquad (2\text{-}3)$$

$$Q_s = Q\frac{R_f}{R_f + R_s} \qquad (2\text{-}4)$$

From these two last equations, we see that the modes of heat transfer through the solid and through the fluid are inter-related and this is due to the fact

that the conductance of heat is sensitive to the resistance of each path which in turn is influenced by the amount of heat flowing through it.

2.2 Heat transfer through metallic contact areas

When heat flow reaches a contact, part of it will be transmitted through the metallic junctions and the rest across the interstitial space. The shape, the size and the distribution of these junctions all have profound importance in the heat transfer characteristics of a metallic contact. Before making a study under idealised conditions, it is necessary first to examine the problem in a general aspect and then to try to seek a solution which may achieve some degree of success from the practical point of view.

2.2.1 Contact area

One of the major obstacles in the study of thermal contact problems is the uncertainty of conditions in the actual areas of contact when two metallic surfaces are placed against each other under pressure. So far the method of calculating contact area has been derived either from two elastically deformed bodies having curvilinear shape (i.e. the Hertz' equation (2)) or from the assumption of fully plastic deformation in which the hardness of the material must be known[3]. The surface of a solid body however carefully prepared is wavy and rough and the study of contact surfaces becomes even more complicated owing to the fact that the roughness formed under load is added to the geometrical roughness itself.

The number and distribution of the contact spots are dependent on the applied load, the mechanical and physical properties of the materials, the surface texture and treatments, the temperatures and the working history. These factors are to a large extent inter-related. When a load is applied, the pressure on the contact areas is distributed irregularly. The peaks of the irregularities in contact will deform, part of them elastically and part plastically. The waves, in which the strain is always much lower, will deform also but mainly elastically. The critical value of strain corresponding to the onset of plastic deformation may be calculated according to Hertz' equation, but there is at present no thecry available which governs the strain conditions between the onset of plasticity and full plasticity[4]. As the metal deforms, work-hardening occurs and the elastic limit of the material increases. The yield stress, however, varies from point to point over the region of indentation. With a spherical body pressed against a flat surface, the amount of work-hardening and hence the elastic limit increases with the size of the indentation as a result of which the yield stress increases. Although the elastic limit is found to be closely related to the hardness of metals, the hardness value itself is subject to variation under the influence of temperature. The rise of temperature causes a reduction in hardness owing to the thermal movement of the atoms, the process of which was described by Holm[5] as atomic diffusion. Through the increase of atomic diffusion with rising temperature, there is a decrease in the hardness in the part caused by work-hardening. Work-hardening may be completely removed

if the temperature exceeds a certain critical value called softening temperature. It follows that the direct consequence of a temperature rise at the interface is an increase in contact area due to plastic deformation of the material. The determination of the actual areas of contact is further complicated by surface film which may grow or boil off depending on the temperature and the environmental conditions. The application of electrical measurements for the determination of contact areas would seem an obvious approach if it were not for the presence of surface films. We shall now consider each aspect of the problem in detail.

2.2.2 Thermal-electric analogy

According to Clerk Maxwell, mathematically the temperature plays the same part in the theory of heat flow as does the electric potential in the theory of electric current. In reality, we know that heat flow in a solid is transmitted partly by elastic waves due to lattice vibrations and partly by the conducting electrons. In metals, it is believed, the electronic component dominates the activity in thermal conductivity. So the same electrons are responsible for both the thermal and electrical conductivities which are related by the simple expression known as the Wiedemann-Franz-Lorenz law. Thus it would seem logical to take electrical resistance measurements across a metallic contact as a convenient means for measurements of the thermal resistance in the absence of an interstitial fluid and with negligible heat transfer by radiation. This could also provide a reasonable measure of the actual area of contact between the metal faces.

When uniform current flow occurs in a solid body, the current density is uniform everywhere because of uniform resistance of the body. The flow

lines run parallel to each other. As the flow lines approach the contact region they are attracted towards paths of least resistance and these usually occur at the metallic contact spots, resulting in their convergence towards those spots. The constriction of the current flow through narrow passages give rise therefore to a resistance termed as constriction resistance. If the two contact surfaces are perfectly clean, the contact members under pressure will adhere as if they are welded at the spots. In this case the thermal constriction resistance can be calculated from measurements of the electric constriction resistance. However, there is still no certainty in the estimate of the number, sizes, shapes and distribution of the individual areas of contact from such measurements. Assuming that the shape of the contact spot is circular and that there are equal spots per unit area evenly distributed over the contact surfaces, the electric resistance due to the constriction of the flow lines over an apparent contact area A_a is

$$R_e = \frac{\rho}{2amA_a} \tag{2-5}$$

where ρ is the electric resistivity, and a the radius of the contact area. The number and radius of the contact areas can be related to each other if we assume that the total area of true contact is equal to the total applied load W divided by the yield pressure H of the softer material, i.e.

$$A = mA_a\pi a^2 = \frac{W}{H} \tag{2-6}$$

Hence we obtain

$$a = \frac{2WR_e}{\pi\rho H} \tag{2-7}$$

and

$$m = \frac{\pi H\rho^2}{4W R_e^2 A_a} \tag{2-8}$$

Although a number of workers have made use of this approach either in formulating a contact theory or in predicting the number and size of the contact areas, yet experimental evidences have frequently shown the existence of large discrepancies between predicted results based on the thermal-electric analogy and test results. For clean surfaces, the constriction resistance concept applies to both thermal and electric contacts; with the presence of surface films, however, the analogy breaks down and the problem requires further examination.

2.2.3 Surface films

A metal surface is usually covered with a layer of tarnish film owing to either physical adsorption or chemical reaction. It is a compound of the metal itself and some constituents of the surrounding atmosphere, an oxide film being the most common one on a metal surface. The film is sometimes relatively thick and visible, such as in the case of a blackened silver; in other cases, it may only be a few atoms thick and invisible, as in the case of aluminium. Under normal conditions, practically all metal surfaces are tarnished with films and they are most difficult to remove except by applying high temperature in vacuo. As soon as the surfaces are exposed to atmosphere, they start to form again. The growth of tarnish films are slow at room temperature and will accelerate with increasing temperature. The rate of oxidation of metals is found to be a parabolic function of time at moderately high temperatures and to be a logarithmic function of time at high temperatures. The cessation of the growth of a tarnish film can be considered to come about only when the film is thick enough to protect the metal against further attack by oxygen (or other gas molecules) from the surroundings.

When two surfaces are brought together, at first only the surface films are in contact. If load is applied, the irregularities on the surfaces may penetrate the film at some local points to establish metallic contact. Since the material of the film usually possesses different properties from those of the underlying metal, it presents a major difficulty in contact problems and renders the thermal-electric analogy inapplicable.

In an electric contact, we may consider that the total resistance consists of constriction resistance and film resistance connected in series. Thus

$$R_e = \frac{\rho}{2amA_a} + \frac{\sigma t}{\pi a^2 m A_a} \qquad (2\text{-}9)$$

where σ is the resistivity and t the thickness of the surface film. In a thermal contact, the situation becomes quite difficult even if we ignore the fact that heat may be transmitted through the interstitial fluid and by radiation. This is because a tarnish film normally has a very high resistance to electricity but not so much to heat. Most surface films are semi-conductors and are considered potential barriers. If the films are thin, say 10 Å, the thermal agitation of the electrons of high energy levels is sufficient to allow them to pass through the barriers according to the quantum mechanical tunnel effect[5]. If the films are thick, the flow of electric current becomes rather restricted. The film thickness and the resistivity value are generally unknown. If the resistance due to the presence of films is to be included in calculations, separate experiments have to be carried out to determine their values. Thus it is apparent that the number and size of contact areas determined by electrical measurements will not include all those which are potential junctions for the

passage of heat flow. The conditions of these films around each contact spot, whether metal-metal with film surrounding it or metal-film-metal, must vary considerably from spot to spot. This situation can be further aggrevated by temperature and time. Thus it explains the reasons for the breakdown of the thermal-electric analogy.

If the pressure on the contact points is increased the surface films may be penetrated by the irregularities to allow actual metallic contact. There are several possibilities for this to happen. First if the irregularities are sharp and the pressure at the tips is high enough. For this reason a rough surface is more likely to give a consistent thermal conductance under the influence of pressure. Secondly, if the basic metal should deform plastically at some local spots, the surface films, having very little elasticity, do not allow themselves to follow large degree of deformation and local ruptures become inevitable. This explains that a soft metal against a harder metal provides a better contact. Thirdly, surface shearing action either due to surface sliding or due to differential thermal expansions is very effective in breaking up surface films as found by Bowden and Tabor in their study on friction[6] and by Anderson on adhesion[7]. The significance of surface films can be realised in the problems of hot and cold welding. In order to increase the actual contact areas, every effort must be made to break through these surface barriers. In the thermal contact problem, however, assumption is usually made that the films are thin and are readily penetrable by surface irregularities. If this is not realistic enough, additional contact resistance must be included,

2.2.4 Surface roughness

The surface of a solid is never perfectly flat or smooth and waviness with irregularities are a part of any surface. Even in cases where a high degree of smoothness has been obtained, the ultimate surface is a crystalline one consisting of various oriented crystal facets and revealing an irregular micro-geometry. Surface texture is usually defined by a simple number in conjunction with the name of the assessment process. The standards used by most countries are either the Mean Line System or the Envelope System[8,9]. In the mean line system the roughness of a surface is defined either by the centre line average values or the root mean square values and the usual technique of measurement is by means of a stylus equipment in conjunction with an electrical integrating meter to indicate the value over a sample length. In the envelope system, no reliable instrument has yet been designed for the measurement[10]. The main object of all these standards is to give a reasonable classification of a surface texture for industrial purposes. Thus the basis of measurement is essentially one of geometry and the fundamental definitions are expressed in geometrical terms. The true measurement of any surface should be three-dimensional. The difficulty involved in making such measurements, however, lies in the transformation of various definitions into a two-dimensional plane for the use in a three-dimensional problem. Machined surfaces would have ridges and waviness whereas ground, polished and lapped surfaces would only have dimples and humps. Other type of surfaces would have irregularities distributed at random and there may be scratches not detectable by optical or stylus methods. The measured value over a sample length may vary considerably from area to area. It is quite possible for

surfaces having widely different texture to have a similar assessed value. In short, a simple roughness measurement is seldom sufficient for the characterisation of a surface in a satisfactory manner. To adequately define a surface texture, it is necessary to know the size, shape, the distribution of the irregularities together with the surface waviness and error of form. This is clearly impossible with the present methods of surface roughness assessment.

When two surfaces are pressed together, metallic contacts are set up. If the surfaces are free from waviness, we expect the higher peaks of the irregularities to be engaged first in contact. But if waviness exists, it is those irregularities on the crests of the waves which first make contact. The manner in which contacts are established is often arbitrary. Even with two surfaces of the same texture, there may be an infinite number of matching configurations and it is rather difficult to repeat the same matching once the contact is disturbed. In the absence of waviness, contact spots may be distributed more evenly; on the other hand they are likely to appear in groups. Under the influence of load, the wavy area will deform elastically while the irregularities in contact will most likely deform plastically. The increase in the real area of contact under load depends not only on the surface texture in its real shape and form but also on the mechanical properties of the materials. The form of the surface affects the distribution of the contact areas whereas the shape of the irregularities affects the conditions of the transition from an elastic to a plastic state, the sharper the irregularities the easier for the transition to take place. Owing to the plastically deformed irregularities, some of the contact junctions will be broken as a result of the elastic recovery of the waves in the event of load release.

Thus it is clear that in order to meet the requirements of a thermal contact problem, the complete definition of surface roughness will require a large number of parameters. Yet too large a number will certainly make the problem more involved and unsolvable. There is a definite relationship between the contact conductance and the area of contact. A meaningful roughness parameter for thermal contact studies, should at least enable prediction of contact areas to be made. This not being available, we can understand why there have been conflicting conclusions when thermal contact conductance was treated as a junction of roughness assessed by common simplified methods. An accurate prediction of the size, number and distribution of the contact areas may never be possible unless the surfaces are specially prepared to produce a controlled texture. In this way, the mechanism of heat transfer at the interface can be more positively examined. For random distribution of irregularities of various sizes there does not seem to be a reliable method of estimating the areas of contact. This is where the theory of statistics may be applied.

2.2.5 Area of contact under idealised conditions

From the above discussions, it is clear that there is hardly any possibility for an accurate estimate of the actual areas of contact when two surfaces are pressed together unless some simplified assumptions be introduced. To begin with we may assume that the surfaces in question are flat and are covered uniformly with irregularities of the same size. The tips of the irregularities may be treated as a portion of a sphere of vanishingly small radius of curvature. On the other hand, we may

assume that the surfaces are covered with uniform ridges. Under both these conditions the number and distribution of the contact spots are defined. This leaves only the size of the contact area to be determined under the influence of pressure.

When the applied pressure is small, we can consider deformations to be elastic. According to Hertz' equation[2] for contact between two spheres with radii r_1 and r_2, the radius of the contact area is given by

$$a = \left(\frac{3}{4}W \left(\frac{1-\nu_1^2}{E_1} + \frac{1-\nu_2^2}{E_2}\right) \left(\frac{r_1 r_2}{r_1 + r_2}\right)\right)^{\frac{1}{3}} \qquad (2\text{-}10)$$

where W is the applied load, E_1 and E_2 are the Young's moduli of the two metals and ν_1 and ν_2 are the corresponding values of Poisson's ratios. In the case of a sphere pressed against a flat surface of similar material, $r_1 = r$, $r_2 = \infty$, $E_1 = E_2 = E$ and we have by taking $\nu_1 = \nu_2 = 0.3$ for most metals

$$a = 1.11 \left(\frac{Wr}{E}\right)^{\frac{1}{3}} \qquad (2\text{-}11)$$

As the load is increased, the mean pressure increases until it reaches a value exceeding the elastic limit of the material when we have the onset of the plastic deformation. This occurs when the mean pressure is equal to about 1.1Y where Y is the yield stress of the material. The load which corresponds to the onset of plasticity is

$$W_{op} = 58P^3\left(\frac{r}{E}\right)^2 = 77.2Y^3\left(\frac{r}{E}\right)^2 \qquad (2\text{-}12)$$

From the equation (2-12) it can be seen that the commencement of plastic flow occurs at a load of extremely small magnitude. As the load is further increased, the mean pressure increases and the region of plasticity grows

until the whole of the material around the region of contact is flowing plastically. The mean pressure at this stage is about 3 times the yield stress which, it must be remembered, increases too as the result of work-hardening during the course of plastic deformation. The load corresponding to the condition of fully plastic flow was found by Tabor[3] to be about 150 times that at the onset of plastic flow. To any further increase of load, the material will just yield plastically and the magnitude of the area of contact will be just sufficient to keep the mean pressure equal to the flow pressure, i.e.

$$A = \frac{W}{H} \tag{2-13}$$

where H is the maximum flow pressure determined directly from hardness measurement (the Meyer hardness value). It is known that on a normal contact surface the actual contact area is only a very small fraction of the apparent area of contact. This means that the local contact pressure can be very high, being sufficient to cause plastic flow. Under this condition equation (2-13) provides for the estimate of the contact area. A represents the total sum of the actual contact areas; it, however, does not indicate the exact number and their sizes. Assuming for a moment that the distribution is uniform with m equal spots per unit area, we obtain the radius of each contact spot as

$$a = \left(\frac{W}{HA_a m \pi}\right)^{\frac{1}{2}} \tag{2-14}$$

where A_a is the apparent area of contact.

If the magnitude of the applied load is insufficient to produce full plasticity, both elastic and plastic deformation exist simultaneously, and there is no obvious means of determining the size of the contact

area. The elastic properties of metals are due to the inter-atomic forces and they are very little affected by the amount of work-hardening to which the material is subjected. On the other hand, the plastic properties depend on the slipping of the crystals along certain crystallographic planes. Although ultimately they are related to the crystalline structure and the inter-atomic forces, there is no simple relationship between the elastic moduli and the yield stress. However, we know that during elastic deformation the diameter of a circular contact area is proportional to $W^{\frac{1}{3}}$ whereas during plastic deformation it is proportional to $W^{\frac{1}{2}}$. If the diameter is plotted against the applied load in log-log scales, we would expect the slope of the elastic deformation curve to be 3 while the slope of the plastic deformation curve to be 2. Within the transition range, the slope varies from 3 to 2 as load is increased. This indicates that some approximate results may be derived from graphical methods. That is, in between the onset of plasticity and full plasticity, a smooth curve can be drawn to represent the variation of the contact area in the transition region. This has actually been done and agrees fairly well with test results, the detail of which is given in chapter 4.

2.3 Heat transfer through the interstitial space

Across the interstitial space heat transfer may be considered to take place through the fluid medium filling the space, and by radiation. Since the surfaces bounding the space are covered with irregularities and have non-uniform temperature distribution, the conditions of heat transfer are also non-uniform and thus the quantity of heat transmitted by each

mode of heat transfer becomes a function of the location. We see also that over the entire contact surface it is possible to find the domination of heat being transferred through the metallic junctions in one part and the domination of heat being transferred through the interstitial space in another part. For any fruitful study, it is necessary to make some simplified assumptions. For example, we shall assume that the surfaces are separated by an effective gap distance and that the solid-fluid interfacial conditions surrounding each solid junction are similar.

2.3.1 Heat transfer through the interstitial fluid.

Heat transfer through the fluid may be by conduction as well as by convection. If the Gashof No., which represents the relationship between the buoyant and viscous forces, is less than 1000[11], free convective heat transfer is practically non-existent. In most contact problems it is true to say that the Gashof No. is very much smaller than this value. Thus only fluid conduction need be considered.

The amount of heat transferred by fluid conduction depends largely on the thermal conductivity of the fluid and on the distance of the fluid gap. If the thermal conductivity of the fluid is higher than that of the solid, most of the flow lines will be attracted towards the fluid region. The convergence of flow lines will similarly give rise to a constriction resistance as in the case when they are attracted towards the solid spots. But because the fluid covers a much greater space, the nett resistance of the contact will still be less than that if the basic metal were to occupy the whole interstitial space.

The possibility of a fluid having a higher thermal conductivity than that of a metal is not very great. More often the interstitial fluid is a gas which usually has a thermal conductivity value very much smaller

than that of a metal. In this case the flow lines will be attracted towards the solid junctions. Owing to the accommodation effect, a temperature drop will occur at each solid-gas interface. This effect is equivalent to adding a gas layer between the solid and the gas with a thickness equal to the so called temperature jump distance which is a function of the gas properties and the accommodation coefficient[12].

$$T_{solid} - T_{gas} = l\frac{\partial T}{\partial n} \tag{2-15}$$

where $\frac{\partial T}{\partial n}$ is the temperature gradient normal to the surface and l is the temperature jump distance which is given by

$$l = \frac{2-a}{a}\frac{4c}{\gamma+1}\frac{k_f}{\mu c_v}\lambda \tag{2-16}$$

where λ is the mean free path of the gas, a the accommodation coefficient, μ the coefficient of viscosity, c_v the specific heat for constant volume, γ the rotio of specific heats, k_f the thermal conductivity of the gas and c is a constant which has a value near to 0.5. For different surface conditions at the two solid-gas interfaces, we have

$$l_1+l_2 = \frac{a_1+a_2-a_1a_2}{a_1a_2}\frac{4}{\gamma+1}\frac{\lambda k_f}{\mu c_v} \tag{2-17}$$

In general metal surfaces are covered with a layer of tarnish film and the additional resistance can be taken as

$$R_o = \frac{t}{k_o} \tag{2-18}$$

where t is the thickness and k_o the thermal conductivity. Combining the effects of surface accommodation and the presence of surface films, an effective fluid thermal conductivity can be obtained, i.e.

$$k_f' = \frac{k_f}{1 + \frac{l_1+l_2}{\delta} + \frac{k_f}{\delta}\left(\frac{t_1}{k_{o1}} + \frac{t_2}{k_{o2}}\right)} \qquad (2\text{-}19)$$

Where the subscripts 1 and 2 refer to surface 1 and 2 respectively, and δ is the mean contact gap distance. Normally t is in the order of 10^2 Å whereas δ may be in the order of 10^6 Å or more. Even if k_o were (say) one hundred times smaller than k_f, the part due to film resistance is negligibly small. Thus equation (2-19) can be written as

$$k_f' = \frac{k_f}{1 + \frac{l_1+l_2}{\delta}} \qquad (2\text{-}20)$$

The thermal conductivity of a gas, however, varies with temperatures, a rise in temperature tending to increase its value since the thermal conductivity of a gas is directly connected with the coefficient of viscosity which is proportional to the square root of the absolute temperature. According to the kinetic theory of gases [12], we obtain the gas thermal conductivity as

$$k_f = \tfrac{1}{4}(9\gamma - 5)\mu C_v$$

$$= \frac{9\gamma-5}{2\sqrt{2\pi}} C_v \rho \lambda \sqrt{\frac{R_g T}{M}} \qquad (2\text{-}21)$$

where ρ is the density of the gas, R_g the universal gas constant and M the molecular weight of the gas. However, it has been found that the thermal conductivity of most gases increases more rapidly than the square root of the absolute temperature T. It is considered that a rise of temperature tends to increase the violence of impacts between molecules more so than equation (2-21) would indicate. If the molecules are not

absolutely hard as assumed in the theory, the net result of a temperature rise lends itself to an increase in the persistance of molecular velocities after each impact. It is also suggested that the mean free path is somewhat shortened by the fact that molecules which pass each other at close range are under the influence of an attractive force between them. To include these effects a modified expression for the coefficient of viscosity was introduced by Sutherland[12]. Since thermal conductivity is directly proportional to the coefficient of viscosity, Sutherland's expression (Kennard page 156) is applied here so that the thermal conductivity at temperature T is given by

$$(k_f)_T = (k_f)_o \left(\frac{T}{T_o}\right)^{\frac{1}{2}} \left(\frac{1 + C/T_o}{1 + C/T}\right) \qquad (2\text{-}22)$$

where $(k_f)_o$ is the thermal conductivity at temperature T_o and C is a constant which can be determined from results at two temperature points - the low temperature point may be from (2-21) while the high temperature point from an experimental result. Equation (2-22) can be further modified to take the form of

$$k_f = b \frac{\sqrt{T}}{1 + \frac{C}{T}} \qquad (2\text{-}23)$$

where b is a constant corresponding to C for a given gas.

By substitution of equations (2-17) and (2-23) into equation (2-20), the effective gas thermal conductivity becomes

$$k_f' = \frac{\delta \frac{b\sqrt{T}}{1 + C/T}}{\delta + \frac{a_1 + a_2 - a_1 a_2}{a_1 a_2} \frac{4}{\gamma + 1} \frac{\lambda}{\mu C_v} \frac{b\sqrt{T}}{1 + C/T}} \qquad (2\text{-}24)$$

Thus the ratio k_f'/δ forms a governing factor on the heat transfer through the fluid.

2.3.2 Heat transfer by free molecular conduction

As the interstitial gas pressure is reduced, the occurrence of intermolecular collisions becomes less frequent and therefore viscosity as well as thermal conductivity become less important. Under normal conditions, the thermal conductivity of a gas is independent of the gas pressure. This, however, is not the case when the pressure is either so low or the contact surfaces so close that the mean free path of the gas molecules is larger than the contact gap dimension. In this case, the molecules transport energy across the interface at a single bound. There is no temperature gradient in the gas field. This is called free molecular conduction and it is considered to exist for the Knudson number (defined as $\frac{\lambda}{\delta}$) to be greater than 10. Let $(k_f')_m$ be the equivalent gas conductivity corresponding to a contact gap distance of δ for free molecular heat transfer. From the kinetic theory of gases we obtain

$$(k_f)_m' = \delta \left(\frac{a_1 a_2}{a_1 + a_2 - a_1 a_2}\right)\left(\frac{\gamma+1}{\gamma-1}\right) p \sqrt{\frac{R_g}{8\pi MT}} \qquad (2\text{-}25)$$

where p is the gas pressure and M the molecular weight. Under the free molecular conduction condition, the fluid heat transfer is governed by the ratio $(k_f)_m'/\delta$.

2.3.3 Fluid gap distance

Since surfaces can never be perfectly flat, we see that the fluid gap distance will vary from point to point. Lack of a definite means of assessing the true roughness of a surface means it is impossible even to find a mean value when the matching of two surfaces in contact is always arbitrary.

Any standard method of assessing a surface texture certainly would not help as it is on a two dimensional basis. Fenech and Rohsenow[13] used a graphical method to work out a mean value along two perpendicular lines on the surfaces and tried to preserve the matching conditions by placing the two surfaces of the test specimens carefully together so that the measured lines of one surface would coincide with those of the other. In practice such a method would be very difficult to carry out. Other workers simply derived a mean value from the measurement of a surface analyser. A more positive approach has been carried out by those who used prepared surfaces where the roughness has a definite pattern. Thus it is not too difficult to find the volume of the void and the mean fluid gap. Since the prediction of a fluid gap distance is closely connected with the definition of a surface texture and the instrument which is employed for such an assessment, and since, however, both the definition and any available instruments are inadequate for giving the required information for a thermal contact problem, simplified assumptions are necessary for any estimation. For example, the surface irregularities may be assumed to be of a regular shape and size according to a certain surface treatment. We could also assume that the irregularities on both surfaces are engaged in pairs. Knowing the average height of the irregularities, it is possible then to find the mean value of the fluid gap distance.

Assuming that the effective mean value of δ is known, we realise that its value is liable to decrease when the contact parts are subject to pressure. In which case the result obtained in Appendix E can be applied with certain modifications to suit the shape of the irregularities. It seems reasonable to assume that the tips of all irregularities are spherical. And if we ignore the deformation of the main body due to

local contact pressure, the reduction in height will be equal to

$$\Delta\delta = 2r\left(1-\sqrt{1-\left(\frac{a}{r}\right)^2}\right) \qquad (2\text{-}26)$$

where r is the radius of the tip and a is the radius of the contact area. Thus the final fluid gap distance is $\delta - \Delta\delta$.

2.3.4 Heat transfer by radiation

During contact, the two surfaces are normally non-isothermal. Heat transfer by radiation therefore depends on the surface emissivity and absorptivity according to the local temperature. If the surfaces are assumed isothermal and 'grey' (for which the emissivity is equal to the absorptivity owing to the monochromatic condition), the heat flux per unit area between two parallel surfaces of very large size compared with the distance separating them is given by

$$q_r = \frac{1}{\frac{1}{\epsilon_1}+\frac{1}{\epsilon_2}-1}\,\sigma\,(T_1^4 - T_2^4) \qquad (2\text{-}27)$$

where ϵ_1 and ϵ_2 are emissivities of surface 1 and 2 respectively and σ is the Stafan-Boltzmann's constant. Equation (2-27) may be written as

$$q_r = \frac{\sigma}{\frac{1}{\epsilon_1}+\frac{1}{\epsilon_2}-1}\,(T_1^3+T_1^2T_2+T_1T_2^2+T_2^3)(T_1-T_2)$$

$$= \frac{k_r}{\delta}\,(T_1-T_2) \qquad (2\text{-}28)$$

where k_r is an equivalent thermal conductivity of an imaginary fluid through a distance δ of which the amount of heat transferred is equal to that by radiation. Thus we write

$$k_r = \frac{\delta\sigma(T_1^3+T_1^2T_2+T_1T_2^2+T_2^3)}{\frac{1}{\epsilon_1}+\frac{1}{\epsilon_2}-1}$$

$$\doteq \frac{4\sigma T_m^3\delta}{\frac{1}{\epsilon_1}+\frac{1}{\epsilon_2}-1} \qquad (2\text{-}28)$$

The second result of equation (2-28) can be used if (T_1-T_2) is small compared with the mean temperature $T_m = \frac{T_1+T_2}{2}$. The amount of heat transferred by radiation as compared with that by conduction of the interstitial fluid can be represented by the ratio k_r/k_f. At moderately high temperature this ratio is very small and the radiation heat transfer is generally ignored. Under low pressure and low contact load conditions, however, when conductance of heat through metallic junctions and the fluid becomes relatively small, the radiation term can be of significance.

Overall effective fluid thermal conductivity

Combining the equivalent thermal conductivity by radiation with the effective fluid conductivity, we obtain the overall effective fluid thermal conductivity. The following are the results of the combination for two different conditions.

1. Normal pressure condition (equations (2-24) and (2-28)

$$k_f'' = \frac{\delta\frac{b\sqrt{T}}{1+C/T}}{\delta+\frac{a_1+a_2-a_1a_2}{a_1a_2}\frac{4}{\gamma+1}\frac{\lambda}{\mu C_v}\frac{b\sqrt{T}}{1+C/T}} + \frac{4\delta\sigma T_m^3}{\frac{1}{\epsilon_1}+\frac{1}{\epsilon_2}-1} \qquad (2\text{-}29)$$

2. free molecular conduction condition (equations (2-25) and (2-28))

$$k_f'' = \delta \left(\frac{a_1 a_2}{a_1 + a_2 - a_1 a_2}\right)\left(\frac{\gamma+1}{\gamma-1}\right) p \sqrt{\frac{R_g}{8\pi MT}} + \frac{4\delta\sigma T_m^3}{\frac{1}{\epsilon_1} + \frac{1}{\epsilon_2} - 1} \qquad (2\text{-}30)$$

To include fluid gap distance reduction due to applied load, δ should be reduced by $\Delta\delta$ which can be obtained from equation (2-26).

CHAPTER III

THEORETICAL STUDY

3.1 Idealised contact model

When two surfaces are brought into contact, we assume that the contact spots are uniformly distributed and are of the same size, so that if the contact members are divided into a number of parallel cylinders, each containing one contact spot at its centre, no heat flow will take place between them. In this case, we need only use one such cylinder to study the manner in which heat is transferred from one member to another across the interface of the contact. The contact spot is also assumed to be a circular cylinder so that the fluid gap distance between the contact members is uniform. Under steady-state condition, the Laplace equation for the axi-symmetrical temperature distribution is

$$\frac{\partial^2 T}{\partial r^2} + \frac{1}{r}\frac{\partial T}{\partial r} + \frac{\partial^2 T}{\partial Z^2} = 0 \qquad (3\text{-}1)$$

where Z and r are the axial and radial coordinates respectively. Since the fluid gap is usually very small compared with the radius of the cylinder R, we assume that there is no radial heat flow between the contact spots and the fluid. The fluid gap distance is divided into δ_1 and δ_2 by a plane of contact which is assumed to have a uniform temperature T_o

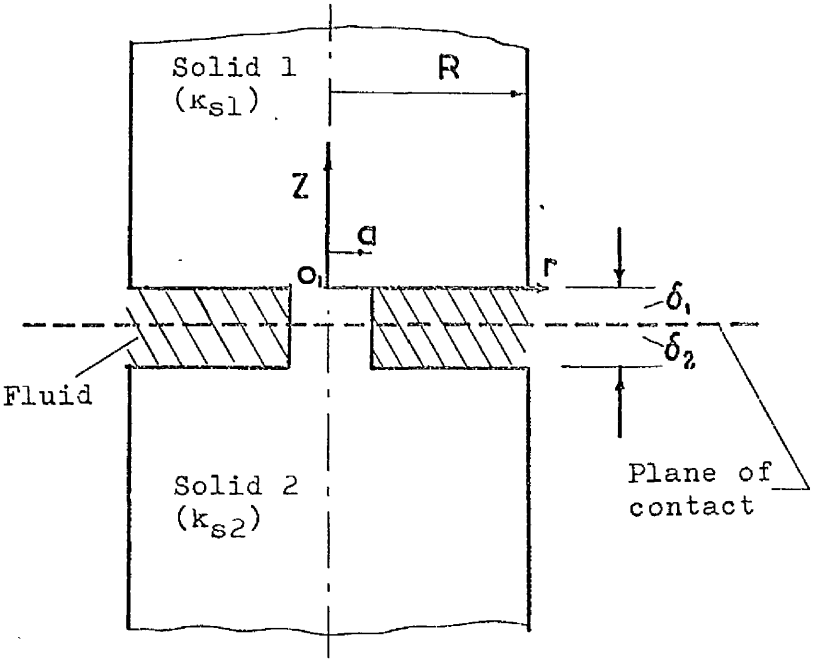

Fig. 3.1 Idealised contact model

The distances are chosen so that $\delta_1 = (\frac{k_{s2}}{k_{s1}+k_{s2}})\delta$ and $\delta_2 = (\frac{k_{s1}}{k_{s1}+K_{s2}})\delta$ where k_{s1} and k_{s2} are the thermal conductivities of solid 1 and 2 respectively and δ is the total distance of the fluid gap which is made up of the height h_1 of the contact spot 1, and the height h_2 of the contact spot 2. By placing the origin at O_1 at a distance δ_1 above the plane of contact (similarly by placing the origin at O_2 at a distance δ_2 below the place of contact when considering solid 2), it is possible to assume that the fluid is replaced by a medium having a heat transfer coefficient $\frac{k_f}{\delta_1}$ and the solid spot by a medium having a heat transfer coefficient $\frac{k_m}{\delta_1}$. To obtain k_m, we consider the heat flowing through the contact spots 1 and 2 against a total resistance of $\frac{h_1k_{s2}+h_2k_{s1}}{k_{s1}k_{s2}}$. Since $\delta = h_1+h_2=\delta_1+\delta_2$ is small compared with R, the resistance from solid 1 and 2 to the plane of contact can be taken as equal to

$$(\frac{h_1k_{s2}+h_2k_{s1}}{k_{s1}k_{s2}})\frac{\delta_1}{\delta} \quad \text{and} \quad (\frac{h_1k_{s2}+h_2k_{s1}}{k_{s1}k_{s2}})\frac{\delta_2}{\delta}$$

respectively. Thus $k_m = \frac{k_{s1}k_{s2}}{h_1k_{s2}+h_2k_{s1}}\delta$ (3-2)

We seek now a temperature distribution which satisfied the following boundary conditions:-

$$\frac{\partial T}{\partial r} = 0 \qquad \text{at} \quad r = 0, \quad 0 < Z < \infty \tag{3-3}$$

$$\frac{\partial T}{\partial r} = 0 \qquad \text{at} \quad r = R, \quad 0 < Z < \infty \tag{3-4}$$

$$T \propto Z \qquad \text{as} \quad Z \longrightarrow \infty \tag{3-5}$$

$$k_{sl}\frac{\partial T}{\partial Z} = \frac{k_f}{\delta_1}(T-T_o) \quad \text{at} \quad Z = 0, \quad a < r < R \tag{3-6}$$

$$k_{sl}\frac{\partial T}{\partial Z} = \frac{k_m}{\delta_1}(T-T_o) \quad \text{at} \quad Z = 0, \quad 0 < r < a \tag{3-7}$$

In general such boundary conditions are difficult to satisfy by one simple expression of T. We therefore divide the solid above the o-r plane into two parts as shown in the figure 3.2 so that in region 1, i.e. $a < r < R_1$, $0 < Z < \infty$

$$\frac{\partial^2 T_1}{\partial r^2} + \frac{1}{r}\frac{\partial T_1}{\partial r} + \frac{\partial^2 T_1}{\partial Z^2} = 0 \tag{3-8}$$

and in region 1', i.e. $0 < r < a$, $0 < Z < \infty$

$$\frac{\partial^2 T_1'}{\partial r^2} + \frac{1}{r}\frac{\partial T_1'}{\partial r} + \frac{\partial^2 T_1'}{\partial Z^2} = 0 \tag{3-9}$$

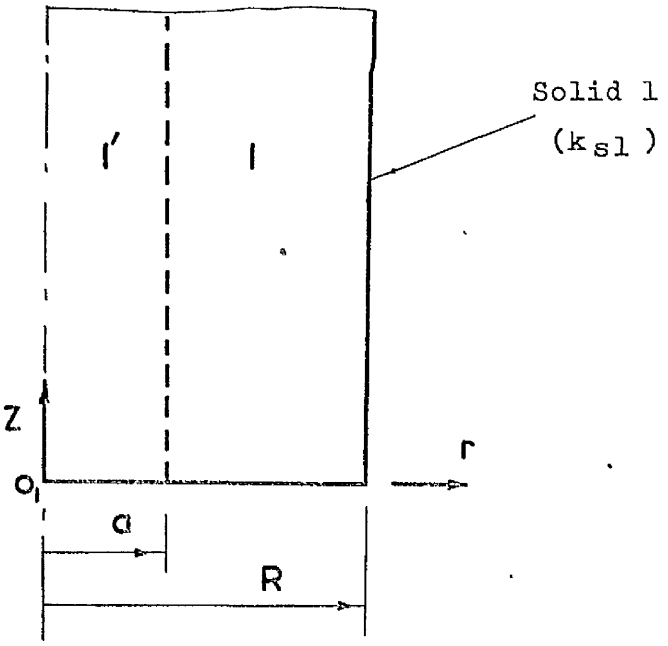

Fig. 3.2 Solid 1 of idealised contact model

Between these two regions, the boundary conditions at r = a are

$$T_1 = T_1' \tag{3-10}$$

$$\frac{\partial T_1}{\partial r} = \frac{\partial T_1'}{\partial r} \tag{3-11}$$

Without suggesting any order of magnitude we may consider the typical longitudinal temperature distributions through the contact spot and through the fluid to be represented in figure 3.3

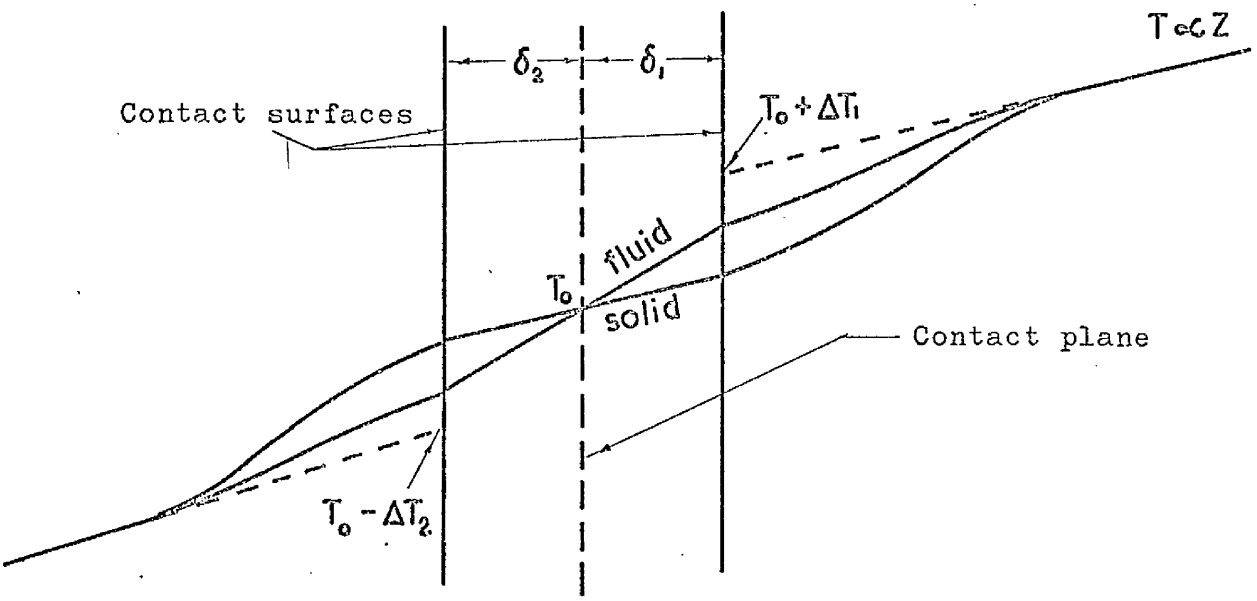

Fig. 3.3 Typical longitudinal temperature distribution in the contact region.

With these considerations and the assumptions made earlier, we introduce the following solutions to the equations (3-8) and (3-9)

$$T_1' = T_o + \Delta T_1 + H_1\frac{Z}{R} - A_1 e^{-\alpha\frac{Z}{R}} J_o\left(\alpha\frac{r}{R}\right) \tag{3-12}$$

$$T_1 = T_o + \Delta T_1 + H_1\frac{Z}{R} - B_1 e^{-\lambda\frac{Z}{R}} J_o\left(\lambda\frac{r}{R}\right) - D_1 e^{-\beta\frac{Z}{R}} Y_o\left(\beta\frac{r}{R}\right) \tag{3-13}$$

The first term on the right hand side of these equations indicates the temperature of the contact plane while the second term the experimental

temperature difference between the contact surface of solid 1 and the contact plane. The third term represents the uniform temperature variation with Z in the absence of flow constriction and the remaining terms in both (3-12) and (3-13) signify the variation of the temperatures as a result of flow constriction. J_o and Y_o are Bessel functions of the first and second kind respectively[15], and A_1, B_1, D_1, H_1, α, λ, β are constants. In order to determine these constants, the boundary conditions are approximately modified. First we assume the average of the heat flux distribution across the contact surface at Z = 0 to be sufficiently accurate to replace equations (3-6) and (3-7), i.e.

$$\int_r^R k_{s1} \frac{\partial T_1}{\partial Z} \, rdr = \int_r^R \frac{k_f}{\delta_1}(T_1 - T_o) rdr \qquad (3\text{-}14)$$

$$\int_o^a k_{s1} \frac{\partial T_1'}{\partial Z} \, rdr = \int_o^a \frac{k_m}{\delta_1}(T_1' - T_o) rdr \qquad (3\text{-}15)$$

We also assume that the average of the temperature distribution and the average of the heat flux distribution at r = a, $0 < z < \infty$ are reasonable conditions to use instead of those given by equation (3-10) and (3-11). They are

$$\int_o^\infty T_1' \, dZ = \int_o^\infty T_1 dZ \qquad \text{at } r = a \qquad (3\text{-}16)$$

$$\int_o^a \frac{\partial T_1'}{\partial r} \, dZ = \int_o^a \frac{\partial T_1}{\partial r} \, dZ \qquad \text{at } r = a \qquad (3\text{-}17)$$

The total heat flux is equal to

$$Q = k_{s1}\left(\frac{T}{Z}\right)_{Z=\infty} \pi R^2 = \pi R k_{s1} H_1 \qquad (3\text{-}18)$$

Hence by definition, the contact resistance between solid 1 and the contact plane is given by

$$R_1 = \frac{\Delta T_1}{Q} = \frac{\Delta T_1}{\pi R k_{s1} H_1} \tag{3-19}$$

The detail of the analysis is given in APPENDIX A. Accordingly we obtain

$$R_1 = \frac{\delta_1}{\pi R^2 k_{s1}} \left[\frac{(1-x^2)(1+\frac{\pi x}{4y_1}\frac{k_m}{k_{s1}}) + x^2(1+\frac{k_f}{y_1 k_{s1}}F(x))}{(1-x^2)(1+\frac{\pi x}{4y_1}\frac{k_m}{k_{s1}})\frac{k_f}{k_{s1}} + x^2\frac{k_m}{k_{s1}}(1+\frac{k_f}{y_1 k_{s1}}F(x))} \right] \tag{3-20}$$

where

$$F(x) = \frac{J_1(3.83x)Y_o(2.2x) + 1.6xJ_1(3.83x)Y_1(2.2x) - J_o(3.83x)Y_1(2.2x)}{3.83J_1(3.83x)Y_o(2.2x) - 2.2J_o(3.83x)Y_1(2.2x)} \tag{3-21}$$

The value of F(x) is plotted against x which is the ratio $\frac{a}{R}$ and is given in figure 3.4. y_1 is the ratio $\frac{\delta_1}{R}$.

If we choose the following temperature distributions in region 2' and 2 of solid 2 with the origin of the r,Z coordinates placed at O_2, such as

$$T_2' = T_o - \Delta T_2 - H_2 \frac{Z}{R} + A_2 e^{-\alpha\frac{Z}{R}} J_1(\alpha\frac{r}{R}) \tag{3-22}$$

$$T_2 = T_o - \Delta T_2 - H_2 \frac{Z}{R} + B_2 e^{-\lambda\frac{Z}{R}} J_1(\lambda\frac{r}{R}) + D_2 e^{-\beta\frac{Z}{R}} Y_o(\beta\frac{r}{R}) \tag{3-23}$$

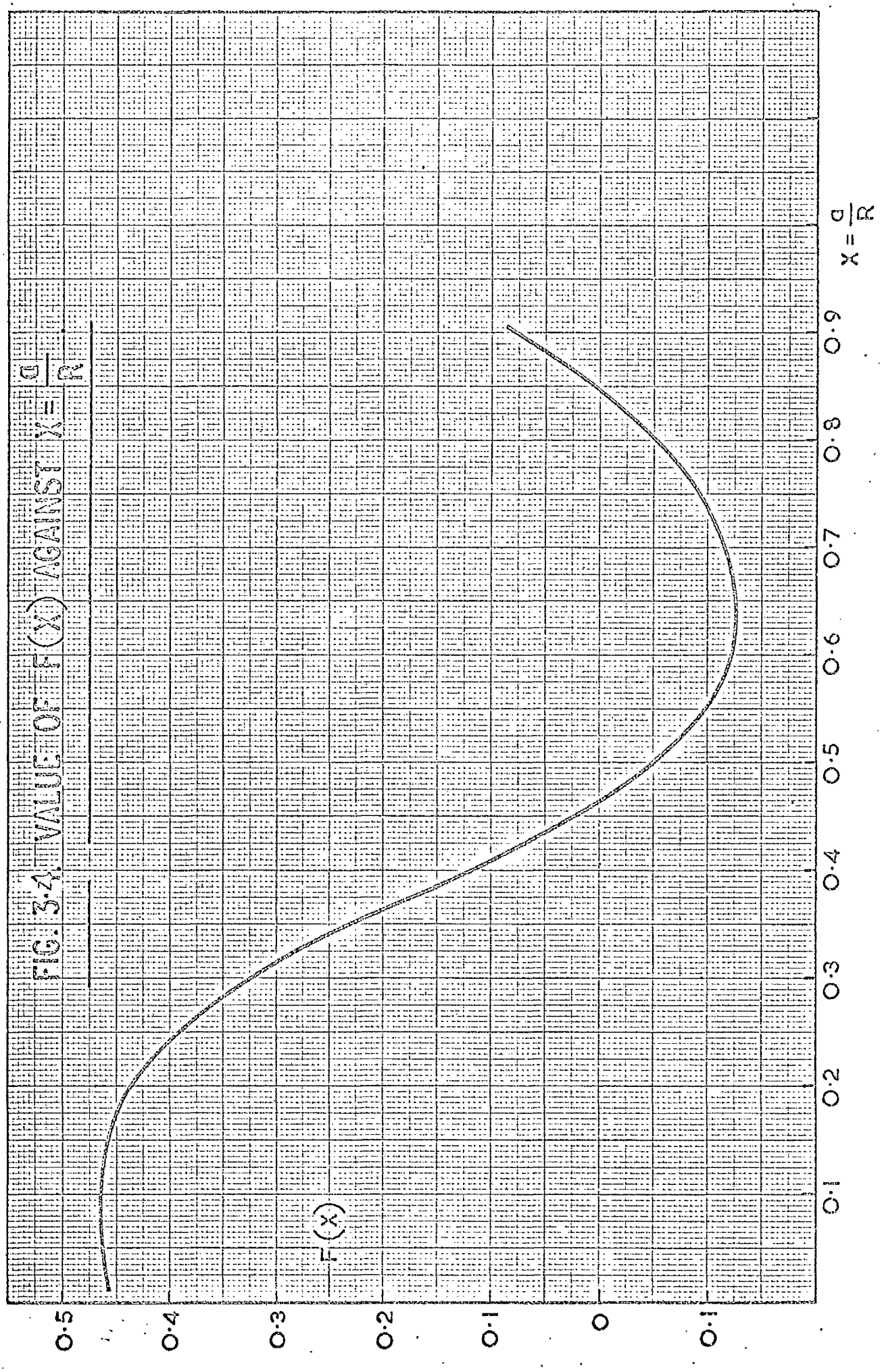

FIG. 3·4. VALUE OF F(x) AGAINST $x = \frac{a}{R}$

We can use the similar approach as with solid 1 and find the contact resistance between solid 2 and the contact plane to be given by

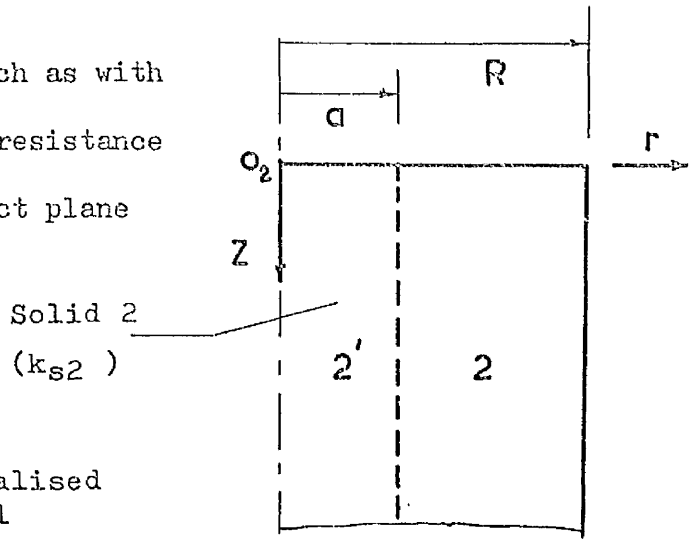

Fig. 3.5 Solid 2 of idealised contact model

$$R_2 = \frac{\delta_2}{\pi R^2 k_{s2}} \left[\frac{(1-x^2)(1+\frac{\pi x}{4y_2}\frac{k_m}{k_{s2}}) + x^2(1+\frac{k_f}{y_2 k_{s2}}F(x))}{(1-x^2)(1+\frac{\pi x}{4y_2}\frac{k_m}{k_{s2}})\frac{k_f}{k_{s2}} + x^2\frac{k_m}{k_{s2}}(1+\frac{k_f}{y_2 k_{s2}}F(x))} \right] \qquad (3\text{-}24)$$

It is interesting to note that the square brackets in each of the equations (3-20) and (3-24) contains a multiplying factor to the contact gap distance δ_1 and δ_2 respectively. This means that the contact resistance could be taken to be that acting against a uniform flow of heat flux through some equivalent lengths of the materials many times larger than the distances δ_1 and δ_2 according to the magnitude of these factors.

Since $y_1 k_{s1} = y_2 k_{s2}$ where $y_1 = \frac{\delta_1}{R}$ and $y_2 = \frac{\delta_2}{R}$, we introduce a solid contact parameter K_s and a fluid contact parameter K_f such that

$$K_s = \frac{k_m}{y_1 k_{s1}} = \frac{k_m}{y_2 k_{s2}} \quad \text{and} \quad K_f = \frac{k_f}{y_1 k_{s1}} = \frac{k_f}{y_2 k_{s2}}$$

The combination of equations (3-20) and (3-24) gives the total contact resistance

$$R_t = R_1 + R_2 = \frac{1}{\pi R}\left[\frac{(1+\frac{\pi x}{4}K_s - x\frac{2\pi x}{4}K_s) + x^2 K_f F(x)}{(1-x^2)(1+\frac{\pi x}{4}K_s)K_f + x^2 K_s(1+K_f F(x))} \right] \left(\frac{k_{s1}+k_{s2}}{k_{s1}k_{s2}}\right)$$

(3-25)

The total contact conductance is

$$C_t = \frac{1}{R_t} = \pi R\left(\frac{k_{s1}k_{s2}}{k_{s1}+k_{s2}}\right)\left[\frac{(1-x^2)(1+\frac{\eta x}{4}K_s)K_f + x^2K_s(1+K_fF(x))}{(1+\frac{\eta x}{4}K_s - x^2\frac{\eta x}{4}K_s) + x^2K_f F(x)}\right] \quad (3\text{-}26)$$

It can be seen that as x becomes very small, C_t tends to $\frac{\pi R^2 k_f}{\delta}$. On the other hand when x approaches unity, C_t tends to $\pi R^2\left(\frac{k_{s1}k_{s2}}{h_1k_{s2}+h_2k_{s1}}\right)$. These results are all in accordance with what was expected.

To find the solid contact conductance C_s and the fluid contact conductance C_f, we determine first the amount of heat transferred through each path. The analysis is given in APPENDIX A. We need only quote the results here. They are

$$C_s = \pi R K_s x^2\left(\frac{k_{s1}k_{s2}}{k_{s1}+k_{s2}}\right)\left[\frac{(1+\frac{\eta x}{4}K_f - x^2\frac{\eta x}{4}K_f) + x^2K_f F(x)}{(1+\frac{\eta x}{4}K_s - x^2\frac{\eta x}{4}K_s) + x^2K_f F(x)}\right] \quad (3\text{-}27)$$

$$C_f = \pi R K_s(1-x^2)\left(\frac{k_{s1}k_{s2}}{k_{s1}+k_{s2}}\right)\left[\frac{(\frac{K_f}{K_s}+\frac{\eta x}{4}K_f - x^2\frac{\eta x}{4}K_f)+x^2K_f F(x)}{(1+\frac{\eta x}{4}K_s - x^2\frac{\eta x}{4}K_s) + x^2K_f F(x)}\right] \quad (3\text{-}28)$$

The ratio between C_f and C_s is given by

$$\frac{C_f}{C_s} = \left(\frac{1}{x^2}-1\right)\left[1 - \frac{1-\frac{K_f}{K_s}}{(1+\frac{\eta x}{4}K_f - x^2\frac{\eta x}{4}K_f) + x^2K_f F(x))}\right] \quad (3\text{-}29)$$

For C_s to be equal to C_f we find from equations (3-27) and (3-28) the relationship between the solid contact parameter K_s and the fluid contact parameter K_f, i.e.

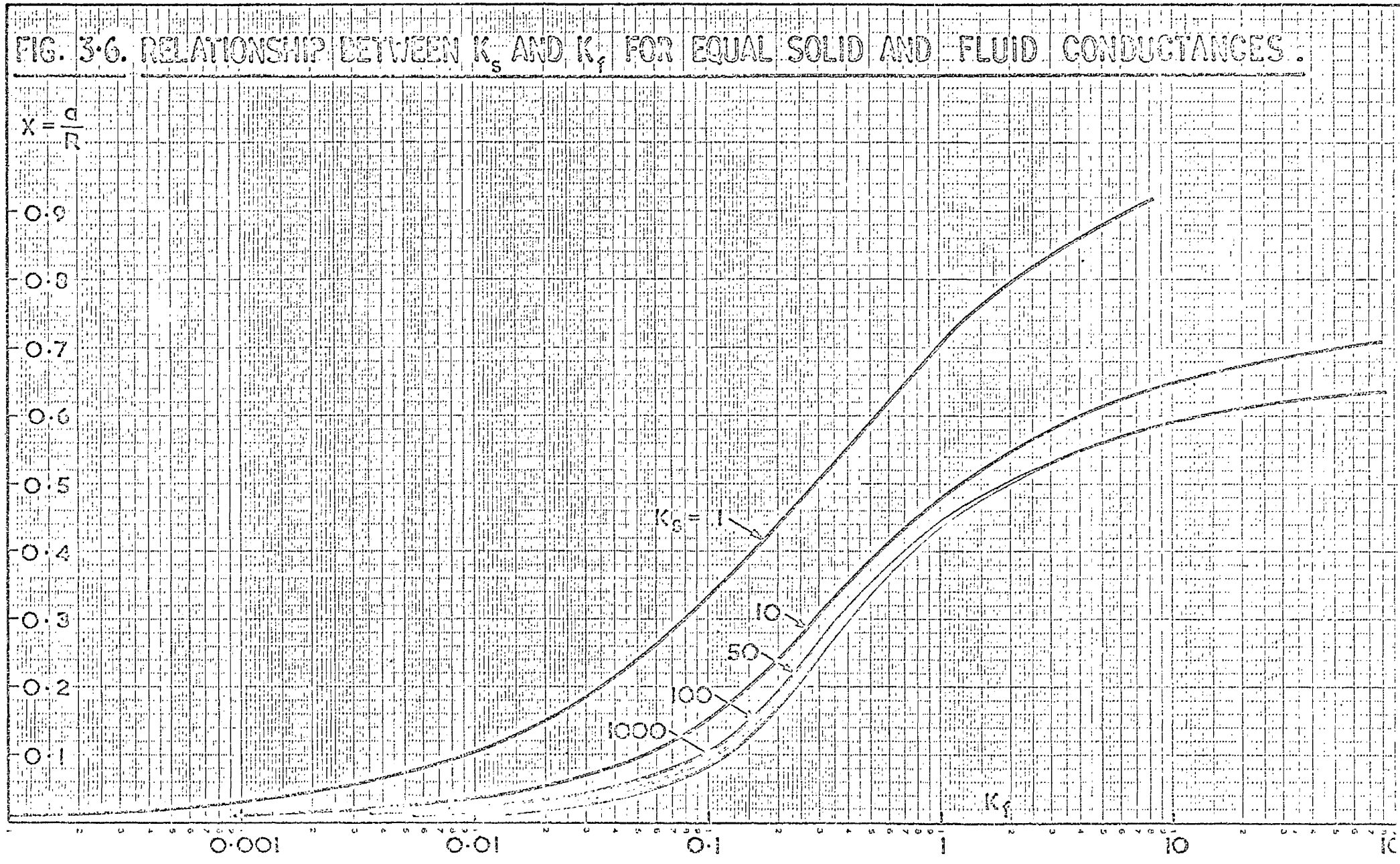

FIG. 3·6. RELATIONSHIP BETWEEN K_s AND K_f FOR EQUAL SOLID AND FLUID CONDUCTANCES.

$$K_f = \frac{x^2 K_s}{(2x^2(1-x^2)F(x) + (1 - 3x^2 + 2x^4)\frac{\pi x}{4})K_s + (1-x^2)} \qquad (3\text{-}30)$$

The $K_f - K_s$ relationship for varying values of x is plotted in Fig. 3.6. As can be seen, when K_s is larger than 10, K_f is mainly influenced by x. To obtain equal conductances for x greater than 0.6, K_f has to be a great deal larger than K_s. For x to be greater than 0.75, no equal conductances can be obtained no matter how large the value of K_f is, unless the value of K_s is reduced. When K_s is smaller than 10, its influence on K_f is quite noticeable.

3.2 A more realistic contact model

From results of surface analyses of a metallic face we realise that the shape of the protruding asperities is more likely to be a circular pyramid rather than a circular cylinder, although it is quite understood that the assumption of the cylindrical contact spots while dealing with a thermal contact problem is more for the convenience of mathematical treatment.

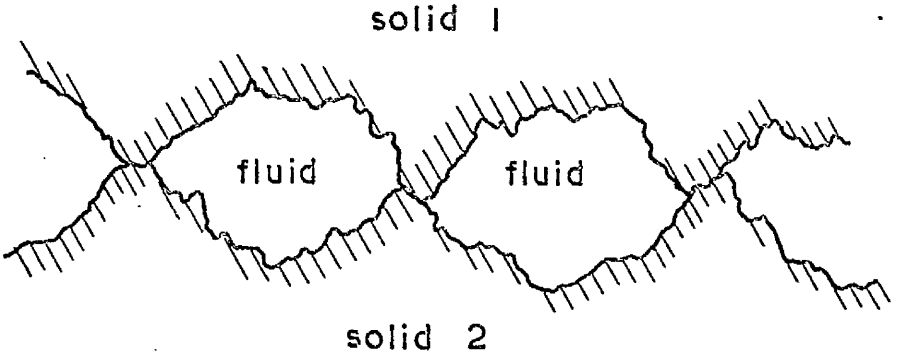

Fig. 3.7 A typical profile of two surfaces in contact.

We realise also that when two surfaces are brought together it is the summits of these hill shaped asperities which are in contact. Although the actual area of contact at the tips is very small, the area at the base can be a great deal larger. This indicates that apart from the constriction of the flow lines in the main body to the base of the asperity, there is also a secondary constriction of flow lines from the base to the tip in the asperity itself. The constriction as well as the material resistance in the engaging pair of asperities determines the amount of heat to be transferred through the solid spot and through the fluid gap. Further, if a tarnish film is present between the tips of the asperities, additional film resistance will result. In other words, the constriction resistance in the main body is sensitively influenced by the total resistance along the asperities which form the metallic passage of heat flow. We see, therefore, that it is nearer to the truth if the asperities are described as conic frusta instead of circular cylinders. The contact model appears as in the figure 3.8, in which it is shown the constriction of the flow lines along the main body as well as along the asperity. The determination of constriction and material resistance of a conic frustrum is given in APPENDIX B.

The total resistance consists of the constriction and material resistances of the conic frustum 1 and those of conic frustum 2 connected in series. Any film resistance can be included if necessary. In this case we shall require to know the film thickness t and its

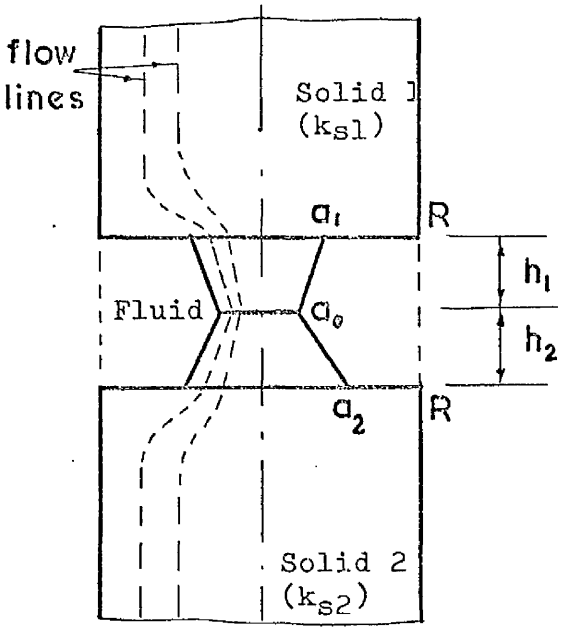

Fig. 3.8 A more realistic contact model

thermal conductivity k_o in order to calculate this additional resistance according to

$$R_o = \frac{t}{\pi a_o^2 k_o} \tag{3-31}$$

Normally a surface film may only be several hundred Angstrom in thickness and is quite readily penetrable by the tips of the asperities under high pressure. In this case we can ignore its existence. From the results obtained in APPENDIX B, we find that the constriction resistance of a conic frustum is

$$R_{cf} = \frac{\frac{a}{a_o} - 1}{4\pi a k_s} \frac{\beta}{\sqrt{1+\beta^2} - \beta} \tag{3-32}$$

The value of R_{cf} multiplied by ak_s is plotted against $\theta_o = \tan^{-1}(\frac{a-a_o}{h})$ for various $\frac{a}{a_o}$ as shown in figure 3.9. The material resistance is equal to

$$R_{mf} = \frac{h}{\pi k_s a a_o} \tag{3-33}$$

The total resistance per unit area for a pair of conic frusta engaged in contact is therefore equal to

$$R_a = \frac{a_1}{4k_{s1}} \frac{(\frac{a_1}{a_o}-1)\beta_1}{\sqrt{1+\beta_1^2}-\beta_1} + \frac{a_2}{4k_{s2}} \frac{(\frac{a_2}{a_o}-1)\beta_2}{\sqrt{1+\beta_2^2}-\beta_2} + \frac{a_1 h_1}{a_o k_{s1}} + \frac{a_2 h_2}{a_o k_{s2}} \tag{3-34}$$

where $\beta_1 = \frac{a_1 - a_o}{h_1}$, $\beta_2 = \frac{a_2 - a_o}{h_2}$ and the dimensions a_1, a_2, a_o, h_1 and h_2 are defined as according to the figure 3.8.

To find the overall thermal conductance of the system, the approach used in section 3.1 can be applied here provided that the fluid gap distance (i.e. $\delta = h_1 + h_2$) is small compared with the radius R of the cylinder and

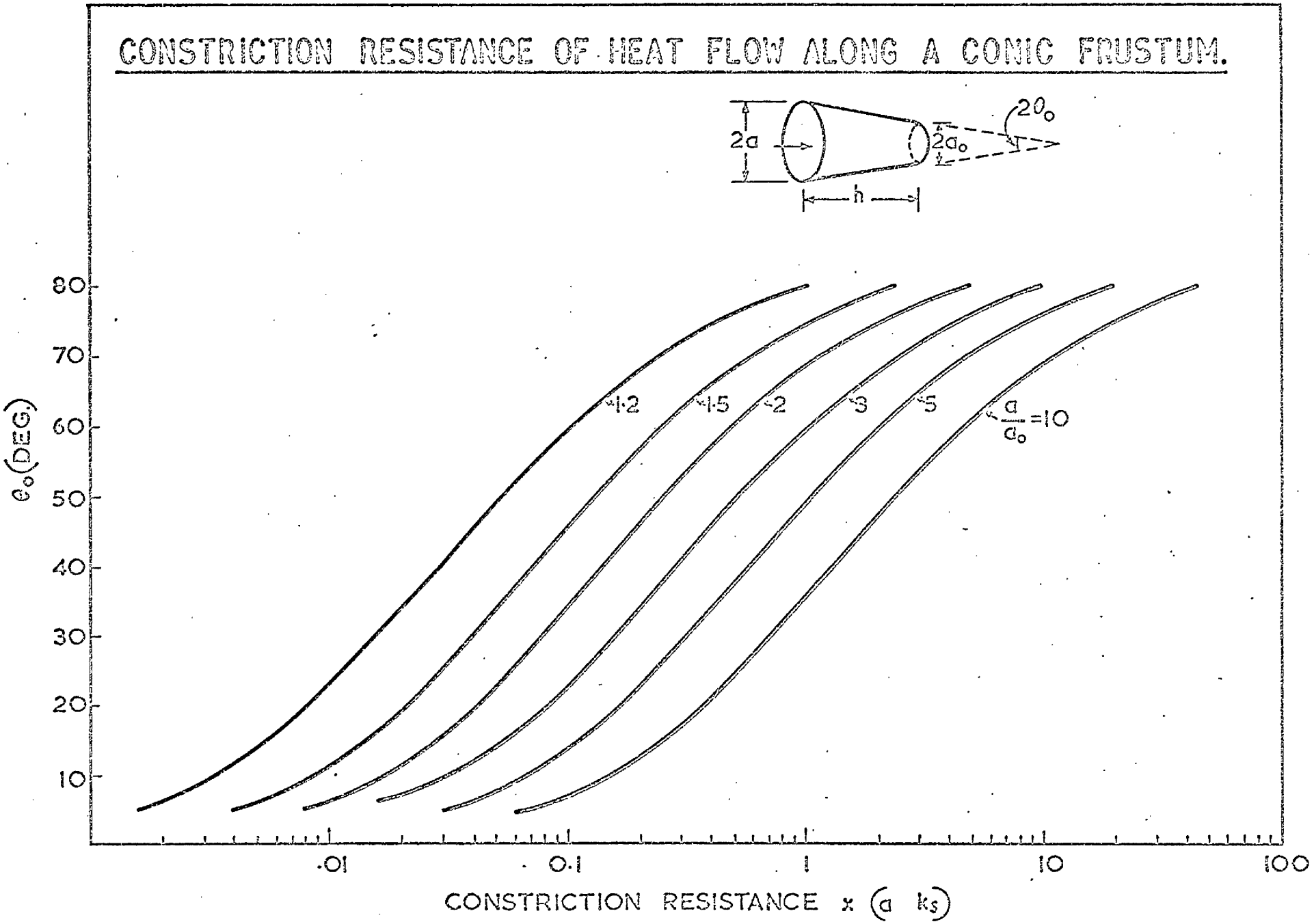
CONSTRICTION RESISTANCE OF HEAT FLOW ALONG A CONIC FRUSTUM.
2a
2a₀
2θ₀
h
θ₀ (DEG)
80
70
60
50
40
30
20
10
1·2
1·5
2
3
5
a/a₀ = 10
·01
·0·1
1
10
100
CONSTRICTION RESISTANCE x (a k_s)

FIG. 3·9.

provided that no heat transfer takes place between the fluid and the solid spots. Under such circumstances the results obtained in section 3.1 apply directly to the case with asperities of any regular shape including a conic frustum. What will be required is the establishment of the value of k_m. In what follows we shall attempt only to determine k_m for the solid contact spots formed by a pair of conic frusta.

We use the same approach as that already shown in section 3.1 and assume an isothermal contact plane to be placed at distances δ_1 and δ_2 from the contact surfaces where

$$\delta_1 = \frac{k_{s2}}{k_{s1}+k_{s2}}\delta \quad \text{and} \quad \delta_2 = \frac{k_{s1}}{k_{s1}+k_{s2}}\delta$$

The heat transfer coefficients from solid 1 to the contact plane and from solid 2 to the contact plane are given by $\frac{k_m}{\delta_1}$ and $\frac{k_m}{\delta_2}$ respectively. Since the corresponding resistance for the two portions separated by the contact plane is taken as

$$R_a \frac{\delta_1}{\delta} \quad \text{and} \quad R_a \frac{\delta_2}{\delta}$$

it follows from equation (3-34) that

$$k_m = \delta \left[\frac{a_1}{4k_{s1}} \frac{(\frac{a_1}{a_o}-1)\beta_1}{(\sqrt{1+\beta_1^2}-\beta_1)} + \frac{a_2(\frac{a_2}{a_o}-1)\beta_2}{4k_{s2}(\sqrt{1+\beta_2^2}-\beta_2)} + \frac{a_1 h_1}{k_{s1} a_o} \frac{a_2 h_2}{k_{s2} a_o} \right]^{-1} \qquad (3\text{-}35)$$

As can be seen, the value k_m decreases with the increase of the ratios $\frac{a_1}{a_o}$ and $\frac{a_2}{a_o}$ and it tends to that in equation (3-2) as $\frac{a_1}{a_o}$ and $\frac{a_2}{a_o}$ approach unity.

3.3 A simplified method.

When heat flows in a solid it does so in the same manner as an electric current in a conductor. Thus a solid when uniformly conducting heat, can be imagined to constitute n number of tubes of flow and the thermal conductance per unit area of the body over a given distance is the summation of the thermal conductance of each individual tube with an equivalent thermal conductivity of $\frac{1}{n}$ that of the body. We see that the same result can be obtained if we consider that the tubes are enlarged to take up the same boundary of adiabatic condition as the body but with the conducting strength of k/n for each one. It is equally possible for the tubes to possess different strengths in conductivity so long as the total strength adds up to that of the body. For example, when heat flows axially along a solid rod of a thermal conductivity k, it can be imagined to flow along two same-sized rods, one superposed on the other, with one having a thermal conductivity of fk while the other of (1-f)k, where f is a fraction. If the same rod has a contact joint at some point along its length, the homogeneity of the material and consequently the uniformity of the flow is now interrupted. By virtue of the definition of a contact conductance which is equal to the heat flux divided by the fictitious temperature drop across the contact, the flow lines can be regarded as behaving uniformly right up to the surfaces on both sides of the joint. The temperature drop is in effect a measure of the constriction resistance of the flow as well as the resistance of the materials occupying the contact gap and it is regarded as representing solely the heat transfer characteristics of the contact. Since the contact gap is occupied by some solid junctions surrounded by a fluid, it is convenient to divide the conducting strength of the rod into two groups, one having a thermal conductivity of k_f and the other of

$(k_s - k_f)$. The one which has the same thermal conductivity as the fluid, will suffer no interruption whereas the other will have flow constriction. By such an arrangement, the problem is very much simplified as the heat transfer through the fluid and through the solid can be dealt with separately, but the interdependent nature of the two lies in the grouping of the conducting strength. The total thermal conductance of the contact is then the sum of the two parts.

Using the same contact model as in section 3.1 and considering first the heat transfer between solid 1 and the contact plane, we find, with δ_1, x, k_m defined earlier, that the resistance to the flow with the group strength k_f is $\frac{\delta_1}{\pi R^2 k_f}$ while the resistance to the flow with the group strength $(k_{s1} - k_f)$ is $\left(\frac{\delta_1}{\pi a^2(k_m - k_f)} + \frac{1 - x^2}{4a(k_{s1} - k_f)}\right)$

The first term in the square bracket represents the material resistance of the solid spot which by the assumption made in section 3.1 has an equivalent thermal conductivity of k_m instead of k_{s1}. The second term in the square bracket represents the constriction resistance in the solid 1. Since the fluid and solid resistances are in parallel, the total resistance can be found from

$$\frac{1}{R_{1s}} = \frac{1}{\frac{\delta_1}{\pi R^2 k_f}} + \frac{1}{\frac{\delta_1}{\pi a^2(k_m - k_f)} + \frac{1 - x^2}{4a(k_{s1} - k_f)}} \qquad (3\text{-}36)$$

Substituting the contact parameters K_s and K_f, we find

$$R_{1s} = \frac{1}{\pi R} \frac{1}{k_{s1}} \frac{(1 + \frac{\pi x}{4} K_s - x^2 \frac{2\pi x}{4} K_s) + (1 - x^2)\frac{\pi x}{4} K_f \left(\frac{k_m - k_{s1}}{k_{s1} - k_f}\right)}{(1 - x^2)(1 + \frac{\pi x}{4} K_s) K_f + x^2 K_s + (1 - x^2)\frac{\pi x}{4} K_f^2 \left(\frac{k_m - k_{s1}}{k_{s1} - k_f}\right)} \qquad (3\text{-}37)$$

Likewise we find the resistance between solid 2 and the contact plane to be expressed by

$$R_{2s} = \frac{1}{\pi R}\left[\frac{1}{k_{s2}}\,\frac{(1+\frac{\pi x}{4}K_s - x^2\frac{\pi x}{4}K_s)+(1-x^2)\frac{\pi x}{4}K_f(\frac{k_m-k_{s2}}{k_{s2}-k_f})}{(1-x^2)(1+\frac{\pi x}{4}K_s)K_f+x^2K_s+(1-x^2)\frac{\pi x}{4}K_f^2(\frac{k_m-k_{s2}}{k_{s2}-k_f})}\right] \qquad (3\text{-}38)$$

The combination of equations (3-37) and (3-38) gives the total resistance of the contact, i.e.

$$R_{ts} = R_{1s} + R_{2s} \qquad (3\text{-}39)$$

Hence we can obtain the total thermal conductance from the expression

$$C_{ts} = \frac{1}{R_{ts}} \qquad (3\text{-}40)$$

It must be pointed out that solutions obtained from such a simplified method would not satisfy all the boundary conditions especially at the interface unless the temperature gradient normal to the surface is uniform over the fluid contacting surface. This can be approximately achieved if we have either the value of x or the fluid contact parameter to be very small. By comparing equation (3-39) with (3-25), we see that the discrepancy of results between the two approaches lies in the term containing $(\frac{k_m-k_s}{k_s-k_f})$ in the former and that containing F(x) in the latter. The significance of the discrepancy can be observed easily if we take $k_{s1} = k_{s2} = k_s$ to simplify the expressions. Thus equation (3-39) reduces to

$$R_{ts} = \frac{\delta}{\pi R^2 k_s}\left[\frac{(1+\frac{\pi x}{4y} - x^2\frac{\pi x}{4y})}{(1-x^2)(1+\frac{\pi x}{4y})\frac{k_f}{k_s}+x^2}\right] = \frac{\delta}{\pi R^2 k_s} I_{ts} \qquad (3\text{-}41)$$

Whereas equation (3-25) reduces to

FIG. 3.10. CONTACT RESISTANCE FROM SIMPLIFIED METHOD.

$$R_t = \frac{\delta}{\pi R^2 K_s}\left[\frac{(1+\frac{\eta x}{4y}-x^2\frac{\eta x}{4y})+x^2\frac{k_f}{yk_s}F(x)}{(1-x^2)(1+\frac{\eta x}{4y})\frac{k_f}{k_s}+x^2+x^2\frac{k_f}{yk_s}F(x)}\right]=\frac{\delta}{R^2 k_s}I_t \qquad (3\text{-}42)$$

where $y = \frac{\delta}{2R}$ and I_{ts}, I_t, which are magnification factors of δ as a measure of the equivalent lengths, are self-evident. The values of I_{ts} plotted against $(\frac{k_f}{k_s})$ for various values of x is given in figure 3.10. We can now see it more clearly that the results predicted by the simplified method can be sufficiently accurate if the term $(x^2 K_f F(x))$ where $K_f = \frac{k_f}{yk_s}$. is small. The percentage of discrepancy between the two results may be calculated from

$$\eta = \frac{I_{ts}}{I_t} - 1$$

$$= \left[\frac{(1-x^2)(1+\frac{\eta x}{4y})\frac{k_f}{k_s}+x^2+x^2\frac{k_f}{yk_s}F(x)}{(1+\frac{\eta x}{4y}-x^2\frac{\eta x}{4y})+x^2\frac{k_f}{yk_s}F(x)}\right]\left[\frac{1+\frac{\eta x}{4y}-x^2\frac{\eta x}{4y}}{(1-x^2)(1+\frac{\eta x}{4y})\frac{k_f}{k_s}+x^2}\right] - 1 \qquad (3\text{-}43)$$

Since the term $x^2 K_f F(x)$ in the denominator is usually very small compared with $(1+\frac{\eta x}{4y})$ for x smaller than 0.5, its omission can only give slightly pessimistic results. Hence we drop this term and equation (3-43) reduces to

$$\eta = \frac{K_f F(x)}{1+(\frac{1-x^2}{x})(\frac{y}{x}+\frac{\eta}{4})K_f} \qquad (3\text{-}44)$$

Table (3.1) shows the value of η in percentage for various values of K_f, x and y.

TABLE 3.1 Percentage of discrepancy of the contact resistance obtained from the simplified method and the analytical method.

y	K_f	10	5	1	0.2	0.1	0.01
.005	x = .01	0.35	0.35	0.35	0.34	0.33	0.20
	.05	2.59	2.58	2.47	2.03	1.66	0.39
	.1	5.61	5.51	5.02	3.50	2.55	0.43
	.2	10.9	10.6	8.90	4.85	3.14	0.42
	.3	11.7	11.3	8.85	4.24	2.57	0.32
	.4	6.78	6.41	4.50	1.81	1.03	0.12
.01	x = .01	0.26	0.25	0.25	0.25	0.24	0.17
	.05	2.33	2.31	2.23	1.86	1.55	0.38
	.1	5.25	5.18	4.77	3.38	2.48	0.43
	.2	10.6	10.35	8.70	4.82	3.10	0.41
	.3	11.4	11.1	8.70	4.20	2.55	0.31
	.4	6.67	6.32	4.44	1.79	1.03	0.10
.1	x = .01	0.04	0.04	0.04	0.04	0.04	0.04
	.05	0.82	0.82	0.81	0.76	0.70	0.29
	.1	2.60	2.60	2.48	2.05	1.68	0.39
	.2	6.95	6.85	6.07	3.90	2.69	0.41
	.3	8.47	8.25	6.85	3.72	2.36	0.31
	.4	5.28	5.06	3.78	1.67	1.00	0.12

The values in the table show that for $x < 0.5$ the simplified method always gives a higher estimate in the value of the contact resistance. It can be seen that the discrepancy is extremely small for $K_f < 0.01$ independent

of the values of x and for $x < 0.01$ independent of the values of K_f. Table 3.2 shows the thermal conductivity values of some commonly used metals and gases.

Table 3.2 Thermal conductivity of some commonly used metals and gases at about 100°C [16,17].

Metal	k_s(cal cm^{-1} sec^{-1} $^oC^{-1}$)	Gas	k_f(cal cm^{-1} sec^{-1} $^oC^{-1}$)
Copper	0.97	Hydrogen	0.00050
Aluminium	0.53	Helium	0.00041
Duralumin	0.41	Nitrogen	0.000078
Titanium	0.050	Oxygen	0.000077
Stainless steel	0.068	Carbon dioxide	0.000054
Magnox	0.30	Ammonia	0.000077
Cast iron	0.13	Steam	0.000059
Steel	0.13 - 0.08	Argon	0.000052
20 Ni Steel	0.045	Air	0.000074
Uranium	0.07		

From Table 3.2, we find that the maximum k_f to k_s ratio is about 0.01 whereas the minimum ratio is about 0.00005. The average value may be represented by k(air) to k(steel) ratio which is about 0.0008. Therefore, even with the fluid gap to cylinder radius ratio of y = 0.01, the fluid contact parameter K_f is only about 0.08. The maximum discrepancy will be about 3%. Normally we expect the value of x to be less than 0.1. Hence any discrepancy is quite negligibly small.

3.4 Discussion of various theories

Among the thermal contact theories in the literature, those presented by Cetinkale and Fishenden[18] and Fenech and Rohsenow[13] can be considered as most thorough. They carried out their analyses on the general manner in which the dependence of the thermal contact conductance on both the fluid and the solid spots at the interface was investigated and their results show clearly the inter-dependence of the two. It is true that the amount of heat flows through each path not only governed by the resistance of that path but also by the resistance in other paths. Most other workers formulated their theories rather on how the contact areas should be determined and incorporated in the part which represents the thermal conductance through the solid spots. Often the fluid and solid conductances were treated separately and the inter-dependent nature of the two was therefore omitted. The determination of the distribution and the size of the contact areas, however, has not been very successful owing to the difficulties in relating them with the applied pressure and the surface roughness index as described earlier. The exceptional cases are those where contact surfaces were specifically prepared to give a uniform distribution of contact spots during contact. Laming's work[19] is one good example. In this case it is possible to assume the contact spots to be of equal size and the condition of heat transfer around one contact spot is the same for all spots. If contacts are made under arbitrary conditions, no accurate predictions so far are available. A recent paper by Greenwood and Williamson[20] on contact areas of flat surfaces may suggest one line of approach to this important problem. Since no attempt has been carried out in the present work to determine the actual contact areas under random conditions, our comments will be made only on the theories presented in

references (18) and (13).

3.4.1 Cetinkale-Fishenden theory

Cetinkale and Fishenden's work is one of the first thorough analyses on a thermal contact problem in which they considered the simultaneous existence of both of solid and fluid conductances. They derived their contact resistance equation by first considering the solid and fluid resistance separately. To do this they assumed a flow dividing surface on one side of which heat was considered to flow across the circular solid spot while on the other side across an uniform fluid layer. The fluid resistance, which was determined by a relaxation method, is given by

$$R_f = \frac{\delta}{\pi R^2 k_f} \tag{3-45}$$

The solid resistance was calculated by considering isothermal surfaces in the form of ellipses and it is given by

$$R_s = \frac{\tan^{-1}(\frac{w}{a})}{\pi\, a\, k_s} \tag{3-46}$$

Where w is a parameter, a/the vertical semi-axis of an ellipse. They deduced then on the basis of the relaxation method results the value of w to be equal to $(r_d - a)$ where r_d is the radius of the flow dividing surface measured from the longitudinal axis of the contact cylinder. Putting r_d to be equal to $R\sqrt{1-\frac{c_f}{c_t}}$, the total contact conductance is given by

$$C_t = C_f + C_s = \frac{1}{R_f} + \frac{1}{R_s} = \frac{\pi R^2 k_f}{\delta} + \frac{\pi\, a\, k_s}{\tan^{-1}\left(\frac{R}{a}\sqrt{1-\frac{\pi R^2 k_f}{\delta C_t}} - 1\right)} \tag{3-47}$$

Use $B = \frac{C_t \delta}{R^2 k_f}$, $x = \frac{a}{R}$ and $K_f = \frac{2R k_f}{\delta k_s}$ so that equation (3-47) can be written as

$$B = 1 + \frac{\frac{2x}{K_f}}{\tan^{-1}\left(\frac{1}{x}\sqrt{1-\frac{1}{B}}-1\right)} \qquad (3\text{-}48)$$

It can be realised that in fact

$$B = \frac{R^2}{R^2 - r_d^2} \qquad (3\text{-}49)$$

which is always great than unity. We can now examine the results more closely.

As $k_f = 0$, no heat is transferred across the fluid gap and the contact resistance as given by equation (3-46) if we neglect the material resistance of the solid spots. As $k_f = k_s$ we expect the contact conductance (hence B) to be a constant, independent of x. This is achieved approximately well when δ is small compared with R as in this case the second term in equation (3-48) is of little importance. However, when B is a constant, we expect r_d (equation 3-49) to be of a specific value so that by the definition of of the flow dividing surface r_d/R should be equal to x. But this is clearly not satisfied. On the other hand, if the value of the ratio r_d/R is made to approach that of x (i.e. $B \to \frac{1}{1-x^2}$) we find that K_f will approach a value corresponding to $\frac{2}{\pi}\left(\frac{1}{x} - x\right)$. This can be achieved only by giving δ a definite value so that $\delta/R = \pi/\left(\frac{1}{x} - x\right)$ (since k_f is taken to be equal to k_s). If this must be so, it would contradict the fact that δ is an independent parameter of a contact joint. The association of δ with x (by no means in a definite relationship) will come into existence in the contact conductance equation when the material resistance of the contact spots is taken into account. We see, therefore, if the material resistance of the solid spots is included, we find that we can obtain results to satisfy all cases. Thus

we modify equation (3-47) to take the form

$$C_t = \frac{1}{\frac{\delta}{\pi(R^2-a^2)k_f} + \frac{1}{\tan^{-1}\left(\frac{R}{a}\sqrt{1-\frac{\pi(R^2-a^2)k_f}{\delta C_t}}-1\right) + \frac{\delta}{\pi a^2 k_s}}} \qquad (3\text{-}50)$$

Using $B = \frac{C_t \delta}{\pi(R^2-a^2)k_f} = \frac{R^2}{R^2-r_d^2}$, $K_f = \frac{2Rk_f}{\delta k_s}$, $x = \frac{a}{R}$ and $y = \frac{\delta}{2R}$, equation (3-50) reduces to

$$B = 1 + \frac{\frac{2x}{(1-x^2)K_f}}{\tan^{-1}\left(\frac{1}{x}\sqrt{1-\frac{1}{B}}-1\right) + \frac{2y}{x}} \qquad (3\text{-}51)$$

When $k_f = 0$, the contact conductance is now given by

$$C_t = \frac{\pi a k_s}{\tan^{-1}\left(\frac{1}{x}-1\right) + \frac{2y}{x}} \qquad (3\text{-}52)$$

When $k_f = k_s$, we find $r_d = a$, $B = \frac{1}{1-x^2}$ and $K_f = \frac{1}{y}$ as was expected. Further, when $x = 0$, we find $C_t = \frac{\pi R^2 k_f}{\delta}$, and when $x = 1$, $C_t = \frac{\pi R^2 k_s}{\delta}$. These satisfy the expected conclusions.

The modification of Cetinkale and Fishenden's result has not in any way contradicted their analysis but can be considered to be consistent with the simplified method given in section 3.3. It becomes clear that the inclusion of the resistance of the solid spots is essential in estimating the amount of heat to be transmitted through the solid junctions. Its importance, however, is less obvious when either k_f is very much smaller

than k_s or when a is very much smaller than R, because under these conditions the resistance of the solid spots is small compared with the flow constriction resistance.

3.4.2 Fenech-Rohsenow theory

The authors carried out a comprehensive analysis in which they treated the thermal contact problem mathematically as a whole. They used the same contact model as Cetinkale and Fishenden and divided each solid contact member into four regions one of which was occupied by a common fluid layer. They then introduced a temperature distribution for each solid region and obtained the constants of the equations according to the boundary conditions. The contact conductance of their results is given by

$$C_t = \pi R^2 \frac{\frac{k_f}{h_1+h_2}\left[(1-x^2)\left(\frac{2.4\frac{h_1}{a}+1}{k_{s1}} + \frac{2.4\frac{h_2}{a}+1}{k_{s2}}\right) + 1.1x\,f(x)\left(\frac{1}{k_{s1}}+\frac{1}{k_{s2}}\right)\right] + 2.4\,\frac{x}{R}}{(1-x^2)\left[1-\frac{k_f}{h_1+h_2}\left(\frac{h_1}{k_{s1}}+\frac{h_2}{k_{s2}}\right)\right]\left[\frac{2.4\frac{h_1}{a}+1}{k_{s1}} + \frac{2.4\frac{h_2}{a}+1}{k_{s2}}\right]}$$

(3-53)

By taking $k_{s1} = k_{s2} = k_s$, $\frac{\delta}{2} = h_1 = h_2$ and $y = \frac{\delta}{2R}$, equation (3-53) reduces to

$$C_t = \frac{\pi R^2 k_f}{\delta\left(1-\frac{k_f}{k_s}\right)}\left(1 + \frac{1.1\,x\,f(x)}{(1-x^2)(2.4\frac{y}{x}+1)}\right) + \frac{1.2\,\pi\,a\,k_s}{(1-x^2)(1-\frac{k_f}{k_s})(2.4\,\frac{y}{x}+1)}$$

(3-54)

where f(x) is a function of x. We can now consider the results for all the particular cases. When either $x = 1$ or $k_s = k_f$ we obtain from equation

(3-54) an infinite conductance which indicates that no resistance of the materials occupying the interface has been included. When $k_f = 0$, equation (3-54) reduces to

$$C_t = \frac{1.2\,\pi a\, k_s}{(1-x^2)(2.4\,\frac{y}{x}+1)} \qquad (3\text{-}55)$$

In the case where both the fluid resistance and the solid spot material resistance are absent, the contact conductance is the reciprocal of the flow constriction resistance of the main body, and the fluid gap distance (i.e. y) has no effective influence on its value. Since the total heat flux must pass through the solid contact spot as the sole heat path, we reason that the flow lines can only be affected by the size of the contact spot (i.e. x) and not by its depth. The existence of y in a flow constriction resistance equation does not fit into this case. We can see it more clearly when we set x to be a very small value, as we expect C_t in equation (3-55) to tend to a limiting value of $2a\,k_s$ as given in classical text books mentioned earlier. For C_t to approach this value, it is necessary for y to be related to x in a definite manner (i.e. in this case it is necessary for $y = 0.368\,x$). But y is an independent parameter of a contact and its position here is in question. We can also examine another case the result of which is known. For example, for the fluid conductance to be equal to the solid conductance when $k_f = k_s$, we expect $x = \frac{1}{\sqrt{2}}$. From equation (3-54) we find

$$\frac{C_f}{C_s} = \frac{k_f}{k_s}\left[\frac{(1-x^2)\,(2.4\,\frac{y}{x}+1)+1.1\,x\,f(x)}{2.4\,x\,y}\right] \qquad (3\text{-}56)$$

For the above condition to be satisfied, the value in the square bracket must be equal to unity. But then x becomes a function of y and this is undesirable for the reason stated earlier. Taking for the moment $y = 0.368\ x$ and the value of f(x) from reference (13), we obtain $x = 0.925$ instead of $1/\sqrt{2}$. The reason for these disagreements could well be in the choice of the boundary conditions in the analysis. Since it is not the purpose of the writer to cast any doubt on a piece of outstanding work by these two authors, it suffices to say that the omission of the resistance due to the materials occupying the interface must give rise to some influential effect on the final results. This effect is less marked when the fluid gap distance is of the same order of magnitude as the radius of the contact area. Speaking in a general sense, we realise that the amounts of heat transferred through the fluid and the solid junctions must essentially be governed by the overall resistance existing along each path across the interface, and the resistance of the materials, however small it may be compared with the constriction resistance can not be categorically ignored except in the case where there is only one single path for heat transfer.

3.4.3 Present theories

The contact conductance for the idealised contact model is given by equation (3-26). To examine its validity for those cases of known results, let us take $k_{s1} = k_{s2} = k_s$. Thus the equation reduces to

$$C_t = \frac{\pi R^2 k_s}{\delta}\left[\frac{(1-x^2)(1+\frac{\eta x}{4y}\frac{k_f}{k_s}) + x^2 + x^2 K_f F(x)}{(1+\frac{\eta x}{4y} - x^2\frac{\eta x}{4y}) + x^2 K_f F(x)}\right] \qquad (3\text{-}57)$$

For $k_f = 0$, the total contact conductance is the result of the constriction resistance plus the solid spot resistance connected in series and it is represented by

$$C_t = \frac{\pi R^2 k_s}{\delta} \left[\frac{x^2}{1 + \frac{\pi x}{4y} - x^2 \frac{\pi x}{4y}} \right] \qquad (3\text{-}58)$$

According to equation (3-58), when $x = 0$ we obtain $C_t = 0$ and when $x = 1$, we obtain $C_t = \frac{\pi R^2 k_s}{\delta}$.

If we now set $k_f = k_s$, we obtain again $C_t = \frac{\pi R^2 k_s}{\delta}$ which is independent of x but is inversely proportional to the fluid gap distance. For the solid conductance to be equal to the fluid conductance we can use the x, K_s and K_f relations which are plotted in figure 3.6 according to equation (3-30). As can be seen, when $k_f = k_s$, we obtain the expected value $x = \frac{1}{\sqrt{2}}$.

The contact conductance for a more realistic contact model presented in section 3.2 will follow the same trend as that presented in section 3.1 if examined under different particular conditions provided that the assumption for no heat transfer between the solid spots and the fluid is valid. This could be acceptable if the taper ratio of the conic frustum is small. However, when the taper ratio is high as in the case of very smooth surfaces in contact, heat transfer will certainly take place between the solid junctions and the fluid. In this case the resistance of the solid path will be reduced, as a portion of heat can by pass the tips of the conic frusta and re-enter the solid junction from the fluid region. Unfortunately the boundary conditions at the solid-fluid interface would be rather complex for any mathematical solutions to be obtained.

Under such circumstances the simplified method presented in section 3.3 may give a reasonable approximation, since in this method the amount of heat transferred along the part with a conducting strength designated by k_f would cover, if not exactly, some of the heat transferred between the solid junctions and the fluid whenever the solid faces incline at an angle to the longitudinal axis. The simplified method, though lacking in any exact mathematical justification for a general case, has the advantage of its simple formulation for a practical problem. In this way even if a contact model be as complex as the one suggested by Archard[21] the simplified method can still be applied. An examination of all particular cases will show that the results are satisfied.

CHAPTER IV

EXPERIMENTAL STUDY

In chapter 2 we discussed the number of uncontrollable factors which render the thermal contact a very complex problem. One of the difficulties lies in estimating quantities such as the actual areas of contact and the actual fluid gap distance. If the surfaces are pre-arranged to have a definite roughness pattern, either by a machining process or by ruling with a cutter, the number of contact spots and the size of the contact areas become more assessable, but it is still necessary to assume the surfaces to be initially flat and having no out of form during matching. For the purpose of studying the fundamental phenomena of heat transfer across the contact, it is desirable to have a greater degree of certainty regarding the number and size of these contact spots under a given loading condition. For this reason, it is better to avoid the use of a roughness index and if at all possible the complicated situation aggravated by the presence of the surfaces film. We propose to create a favourable contact condition by the introduction of artificial metallic junctions between the contact members distributing in a definite pattern so that when the contact members are pressed against them, a reasonable estimate of their bearing areas can be obtained. Two different types of junctions have been used in the present experiment. They are described in the following sections.

4.1 Insertion of steel balls

Small steel balls in large numbers, when inserted between two highly finished flat surfaces, will have a more or less uniform distribution of contact spots over the surfaces. When they are closely packed the pattern

is hexagonal. Since the dimension of the surface roughness is very small compared with the size of the balls we expect the size of the spots to be solely determined by considering the contact area between a sphere and a flat surface under a given applied load. Also since the deviation from perfect flatness of a highly prepared surface and the deviation from true spherity and diameter of carefully finished steel balls are very small compared with the size of the contact surfaces and the balls, we expect, therefore, the contact spots to be of equal size when the load is applied uniformly over the contact surfaces. The pressure over these contact areas is most likely to be very high even under a moderately low load condition to ensure the break down of any surface film. The presence of the balls acting as metallic contact junctions will cause no constraint to any thermal expansion, as would the surface irregularities for they are integral parts of a surface. Under these circumstances, the phenomena of heat transfer from one cylindrical specimen to another across the inserted balls can be represented by the contact model containing only one ball as shown in figure 4.1.

The radius of the specimen block used is 2.54 cm. Let n be the number of balls. Thus the radius of the model cylinder is

$$R = \frac{2.54}{\sqrt{n}} \text{ cm.}$$

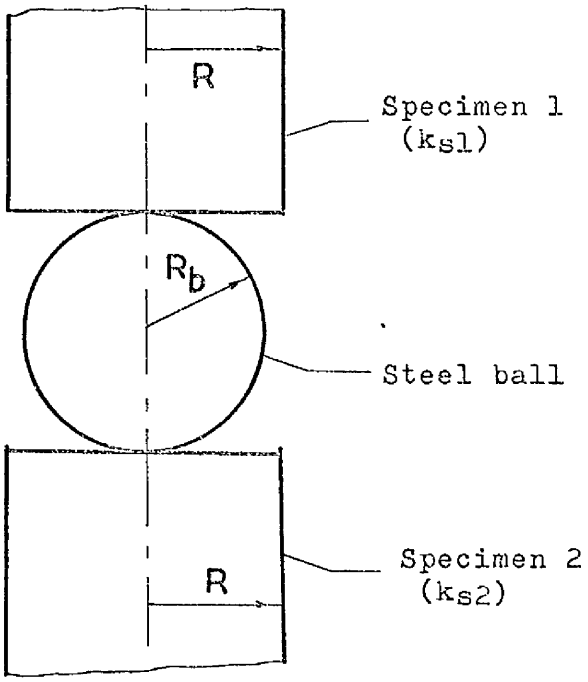

Fig. 4.1 Contact model with the insertion of a steel ball.

From the analysis given in APPENDIX C we obtain the constriction resistance of the steel ball when it is in contact with plane surfaces.

$$R_{cb} = \frac{1}{2k_b}\left(\frac{1}{a} - \frac{1}{R_b}\right) \qquad (4\text{-}1)$$

where a is the radius of the contact area which will be determined in section 4.3.

The material resistance of ball is determined in APPENDIX D and it is

$$R_{mb} = \frac{1}{k_b \pi R_b} \log\left(\frac{1 + \sqrt{1-\left(\frac{a}{R_b}\right)^2}}{1 - \sqrt{1-\left(\frac{a}{R_b}\right)^2}}\right) \qquad (4\text{-}2)$$

A comparison of the material resistance with the constriction resistance can be made by dividing the result of equation (4-2) by that of (4-1). Thus

$$\frac{\text{material resistance}}{\text{constriction resistance}} = \frac{2 \log\left(\frac{1+\sqrt{1+(a/R_b)^2}}{1-\sqrt{1-(a/R_b)^2}}\right)}{\pi\,(R_b/a - 1)} \qquad (4\text{-}3)$$

Table 4.1 shows the value of the ratio for various a/R_b.

TABLE 4.1 material resistance to constriction resistance ratio of a sphere

$\frac{a}{R_b}$	0.01	0.02	0.05	0.1	0.2	0.3	0.4	0.5
$\frac{\text{material resistance}}{\text{constriction resistance}}$	0.068	0.128	0.248	0.424	0.732	1.02	1.312	1.662

It can be seen that as the actual area of contact is small compared with the size of the ball, resistance is largely attributed to the constriction of heat flow.

Now the total ball resistance can be obtained from equations (4-1) and (4-2), i.e.

$$R_{tb} = \frac{1}{R_b k_b}\left[\frac{1}{2}\left(\frac{R_b}{a}-1\right) + \frac{1}{\pi}\log\left(\frac{1+\sqrt{1-(a/R_b)^2}}{1-\sqrt{1-(a/R_b)^2}}\right)\right] \qquad (4\text{-}4)$$

According to section 3.1 the heat transfer coefficients of the solid spots are k_m/δ_1 and k_m/δ_2. The equivalent thermal conductivity k_m referred to the contact area can now be determined. This is derived as

$$k_m = \frac{\delta R_b k_b}{\pi a^2}\left[\frac{1}{2}\left(\frac{R_b}{a}-1\right) + \frac{1}{\pi}\log\left(\frac{1+\sqrt{1-(a/R_b)^2}}{1-\sqrt{1-(a/R_b)^2}}\right)\right]^{-1} \qquad (4\text{-}5)$$

where δ is the fluid gap distance and is approximately equal to (see APPENDIX E)

$$\delta = 2R_b\sqrt{1-(a/R_b)^2} \qquad (4\text{-}6)$$

Using $N = \frac{a}{R_b}$ and substituting equation (4-6) into equation (4-5) we find

$$k_m = \frac{2\sqrt{1-N^2}}{\pi N^2} k_b\left[\frac{1}{2}\left(\frac{1}{N}-1\right) + \frac{1}{\pi}\log\left(\frac{1+\sqrt{1-N^2}}{1-\sqrt{1-N^2}}\right)\right]^{-1} \qquad (4\text{-}7)$$

The total thermal conductance of the contact can now be found according to the formulae laid down in Section 3.1. Since, however, the assumption of no heat transfer between the solid spots and the fluid may not be entirely acceptable in this case where the fluid gap is comparatively large, we consider that the simplified method could give a better approximation for the reason explained earlier, especially where, in this case, the fluid contact parameter K_f is small. Thus according to this method we obtain the total thermal conductance of the contact from

$$C_t = \frac{1}{\frac{\delta}{\pi R^2 k_f} + \frac{1}{R_b(k_b-k_f)}\left[\frac{1}{2}\left(\frac{1}{N}-1\right)+\frac{1}{\pi}\log\left(\frac{1+\sqrt{1-N^2}}{1-\sqrt{1-N^2}}\right)\right]+\frac{1-x^2}{2a(k_s-k_f)}} \qquad (4\text{-}8)$$

where k_f is obtained either from equation (2-29) or equation (2-30) depending on whether the condition is a normal pressure or a free molecular condition respectively, and k_s is the thermal conductivity of cylindrical specimen blocks. δ is obtained from equation (4-6), if the solid junctions are cylindrical otherwise δ should be replaced by an effective fluid gap distance δ_e. This will be discussed in Chapter 7.

4.2 Insertion of aluminium discs

With the insertion of small aluminium discs between the flat surfaces of two cylindrical blocks to form the metallic contact junctions we will have the idealised contact model as described in section 3.1. The aluminium disc material has a very low hardness value and a high thermal conductivity value. When a soft material is compressed between two surfaces of a much harder material, a large area of contact can be expected even though there may be irregularities over the surfaces. Furthermore when the applied load is sufficiently high but not too high to cause spreading of the soft material, a full area of contact can be established corresponding to the size of the discs. When this condition is reached the areas of contact become independent of the applied load and needless to say independent of the surface roughness index. We choose a small thickness for the disc so that the solid contact parameter K_s becomes large, but not too small to involve a large percentage of contact error due to any deviation in thickness. Thus such a contact model will enable us to study the contact problem in the range outside the previous case with the insertion of steel balls. The essential factor in

this investigation lies in the accurate production of the discs which will be reported in section 4.3. For the calculation of the thermal conductance of the contact, we can use the formulae laid down in both section 3.1 and section 3.3. In both cases, $k_m = k_a$ (the thermal conductivity of the aluminium disc.) Thus equation (3-26) becomes

$$C_t = \frac{\pi R k_s}{2}\left[\frac{(1-x^2)(1+\frac{\pi x}{4}K_s)K_f + x^2K_s(1+K_f F(x))}{(1+\frac{\pi x}{4}K_s - x^2\frac{\pi x}{4}K_s) + x^2 K_f F(x)}\right] \qquad (4\text{-}9)$$

and equation (3-40) becomes

$$C_t = \frac{\pi R k_s}{2}\left[\frac{(1-x^2)(1+\frac{\pi x}{4}K_s)K_f + x^2 K_s + (1-x^2)\frac{\pi x}{4}K_f{}^2(\frac{k_a-k_s}{k_s-k_f})}{(1+\frac{\pi x}{4}K_s - x^2\frac{\pi x}{4}K_s) + (1-x^2)\frac{\pi x}{4}K_f(\frac{k_a-k_s}{k_s-k_f})}\right] \qquad (4\text{-}10)$$

where $K_s = \frac{k_a}{yk_s}$ and $K_f = \frac{k_f}{yk_s}$, and y is the half thickness of the disc divided by the radius of the contact model cylinder $R = \frac{2.54}{\sqrt{n}}$. n is the number of discs inserted. We obtain k_f either from equation (2-29) or equation (2-30) according to the gas pressure condition.

4.3 Supplementary experiments.

4.3.1 Area of contact between a steel ball and a flat metal surface

This experiment was carried out to determine the diameter of the area of contact between a steel ball and the flat surface of the material used as the specimen, over a load range covering also the region between the onset of plasticity and full plasticity. The Hounsfield Tensometer test machine was first used but it did not give the accuracy required. A testing

device was therefore designed which is shown in figure 4.2.

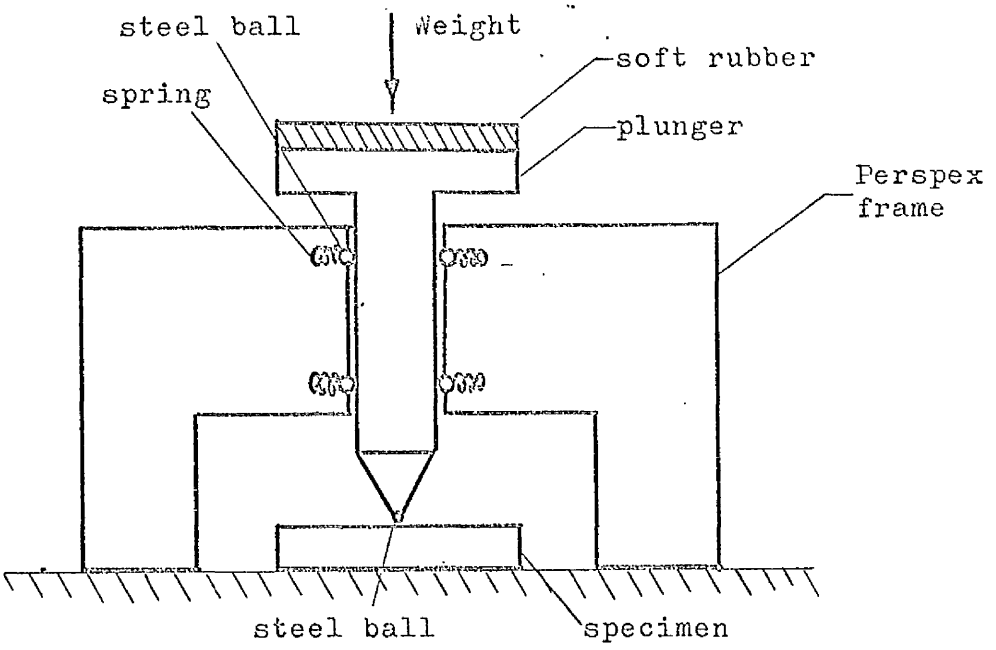

Fig. 4.2 Indentation testing device.

The steel balls fixed at the tip of the plunger, one at a time, were of diameters 0.792 mm and 1.585 mm which are the two sizes used in the contact model. The specimens are En 8 steel and Armco Iron. The load was applied by carefully placing a weight on top of the plunger for 30 seconds and the diameter was measured afterwards by means of an optical microscope. Several runs for each load were made separately and the results are plotted in figures 4.3 - 4.6. As can be seen, for full plasticity the load-diameter slope has a value of about 2 which is expected. Between the onset of plasticity and full plasticity the results follow a smooth curve having a slope of about 2.6. No accurate measurements of the indentation could be obtained when the applied load was below 0.2 kg, because at such low load levels, deformation is mainly elastic and there revealed no clear boundary line of the indentation. Elastic recovery of the metal on removal of the applied load has prevented proper observations on the exact size of the indentation.

INDENTATION OF EN 8 STEEL.

BALL DIAMETER. 0·792 mm.

x — MEAN VALUE OF 4 RUNS.

FIG. 4·3

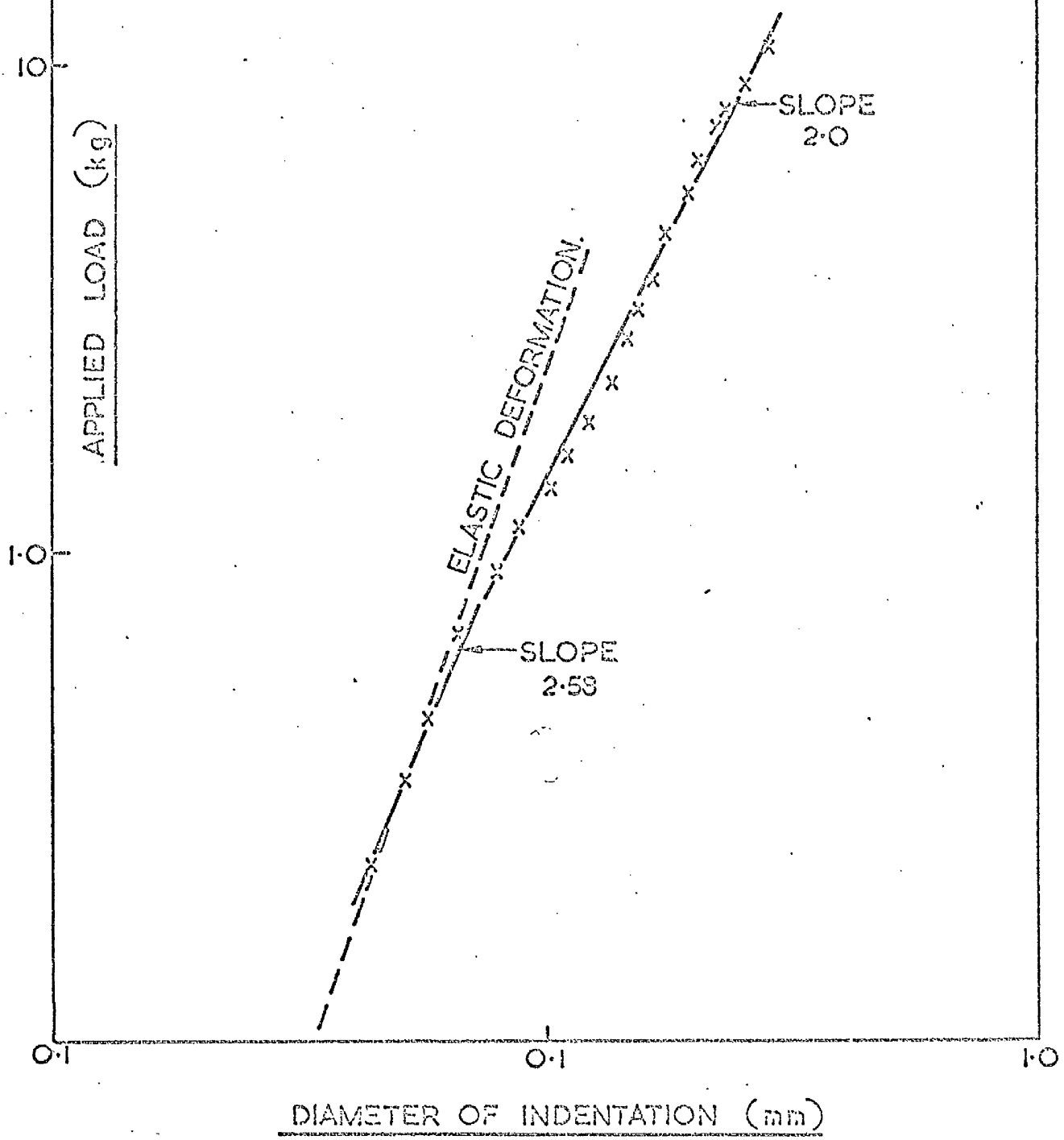

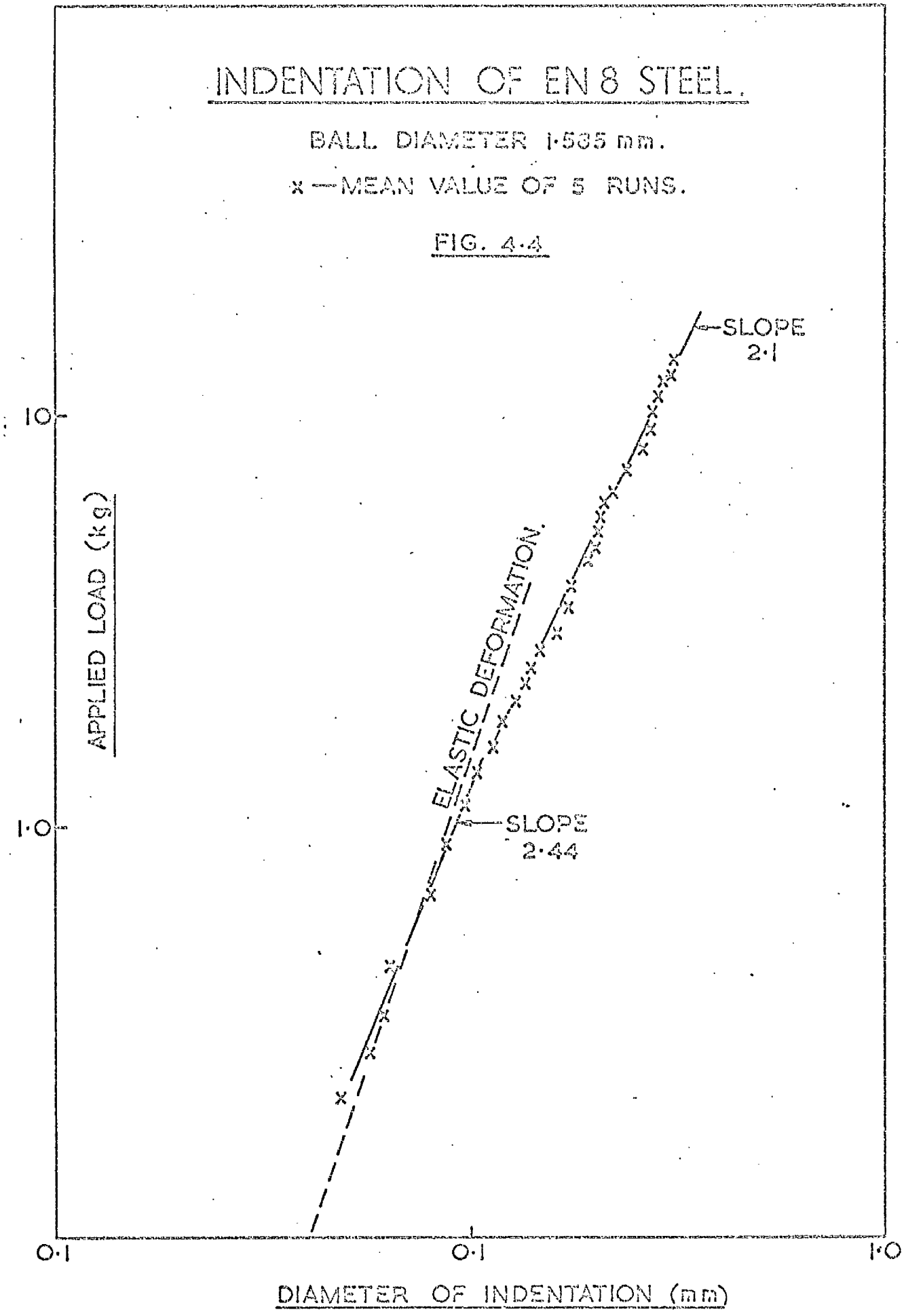
INDENTATION OF EN 8 STEEL.
BALL DIAMETER 1·535 mm.
x — MEAN VALUE OF 5 RUNS.
FIG. 4·4
SLOPE 2·1
SLOPE 2·44
ELASTIC DEFORMATION.
APPLIED LOAD (kg)
10
1·0
0·1
0·1
1·0
DIAMETER OF INDENTATION (mm)

INDENTATION OF ARMCO IRON.

BALL DIAMETER 0·792 mm.

x — MEAN VALUE OF 2 RUNS.

FIG. 4·5

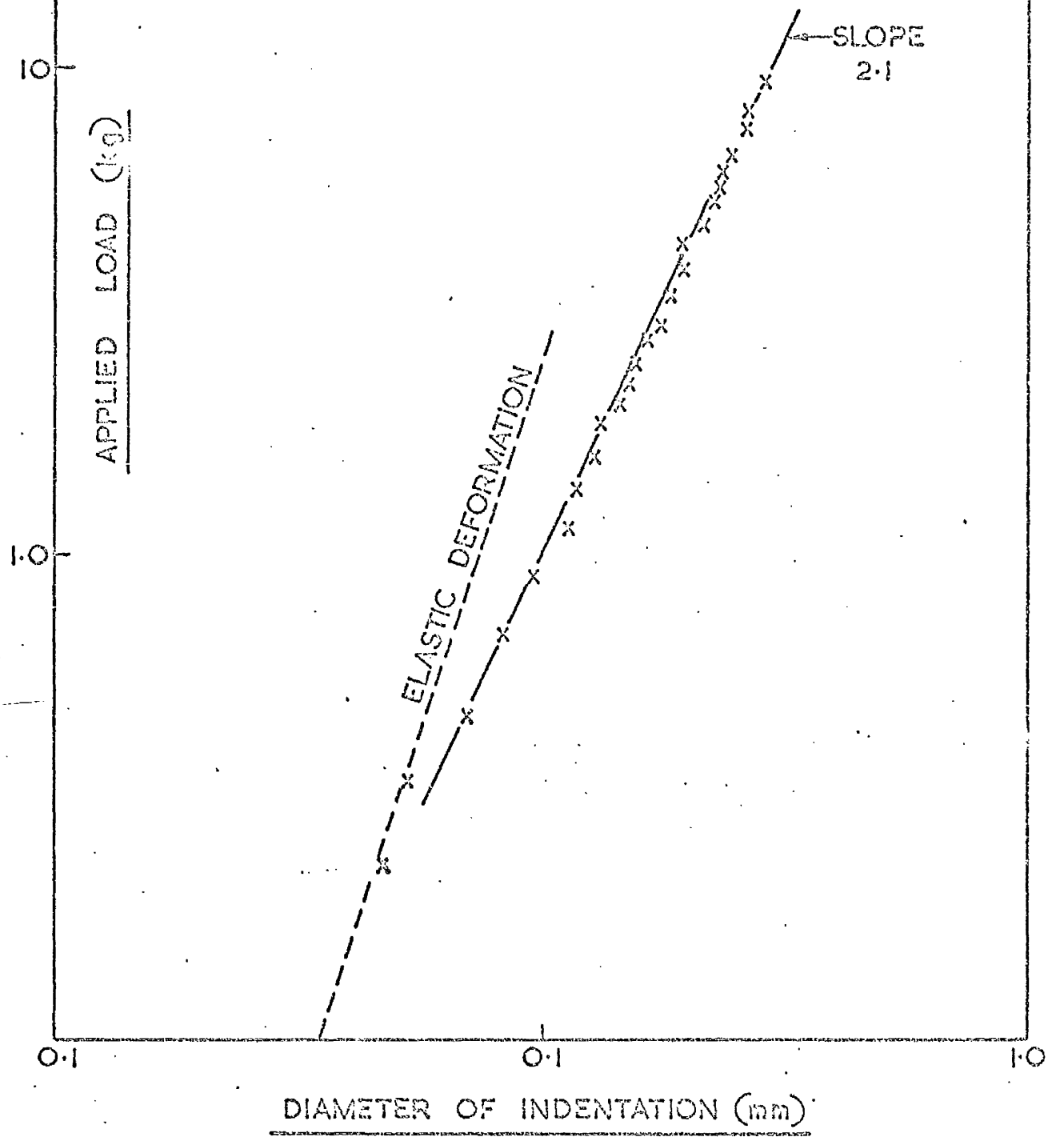

INDENTATION OF ARMCO IRON.

BALL DIAMETER 1·585 mm.
x—MEAN VALUE OF 2 RUNS.

FIG. 4·6

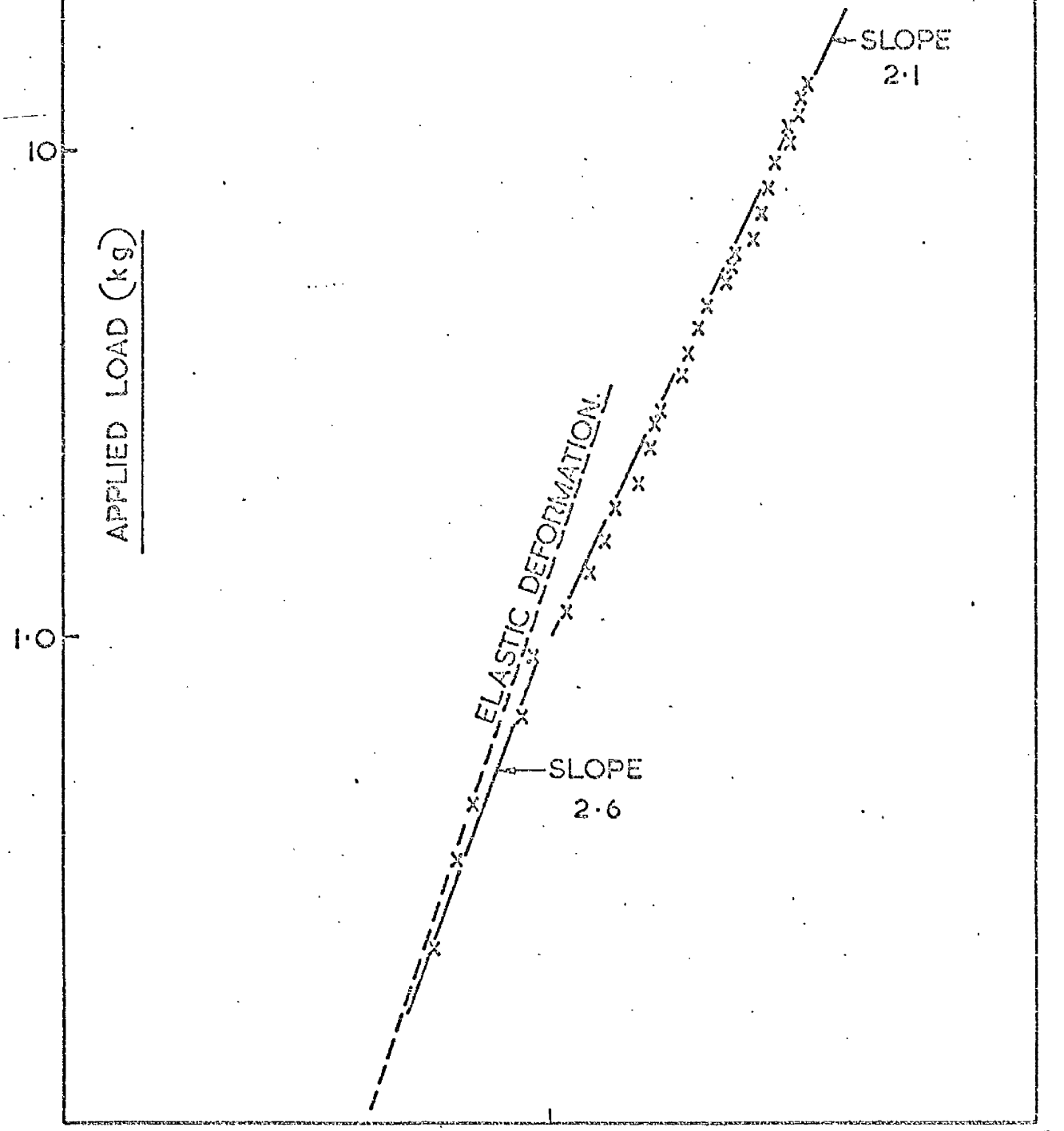

According to Dr. Tabor of Cambridge University in a private communication, accurate measurements of any elastic indentation of such a small size can be made only with special care and by first etching the ball surface.

The results given in figures 4.3 - 4.6 will provide the information regarding the size of the contact area under a given pressure. This will be used for the main experiments.

4.3.2 Hardness testing at elevated temperature

The indentation measurements described in the previous section was carried out at room temperature. The results compare fairly well with that obtained from equation (2-14) for full plasticity. At elevated temperatures, however, we expect the hardness value to decrease owing to atomic diffusion resulting in an increase of contact area under the same contact pressure. In order to investigate the effect of temperature on the hardness of both the En 8 and Armco Iron specimen , a testing device was designed to incorporate into the working capacity of a Hounsfield Tensometer. The detail of the design and its performance are described in reference (24). The results of both materials are given in figures 4.7 and 4.8. Contrary to expectation, the hardness, after a steady decrease, increases to a value higher than that measured at room temperature around the temperature range between 175°C to 275°C. This was found to be due to ageing. We see therefore that the hardness of a metal depends both on temperature and time. Even though a working temperature may not be the ageing temperature the hardness of metal will change constantly with time usually in a decreasing manner. Such a phenomenon may be considered as creep in contact. We did not carry out further investigation to find out the effects of both working history and temperature on the hardness value; we realise, however, that

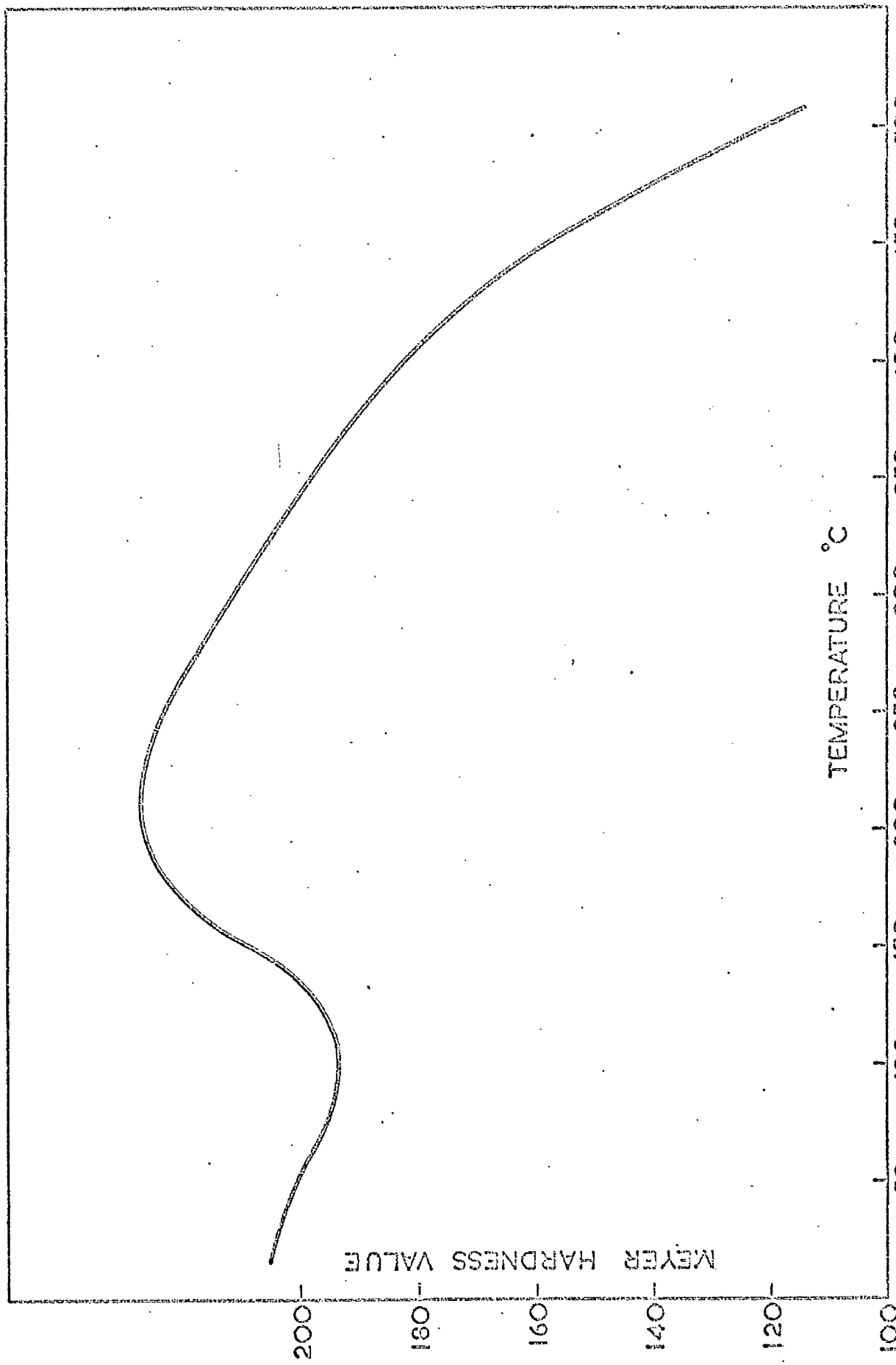

HARDNESS OF NORMALISED EN 8 STEEL AT ELEVATED TEMPERATURE.

FIG. 4.7

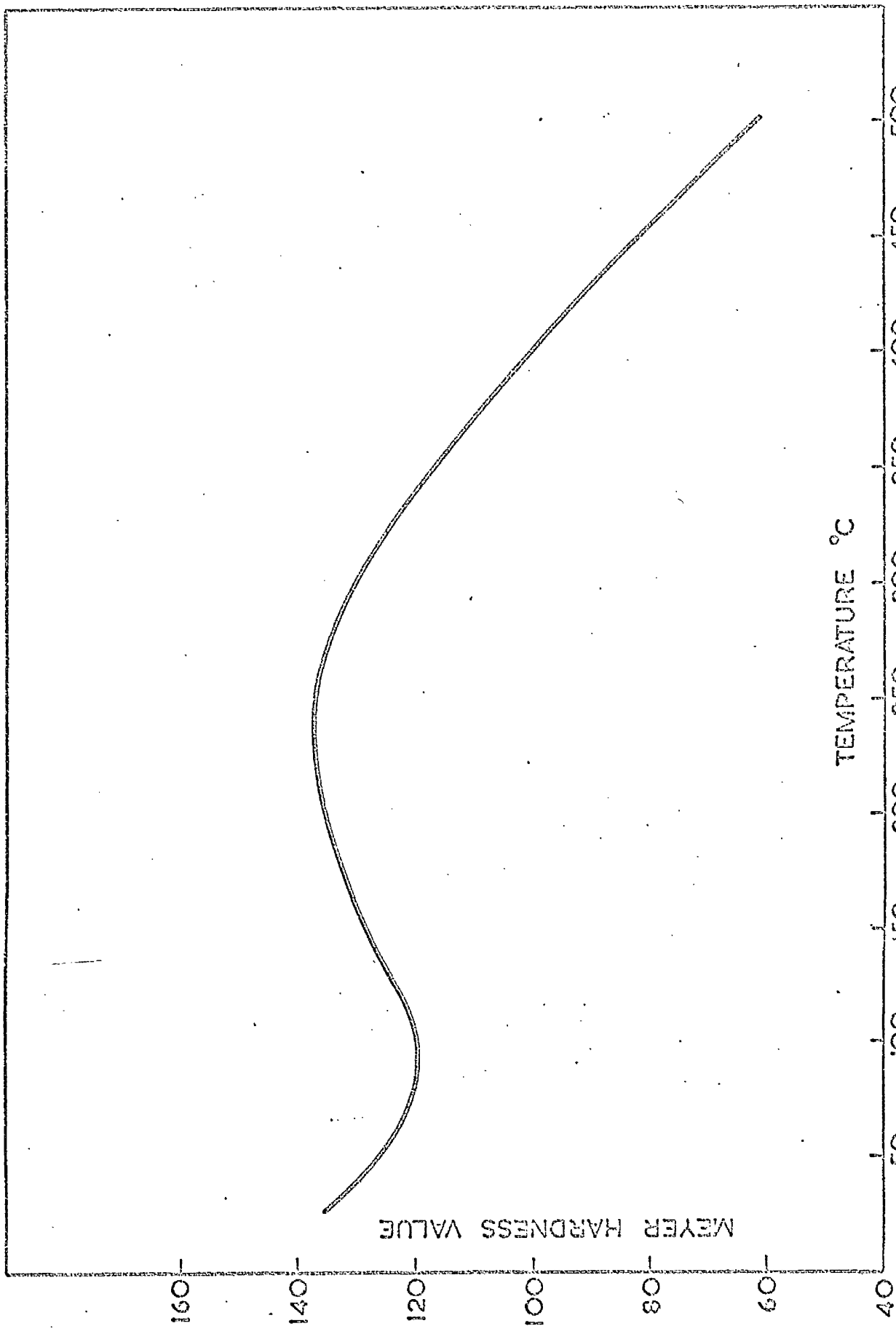

HARDNESS OF ARMCO IRON AT ELEVATED TEMPERATURE.

FIG. 4.8

the contact areas derived from our test results are quite likely to be smaller than what would actually occur during our main experiments each of which usually took several months to complete.

4.3.3 Vacuum seal

There are a number of methods available for bringing thermocouple wires or power leads through a vacuum chamber, and the most common one is the use of the glass-metal seals. In this method the wires are soldered to the metal terminals of the seal on either side of the chamber. For accurate temperature measurements, however, it is desirable that the continuity of the thermocouple wires should be preserved and if not the terminals should be kept in a uniform temperature field. The number of thermocouple wires in the present investigation is rather large. The following method was therefore developed. During the first attempt, the thermocouple wires were threaded through two Tufno discs, between which some synthetic rubber (supplied by Midland Silicone Rubber Co.) was casted and allowed to set. Pressure was then applied on the entire sandwiched block against an 'O' ring placed in the groove of the flange of the vacuum chamber port. Owing to the difficulty of getting rid of air bubbles from the synthetic rubber, this method proved to be unsuccessful. The synthetic rubber was then replaced by a piece of soft natural rubber and satisfactory results were obtained. This method worked very well until the number of the wires became too large, in which case some of the wires would occupy the region near the edge of the rubber disc and cause leakage. The reason for the leakage is believed to be due to the displacement of the rubber under compression which jeopardizes the uniform pressure required for the purpose of sealing the rubber to the wire. A metal ring with a slight taper along the inner surface was placed around the rubber disc as shown in figure 4.9,

to prevent the spreading of the rubber. The result was found to be remarkably good. With a layer of exposy resin coated on the chamber facing surface of the inner Tufuo disc to reduce the effect of out-gassing and with the liberal application of silicon grease to help to seal any minute leak holes, a seal capable of taking 50 wires was found to work successfully under a chamber pressure of about 10^{-6} torr. Such seals have been employed in other experiments with equal success. The detail of the method and its performance was given in reference (25).

4.3.4 The making of small aluminium discs

The essential features of the aluminium discs for our experimental purpose must be of equal size and thickness and perfectly round without any distortions along the edges. The first method used to produce the discs was by punching. This was carried out by clamping a thin sheet of aluminium between two steel plates, with a line of holes pre-drilled in each plate so that when they were clamped together the holes faced each other. The plunger was made of hardened steel and ground to give a sharp edge. However carefully the process was carried out, the aluminium discs produced were always bowed and the edges jagged. The second attempt was by parting of the discs off an aluminium wire. But this was equally unsuccessful, since pure aluminium does not machine readily and it hardly has any mechanical strength to withstand the parting tool. We then tried to machine a pack of over-sized aluminium discs sandwiched between stronger aluminium alloy discs and the whole pack was clamped tightly in a turning machine. It was thought that this would ensure perfect edges when the quasi solid rod was machined to the diameter. It was found, however, that the pack when reduced to a diameter of 0.16 cm has very little strength to withstand machining and was shattered. If the over-sized discs were first bonded firmly together

by some suitable material to form a rod, the chance being thought greater for the rod to be machined to the required diameter. But the material suitable for the bonding must be dissoluable for the discs to be recovered afterwards. Among the number of materials investigated plastic material turned out to be quite satisfactory. Unfortunately this did not work either as the rod always broke before it was machined down to the required diameter. The strength of a plastic material was obviously too weak. If stronger bonding materials were used, it might require either acid or heat for its removal and this would certainly affect the properties of the aluminium discs. Investigation was then carried out along another line. This was by trepanning with a hollow drill. First a hollow drill with a bore of 0.158 cm diameter was produced. This drill had a number of sharp teeth at one end and a spring loaded pin inserted in the tube to recover the discs when drilled. It was thought that if the drilling speed was kept very high (25000 r.p.m.) and the lowering force kept very low, we might manage to produce the discs we required. Results showed the opposite, because the drill teeth, even hardened, started to wear away very quickly and the finishing of the discs was not good enough.

Among all the unsuccessful attempts, it was found that results produced by punching still showed some hope, if only the bowing of the discs during punching could be avoided. When avoidance of bowing was found impossible, the removal of the bowing after punching was pursued. To carry out this investigation, a punching device for making discs of diameter 0.158 cm and diameter 0.119 cm was designed to incorporate in the working capacity of the Tensometer testing machine. This device gives a much better accuracy than the one used previously. In the design there are several essential points to be observed. First the punching pin must be sharp and it must

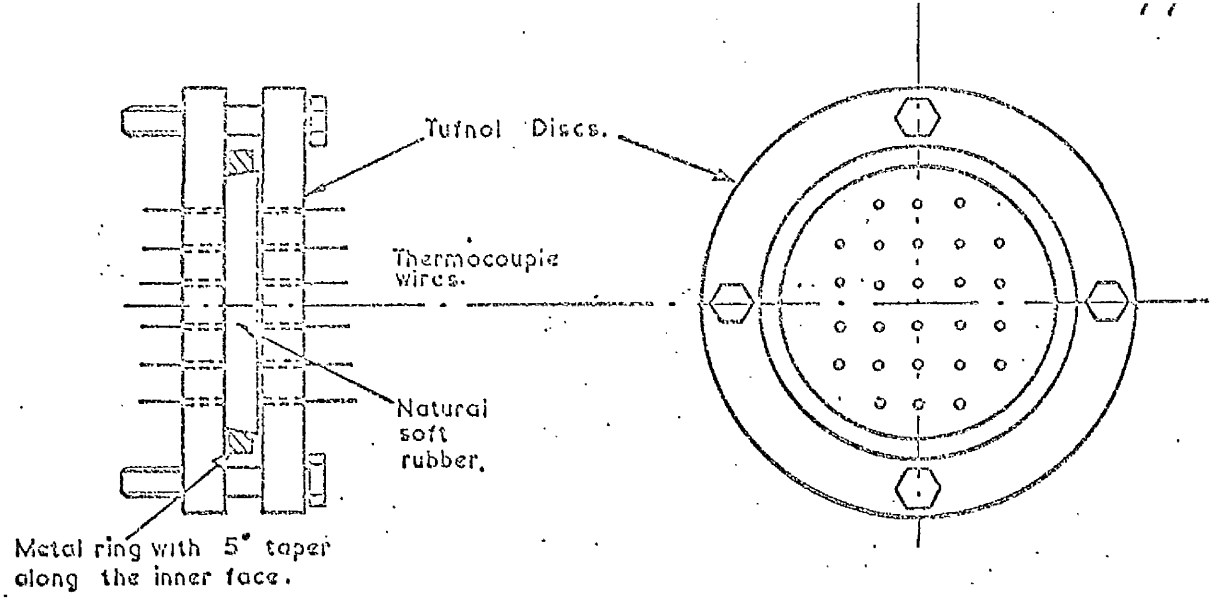

FIG. 4.9 MULTI-WIRE SEAL.

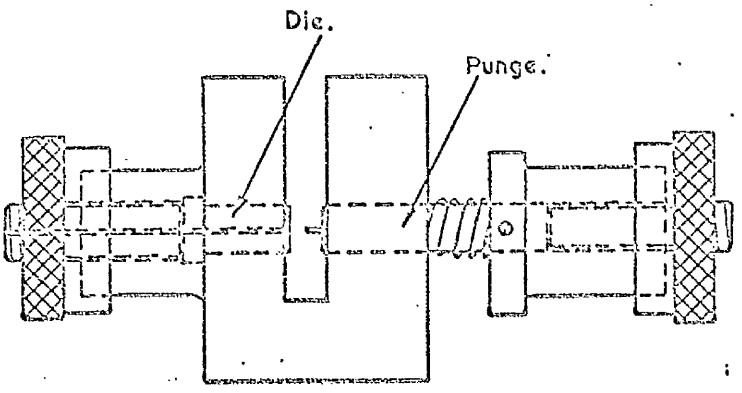

ALUMINIUM DISCS PUNGING DEVICE.

FIG. 4.10 a

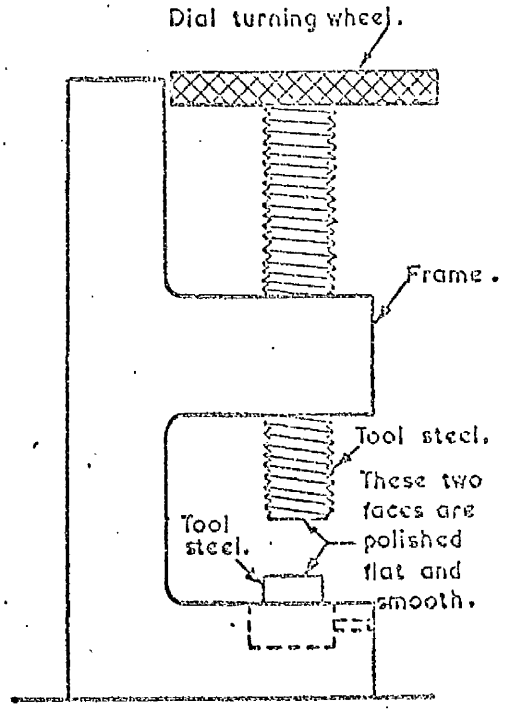

ALUMINIUM DISCS FLATTENING DEVICE

FIG. 4.10 b

meet the die uniformly around the edge. The tolerance between the pin and the hole along the die was maintained at less than 5 thousandth of a mm. Both the die and the pin were made of special hardened steel and the pin could be readily replaced by a fresh one to ensure a keen cutting edge. The device is shown in figure 4.10a. The results obtained were satisfactory although there were still slight bowing occurring on the discs. To remove the disc bowing a clamp in the form of a micrometer was used for compressing the discs, one at a time, to a point where its faces were just flattened. This device is shown in figure 4.10b. The scale along the micrometer head ensures not only the consistent force to be applied during the process, but also all the discs bearing the same thickness to the accuracy of the scale. By means of a selective method afterwards, discs having the same diameter were used for each experiment. The work was laborious, but it was worth while, as we now know that under sufficiently high load, these inserted discs between the specimens at the interface provide full areas of contact, the areas of which can be measured to some degree of accuracy.

4.3.5 Examination of surface finish and flatness of test specimens

The En 8 steel blocks and Armco iron blocks of 5.08 cm in diameter were lapped on both ends. The end which was subsequently used as contact surface was polished to a mirror finish. Samples of these specimens were examined at the National Engineering Laboratory in respect of surface finish and flatness by means of the micro-interferometer. The typical result is reproduced here.

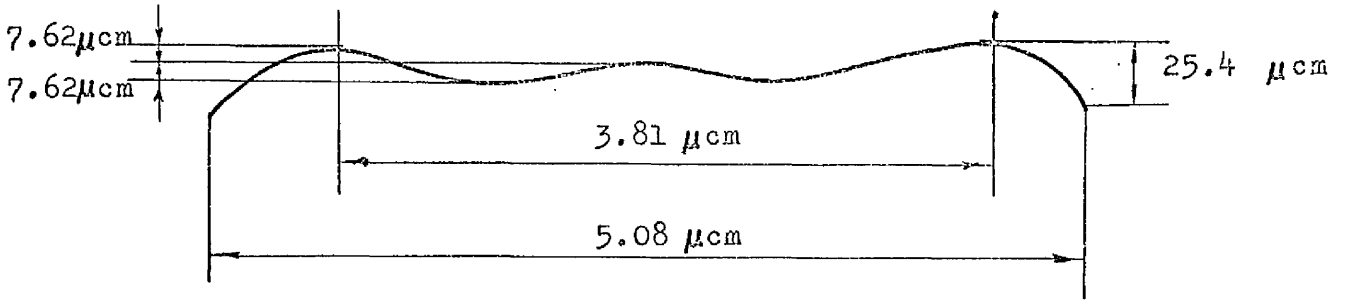

Fig. 4.11 Sectional profile of a contact surface.

The maximum flatness deviation as shown in figure 4.11 is about 8 μcm. We can make an estimate to find out the deviation of the contact areas caused by the surface deviation of such a magnitude in the worst possible case. We find for En 8 steel specimen with 0.795 mm diameters steel balls, the maximum deviation of contact areas is about 2% when x = .01. But the required load to produce an indentation corresponding to x = 0.01 is only about 10 gm. This is indeed a very small load. With a higher load, any deviation of contact areas will be exceedingly small for the contact surface to be treated as flat and smooth.

4.3.6 Determination of Young's modulus.

Since no information concerning the Youngs modulus of En 8 steel and Armco Iron was available to the author, it was decided to carry out the necessary measurement. An En 8 steel block of 5.08 cm in diameter and 7.62 cm in height, with four Tinsley wire electric strain gauges attached longitudinally on four sides, was subject to compressive loads in an Olson testing machine. An arrangement was made so that the load was acting centrally through the specimen. The measurement of the strains was taken by means of a Tinsley Vernier potentiometer and then converted by the

appropriate gauge factor. Load was increased by equal increments and a strain-stress relationship was thus derived. The Olson machine has also a device for plotting the load-deflection relationship, but the potentiometer method is considered much more accurate. The stress-strain curve thus obtained shows a very linear characteristic. From the slope of this curve we obtain the Young's modulus which is equal to 2.11×10^6 Kg. cm^{-2}. The results of the stress-strain relationship of Armco iron also give the same Young's modulus value of 2.11×10^6 Kg. cm^{-2}.

4.37 Thermocouple calibration

In order to reduce the error in temperature measurement due to the inevitable heat conduction along the thermocouple wires, junctions made from materials of relatively low thermal conductivity and of small gauge were preferred. The choice of 40 S.W.G. (0.122 mm diameter) Eureka/Nichrome was made on this basis. Nine thermocouples composed of wires taken from various portions of the reels were produced by arc welding in the presence of coal gas and they were sent to the National Physical Laboratory for e.m.f. - temperature calibration. The variation of results among the nine thermocouples is very small. The average values which are used in the present calculations are shown in Table 4.2.

TABLE 4.2. The e.m.f.-temperature calibration of Eureka/Nichrome thermocouple

Temperature °C	25	50	100	150	200	250	300	350	400	450	500	550
e.m.f. (mv)	1.08	2.22	4.659	7.282	10.06	12.976	16.015	19.163	22.373	25.653	28.917	32.356

In any thermocouples there is a possibility that the wires may not be uniform nor the junction formation be consistent, and these may affect the e.m.f.-

temperature relationship. For accurate temperature measurements it is desirable to carry out separate calibration of those thermocouples to be used in the experiment. The most convenient way is to use the calibrated thermocouples as standards. The equipment required was an oven with the ability to maintain uniform temperature at the working section. Such an oven was designed and constructed. It is shown in figure 4.12. Since the oven design does not have any direct connection with the present problem, any detailed description would not seem necessary. It suffices to say that its performance for the purpose of calibration was satisfactory. By means of a power stabilizing unit a steady temperature could be maintained at any level up to 500°C.

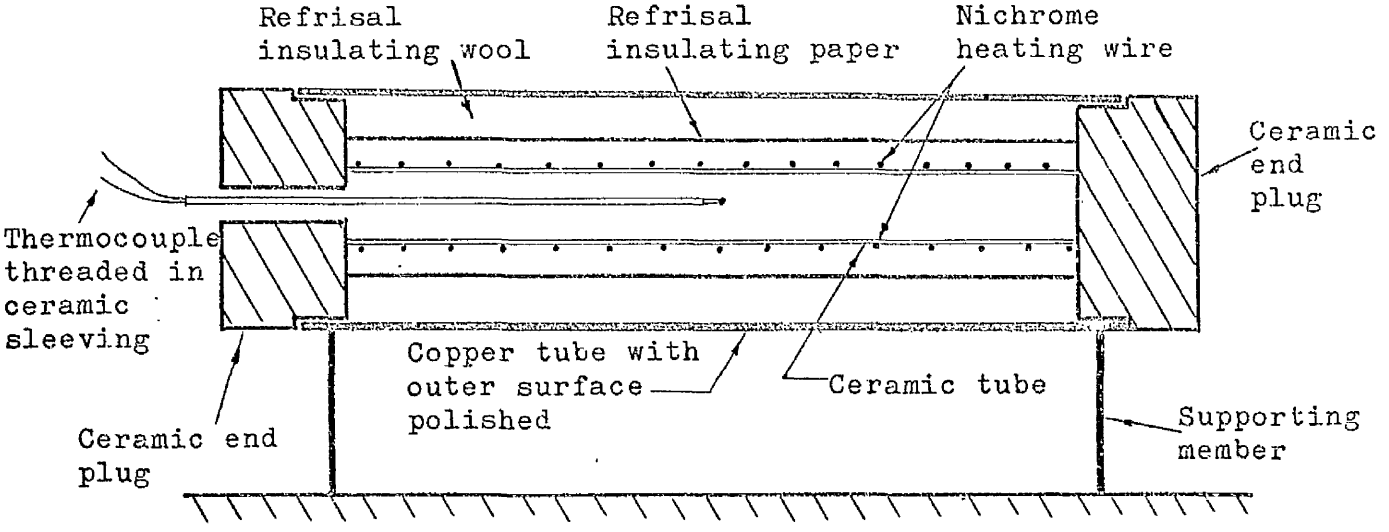

Fig. 4.12 Oven for calibrating thermocouples.

Twelve thermocouples together with two standard thermocouples were inserted into the oven so that the junctions were all situated very close together in the mid-region of the oven. The e.m.f. output of each thermocouple was taken by means of a vernier potentiometer, as the temperature was increased by an increment of approximately 50°C from room temperature to

500°C, and then by 50°C decrement back to room temperature. Two separate sets of calibrations were carried out. The maximum deviation of e.m.f. output of the working thermocouples from that of the standard thermocouple was found to be only about 0.3%. Such a consistency of results was also confirmed in other work using the same thermocouples. It was decided, therefore, that no further calibration of Eureka/Nichrome thermocouples from the same reels of wire would be necessary.

CHAPTER V

APPARATUS AND EXPERIMENTAL SET-UP

5.1 Apparatus

For the purpose of carrying out experimental studies of the heat transfer phenomena across an artificially created contact, an apparatus was designed with the following considerations in mind.

1. Thermal conductance through the metallic contact junctions

If two surfaces are in contact in the absence of any interstitial fluid, heat transfer will take place only by means of metallic conduction and by radiation. At zero load application one surface (e.g. the upper surface for convenient reason) can be arranged to be just not touching the inserted objects so that heat transfer is mainly by radiation. This enables the surface property such as the emissivity to be determined with the upper surface brought subsequently to just touching the inserted objects, the amount of heat transferred by radiation should more or less be unaltered while the influence of metallic contacts begins to take effect. When an axial load is applied, the contact areas are established and they will increase with load. Heat transferred by radiation is expected to decrease owing to the reduction of the temperature difference between the contact surfaces. Such a quantity can be calculated as the overall surface emissivity has been deduced earlier. Thus the thermal conductance by metallic contacts alone can be estimated from observed results. In the case with the insertion of steel balls, any surface films can be readily ruptured by the high pressure exerted at the contact points. This facilitates the study of thermal-electric analogy of current flow to be carried out. The measurements of electric

conductance can be made simultaneously with the measurement of thermal conductance under these conditions. In the case of aluminium discs insertion, surface films between the contact surfaces are likely to exist and they may be detected by such measurements.

2. Thermal conductance in the presence of an interstitial fluid

The influence of the interstitial fluid on the thermal contact conductance can be examined when a specific gas is introduced into the already evacuated chamber. It is important that such a gas should not cause oxidation of the materials and thus affect the interface contact conditions. We chose to use helium for its high thermal conductivity and argon for its relative low thermal conductivity, each gas to be introduced into the chamber in turn during each load increment and decrement. The combined effect of fluid conduction and radiation can be observed for the whole loading range including the case where metallic contacts are entirely absent.

The apparatus which is required to provide such facilities consists of the following systems.

5.1.1 Heating system

Main heater - The main heater is situated in a cylindrical cavity at the upper end of the heat flux meter which is made of Armco iron for its known thermal conductivity at elevated temperatures [30, 31]. The heating element is a nichrome heating coil wound in a spirally cut groove in a Pyrophillite disc, 3.2 cm. in diameter and 1.0 cm. in thickness. The groove is in a "U" shape with a narrow opening so that when the heating coil is threaded to lie in it, it is kept from falling out of the former. After experiment I, when the heating burned out after only about 80 hours of operation, it was decided to cover the face and the groove of the former with a layer of Fibrefrox cement mixed with

graphite powder to protect the nickel oxide film from evaporation when it has to operate for a long period in vacuo. The graphite element is to increase the surface emissivity. The experience gained in this incident will be described in Chapter 6. The placing of the main heater at the upper end of the specimen column, consisting of the top and bottom specimen blocks and the heat flux meter, is to reduce the possibility of convection occurring at the interface when the upper contact surface will be hotter than the lower contact surface. The amount of heat thus generated will flow mainly through the heat flux meter, through the upper specimen, across the contact section, and through the lower specimen to a main heat sink at the very bottom of the specimen column.

Guard heaters - In order to reduce any radial heat transfer, the specimen column is surrounded along its entire length by two guard tubes, of 10 cm in outside diameter and of 0.35 cm in thickness, one placed on top of the other with the junction situated in the same plane as the test contact section. There are three heaters along the guard tubes, one situated at the same level as the main heater, one near the top of the lower guard tube and the third one on the upper guard tube at about 5 cm above the junction of the guard tubes. They are formed by winding nichrome wire around the guard tubes on top of a layer of Refrisal insulating paper. This type of paper was found to withstand a temperature of 1000^{o}C satisfactorily. It has a resilient texture which helps to retain the heating wire in position when it expands under heating. The heating elements are pasted with a coat of Fibrefrax cement to protect them against evaporation. The base of the lower guard tube fits snugly into a recess which forms an extension of the main heat sink, thus being held in position.

The power leads are brought through the vacuum chamber by means of

the single pin type glass-metal seals. The power to all the heaters is supplied from a power stabilising unit connected to the electric main, and is controlled by individual Variac transformers supplemented by the reading on an ammeter.

For the best matching of the temperature distribution along the specimen column and along the guard tubes, the materials used for the guard tubes should be similar to those along the specimen column. Thus two types of materials are employed, namely En 8 steel and Armco iron according to the requirement of the experiments.

The edges of the guard tubes at the junction are shaped at 45 degrees to match each other in order to compensate for a large temperature drop occurring at the specimens' contact interface. Owing to the large range of contact conditions to be investigated, it is obvious that a fixed contact setting between the guard tubes can never give a satisfactory matching of temperatures to all cases. Hence it was decided to introduce a device by which the contact condition at the junction between the two guard tubes can be altered at will from outside the vacuum chamber during the experiment. The working principle of this device is shown in figure 5.1. Essentially, the upper guard tube is supported by four spring loaded pillars which with the full extension of the springs lift it into a position just not touching the lower guard tube. At the interface of the guard tubes a corrugated thin copper strip wrapped with four layers of aluminium foil is inserted to provide various contact areas when an external load is applied through a lever-pulley-cable system to pull the upper guard tube against the inserted copper strip. The whole system emerged as the result of many experiments after the main apparatus had been constructed. Although it may not appear as efficient as we would have liked, it does improve the temperature matching conditions a great deal.

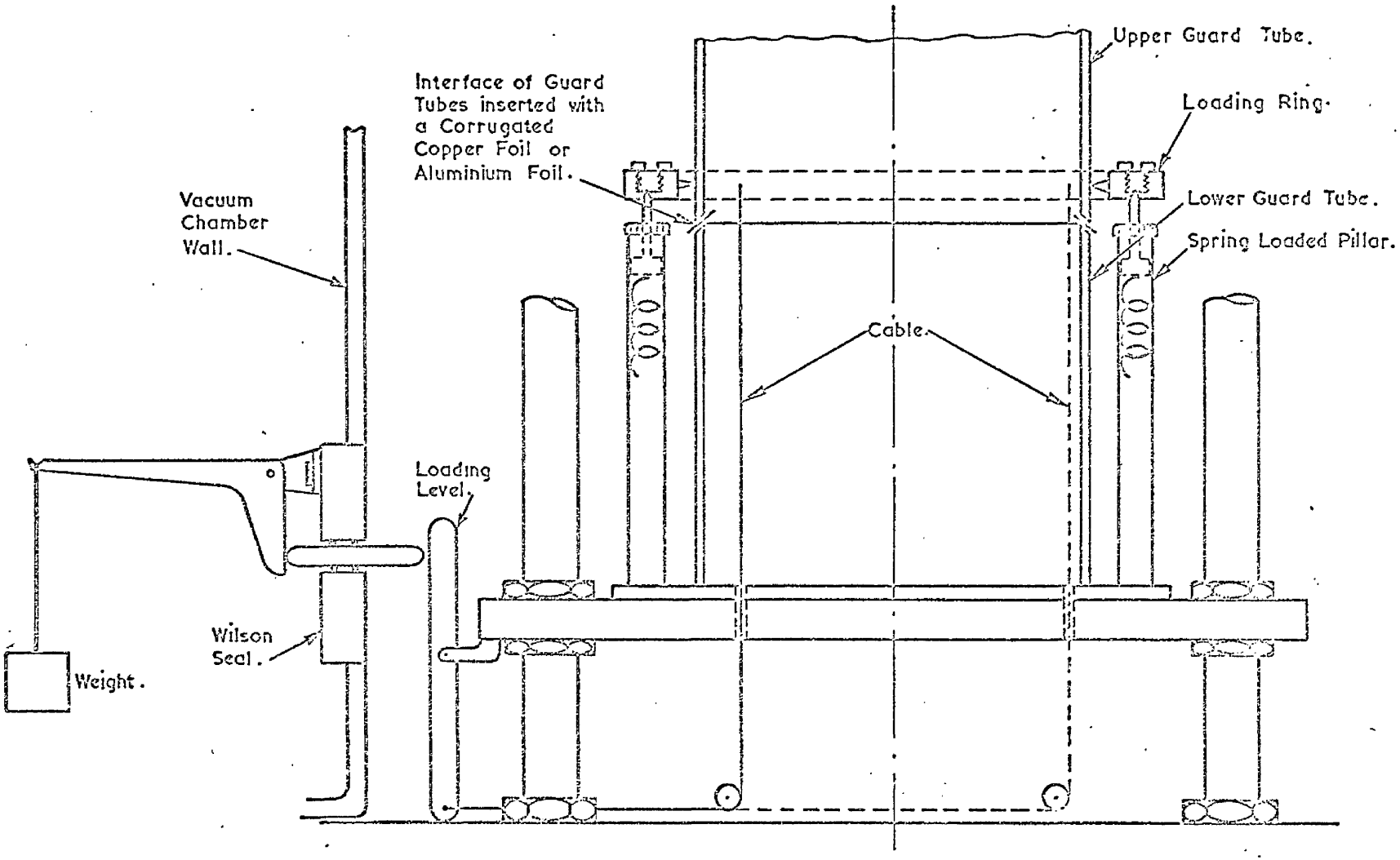

MECHANISM FOR CONTACT ADJUSTMENT AT THE GUARD TUBE INTERFACE.

FIG. 5·1

However, owing to the sudden change in temperature gradients which occur at the junctions in the specimen column, an exact matching even by controlling the guard tube contact junction is still not possible, and in these cases a small correction has to be applied before the true heat flux passing through the specimen contact interface can be estimated. The radial heat transfer correction is determined according to APPENDIX F. Insulation -- the space between the specimen column and the guard tubes is packed with the Silocel insulating powder except in the specimens contact region where ceramic beads are used, so that through two breathing tubes inserted through the powder the gas at the contact interface can be introduced or evacuated in accordance with the experiments. The insulating powder having a very low thermal conductivity reduces the correction that has to be applied for any mis-match of temperatures.

Initially a ceramic shield in two semi-circular halves was used to surround the guard tubes. This, however, proved to be very awkward for bringing out the power leads as well as the thermocouple wires. Instead, an aluminium shield, also in two semi-circular halves but with a much larger diameter, is used and the space between it and the guard tubes is filled with the insulating powder. In this way the leads and wires can be brought out through the powder. The insulating capacity of the system is also improved.

It is desirable that the specimen column should be insulated thermally as well as electrically. This is accomplished by sitting the main heat sink at the bottom of the specimen column on a syndanio plate which is fixed in the centre of the supporting steel plate. On top of the heat flux meter at the other end there is a ceramic cup which has a recess large enough to adopt the heat flux meter block, and widens in diameter to 7.62 cm to support a steel platen for the application of the axial load.

5.1.2 Temperature measurement system

Temperature measurements along the heat flux meter, the specimens and along the guard tubes is made by means of Eureka-nichrome (40 S.W.G.) thermocouples. The junctions of these thermal thermocouples were formed as small beads by electric arc welding in the presence of the coal gas; and the bead, after being covered with a coat of silver paint to facilitate contact, was securely fixed in a shallow hole by means of a soft pencil point at intervals along the above mentioned parts. There are three thermocouple positions on the lower specimen block at 0.476 cm, 3.216 cm and 5.756 cm measured from the lower contact surface, and three positions on the upper specimen block, again at 0.476 cm, 3.216 cm and 5.756 cm measured from the upper contact surface. There are four positions on the heat flux meter block at 0.63 cm, 2.54 cm, 4.45 cm and 6.35 cm measured from the junction between the heat flux meter and the upper specimen. In three experiments where the heat flux meter and the upper specimen are in the same continuous block, there are five thermocouple positions, at 0.476 cm, 3.01 cm, 5.55 cm, 8.10 cm and 10 cm measured from the upper contact surface. In the same plane as the one placed nearest to the upper contact surface and the one nearest to the lower contact surface, two additional thermocouples are fixed at 120 degrees from it, to enable any difference in temperature around the specimens to be detected. In all there are 14 thermocouples (in those experiments where the upper specimen and the heat flux meter are one integral part there are 12 thermocouples) along the specimen column. Ten thermocouples (8 thermocouples in the other three cases of experiment) are fixed to the guard tubes at positions directly opposite to those along the specimen column.

The thermocouple wires are insulated by small twin-bore ceramic

sleevings and by Refrisal sleevings. They are then attached to ceramic rods erected vertically in the space between the specimen column and the guard tubes and just outside the guard tubes so that the wires are brought upward to clear the insulating powder. They are then brought out of the vacuum chamber through the multi-wire vacuum seals described earlier. The wires are always arranged to traverse from the thermocouple junctions to the ceramic rods horizontally, to reduce any transmission of heat due to wire conduction.

Outside the vacuum chamber the thermocouple wires are connected to a double-pole selector switch, and from there two common wires (Eureka and nichrome) are taken to an ice bath. The connection between the ice bath and a Tingsley Vernier Potentiometer capable of measuring volts is by two copper wires. Other equipment includes a highly sensitive Tingsley galvanometer, a standard cell and a 10-ampere-hour two volts battery. The circuit diagram is shown in figure 5.2. The measurement of the thermal e.m.f. output is based on the null method and therefore wire resistance need not be considered.

5.1.3 Electric conductance measurement system

The electric conductance measurements are made by the method involving a comparison of the potential differences across a specific section of the specimens, and across the contact interface, with that established across a standard resistor when carrying the same current. The practical problem is that of finding the total resistance in the circuit so that a current of just sufficient quantity can be passed through to enable the potential differences to be measurable, but not too high to cause unnecessary heating to the contact spots. Another problem is that of finding a stable source of direct current. The current supply from an

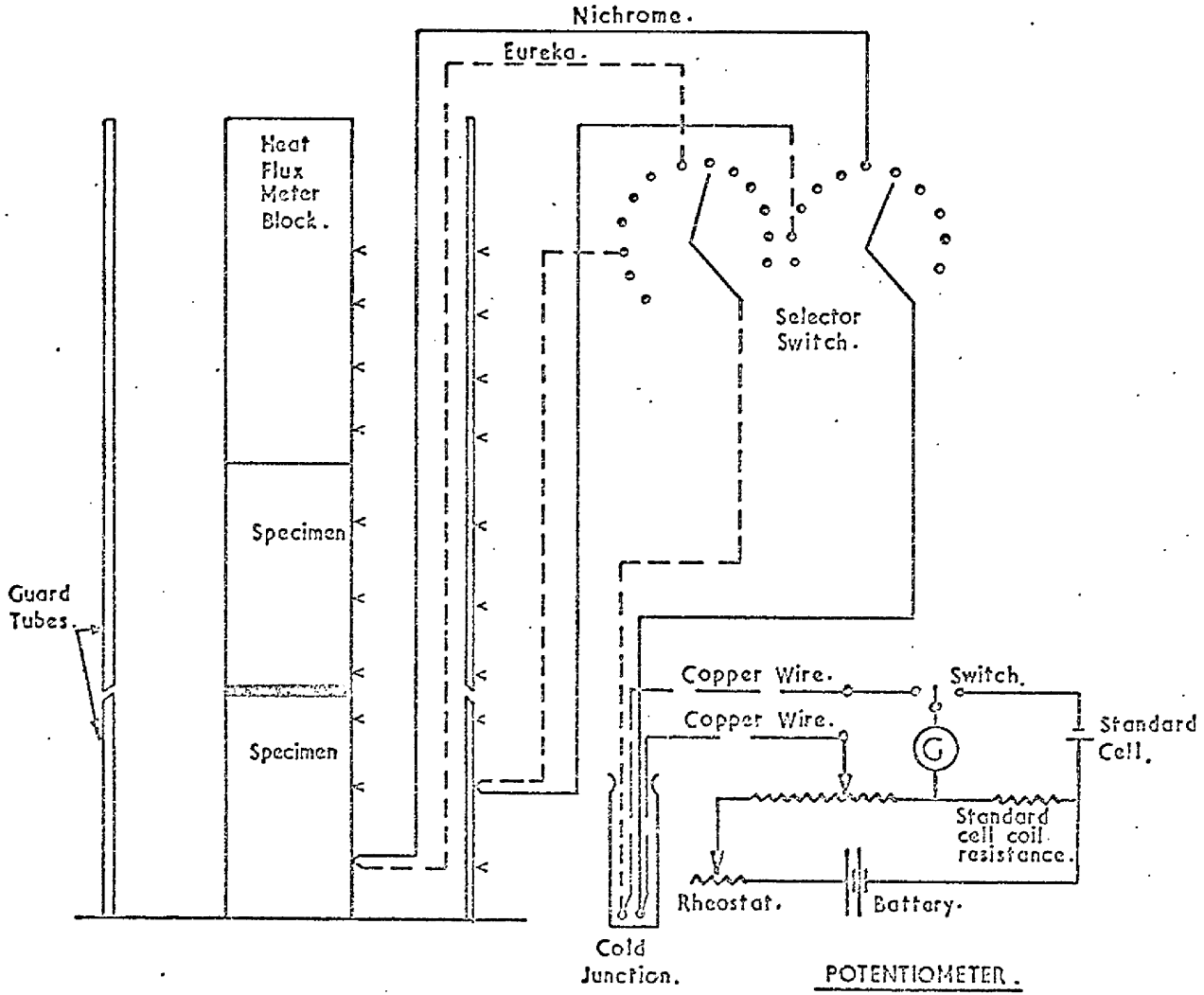

THERMOCOUPLE CIRCUIT FOR TEMPERATURE MEASUREMENT.

FIG. 5·2

accumulator is never stable but varies with time. It does, however, become quasi-steady after a long period of operation if the discharging current is relatively small. In the circuit a current of between 1 and 2 amperes will be required if the standard resistance used is one ohm. After some investigation, it was found adequate to join four 100-ampere-hour accumulators, of 2-volt potential each, in parallel, and to allow at least 30 minutes of switch-on before taking any readings.

The thermocouple wires attached to the specimens are used as the potential leads and the readings are taken with the current flowing alternatively in the positive and negative directions by means of a reversing switch to eliminate the thermoelectric effects. The circuit diagram is shown in figure 5.3.

5.1.4 Cooling system

The main heat sink situated at the lowest part of the specimen column is made of brass through which cooling water is passed around a spiral copper strip to facilitate uniform cooling. In the design, consideration is also given to the fact that this unit has to withstand a maximum compressive load of 10,000 kg. Two rubber 'O' rings are incorporated to ensure perfect sealing. The base of the unit is extended wide enough to adopt the base of the lower guard tube around which two coils of copper tube are soldered for circulating cooling water to act as the heat sink for the guard tubes. PTFE (polytetrafluoroethylene) tubings, which possess excellent thermal and vacuum properties, are used in conjunction with the Wade couplings (supplied by Wade Couplings Limited) which have been modified for the purpose of circulating water inside the vacuum chamber.

Provision is also made for the cooling of the vacuum chamber and for the diffusion pump. A water relay switch was designed and made to safeguard

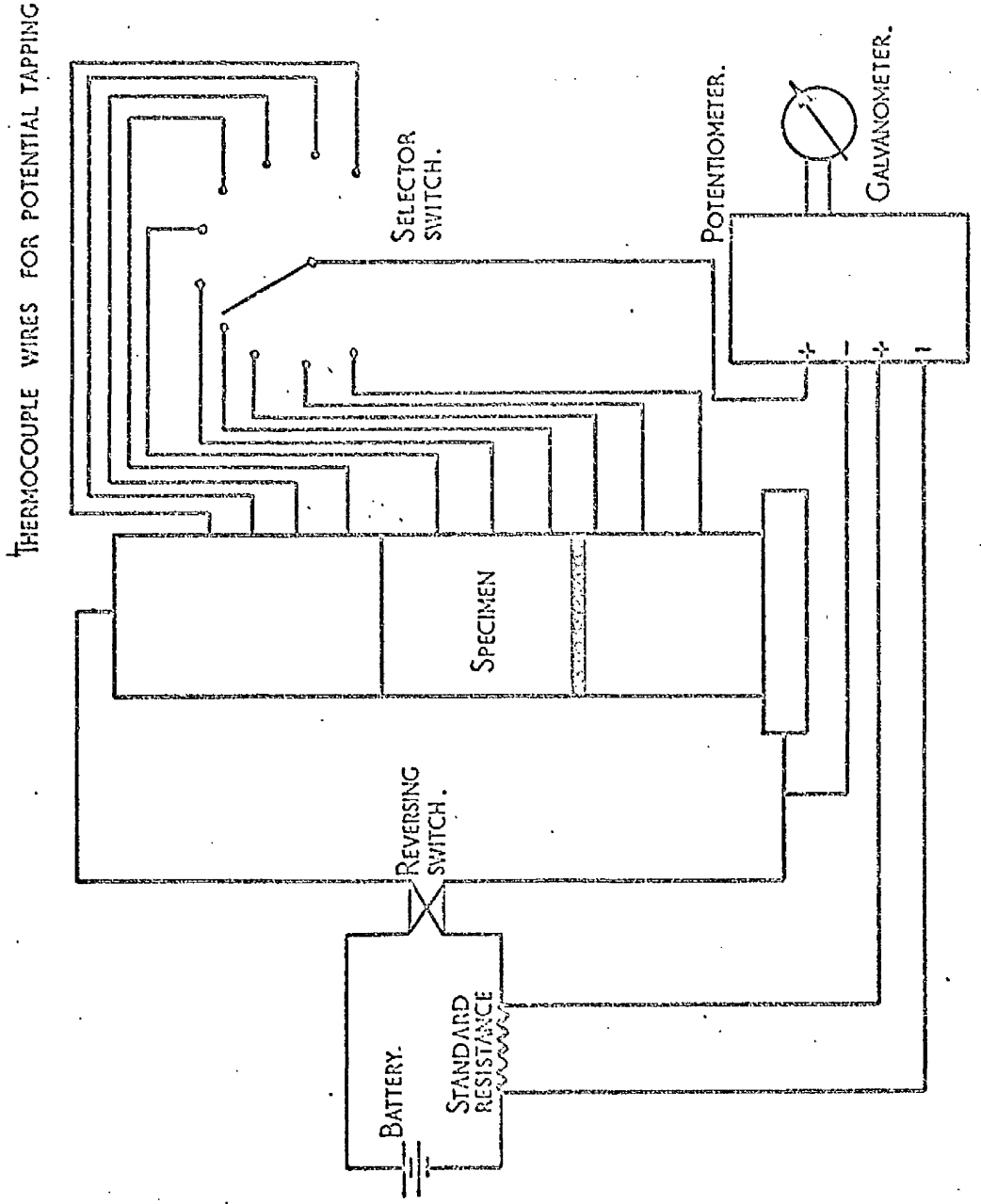

CIRCUIT FOR MEASURING ELECTRIC CONDUCTANCE.

FIG. 5·3

the pumping unit against any failure in water supply.

In all four independent cooling circuits are required. Water for cooling is supplied from a water tank mounted about 8 feet above the floor. An overflow pipe and a float-chamber valve are used to control the level of water in the tank. When it was discovered that the water head thus provided did not give adequate pressure to the cooling circuits inside the vacuum chamber, a water-pump connected with a constant water flow control unit was added to the whole system. There are separate valves for each circuit for controlling the water flow rate. The temperature distribution in both the specimens and the guard tubes are sensitive to the cooling rate of their heat sinks. By adjusting the water flow rate appropriate for each circuit, it is possible to give additional refinement to the matching of temperatures between the specimen column and the guard tubes.

5.1.5 Vacuum system

A vacuum chamber was designed with provision for load transmission and for other mechanical movements through the chamber wall. It was constructed in three sections to facilitate assembly and it has the working dimensions of 30.5 cm in diameter and 56 cm in height. The base plate has a circular recess to fit onto the platen of the compression machine which will be described later. This, unfortunately, rather hinders the connection of the vacuum pump directly on to the vacuum chamber, an asset of having low circuit resistance. The pumping unit consists of an Edwards 4-in diffusion pump backed by a single-stage rotary pump (1 SC 450B). A Pirani vacuum gauge with twin gauge heads, one connected to the vacuum chamber and the other to the pipe line is used for measuring the pressure. Along the pipe line there is also a gas admittance valve which has a connection

either to a helium bottle or to an argon bottle for admitting the gas to the chamber. The system is shown in figure 5.4.

5.1.6 Loading system

During the experiments it is desired to press the upper specimen against the inserted objects at the interface so that various contact areas can be produced under the applied loads. A compressive load ranging from zero to 10,000 kg. is required. A dead weight and lever system was first thought of but this requires a rather long lever arm. A hydraulic system may be more suitable but an objection to this is its tendency for the applied load to creep with time. A compression machine, originally designed by the Clockhouse Engineering Limited for the purpose of soil mechanics experiments, was modified and adopted for our use. Its operation is based on the warm gear principle and it has a sensitivity of 6.4 kg. per division of the dial indicator fitted in the machine. The maximum load capacity of this machine is 10,180 kg. The applied load can be held constant and it has a working space adequate for housing the entire vacuum chamber.

During the experiments it is essential that the applied load should act through the centre of the contact section between the two specimens so that there is a uniform pressure over the contact surfaces. To achieve this, first an adjustable support frame was designed and installed inside the vacuum chamber. The supporting plate holds the specimen column as well as the guard tubes in a vertical and central position. At the tope of the frame there is a cross supporting bar which has two functions, one is to hold a steel loading pin in an upright position to transmit the applied load to the specimen column and the other is to take four springs which, when connected with four fine tungsten wires, are used to lift the upper specimen to a position just not touching the inserted solid objects at the

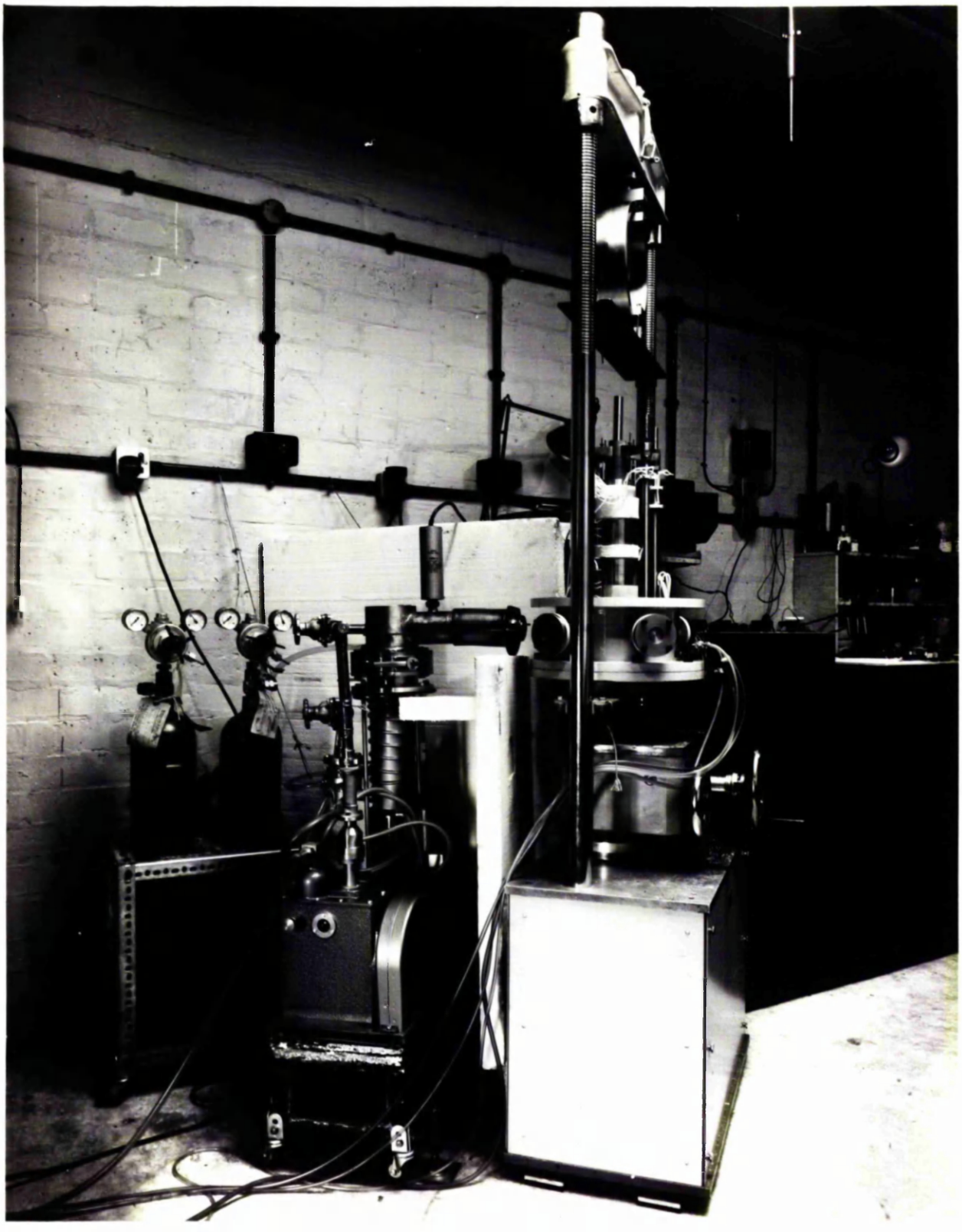

FIG: 5.4 GENERAL VIEW OF VACUUM SYSTEM

contact interface at zero load condition. The gap distance for the lifting which must allow also for the thermal expansions of the parts during heating is controlled by a Pyrophillite distance tube inserted between a steel loading platen and the cross bar. This steel platen of 7.62 cm in diameter has one flat surface to sit on the ceramic insulating cap mentioned earlier and a spherical top surface with the centre of the sphere falling at the centre of the upper contact surface to ensure a uniform applied pressure over the contact, in the event that the applied load should be out of line of the longitudinal axis. Between the steel platen and the loading pin and again between the loading pin and the proving ring of the machine outside the chamber, there is inserted a large sized steel ball to help to keep the load central and to eliminate any undesirable moments to be transmitted to the specimen column. The whole arrangement proves to be satisfactory.

5.1.7 Specimens

The choice of material for the specimens has no particular importance so long as its properties are reasonably stable throughout the range of the experimental temperature for the contact heat transfer phenomena to be studied. Although metals having a relatively high hardness value and a relatively small grain size are preferred because they offer a better surface finish under treatment, these are not primary factors. The choice of En 8 normalised steel for the steel ball insertion experiments is largely because it is more easily obtainable and it has known thermal conductivity values at elevated temperatures (28, 29). The upper and lower specimens are made of the same materials. They are in the form of cylindrical blocks, 5.08 cm in diameter and 7.62 cm in height. The ends of each block were ground flat and perpendicular to the longitudinal axis. They were then lapped and optically polished to attain a smoothness of less than 8 μcm. For use in

the same experiments the heat flux meter is an Armco iron cylindrical block, 5.08 cm in diameter and 11.4 cm in height. One end of the block has an Armco iron lid for covering over the main heater cavity for transmitting loads. Both ends were lapped flat and parallel. In other experiments with aluminium discs insertion and also with steel ball insertion, the upper specimen and the heat flux meter are one continuous block of 5.08 cm in diameter and of 16.5 in height. This block and the lower specimen which is 7.62 cm in height are all made of Armco iron.

The steel balls for insertion at the contact interface are of 1% chrome carbon steel. Two sizes of balls were used in separate experiments, one 1.585 mm. in diameter and the other 0.793 mm in diameter. The tolerance on the diameter is $\pm$ 0.00025 mm and the tolerance on the sphericity is $\pm$ 0.0001 mm.

The aluminium discs for insertion at the interface are made from a 0.203 mm thickness aluminium sheet with a specification number $2S\frac{1}{2}H$ supplied by the Alcan Industries Limited. There are two sizes of diameter for separate experiments, i.e. 1.585 mm and 1.193 mm. The surface finish of the discs is as received.

5.2 Experimental set-up

The general layout of various systems composing the whole apparatus and the detailed arrangement inside the vacuum chamber are shown in figures 5.5 and 5.6 respectively. The general view of the equipments is shown in figure 5.7.

To begin with, the supporting frame is set as accurately as possible at the centre of the vacuum chamber. This involves the use of an electronic

FIG. 5.5 GENERAL LAYOUT OF APPARATUS.

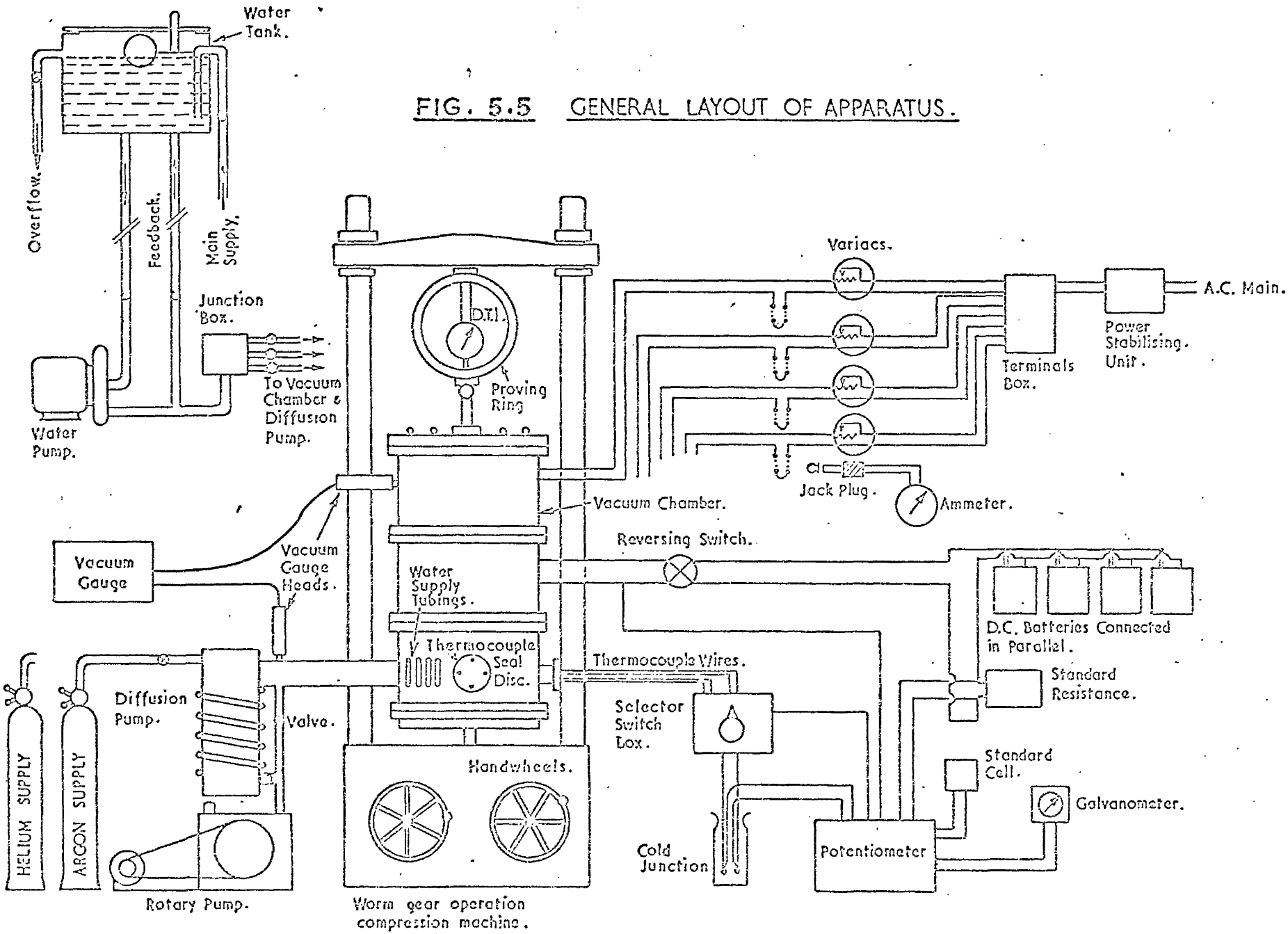

General Layout in Testing Chamber

Vacuum chamber outlet to pump is from the side of the first section.

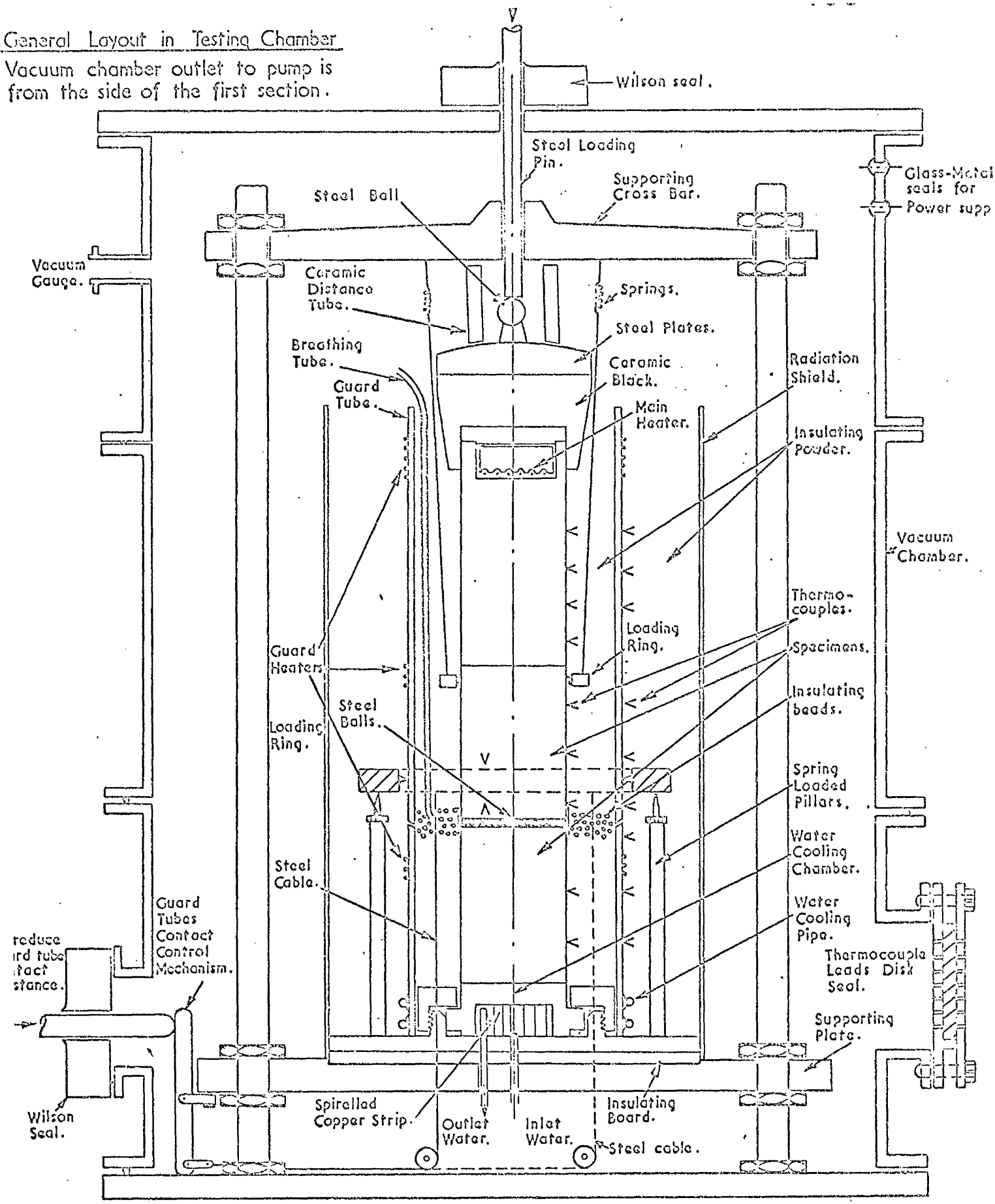

GENERAL LAYOUT INSIDE TESTING CHAMBER.

Vacuum chamber outlet to pump at the side of bottom section not shown.

FIG. 5·6

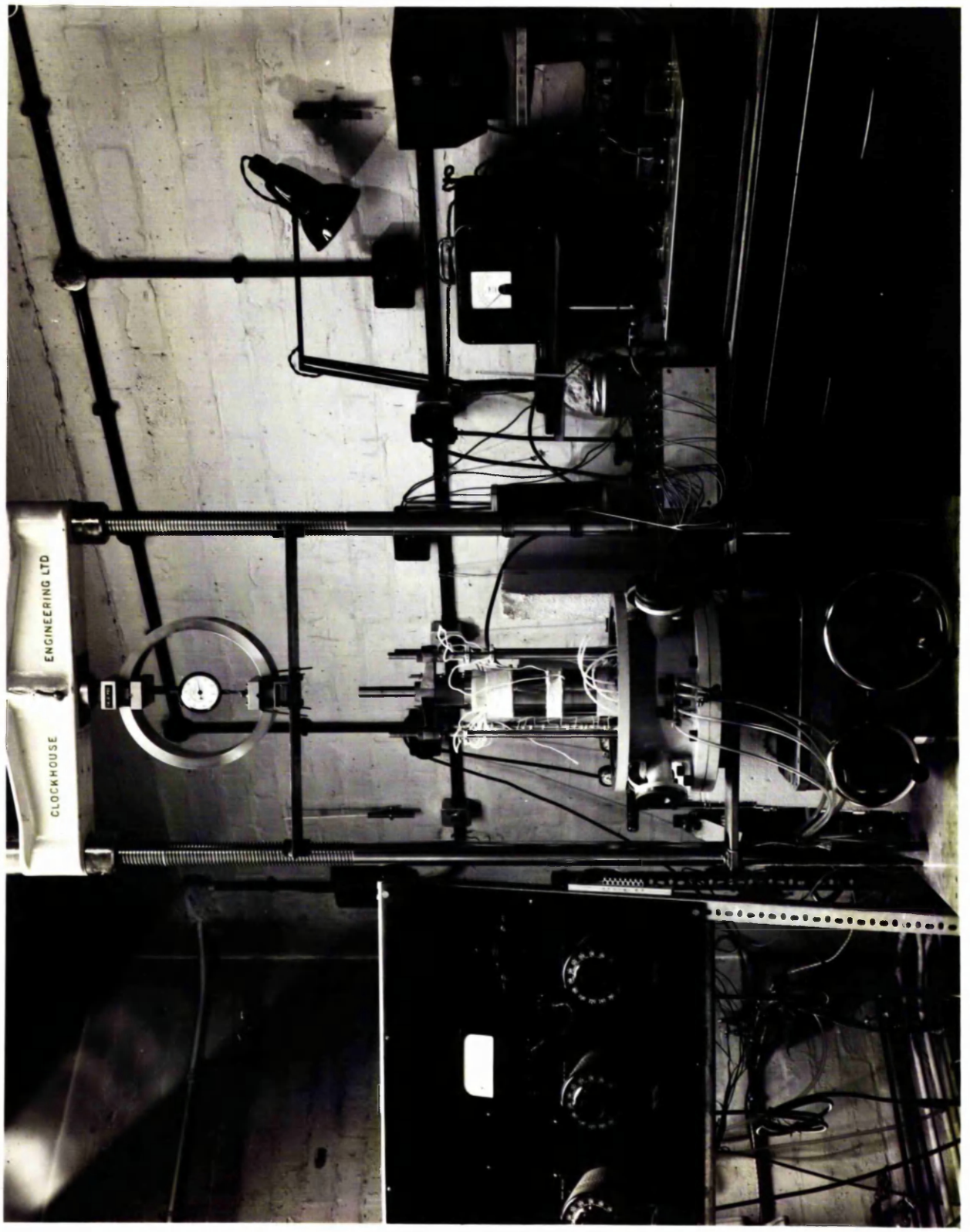

FIG. 5.7 GENERAL VIEW OF EQUIPMENT

levelling instrument and other precision devices. On the base plate of the frame sits the main heat sink, on top of which is placed the lower specimen with a thin aluminium foil inserted at the junction to promote heat transfer. The specimens as well as the steel balls or the aluminium discs as the case may be were thoroughly cleaned with trichlorethylene, acetone and pure alcohol and were allowed to dry in a warm atmosphere. Around the upper contact surface of the lower specimen a strip of PTFE was fixed to prevent the balls from falling out and to hold the upper specimen in position. The PTFE has a maximum working temperature of 270°C which is above the temperature intended to be reached at the interface. The placing of the steel balls on the specimen presented some small problems. They have to be dropped through a hole at the bottom of a plastic container one by one as they bound very readily whenever they hit on a hard surface. Owing to static electrical charges, these balls (weighing only 0.002 gram for the 0.792 mm diameter ball) were subject to forces greater than their own weight and would scatter in an uncontrollable manner. Various methods were used to overcome this, and a simple yet effective cure was by dipping them in acetone and thereafter dropping them directly onto the surface of the specimen. Over three thousand of these balls were then arranged in an array of hexagons leaving just sufficient space between each ball for thermal expansion. The final setting is shown in figure 5.8. The upper specimen was then lowered to rest on the balls. Care was taken not to disturb the setting of the balls nor to cause any undesirable indentation to the surface of the specimens before the upper specimen was clamped rigidly to the lower specimen for the time being for fixing the thermocouples. Since the space between the specimen column and the guard tubes is very restricted, the bringing out of thermocouple wires was done in a most

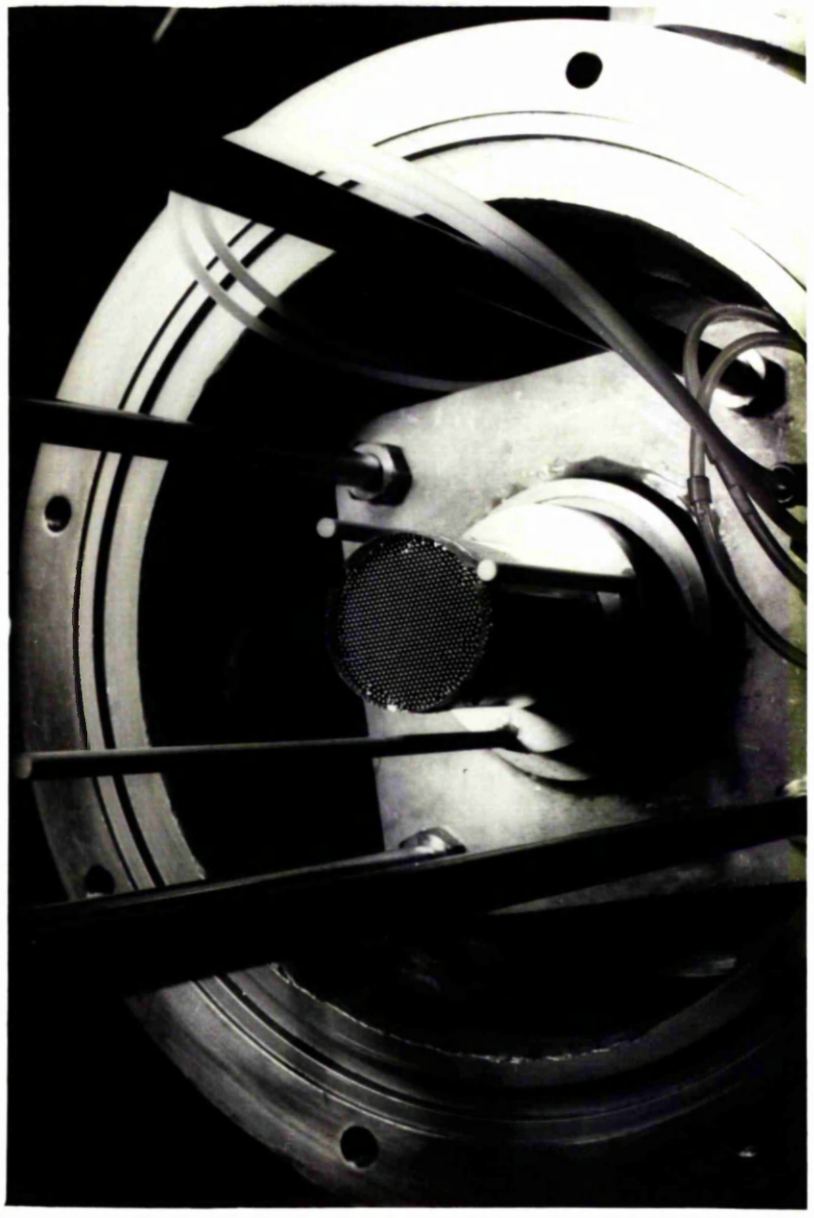

FIG. 5.8 FINAL SETTING OF STEEL BALLS ON SURFACE OF SPECIMEN

intricate manner. The way in which this was carried out and the final setting of the thermocouples can be seen from figures 5.9 and 5.10. When placing the aluminium discs on the lower specimen in other experiments, a special jig made of Perspex was first drilled with holes in a required pattern. These holes were just big enough to admit the aluminium discs. They also served the purpose of checking the exact diameter of the discs so that none of them should be unduly deformed by the clamping process described in section 4.3.4. Figure 5.11 shows the arrangement of the holes in the Perspex jig.

The insulating powder was thoroughly dried before being used to fill in the space inside and outside the guard tubes. After placing the ceramic insulating cup and the steel loading platen on top of the heat flux meter, the cross supporting bar was lowered to position allowing just sufficient space for the Pyrophillite distance tube plus a gap of 1.8 mm for thermal expansion of the specimen column. The upper specimen and the heat flux meter with a thin aluminium foil inserted between them for better heat transmission were then lifted up against the distance tube by four springs attached to the cross supporting bar. This being done, the loading pin was placed in position with one end resting on a steel ball on top of the loading platen and the other end protruding out through the covering plate of the vacuum chamber. The specimen column is connected to a separate electric circuit through which there is an electric indicating light to show when the upper specimen is in contact with the inserted solid objects at the contact interface. The whole chamber appears as in figure 5.12. The apparatus is now ready for the conducting of the experiments.

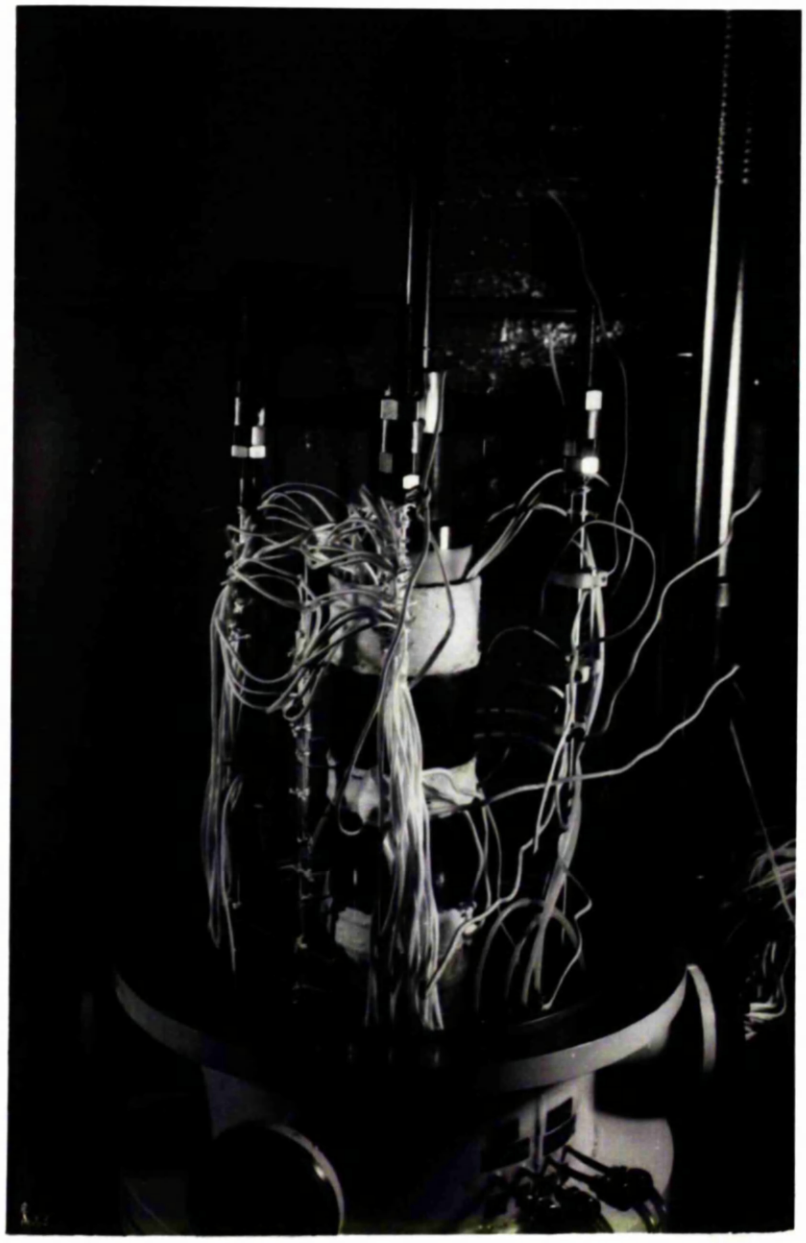

FIG. 5.10 SETTING OF THERMOCOUPLES WITH GUARD TUBES IN POSITION

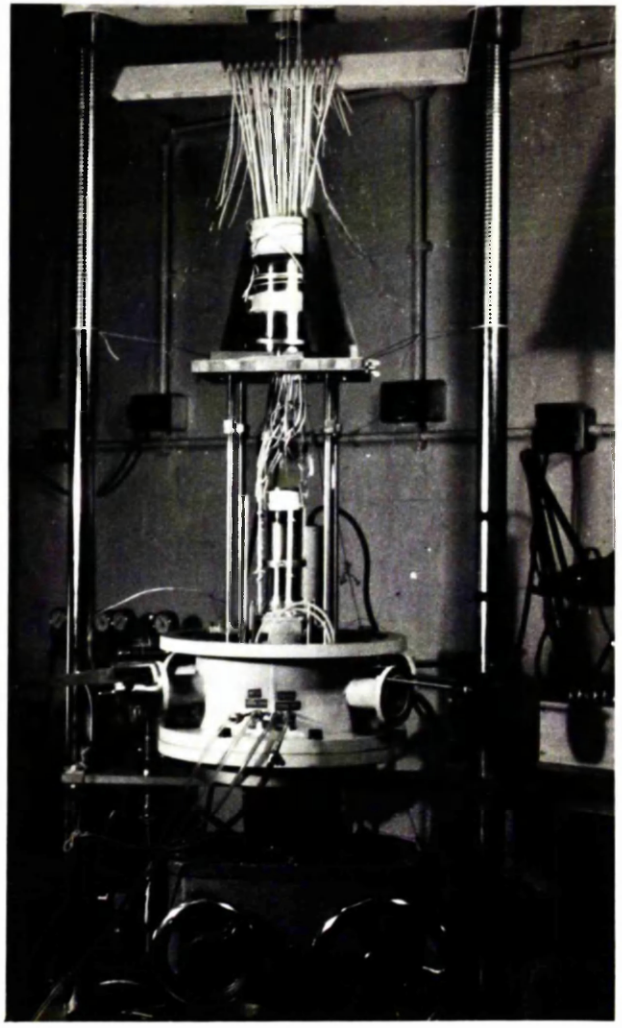

FIG. 5.9 FIXING THERMOCOUPLES TO SPECIMENS

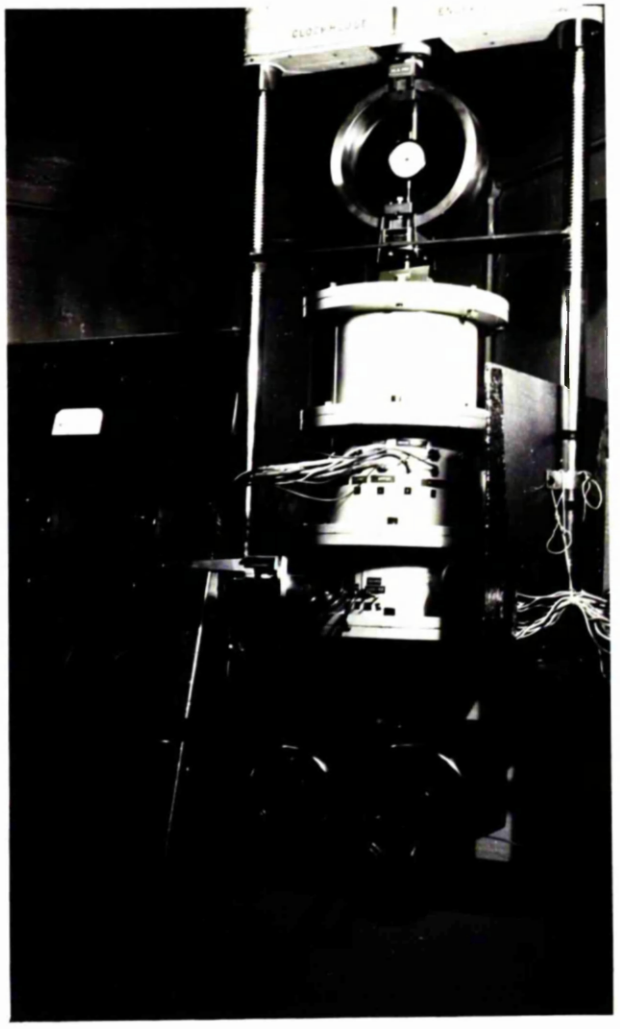

FIG. 5.12 VACUUM CHAMBER

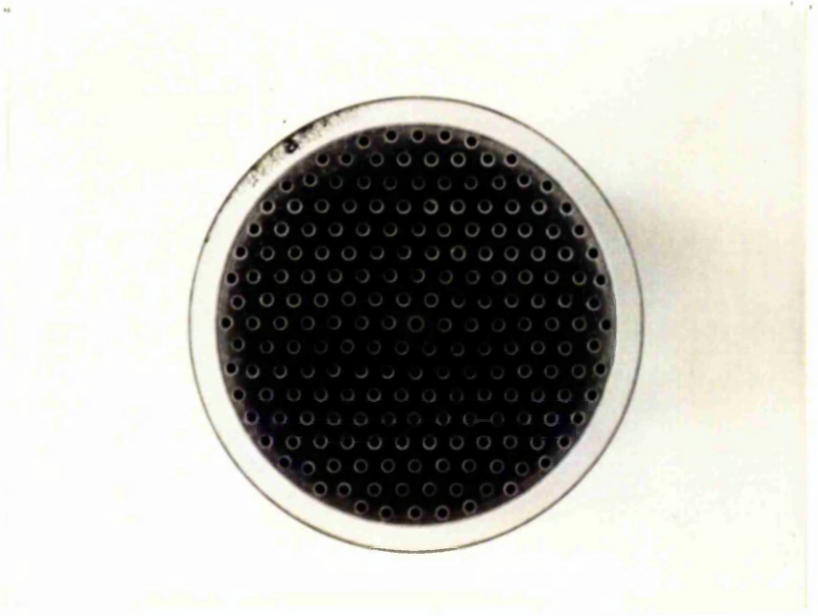

FIG. 5.11 DISTRIBUTION OF ALUMINIUM DISCS ON SURFACE OF SPECIMEN

CHAPTER VI

EXPERIMENTAL PROCEDURE AND TEST RESULTS

6.1 Experimental procedure

During each experiment the following procedure is carried out.

1. The vacuum chamber is first evacuated by the rotary pump alone, during which time the vacuum valve in the coarse pump line is opened only very slowly in order not to disturb the insulating powder inside the chamber.
2. When the gas pressure is reduced to below 0.2 torr, evacuation is taken over by the fine pumping line through the diffusion pump. The object is to reduce the chamber pressure to about one micron. If pumping is carried out for the first time after the apparatus has been freshly set up, it usually takes a long time to reach this pressure. The speed of pumping down the pressure depends on the quantity of the various items housed in the chamber, on whether their setting is likely to trap gases and on the out gassing nature of the materials contained in the chamber. The set-up of the apparatus in our vacuum chamber is certainly not favourable for reaching a required pressure in a short time. The situation was found to have improved considerably when metal surfaces were covered wherever possible with a thin layer of epoxy resin and PTFE to reduce the effect of out gassing.
3. When the chamber pressure is reduced to the test pressure, the indicating light circuit is connected, so that at a signal the contact surface of the upper specimen can be brought, by applying a small load, to be just not touching the inserted solid objects at the contact interface.
4. When a low enough pressure is reached (say 5 microns) the main heater as well as the guard heaters are switched on. Adjustments of the guard

heaters and the rates of water flow are carried out in order to establish the best temperature match between the specimen column and the guard tubes. A steady temperature usually takes 3 to 4 hours to reach, with a longer time needed for the vacuum condition than for the gas condition. With experience the number of adjustments required can be substantially reduced. When the heating capacity is increased, out gassing of the materials is accelerated, resulting in an increase in the chamber pressure. This may require a further period of pumping to bring the chamber pressure to the required level.

5. Temperature readings are taken during each adjustment of heaters to assess the condition of heat balance, and the final readings are recorded.

6. After pumping is stopped, helium gas is admitted into the chamber while the contact setting remains unchanged. The gas pressure is arranged to be about one atmosphere. It is usually quite noticeable that there is a considerable decrease in the temperature drop across the contact when helium gas is admitted. During the admittance of gas, the thermodynamic effect adds a certain amount of heat to the chamber and this results in the temporary expansion of the specimen column. The reverse is true during evacuation.

7. Adjustment of the heaters is again carried out to arrive at a satisfactory temperature match. When this is accomplished, the final temperature readings are recorded.

8. Helium gas is then evacuated and the vacuum process repeated. The purpose is to arrange the vacuum experiment at intervals between the two gas experiments. This not only speeds up the programme of the experiment series but also eliminates the possibility of a certain amount of one type of gas remaining behind to mix with another. Thus after the vacuum experiment, the argon gas experiment is carried out.

9. A load equivalent to 50 division on the dial indicator (328.4 kg.) is applied. Metallic contacts are now established, and a reduction of contact temperature drop should be quite noticeable. The same procedure is repeated under the three conditions, namely with argon, vacuum and helium.

10. During the vacuum experiments the electric potential drop between locations marked by the thermocouple positions is recorded together with that across the standard resistor. This involves switching on the accumulator circuit for about 30 minutes prior to taking any readings. The current is then reversed and the readings taken again.

11. Henceforth the procedure will be repeated for every increment of load up to a maximum value corresponding to 1400 divisions of the dial indicator (i.e. 9095 kg.) and for every decrement of load back to the zero load case. The full programme for the steel balls insertion experiments is shown in table 6.1.

12. In the experiment with insertion of aluminium discs, the applied load is increased steadily, until any small increment of load no longer changes the temperature readings. Under such conditions full contact of the specimens with the discs is assumed.

6.2 Experiments

The following gives a brief description of each experiment which has been carried out.

Experiment 1

Table 6.1 Programme of experiment with steel balls insertion.

Applied load	Environmental condition	Readings taken (e.m.f.), (volt)
zero	vacuum helium vacuum argon	temperature temperature temperature temperature
50 divisions (328.4 kg.)	argon vacuum helium	temperature temperature, electric P.D. temperature
100 divisions (656.8 kg.)	helium vacuum argon	temperature temperature, electric P.D. temperature
200 divisions (1311.8 kg.)	argon vacuum helium	temperature temperature, electric P.D. temperature
1400 divisions (9095.3 kg.)	argon vacuum helium	temperature temperature, electric P.D. temperature
1200 divisions	helium vacuum argon	temperature temperature, electric P.D. temperature
zero load	helium vacuum argon	temperature temperature temperature

Experiment 1

Inserted objects - 875 steel balls of 1.585 mm diameter

Specimens - En 8 steel.

Heat flux meter - Armco iron, a separate part from the upper specimen.

The matching of the temperature distribution along the guard tubes with that along the specimen column was very difficult to achieve during the zero load and vacuum conditions. The temperature drop across the specimens was far greater than that across the guard tubes. It was decided that a mechanism which could vary the contact condition at the guard tube contact junction should be incorporated in the apparatus for subsequent experiments.

At 400 divisions of applied load, the main heater burned out. An attempt to repair it was made without much success. Even with extreme care, the setting of the apparatus was bound to be disturbed. The effort of holding the heat flux meter block in its original position required great delicacy and would have been just as awkward as re-setting a new experiment.

Experiment 2

This experiment was to repeat experiment 1 with the following modifications.

1. A mechanism to control the contact condition at the guard junction was added. In this experiment the corrugated copper strip was not provided. An oscillating contact phenomenon was observed, which will be described later.

2. The heating element for the main heater is made of nickel chromium material. It has a relatively high electric resistivity and in particular has an excellent electric insulation property when covered with an oxide film so that even when the heating coils are actually touching each other no short-circuiting will occur. This oxide film also possesses a relatively

high surface emissivity. Unfortunately, owing to the high rate of evaporation as well as the high rate of evolution of gases at elevated temperatures in vacuo, this thin layer of oxide film becomes rather unstable and the result of this is the serious reduction of the life of the heating element. This was thought to have happened to the main heater in the previous experiment. If the heating element could be completely sealed off within the heater former, the chance of preserving the oxide film would increase. Following this line of reasoning, high temperature cement (trade name Fibrefax) mixed with graphite powder to improve the surface emissivity was used as the sealing compound. The result was very good. One heater prepared in this way was still in operational condition after 2000 hours of continuous heating. This method has been adopted in other experiments with equal satisfaction.

3. A water pump connected with a constant flow controll unit was added to the cooling system.

This experiment unfortunately did not survive very long owing to some accident in the laboratory.

Experiment 3

This experiment was to repeat experiments 1 and 2 with all the modifications carried out previously. A corrugated copper strip was provided at the junction of the guard tubes. This rendered the contact condition much more controllable and also eliminated the oscillating contact phenomenon.

The applied load was increased by specific increments according to the programme up to a maximum load of 9095 kg. (1400 load divisions). It was then decreased by constant decrement to a minimum load of 656 kg. (100 load divisions). As the experiment progressed smoothly, it was decided to proceed with another run of increasing loads. The last increment brought the load up to its maximum value of 9095 kg.

Experiment 4

Inserted objects - 3398 steel balls of 0.792 mm diameter

Specimens - En 8 steel

Heat flux meter - Armco iron, a separate part from the upper specimen.

The experiment was carried out according to the programme. No second run of increasing loads was made.

Experiment 5.

Inserted objects - 3388 steel balls of 0.792 mm diameter

Specimens - Armco iron

Heat flux meter - Armco iron, an integral part of the upper specimen.

The Armco iron is a softer material than the En 8 steel. Therefore if it is used as specimens, one can expect the areas of contact under the same applied load to be greater than those in experiment 4 whilst the number and the distribution of the contact points remain more or less the same.

Two cyclic runs of increasing loads and decreasing loads were carried out. At the end of the first cycle, it was intended to reduce the load to practically zero while the contact junctions, which could have been welded to the contact surfaces, remained unbroken. This would have enabled us to observe any difference in the heat transfer characteristics of the contact during the second cycle of loadings. Unfortunately the forces exerted from the specimen lifting mechanism must have broken these junctions for at zero load the electric indicating light gave the signal of no contact made. However, the programme was carried out as planned and the whole experiment took 85 days to complete.

Experiment 6

Inserted objects - 199 aluminium discs of 1.585 mm in diameter and 0.2 mm in thickness.

Specimens - Armco iron.

Heat flux meter - Armco iron, an integral part of the upper specimen.

No specific programme has been laid down for the experiment. A compressive load was applied with the object of bringing the upper and lower contact surfaces of the specimens into full contact with the discs. As it was not certain when this condition was reached, the magnitude of the applied load had to be increased gradually. At each load increment, thermocouple readings were taken both for the vacuum condition and for the gas conditions. From 45 to 55 divisions of load the changes of temperature readings were reasonably small. This load was then regarded as having compressed the specimens sufficiently to establish full contact with the discs. Nevertheless the applied load was increased steadily until it reached 80 divisions of load while temperature readings were taken. In this experiment the junction between the guard tubes had only two layers of aluminium foil inserted which worked very satisfactorily.

Experiment 7

Inserted objects - 199 aluminium discs of 1.193 mm in diameter and 0.2 mm in thickness.

Specimens - Armco iron.

Heat flux meter - Armco iron, an integral part of the upper specimen.

This experiment was carried out in the same way as in experiment 6. The maximum load applied was 625 kg.

6.3 Some phenomena observed during experiments

Some phenomena which have a connection with thermal contact problems have been observed during the experiments. They are described in the following sections.

6.3.1 Thermal switch effect.

As described earlier, the edges of the upper and lower guard tubes were shaped at 45 degrees so that they fitted onto each other snugly and formed a contact joint. In experiment 2, a mechanism was installed by which the upper guard tube could be pulled against the lower guard tube in order to change the contact areas and hence the contact resistance. During the experiment it was observed that the thermocouple readings along the guard tube fluctuated with the maximum magnitude of deviations at those points adjacent to the junction and with gradual decreasing magnitudes from the junction. The period of oscillation was fairly constant (app. 108 seconds) for all affected thermocouples, and there was a definite time lag between those situated at different distances from the junction. No such fluctuation of thermocouple reading was found to occur in the specimen column. The cause of this phenomenon can be explained as follows. The surface of a solid however carefully prepared is wavy and rough on a microscopic scale. When two nominally flat surfaces are brought together, it is well known that the topography of each surface is such as to make the actual area of contact very small in comparison with the apparent area of contact. Owing to a greater amount of heat transferred through the metallic junctions, the local temperature at those contact points on the upper surface would be lower than that at those areas where no actual contact was established. Some asperities on one surface might be just not touching those on the other surface. The parts with a higher temperature would now expand and consequently would

establish contact with the lower surface. This in turn would cause more heat to be transferred to the lower surface from these areas which would then cool down somewhat and contract. The whole cycle would repeat again. This process of thermal cyclic expansion and contraction between local points of two contact surfaces can be regarded as a thermal switch, where the heat flow is 'on' and 'off' through some local regions. Such a phenomenon is likely to exist in any contact joint unless metallic contact junctions are firmly established. With the insertion of soft aluminium foils at the junction between the guard tubes, the oscillation phenomenon was found to disappear.

6.3.2 Seizure of metallic junctions

The steel balls and the aluminium discs inserted at the contact interface for experiments were found to have adhered firmly to the contact surfaces after the experiment. A certain amount of force was needed to move them. This phenomenon is not unusual as adhesion of metal surfaces has been known in the study of friction and wear. It occurs when surface barriers such as the tarnish films and adsorbed gases are removed so that the underlying metals are brought into atomically close contact for the primary chemical bonds to take place. When this happens the two solids then become as one. In a thermal contact problem, the seizure of contact points may alter the normal approach of assessing contact areas especially when the problem takes place in a vacuum environment. This is because both high temperature and vacuum are the most effective agents for cleaning metal surfaces, and seizure of metallic junctions occurs very readily after the degradation of surface films. Further, high temperature, which provides an activation energy, produces atomic diffusions between the contact members, the result of which is a larger degree of plastic deformation at the contact

spots. For clean metallic surfaces, this leads to increase in contact areas which, once formed, will not diminish unless the recovering force is greater than the weld strength. It follows therefore that under such circumstances the thermal conductance of a contact cannot be simply related with the applied pressure; it involves also the interface temperature, the duration of operation and the application history of loads.

6.4 Analysis of test results

6.4.1 Thermal conductance measurements

First the thermocouple readings were converted into temperatures. They were then plotted against the distance according to the locations of the thermocouples using the upper and lower contact surfaces as the datum lines. The mean temperature at the contact interface and the temperature drop across the contact were determined by means of the extrapolation of the temperature distributions along the upper and lower specimens to these lines.

The temperature distribution along the heat flux meter enables the heat flux value to be determined according to equation (F-1). The radial heat transfer correction was then calculated using equation (F-7). The true heat flux passing through the contact per unit area was then obtained from equation (F-2). To compute the thermal conductance per each contact model we used the following expression

$$C_t = \frac{q_c \pi R^2}{T_1 - T_2} \qquad (6\text{-}1)$$

where R is the radius of the contact model cylinder and T_1 and T_2 are the

extrapolated contact surface temperatures of the upper and lower specimens respectively. Since the thermal conductivity of the specimens is known, we also used its mean value (with reference to temperature) together with the temperature gradient in the upper specimen to check the heat flux value which had been calculated from the temperature gradient distribution along the heat flux meter. They usually agreed very well. The maximum discrepancy was never more than 3%. Since the thermal conductivity of Armco iron at elevated temperatures has been carefully measured as a standard material, it was considered to give a more accurate result. Hence the first method was adopted through out the analysis for determining the heat flux value.

6.4.2 Electric conductance measurements

The current passed through the specimen column was measured by converting the potential drop across the standard resistor in the same circuit. From the potential tappings at each thermocouple position the potential drop between two adjacent positions was obtained. Since it was found that there was no appreciable change in potential in each solid specimen block, it was not necessary to extrapolate the potential tapping for the determination of the potential drop across the contact. Instead the difference of the average values of the three potential tappings from the three thermocouple locations adjacent to the contact surface of the upper specimen and of the lower specimen were used to represent the potential difference across the contact. When the current was reversed, the potential difference acquired a different value. The electric resistance of the contact was obtained by dividing the sum of the absolute values of the potential difference by the sum of the current when flowing in either direction. The electric conductance per contact model was calculated from

$$C_e = \frac{1}{R_e{}^n} \qquad (6\text{-}2)$$

where n is the number of solid objects inserted at the contact interface.

6.5 Test results

The test results are given in tables 6.2 - 6.11. The results of experiment 1 which was curtailed by the burn-out of the main heater, were plotted in figures 6.1, 6.2 and 6.3 designated for experiment 3. Figures 6.1 - 6.9 give a comparison between the test and the calculated results of thermal conductance of the contact models whereas figures 6.12 - 6.15 give the percentage of the fluid conductance to the total contact conductance based both on test and calculated results. The electric conductance of experiments 4 and 5 are plotted against the applied load and are shown in figures 6.10 and 6.11 respectively. The electric conductance measurements of experiment 3 do not follow any reasonable trend and have not been included in figure plotting. The discussion of the results will be given in chapter 7.

Table 6.2: Test results of experiment 1.

Load per contact model kg.	Test condition	Mean temperature at contact interface °C	Temperature drop across contact °C	Heat flux cal. sec^{-1}	Thermal conductance cal.sec^{-1} $^{o}C^{-1}$
zero	argon	174	176	.0189	.000108
	vacuum	199	222	.0158	.000071
	helium	138	55	.0241	.000436
0.376	helium	128	37.5	.0254	.000677
	vacuum	178	74	.0167	.000226
	argon	190	69	.0241	.00035
0.751	argon	133	55	.0246	.000447
	vacuum	136	61	.0219	.000359
	helium	134	35	.0254	.000726
1.128	helium	130	31.5	.0254	.000806
	vacuum	127.5	51	.0224	.000477
	argon	129.5	47	.0248	.000527
1.504	argon	127.5	43	.0243	.000565
	vacuum	119	42.5	.0212	.00050
	helium	131	31	.0264	.000852
1.870	helium	130	27	.0265	.000982
	vacuum	118.5	35	.0231	.00066
	argon	131.7	41.5	.0255	.00062
3.37	argon	120.5	31	.0244	.000787
	vacuum	113.7	30.3	.0216	.000713
	helium	122.5	23	.0262	.001133
4.48	helium	127.1	22.2	.0271	.00122
	vacuum	117.8	27.5	.0238	.000872
	argon	128	28.7	.0254	.000885

Experiment abandoned owing to main heater burn-out. Results plotted in figures 6.1, 6.2 and 6.3.

Table 6.3: Test results of experiment 2

Load per contact model kg.	Test condition	Mean temperature at contact interface ^{o}C	Temperature drop across contact ^{o}C	Heat flux $cal.sec^{-1}$	Thermal conductance $cal.sec^{-1}{}^{o}C^{-1}$
zero	argon	152	147	.0152	.000103
	vacuum	234	228	.0156	.000068
	helium	105	41	.0198	.000483
0.373	helium	107.9	34	.0229	.000675
	vacuum	139	64	.0222	.000346
	argon	107	45	.0195	.000432
0.745	argon	109	41	.0192	.000468
	vacuum	-	-	-	-
	helium	-	-	-	-

Experiment abandoned owing to an accident in the laboratory.

Table 6.4: Test results of experiment 3

Load per contact model kg.	Test condition	Mean temperature at contact interface ^{o}C	Temperature drop across contact ^{o}C	Heat flux $cal.sec^{-1}$	Thermal conductance $cal.sec.^{-1}{}^{o}C^{-1}$
Increasing load	argon	188	168	.0174	.000103
zero	vacuum	186	246	.00415	.0000169
	helium	k32	54	.0256	.000473
0.377	helium	132.7	46	.0284	.000616
	vacuum	103	54	.0162	.00030
	argon	137	62	.0251	.000405
0.753	argon	137.8	59.3	.0277	.000467
	vacuum	123.2	53.5	.0232	.000434
	helium	133.5	35	.0293	.000835
1.130	helium	131	34	.0301	.000885
	vacuum	124	48	.0250	.00052
	argon	136.2	52	.0281	.00054
1.504	argon	134	45.2	.0280	.00059
	vacuum	125	44	.0255	.00058
	helium	131.6	32.8	.0294	.000895
2.253	helium	131.0	30.2	.0291	.000965
	vacuum	120.5	38	.0258	.00068
	argon	128.2	37.5	.0276	.000735
3.001	argon	127.7	35.5	.0286	.000806
	vacuum	116.1	34.7	.0249	.000718
	helium	119.5	25	.028	.00112
4.494	helium	124.6	23.0	.0287	.00125
	vacuum	114	28	.0248	.000887
	argon	121.2	28.5	.0270	.000945
5.988	argon	120	26	.0275	.00105
	vacuum	108.2	24.7	.0243	.000985
	helium	123.7	20.3	.0274	.00135
7.475	helium	125.2	19.5	.0279	.00143
	vacuum	107	21.5	.0237	.0011
	argon	118.2	21.4	.0234	.00109

Table 6.4 contd.

8.953	argon	117.7	21	.0256	.00121
	vacuum	108.5	20.5	.0240	.00117
	helium	120.5	17.5	.0276	.00157
10.47	helium	120.8	17.0	.0274	.00162
	vacuum	109.6	20	.0249	.00125
	argon	118	20.0	.0265	.00132
1st decreasing load 8.953	argon	117.5	20	.0266	.00133
	vacuum	110.2	19.5	.0247	.00127
	helium	118.0	18	.0280	.00155
7.475	helium	118.5	17.5	.0278	.00158
	vacuum	105.5	19	.0243	.00128
	argon	117.5	19	.0256	.00135
5.988	argon	115	20	.0263	.00132
	vacuum	107	20	.0249	.00125
	helium	117	18	.0283	.00157
4.494	helium	117.5	19	.0281	.00148
	vacuum	105	20.5	.0237	.00116
	argon	114	21	.0257	.00122
3.001	argon	116.5	23	.0258	.00112
	vacuum	107.5	25	.0245	.00098
	helium	117.9	19.8	.0274	.00138
1.504	helium	117.5	21	.0271	.00128
	vacuum	116	29	.0254	.000875
	argon	121.7	27.5	.0270	.000981
.753	argon	118.9	30.2	.0252	.000838
	vacuum	118.5	32	.0250	.00078
	helium	117.3	22.6	.0265	.00117
2nd increasing load 1.504	helium	116	19.5	.0255	.001305
	vacuum	118	29.6	.0261	.000882
	argon	116.3	26.2	.0253	.000967

Table 6.4 contd.

3.001	argon	119	23.7	.0261	.00110
	vacuum	118	24	.0248	.00103
	helium	118	20	.0276	.00138
4.494	helium	119	18	.0272	.00151
	vacuum	110	20.8	.0242	.00116
	argon	119.1	21.8	.0264	.00121
5.988	argon	118.2	20	.0263	.00132
	vacuum	110	20	.0245	.00122
	helium	120.5	17.8	.0275	.00154
7.475	helium	119.2	17.5	.0276	.00158
	vacuum	111	19	.0244	.00128
	argon	118.5	19	.0254	.00134
8.953	argon	118	18.6	.0253	.00136
	vacuum	105.8	18.5	.0235	.00127
	helium	118.5	17.6	.0277	.00157
10.43	helium	119	17.5	.0278	.00159
	vacuum	110.8	19.5	.0244	.00125
	argon	116.5	19	.0260	.00136

Table 6.5: Test results of experiment 4

Load per contact model kg.	Test condition	Mean temperature at contact interface °C	Temperature drop across contact °C	Heat flux cal.sec^{-1}	Thermal conductance cal.sec.$^{-1}$°C^{-1}
Increasing load	helium	124	124	.00367	.0000297
zero	vacuum	189	215	.000535	.0000025
	argon	119	185	.000603	.00000326
0.0483	argon	116	38	.00546	.000144
	vacuum	118	162	.00107	.0000066
	helium	118	37	.00535	.000145
0.0966	helium	105	19	.00521	.000274
	vacuum	109	41.5	.00421	.000102
	argon	115	38	.00525	.000138
0.193	argon	115	29.5	.00531	.000181
	vacuum	99	25	.0045	.00018
	helium	115	18.5	.00645	.000348
0.290	helium	117.5	17.5	.00646	.00037
	vacuum	109	26.5	.00534	.000202
	argon	116	24.2	.00602	.000249
0.386	argon	118	24	.00608	.000252
	vacuum	118.5	27.5	.00543	.000197
	helium	116.5	16	.00625	.00039
0.578	helium	115.7	13.5	.00626	.000464
	vacuum	117.8	21.3	.00596	.00028
	argon	123.5	22	.00626	.000285
0.770	argon	120.5	19	.00632	.000332
	vacuum	119.5	19	.00584	.000308
	helium	115.2	13.5	.00615	.000455
1.153	helium	114.2	11.5	.00623	.000542
	vacuum	113.5	17	.00581	.000343
	argon	118	16	.00637	.000398

Table 6.5 contd.

1.537	argon	113	13.7	.00614	.000449
	vacuum	112.2	13.5	.00588	.000435
	helium	114.7	10.5	.00646	.000616
1.918	helium	116	10	.00657	.000657
	vacuum	111.7	12.5	.00594	.000475
	argon	112	13.4	.00630	.00047
2.298	argon	111	13	.0065	.00050
	vacuum	105	12	.00585	.000488
	helium	112	9.5	.00636	.00067
2.677	helium	112	9	.00636	.000708
	vacuum	111	12	.00626	.000522
	argon	112.5	11	.00609	.000552
decreasing load 2.298	argon	112	11.5	.00634	.00055
	vacuum	106	11.5	.00605	.000525
	helium	111.5	9	.00645	.000718
1.918	helium	113.5	9	.00645	.000718
	vacuum	111.7	11.5	.00615	.000535
	argon	116	12.5	.00665	.000532
1.153	argon	110.2	12	.00622	.000518
	vacuum	113.2	12.5	.00593	.000475
	helium	114.5	10	.00656	.000656
0.770	helium	115.2	11 .5	.00665	.000578
	vacuum	113.2	14.5	.00596	.000411
	argon	115.5	13.4	.00638	.000476
0.386	argon	115.7	15.5	.00631	.000407
	vacuum	115.5	17	.00615	.000362
	helium	112.4	12	.00638	.00053

Table 6.6: Test results of experiment 5

Load per contact model kg.	Test condition	Mean temperature at contact interface ^{o}C	Temperature drop across contact ^{o}C	Heat flux $cal.sec^{-1}$	Thermal conductance $cal.sec^{-1}{}^{o}C^{-1}$
1st increasing load	argon	133.2	202.5	.00139	.0000069
	vacuum	134.2	205.5	.000346	.0000017
zero	helium	131.2	132.5	.0043	.0000325
0.097	helium	121.7	25.5	.00902	.000354
	vacuum	147	74	.0081	.000109
	argon	140.7	60.5	.00865	.000143
0.291	argon	134	41	.00912	.000229
	vacuum	134.2	44	.00895	.000203
	helium	135	26	.01046	.000403
0.484	helium	132.5	23	.01072	.000466
	vacuum	137	38	.00984	.000258
	argon	134.2	34	.0101	.000296
0.653	argon	135.6	30	.0106	.000354
	vacuum	134	31.2	.01085	.000349
	helium	133.9	21.3	.0107	.000502
0.869	helium	134.2	19.5	.01089	.000557
	vacuum	133.6	26.7	.01045	.000392
	argon	134.5	25	.01015	.000406
1.061	argon	130	22	.01033	.00047
	vacuum	134.3	24.3	.01064	.000437
	helium	135.2	17.5	.01102	.00063
1.253	helium	133	16	.01106	.00069
	vacuum	136	24	.0104	.000434
	argon	131.5	21	.01055	.000502
1.445	argon	131.8	19.6	.01064	.000543
	vacuum	134.3	19.4	.01063	.000548
	helium	132	14.5	.0111	.000765

Table 6.6 contd.

1.637	helium	134.5	15	.01114	.000744
	vacuum	138	19	.01082	.00057
	argon	131.5	18	.01092	.000607
1.828	argon	132.8	16.3	.01082	.000665
	vacuum	134.8	17.5	.01115	.000639
	helium	130.5	15	.01114	.000743
2.019	helium	131.5	13.7	.01107	.000807
	vacuum	135	18	.0109	.000606
	argon	131.2	15.5	.01089	.000702
2.209	argon	132.6	15.3	.01089	.000712
	vacuum	135.3	17.7	.01096	.00062
	helium	128	13.5	.0108	.000795
2.399	helium	128.2	12	.01073	.000894
	vacuum	134	16	.01089	.000677
	argon	131.7	13	.01078	.00083
2.589	argon	129.5	13	.01092	.000842
	vacuum	133.5	14	.0109	.00078
	helium	128.8	12	.01075	.000894
2.778	helium	125.7	11	.01075	.00097
	vacuum	135	14	.01101	.000787
	argon	130.5	13	.01092	.00084
1st decreasing load	argon	133.5	13	.01087	.000836
	vacuum	135.2	14	.011	.000785
2.399	helium	126.6	11.2	.01075	.00096
2.019	helium	127	11	.01078	.000976
	vacuum	134	14	.01087	.000775
	argon	129.2	13	.01073	.000829
1.637	argon	130.6	12.8	.01071	.000836
	vacuum	133.3	14.8	.0108	.00073
	helium	129.5	13	.01097	.000842
1.253	helium	131.7	12.5	.01097	.000875
	vacuum	131	15	.01055	.000703
	argon	131.1	13.8	.0108	.000782

Table 6.6 contd.

0.869	argon	131.7	13.4	.01078	.000803
	vacuum	141.8	15.5	.01103	.000712
	helium	127	14	.0107	.000764
0.486	helium	127.8	14.5	.01075	.000741
	vacuum	129.2	16.5	.0101	.000612
	argon	122.8	16.5	.00984	.000598
zero	argon	127.7	201	.00116	.00000575
	vacuum	113.8	188.7	.000193	.00000101
	helium	114.8	125.5	.00397	.0000316
Weldings at contact junctions were broken by the lifting device when the applied load was reduced to zero.					
2nd increasing load 0.097	helium	116.2	27.7	.00848	.000306
	vacuum	133	66	.00686	.000104
	argon	116.8	50.5	.00704	.000139
0.486	argon	132.8	32.5	.0101	.000311
	vacuum	132.5	37	.00986	.000267
	helium	128.2	22.5	.0105	.000466
0.879	helium	128	18	.01068	.000592
	vacuum	135.2	25.5	.01015	.000398
	argon	128.5	23	.0101	.000439
1.253	argon	130.7	19.5	.0102	.000522
	vacuum	133.9	20.2	.01041	.000515
	helium	130.5	15	.0108	.000718
1.637	helium	131.2	14	.011	.000785
	vacuum	139.4	18.8	.0109	.00059
	argon	133	16	.01067	.000665
2.019	argon	133.8	14.5	.0106	.00073
	vacuum	138.2	16.4	.0109	.000664
	helium	129.8	12.5	.01065	.000855

Table 6.6 contd.

2.399	helium	128.2	11.5	.01068	.000928
	vacuum	140.5	13	.01082	.000834
	argon	135.4	14	.01064	.000755
2.778	argon	138	13	.0108	.00083
	vacuum	140	13	.0109	.00083
	helium	132.5	11	.0106	.000962
2nd decreasing load 2.399	helium	132.5	11	.0106	.000962
	vacuum	140.2	12.5	.0107	.000855
	argon	138.5	12	.01074	.000896
2.019	argon	134.2	12.5	.0107	.000856
	vacuum	137.9	14.2	.01084	.000764
	helium	129.2	11	.01055	.000945
1.637	helium	130.2	11	.01055	.000945
	vacuum	139.1	14.3	.01086	.000760
	argon	132.6	12.8	.01058	.000826
1.253	argon	133.1	12.7	.01052	.00083
	vacuum	132.2	14.5	.01037	.000716
	helium	130.2	11.5	.01066	.00093
0.869	helium	130.2	11.5	.01064	.000924
	vacuum	139.8	15.5	.01087	.000726
	argon	130	14	.01016	.000726
0.484	argon	137.8	16.5	.0105	.000616
	vacuum	133.5	17	.010	.000587
	helium	129	12	.01043	.00087
0.097	helium	130.5	16	.0102	.000637
	vacuum	135.1	29.7	.00848	.000285
	argon	127	26	.00901	.000345
3rd increasing load 0.484	argon	131.8	17.7	.0101	.00057
	vacuum	133.2	17.7	.00989	.000559
	helium	129.5	13	.0104	.00080

Table 6.7: Test results of experiment 6

Load per contact model kg.	Test condition	Mean temperature at contact interface ^{o}C	Temperature drop across contact ^{o}C	Heat flux $cal.sec^{-1}$	Thermal conductance $cal.sec^{-1}{}^{o}C^{-1}$	calculated value from simplified method	calculated value from analytical method
1.320	argon	128	22	0.175	.00795	-	-
	vacuum	122	21	0.167	.00795	-	-
	helium	119	18.8	0.171	.0091	-	-
1.650	helium	118	16	0.168	.0106	.01	.0101
	vacuum	131	19	0.164	.00864	.00928	.00928
	argon	127	18	0.173	.0096	.00939	.0094
1.815	argon	128	14.5	0.170	.0117	-	-
	vacuum	130.5	17	0.170	.010	-	-
	helium	119	10	0.169	.0169	-	-
2.64	argon	122	8.5	0.168	0.0198	-	-
	vacuum	126.5	11	0.166	.0151	-	-
	helium	120	7.5	0.174	.0232	-	-

Only four sets of results are given here.

Table 6.8: Test results of experiment 7

Load per contact model kg.	Test condition	Mean temperature at contact interface ^{o}C	Temperature drop across contact ^{o}C	Heat flux $cal.sec^{-1}$	Thermal conductance $cal.sec^{-1}{}^{o}C^{-1}$	calculated value from simplified method	calculated value from analytical method
1.32	argon	120	19	.158	.0083	.00665	.00669
	vacuum	128	20	.148	.0074	.00655	.00655
	helium	119	13	.162	.0125	.00725	.0073
1.65	helium	123	11	.167	.0152	-	-
	vacuum	137.8	17.5	.152	.00866	-	-
	argon	132	15	.163	.0108	-	-
3.14	helium	125	10	.173	.0173	-	-
	vacuum	138	18	.150	.00832	-	-
	argon	135	19	.157	.00826	-	-

Only three sets of results are given here. It can be seen that the initial applied load of 1.32 kg. is obviously too high.

Table 6.9: Experiment 3 - electric conductance measurement

Load per contact model kg.	Electric current amp.	Potential drop across contact volt	Electric conductance (Ω^{-1})
0.377	1.50854	.12764	.01355
0.753	1.57439	.04655	.03879
1.130	1.58493	.03294	.05517
1.504	1.59503	.02032	.09001
2.253	1.59841	.01627	.11271
Contact was likely to have been disturned owing to fixing a thermo-couple at this stage of the experiment.			
3.001	1.54871	.07086	.02507
4.494	1.56924	.03968	.04535
5.988	1.58247	.02322	.07805
7.475	1.58382	.01577	.11517
8.953	1.58689	.01144	.15905
10.430	1.58317	.00763	.23801
8.953	1.57842	.00754	.24016
7.475	1.57847	.00825	.21952
5.988	1.57566	.00885	.20427
4.494	1.57196	.00985	.18305
2nd increasing load			
3.001	1.55109	.02560	.06948
5,988	1.55783	.02047	.08727
7.475	1.55371	.01858	.09587
8.953	1.55261	.01752	.10165
10.430	1.55035	.01574	.1130

These results are not plotted as they do not seem to follow any reasonable order.

Table 6.10 Experiment 4 - electric conductance measurement

Load per contact model kg.	Electric current amp.	Potential drop across contact volt	Electric conductance (Ω^{-1})
0.048	1.53876	.07141	.00638
0.097	1.36865	.30679	.00132
0.193	1.45826	.19199	.00225
0.290	1.48658	.14920	.00295
0.386	1.50741	.11764	.00379
0.578	1.5333	.08337	.00545
0.770	1.54827	.06487	.00707
1.153	1.56123	.04519	.01024
1.537	1.57100	.03358	.01386
1.918	1.57171	.02678	.01739
2.298	1.56841	.02431	.01911
2.677	1.55381	.01964	.02345
2.298	1.54691	.02092	.02231
1.918	1.52352	.02253	.02013
1.153	1.52195	.02661	.01695
0.770	1.48999	.03687	.01197
0.386	1.48251	.05667	.00775

Table 6.11: Experiment 5 - electric conductance measurement

Load per contact model kg.	Electric current amp.	Potential drop across contact volt	Electric conductance (Ω^{-1})
0.097	1.46897	.17945	.00242
0.291	1.5396	.09206	.00494
0.484	1.56175	.08055	.00572
0.653	1.56124	.07336	.0063
0.869	1.56167	.07076	.00652
1.061	1.56895	.06848	.00675
1.253	1.56760	.06672	.00693
1.445	1.56635	.06427	.00718
1.637	1.56572	.06412	.00722
1.828	1.56251	.06253	.00736
2.019	1.56727	.05996	.00772
2.209	1.56055	.05760	.0080
2.399	1.56922	.05731	.0081
2.589	1.56426	.05696	.00857
2.778	1.56962	.05583	.00832
2.399	1.56583	.055715	.00832
2.019	1.56555	.05672	.00815
1.637	1.56013	.05844	.00788
1.253	1.56117	.06184	.00745
0.869	1.56128	.06570	.0070
0.4835	1.55183	.07478	.00614
Weldings at the contact junctions were broken by the lifting device when the applied load was reduced to zero.			
0.0969	1.29668	.38366	.00101
0.484	1.27476	.41345	.00091
0.869	1.31955	.35878	.00108
1.253	1.34829	.32834	.00122

Table 6.11 contd.

1.637	1.37616	.28798	.00141
2.019	1.40243	.25661	.00162
2.399	1.42617	.2152	.00196
2.778	1.45597	.18044	.00239
2.399	1.45752	.18187	.00237
2.019	1.4680	.18482	.00235
1.637	1.44788	.19295	.00222
1.253	1.42698	.21350	.00201
0.869	1.41697	.22947	.00183
0.484	1.38046	.27455	.00148
0.097	1.30291	.37398	.00103
0.484	1.30333	.37100	.00104

6.6 Sources of error

An examination of the experimental process gives the following possibility of errors involved in the measurements presented in the previous section.

1. Temperature measurements - The thermocouple readings were converted according to the e.m.f. - temperature calibration carried out by the National Physical Laboratory which was stated to give an accuracy of $\pm$ 1°C. An inhomogeneity in the wires was found to be equivalent to a maximum of 0.8°C from the mean readings. The combination of these deviations for the worst possible condition may amount to a large percentage of error in cases where the contact temperature drop is relatively small. But this is unlikely to happen and it is considered that the maximum error can well be within 5%.

2. On account of the large amount of insulation surrounding the apparatus, a long time was usually required for a steady state condition to be reached. It was decided to record readings when a drift was reduced to about 0.1°C per minute. The absolute temperature values could be several degrees from the steady state temperature; the relative temperature difference between the contact surfaces, however, should not be anything appreciable.

3. Heat transfer by conduction of thermocouple wires. The thermal conductivity is 0.0205 cal. cm^{-1} sec^{-1} $^{o}c^{-1}$ and 0.054 cal. cm^{-1} sec^{-1} $^{o}c^{-1}$ for nichrome and Eureka respectively. The amount of heat transmission along the wires from the junction to the ceramic supporting rod is about 1×10^{-5} cal. sec^{-1} per 1°C temperature difference. Since the temperature difference at any one location between the specimen column and the guard tubes was never more than 30°C in a few instances in experiments 1 and 2 (generally the maximum temperature difference never exceeded 10°C for vacuum and low load conditions). This amount of heat transfer is quite negligible.

4. Heat transfer by conduction of the insulating powder is also small. Based

on a 30°C temperature difference a radial heat transfer amounts to about 0.021 cal. sec^{-1} cm^{-2}. This is equivalent to about 8% of the total heat flux for the worst case.

5. However careful one may be in determining the temperature drop across the contact by means of the graphical method of extrapolating the temperature distribution along the specimens, there is always some degree of error involved. A difference of 0.5°C may amount to about 5% in those cases of high applied loads. To eliminate the error larger scales were used in plotting the temperature readings.

6. The applied load readings were based on the maker's calibration of the machine. It is reasonable to say that an error of 2-3% is quite possible.

7. The uniform distribution of the applied load over the contact surface may not be perfect especially in the low load cases. If the load is not evenly distributed, we expect the contact areas to be non-uniform as well. The circumferential temperature readings showed that the maximum variation was about 2%.

8. In taking electrical conductance measurements, the current flow became extremely unstable at very low load conditions. When the applied load was more than 1000 kg. it became fairly stable. The measurements obtained did not appear at all satisfactory. This will be discussed in the next chapter.

Among the possibilities of error, items 1 and 5 attribute the largest percentage. In the worst possible case these may amount to about 10%.

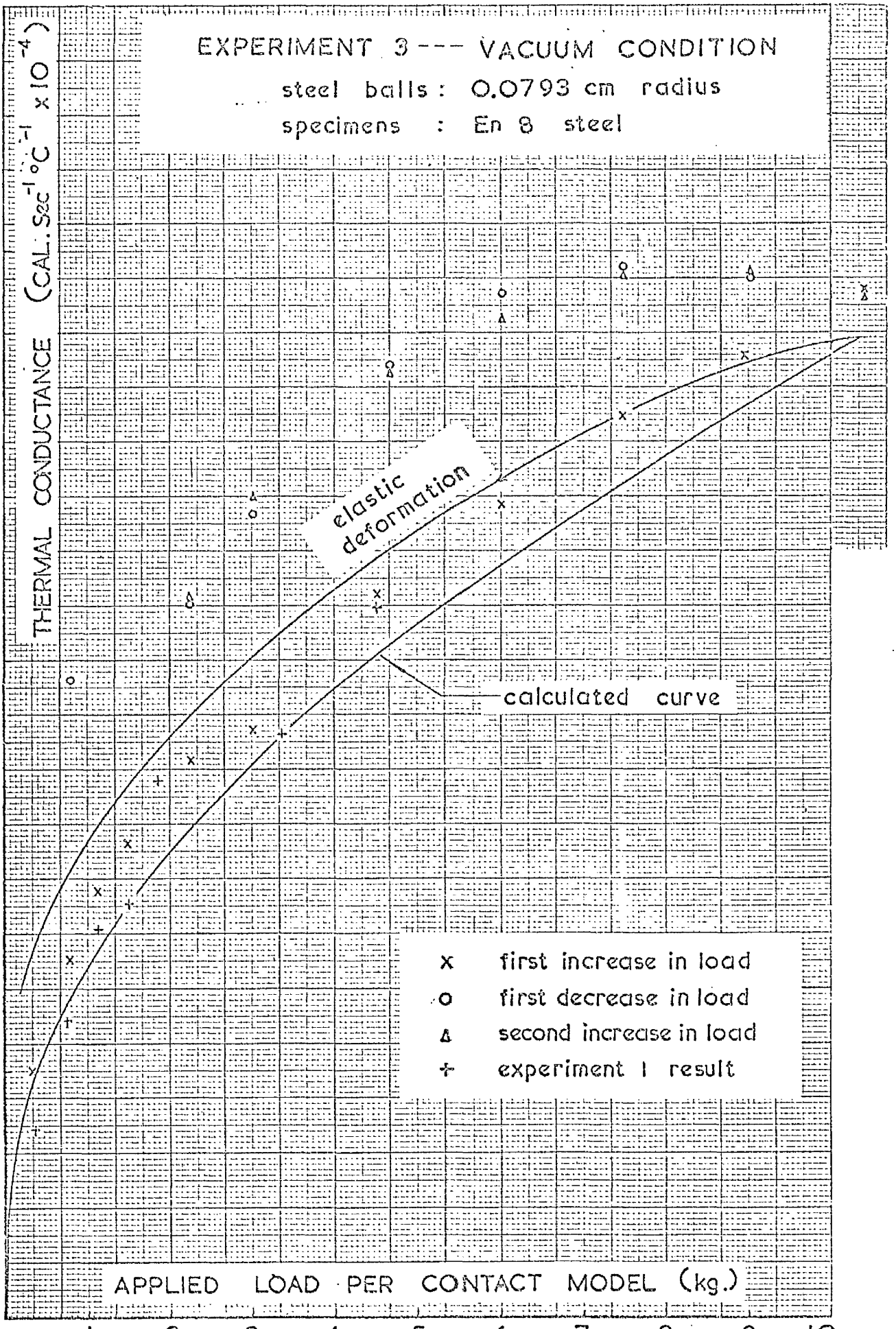
EXPERIMENT 3 --- VACUUM CONDITION
steel balls : 0.0793 cm radius
specimens : En 8 steel
THERMAL CONDUCTANCE (CAL. Sec^{-1} °C^{-1} x 10^{-4})
APPLIED LOAD PER CONTACT MODEL (kg.)
elastic deformation
calculated curve
x first increase in load
o first decrease in load
Δ second increase in load
+ experiment 1 result
1
2
3
4
5
6
7
8
9
10
11
12
13
14

FIG. 6-1

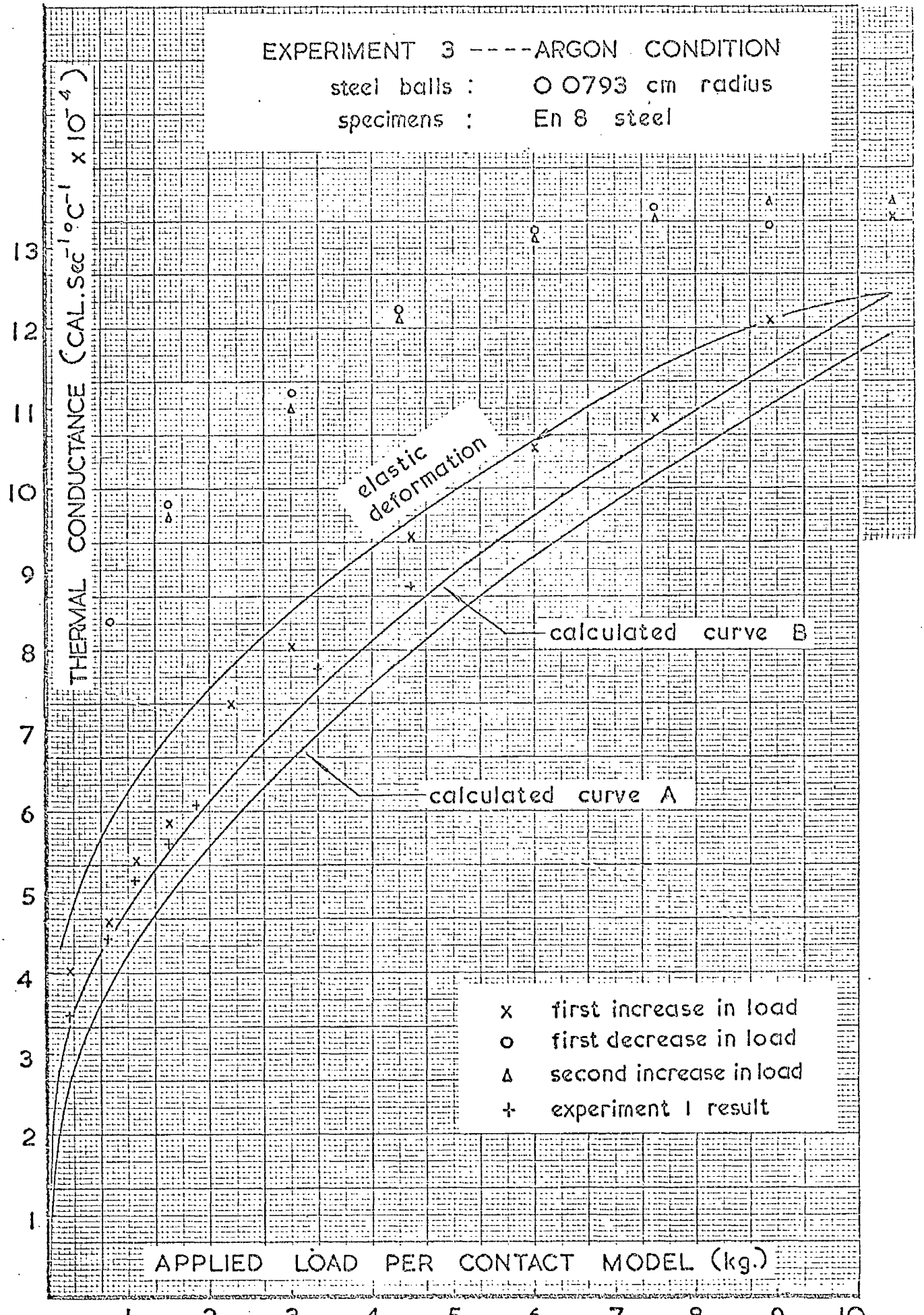
EXPERIMENT 3 ----ARGON CONDITION
steel balls : O 0793 cm radius
specimens : En 8 steel
THERMAL CONDUCTANCE (CAL.Sec⁻¹°C⁻¹ x 10⁻⁴)
APPLIED LOAD PER CONTACT MODEL (kg.)
elastic deformation
calculated curve B
calculated curve A
x first increase in load
o first decrease in load
Δ second increase in load
+ experiment 1 result
1
2
3
4
5
6
7
8
9
10
11
12
13

FIG. 6 · 2

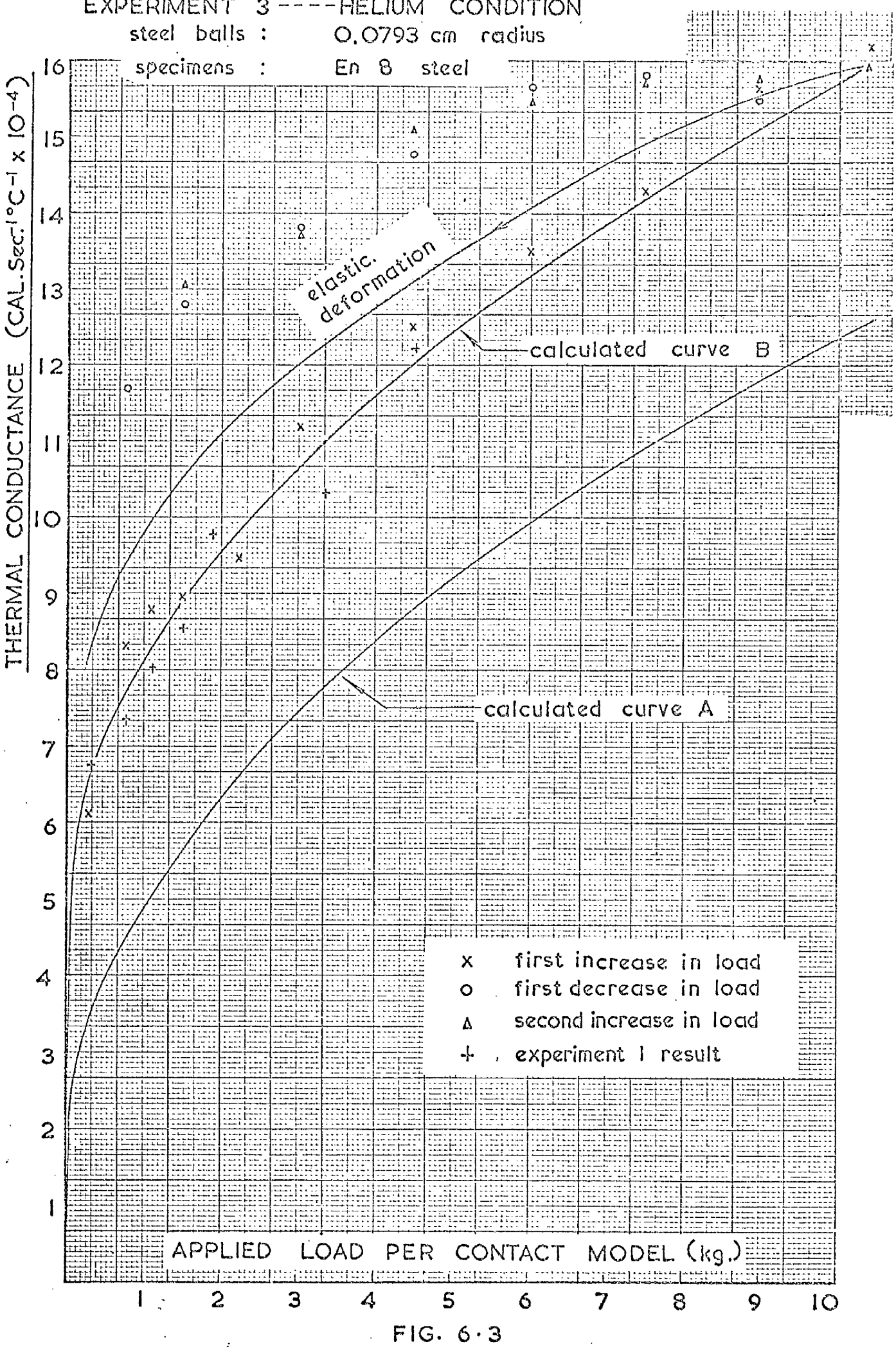
EXPERIMENT 3 ----HELIUM CONDITION
steel balls : 0.0793 cm radius
specimens : En 8 steel
THERMAL CONDUCTANCE (CAL. Sec⁻¹°C⁻¹ x 10⁻⁴)
elastic deformation
calculated curve B
calculated curve A
x first increase in load
o first decrease in load
Δ second increase in load
+ experiment 1 result
APPLIED LOAD PER CONTACT MODEL (kg.)
1 2 3 4 5 6 7 8 9 10
1 2 3 4 5 6 7 8 9 10 11 12 13 14 15 16

FIG. 6·3

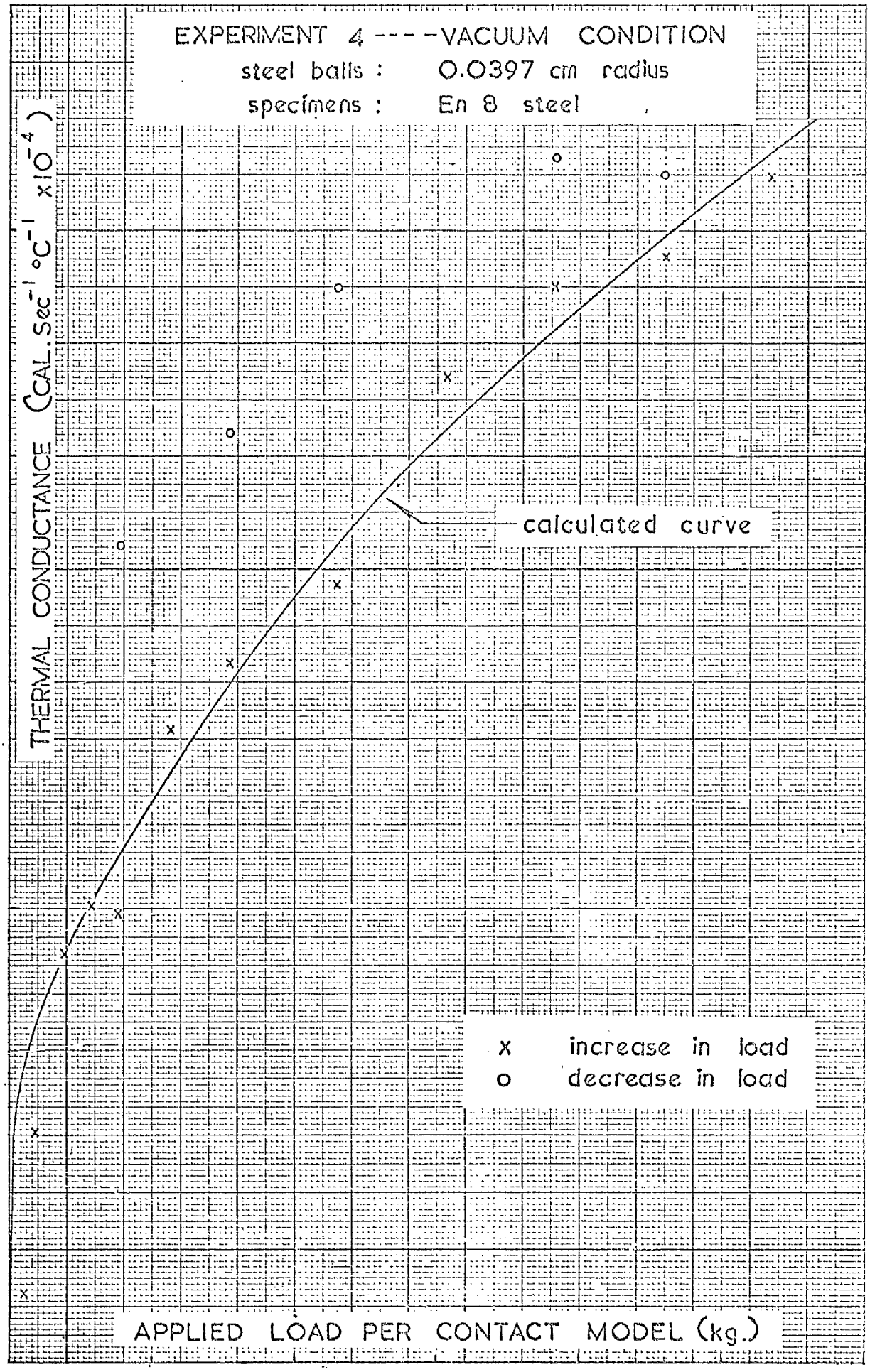
EXPERIMENT 4 ----VACUUM CONDITION
steel balls : 0.0397 cm radius
specimens : En 8 steel
THERMAL CONDUCTANCE (CAL. Sec^{-1} °C^{-1} x10^{-4})
5
4
3
2
1
calculated curve
x increase in load
o decrease in load
APPLIED LOAD PER CONTACT MODEL (kg.)
0·5
1
1·5
2
2·5
3

FIG. 6·4

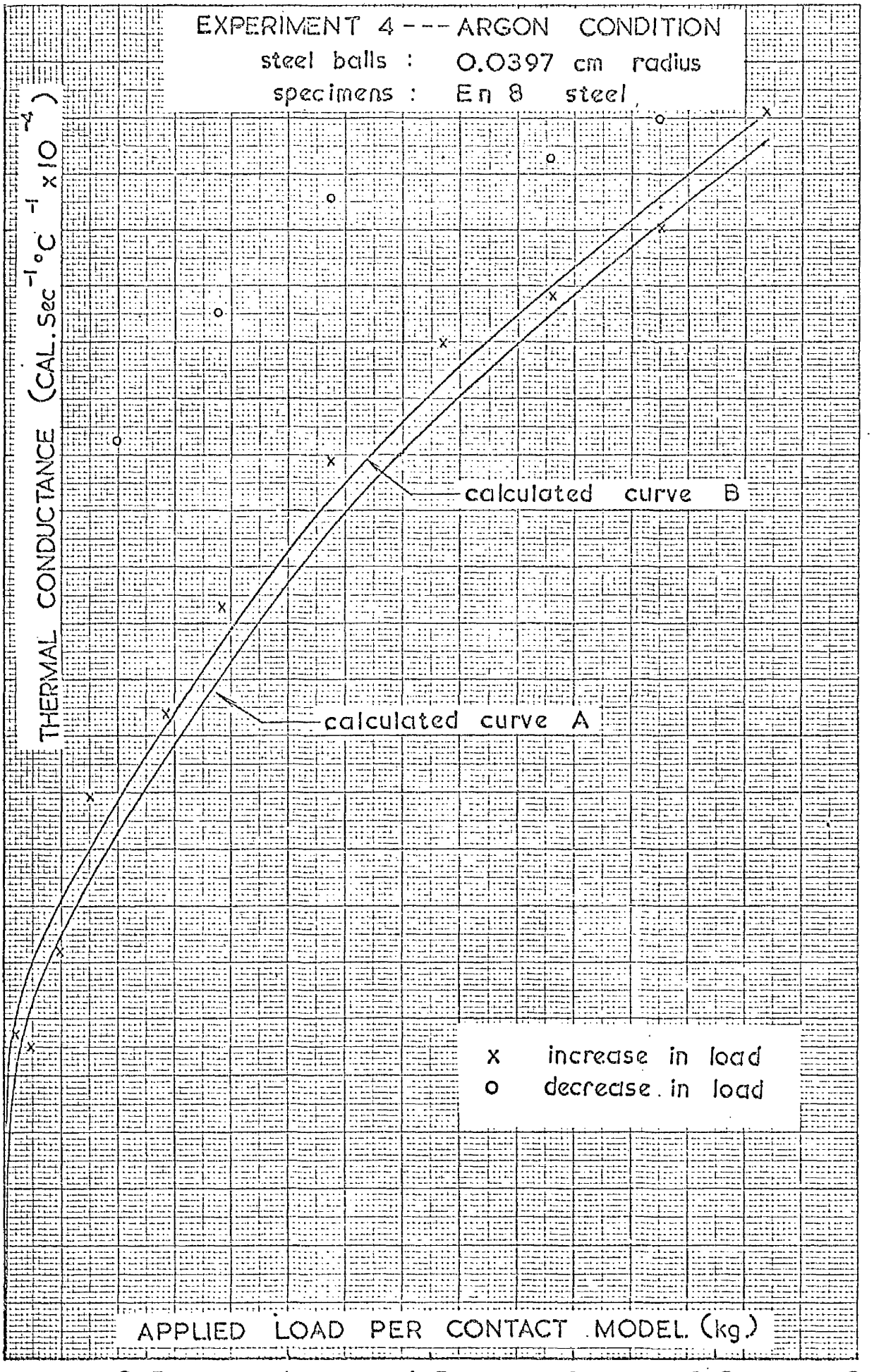
EXPERIMENT 4 --- ARGON CONDITION
steel balls : 0.0397 cm radius
specimens : En 8 steel
THERMAL CONDUCTANCE (CAL. Sec^{-1} °C^{-1} x 10^{-4})
5
4
3
2
1
calculated curve B
calculated curve A
x increase in load
o decrease in load
APPLIED LOAD PER CONTACT MODEL (kg.)
0·5
1
1·5
2
2·5
3

FIG. 6·5

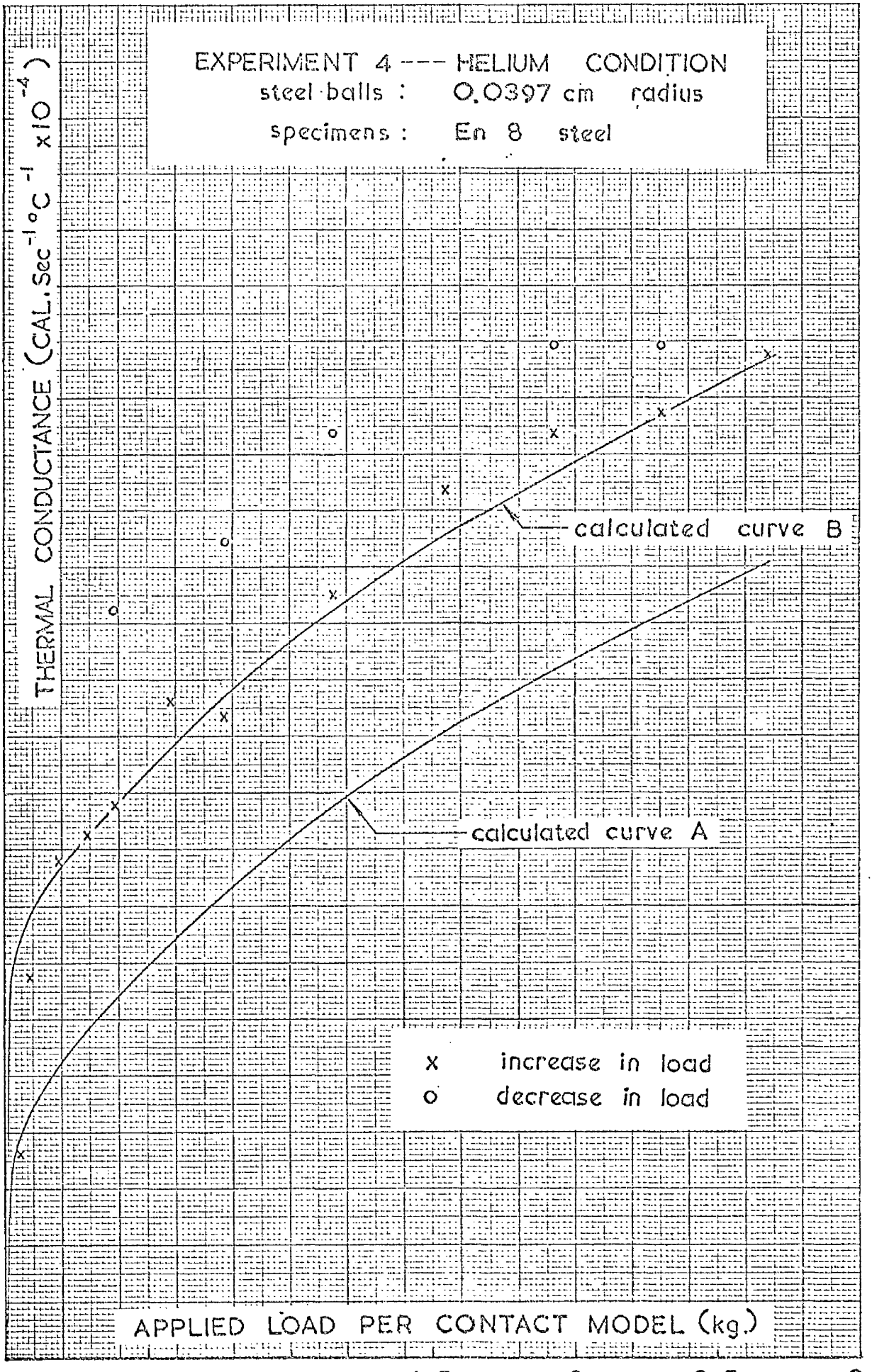
EXPERIMENT 4 --- HELIUM CONDITION
steel balls : 0.0397 cm radius
specimens : En 8 steel
THERMAL CONDUCTANCE (CAL. Sec^{-1} °C^{-1} x10^{-4})
8
7
6
5
4
3
2
1
calculated curve B
calculated curve A
x increase in load
o decrease in load
APPLIED LOAD PER CONTACT MODEL (kg.)
0·5
1
1·5
2
2·5
3

FIG. 6·6

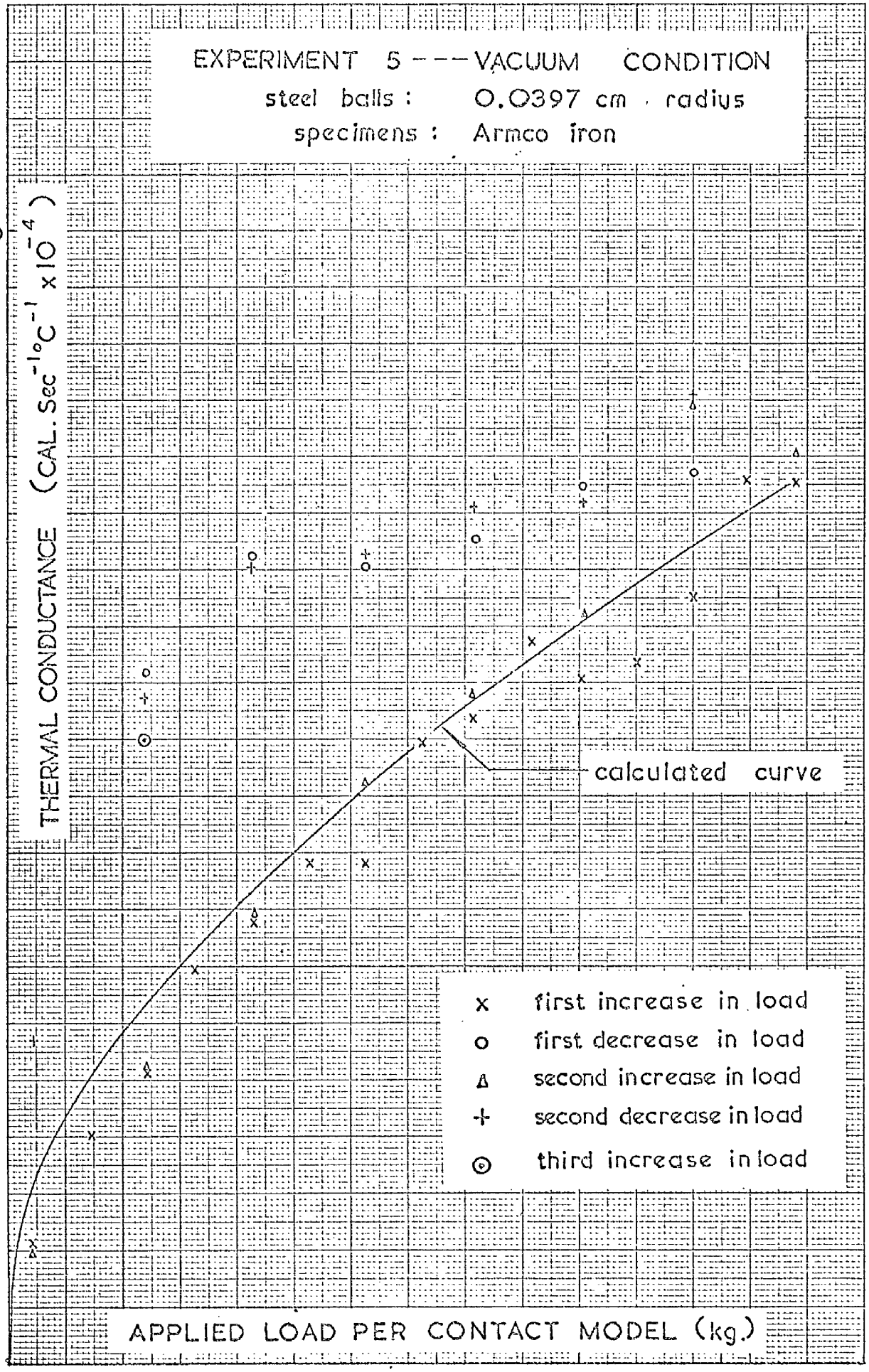
EXPERIMENT 5 --- VACUUM CONDITION
steel balls : 0.0397 cm . radius
specimens : Armco iron
THERMAL CONDUCTANCE (CAL. Sec^{-1}°C^{-1} x 10^{-4})
10
9
8
7
6
5
4
3
2
1
calculated curve
x first increase in load
o first decrease in load
Δ second increase in load
+ second decrease in load
⊙ third increase in load
APPLIED LOAD PER CONTACT MODEL (kg.)
0·5
1
1·5
2
2·5
3

FIG. 6·7

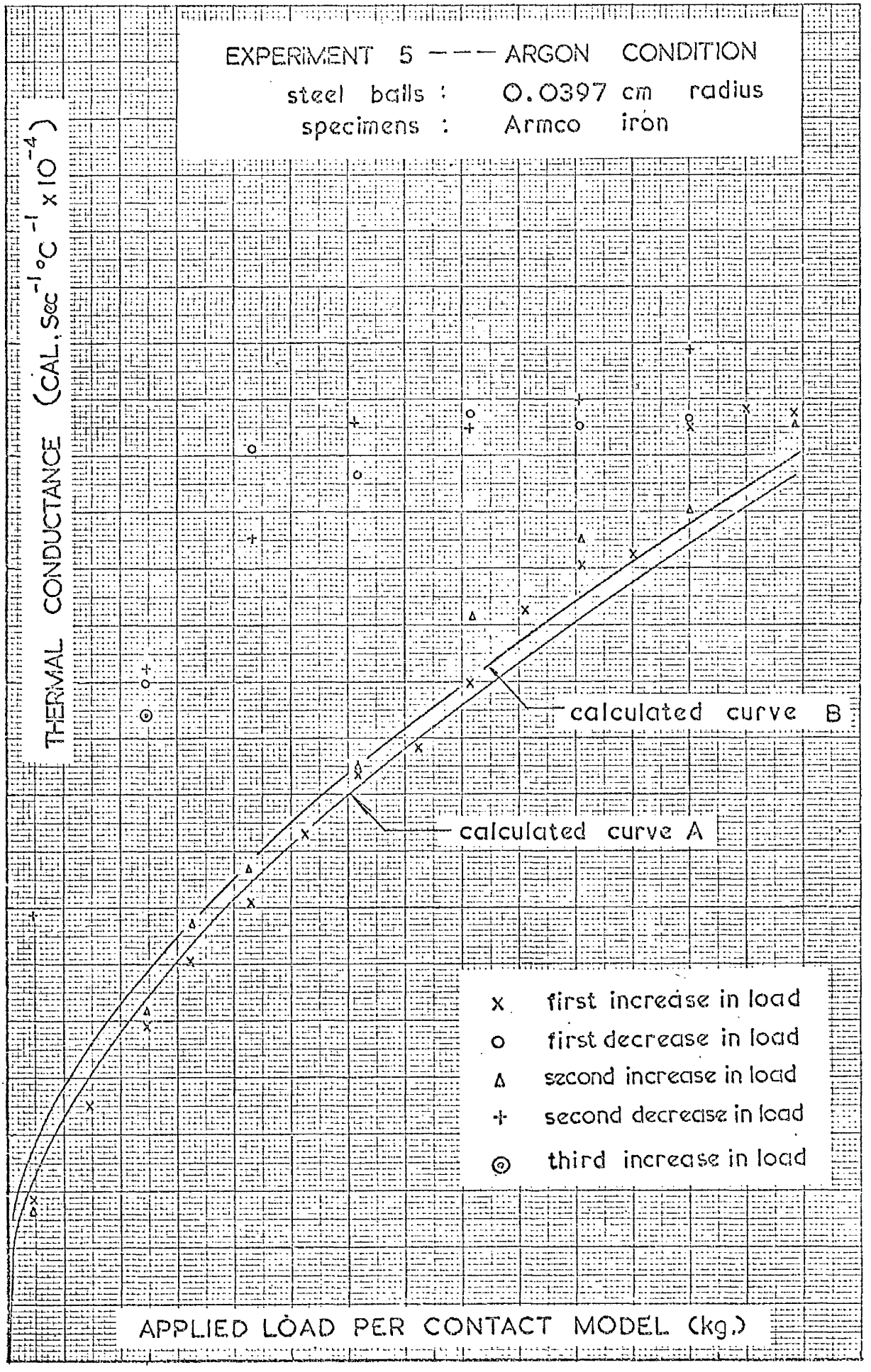
EXPERIMENT 5 --- ARGON CONDITION
steel balls : 0.0397 cm radius
specimens : Armco iron
THERMAL CONDUCTANCE (CAL. Sec^{-1} °C^{-1} x 10^{-4})
10
9
8
7
6
5
4
3
2
1
calculated curve B
calculated curve A
x first increase in load
o first decrease in load
Δ second increase in load
+ second decrease in load
⊙ third increase in load
APPLIED LOAD PER CONTACT MODEL (kg.)
0.5
1
1.5
2
2.5
3

FIG. 6·8

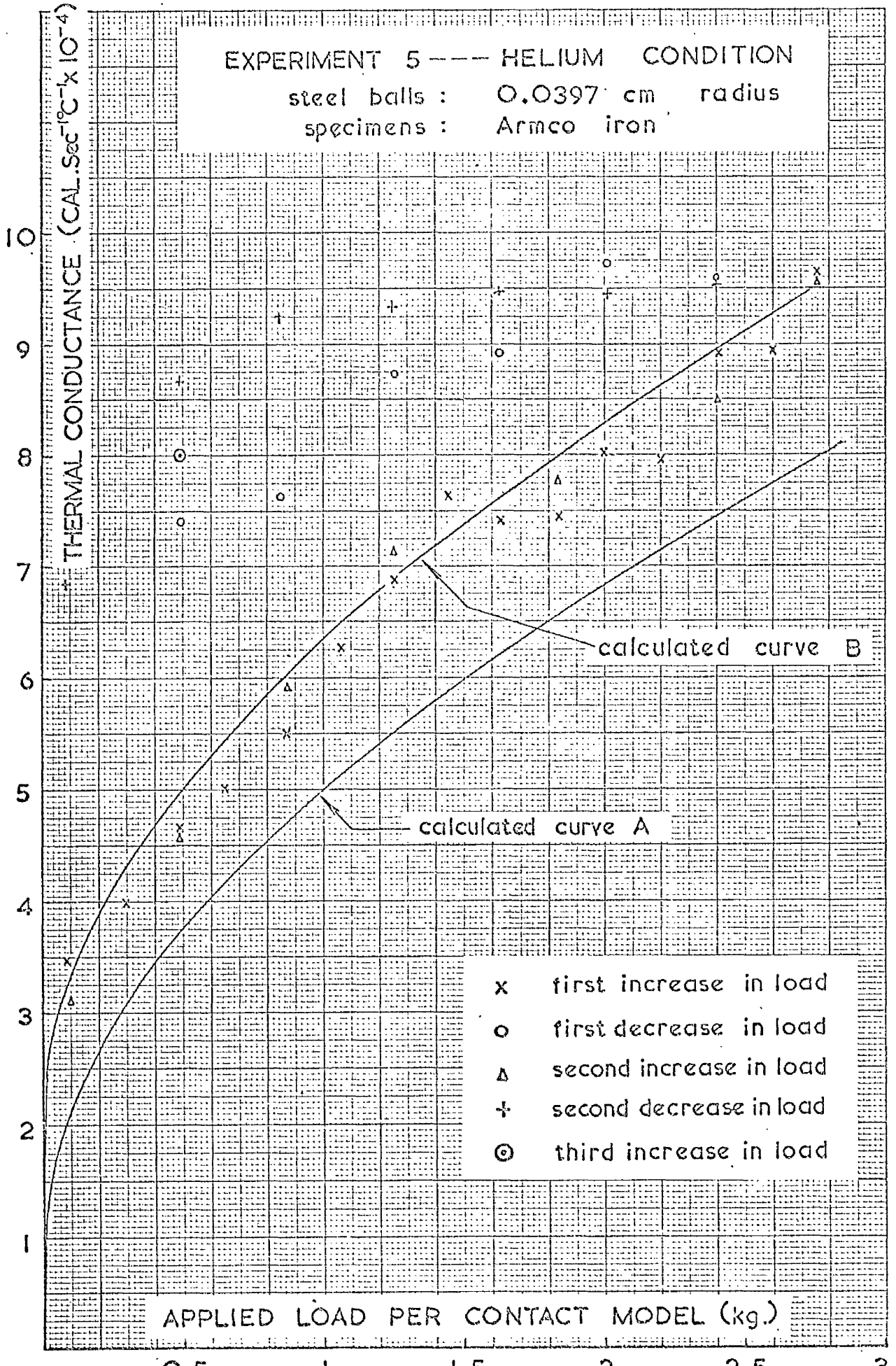
EXPERIMENT 5 --- HELIUM CONDITION
steel balls : 0.0397 cm radius
specimens : Armco iron
THERMAL CONDUCTANCE (CAL.Sec⁻¹°C⁻¹ x 10⁻⁴)
10
9
8
7
6
5
4
3
2
1
calculated curve B
calculated curve A
x first increase in load
o first decrease in load
Δ second increase in load
+ second decrease in load
⊙ third increase in load
APPLIED LOAD PER CONTACT MODEL (kg.)
0·5
1
1·5
2
2·5
3

FIG. 6·9

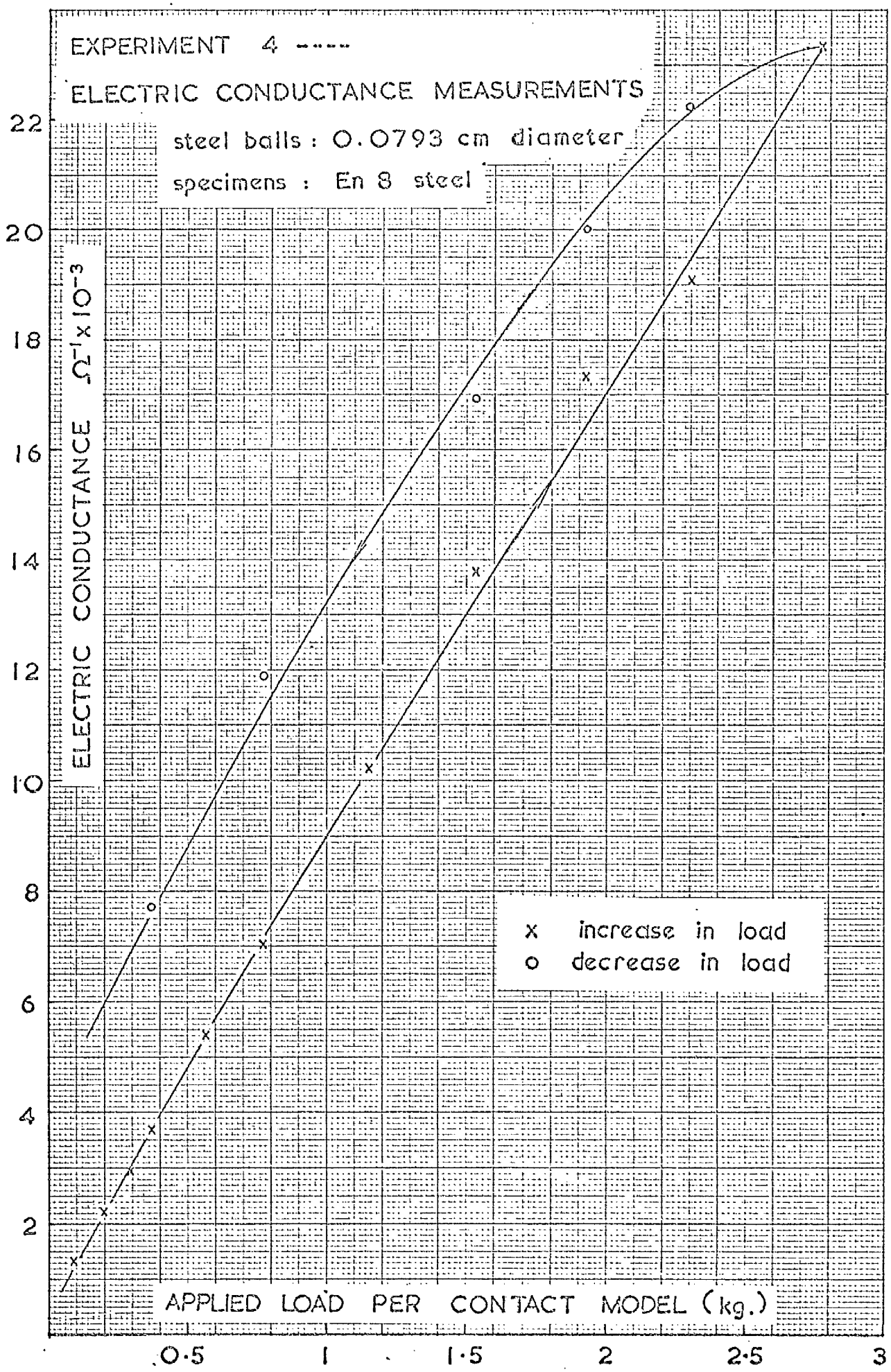
EXPERIMENT 4 ----
ELECTRIC CONDUCTANCE MEASUREMENTS
steel balls : 0.0793 cm diameter
specimens : En 8 steel
ELECTRIC CONDUCTANCE $\Omega^{-1} \times 10^{-3}$
22
20
18
16
14
12
10
8
6
4
2
x increase in load
o decrease in load
APPLIED LOAD PER CONTACT MODEL (kg.)
0·5
1
1·5
2
2·5
3

FIG. 6·10

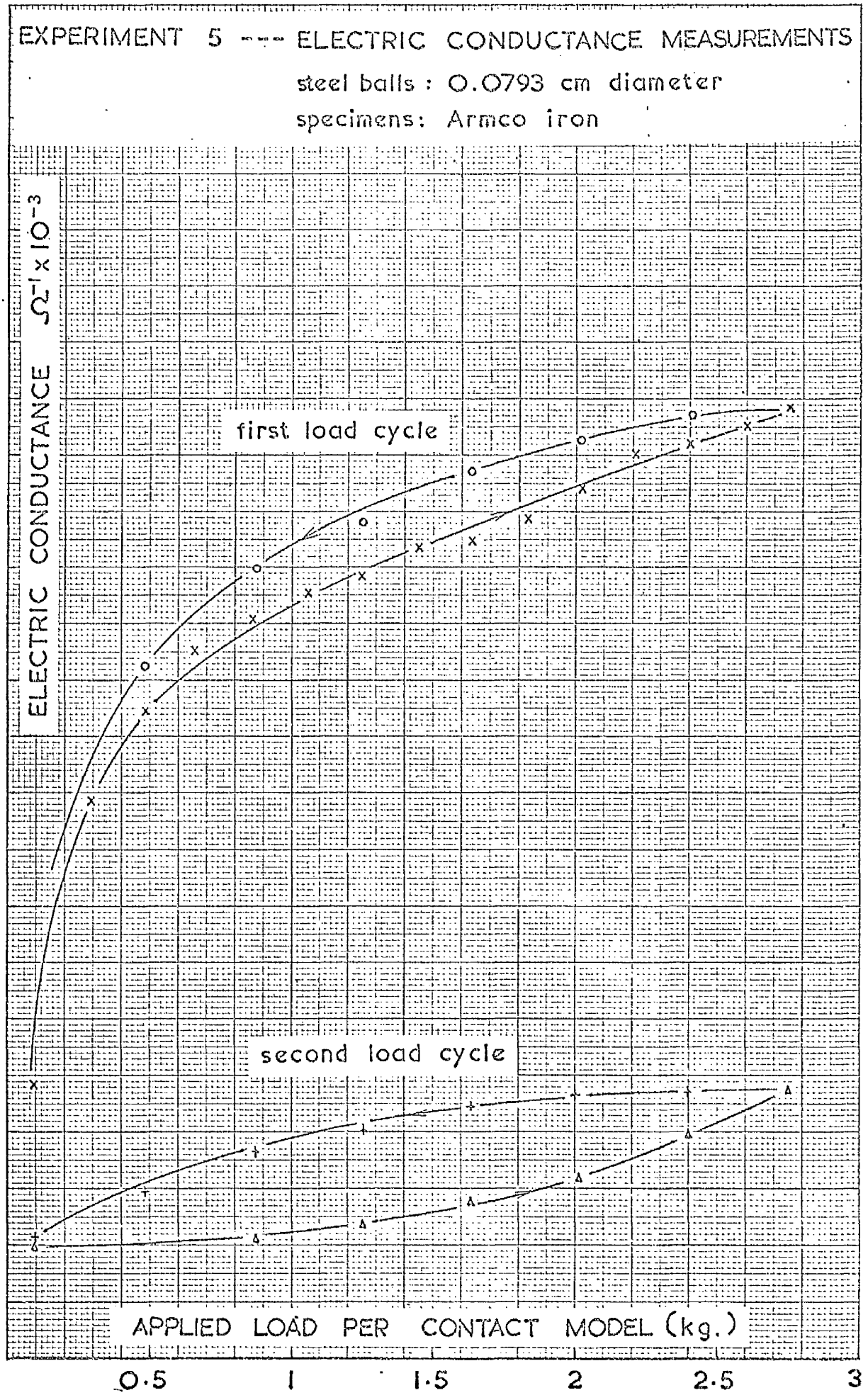
EXPERIMENT 5 --- ELECTRIC CONDUCTANCE MEASUREMENTS
steel balls : 0.0793 cm diameter
specimens: Armco iron
ELECTRIC CONDUCTANCE Ω⁻¹ x 10⁻³
9
8
7
6
5
4
3
2
1
first load cycle
second load cycle
APPLIED LOAD PER CONTACT MODEL (kg.)
0·5
1
1·5
2
2·5
3

FIG. 6·11

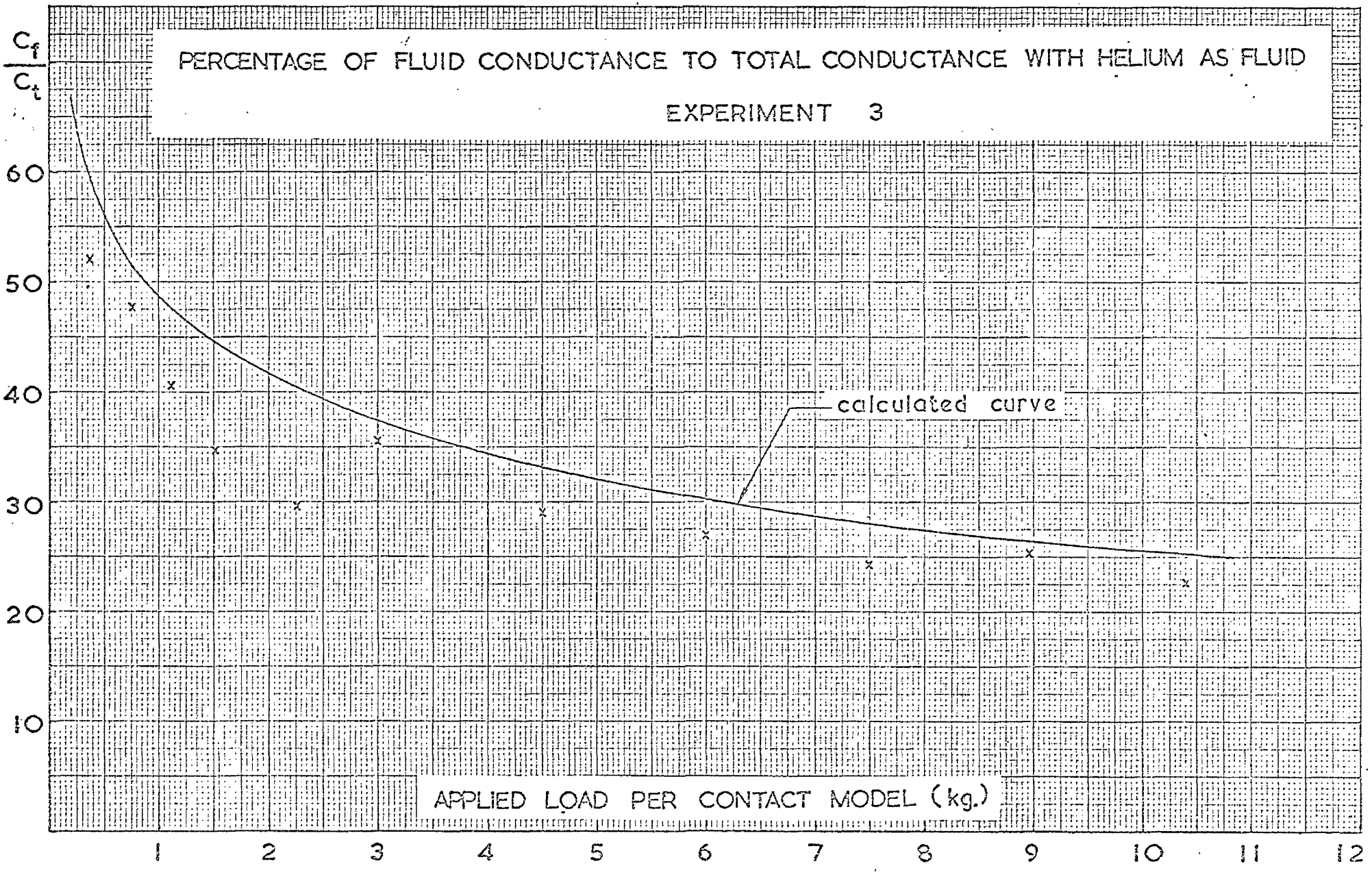
C_f / C_t
PERCENTAGE OF FLUID CONDUCTANCE TO TOTAL CONDUCTANCE WITH HELIUM AS FLUID
EXPERIMENT 3
60
50
40
30
20
10
calculated curve
APPLIED LOAD PER CONTACT MODEL (kg.)
1
2
3
4
5
6
7
8
9
10
11
12

FIG. 6·12

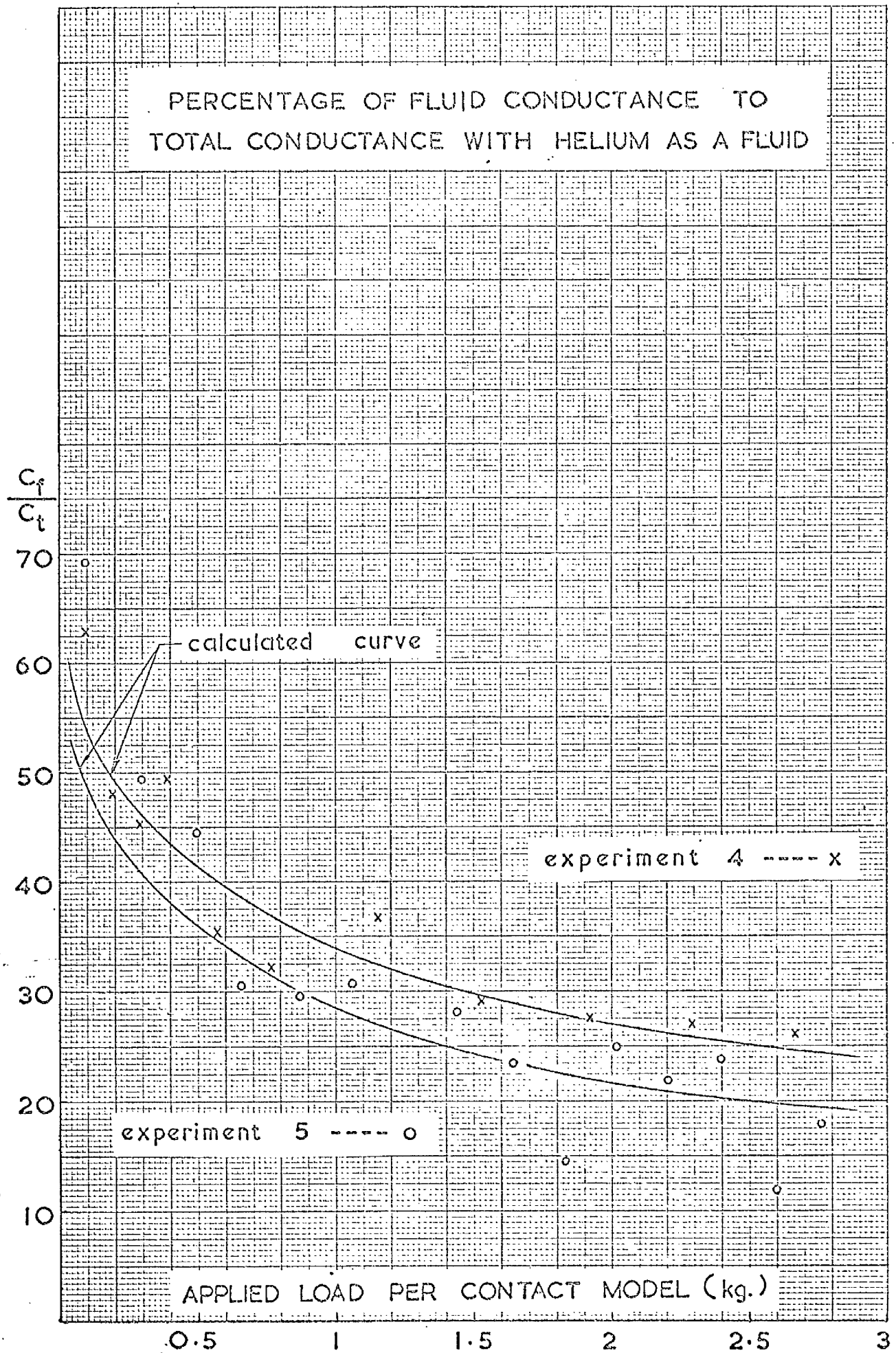
PERCENTAGE OF FLUID CONDUCTANCE TO TOTAL CONDUCTANCE WITH HELIUM AS A FLUID
$\frac{C_f}{C_t}$
70
60
50
40
30
20
10
calculated curve
experiment 4 ---- x
experiment 5 ---- o
APPLIED LOAD PER CONTACT MODEL (kg.)
0·5
1
1·5
2
2·5
3

FIG. 6·13

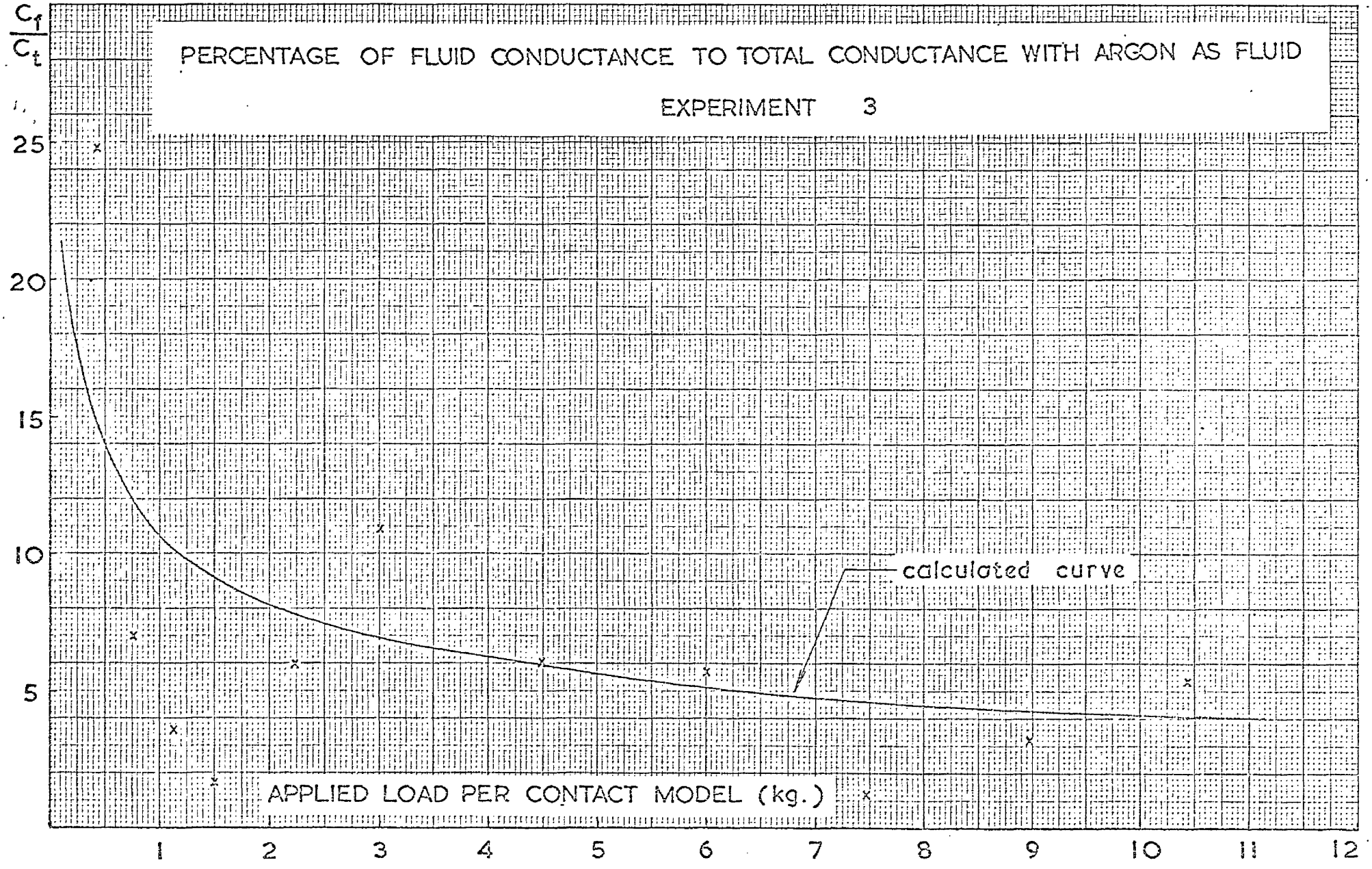
$\frac{C_f}{C_t}$
PERCENTAGE OF FLUID CONDUCTANCE TO TOTAL CONDUCTANCE WITH ARGON AS FLUID
EXPERIMENT 3
25
20
15
10
5
calculated curve
APPLIED LOAD PER CONTACT MODEL (kg.)
1
2
3
4
5
6
7
8
9
10
11
12

FIG. 6·14

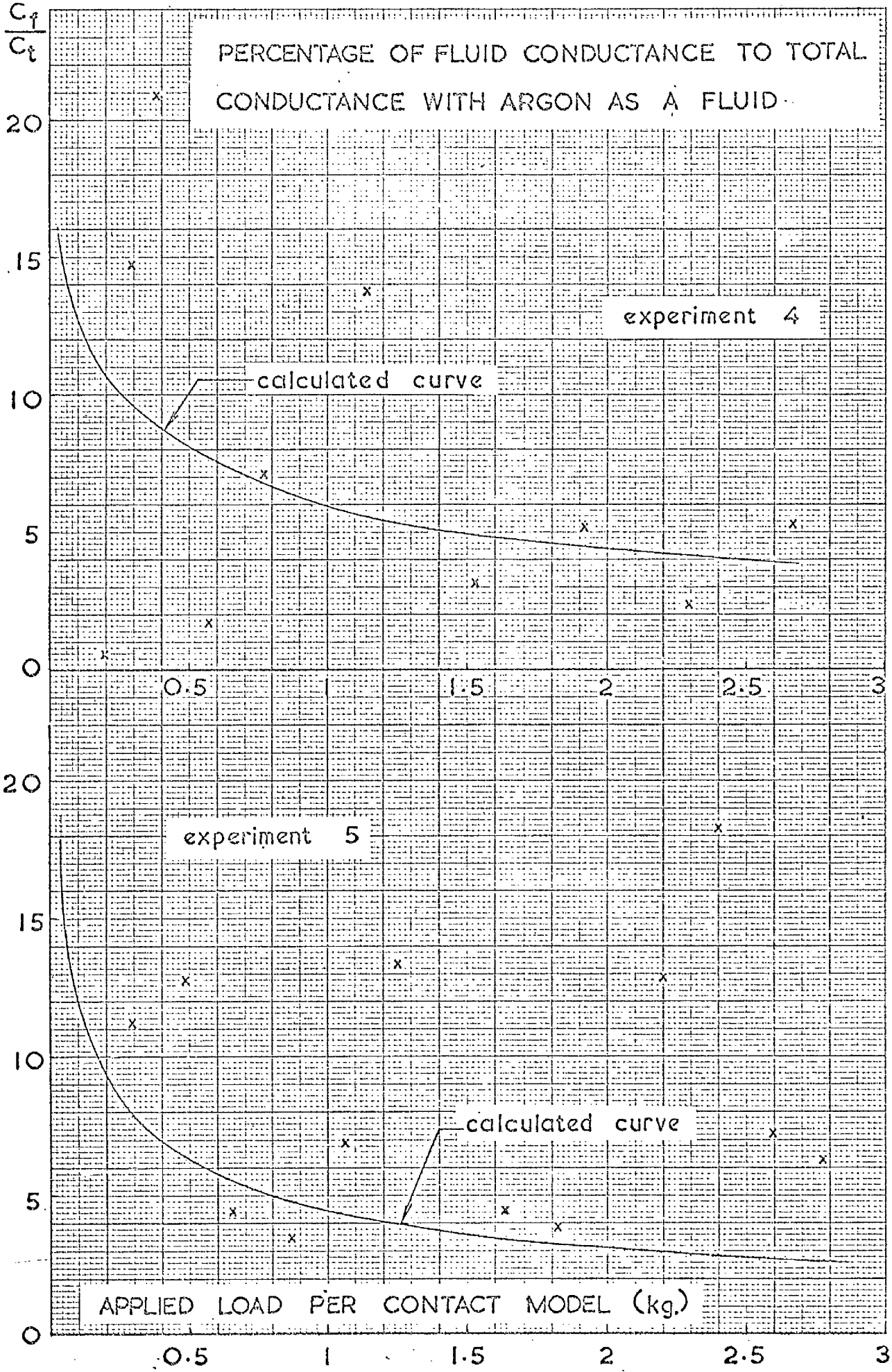
$\frac{C_f}{C_t}$
PERCENTAGE OF FLUID CONDUCTANCE TO TOTAL CONDUCTANCE WITH ARGON AS A FLUID
20
15
10
5
0
experiment 4
calculated curve
0.5
1
1.5
2
2.5
3
20
15
10
5
0
experiment 5
calculated curve
APPLIED LOAD PER CONTACT MODEL (kg.)
0.5
1
1.5
2
2.5
3

FIG. 6·15

CHAPTER VII

DISCUSSIONS AND CONCLUSIONS

We shall now examine the results of the experiments according to the tables and figures presented in Chapter 6.

7.1 Discussion of experimental results with the insertion of steel balls

The applied load range in these experiments lies largely between the onset of plasticity and full plasticity of the test materials. The maximum estimated contact area dimensionless parameter x is 0.2. We can consider that this covers fairly well the x range for a normal contact problem. The mean temperature at the contact interface is kept at about 120°C and not higher in order to reduce as much as possible the effects of high temperature on the properties of the materials, the most important one of which is on the hardness reduction of metals under prolonged heating at high temperatures. The total heat flux passing through the contact is about 24 cal. per sec for experiments 1 to 4 and about 35 cal. per sec for experiment 5. The temperature drop across the contact varies greatly from the vacuum and low load conditions to the helium and high load conditions. Owing to the additional resistance of the steel balls the contact temperature drop is relatively high compared with that in a practical case under similar conditions but without the balls. This is an advantage as it involves a smaller percentage of error in the process of determining the contact temperature drop.

7.1.1 Zero load condition

The results obtained for the zero load condition, in which the upper contact surface is regarded as just not touching the steel balls, appear to be markedly different from the predicted values but not entirely unreasonable.

Table 7.1 shows the results.

Table 7.1: Thermal conductance at zero contact load (cal. $sec^{-1} {}^{o}C^{-1} \times 10^{-6}$)

Test condition	Experiment 1	Experiment 2	Experiment 3		Experiment 4		Experiment 5		
	Test results	Test results	Test results	Calculated values	Test results	Calculated values	Results 1st cycle	Results 2nd cycle	Calculated values
vacuum	71	68	16.9	4.83	2.5	1.05	1.7	1.0	1.06
argon	108	103	103	49	3.26	21.3	6.9	5.75	25
helium	435	483	473	394	29.7	171	32.5	31.6	185

At zero load under vacuum condition, we consider that heat transfer is taking place not only by radiation but also by free molecular conduction if a residue of gas is trapped at the contact interface. This is possible because we realise that the vacuum circuit in our apparatus has a very high resistance and thus the gas pressure at the interface may be much higher than the measured chamber pressure. The calculated values were based on the assumption that the interstitial gas was helium at a pressure of 0.1 torr. With an argon gas these values will be smaller. But at a helium gas pressure of 0.1 torr., the Knudsen number is only 1.2 for experiments 1, 2 and 3 and only 2.4 for experiments 4 and 5. (taking the characteristic length to be the full size of the ball diameter). The assumption of free molecular conduction seems to be pessimistic and yet an assumption of conduction of a gas continuum would be unrealistic. Although there is no reliable theory on the gas conduction in the transtition regime, it is quite likely that the residual gas at the interface plays a greater part in transferring heat than that indicated by the calculated values. The test results of experiments 1 and 2 exceed the

calculated values by more than a decade. This may be explained as due to a mis-match of the temperature distribution between the specimens and the guard tubes especially around the contact junction. When this happens, some of the heat would inevitably be transmitted through the insulating material and re-enter the lower specimen as the temperature difference between the contact surfaces is quite high. The radial heat transfer correction apparently does not cover the existence of such a local heat transfer .

At zero load with gases, the dominant means of heat transfer is by the conduction of the gases, and the thermal conductance depends a great deal on the effective contact gap distance. The calculated values were based on a contact gap distance with the presence of the balls taken into account. Why this has become necessary will be discussed later. The agreements between the test and calculated results of experiments 1, 2 and 3 are exceptionally good. We may regard this as fortunate because any small increase in the contact gap distance, that is, when the upper specimen is raised a little too far from contact making, will considerably reduce the thermal conductance of the contact. This could be the explanation of the large discrepancy in the results of both experiments 4 and 5. In these two experiments the size of the balls is much smaller than that of those used in the previous three experiments and only a 0.1 mm distance increase is sufficient to reduce the thermal conductance by 60%. It is interesting to note the decrease in the thermal conductance values of experiment 5 after the first load cycle. This may be due to the change of the surface properties of the contact when the surfaces has been cleaned after a long period of heating at intervals in vacuo.

7.1.2 Load applied condition

The establishment of metallic contacts (or quasi-metallic contacts from the stand point of heat transfer) commences as soon as load is applied, and this

is shown clearly in the large increase of the thermal conductance value in all experiments. The trend of increase is more parabolic than rectilinear. This suggests that the approach may be an erroneous one, as already attempted by other investigators when trying to estimate the thermal conductance of a contact at zero load by means of the linear extrapolation of the results obtained under load. At low load levels, the size of the areas of contact is very sensitive to the applied load, to the accurate dimensions of the parts composing the contact junction, and furthermore to the conditions of the surface films existing between the contact points. Some large degree of deviation of results can be seen from figures 6.4, 6.6 and 6.7. On the whole the results do indicate a definite trend which is not too greatly different from the predicted one. At high load levels the results do not always follow a steady trend. This may be due to a larger degree of error introduced during the process of determining the temperature drop. But it is more likely due to the presence of some uncontrollable factors which, apart from the applied load, tend to effect the areas of contact. For example, the contact junctions subjected to a high load after a long period of heating are likely to be welded together. But the contact areas were by no means held in a steady rate of increase or decrease according to the sequence of the loading. Instead, it is very possible that they were constantly disturbed from one experimental run to another. When the gas in the chamber is being evacuated, the extraction of heat during the process can cause contraction to all parts in the chamber including the specimen column. The rate of heat extraction depends on the rate of pumping. In our experiment, the evacuation rate was kept to a minimum for reasons mentioned in chapter 5. Nevertheless it is still quite possible to have caused a sudden decrease in temperature of a few degrees. The consequence of a contraction in the specimen column is a sudden relief of

the applied load, and therefore a disturbance to the welded junctions of contact. When a gas is admitted to the chamber for the helium or argon experiment, the release of heat will cause expansion of the parts, the consequence of which is a sudden but temporary increase of the applied load. Thus there are small loading cycles about the main loading cycle throughout the experiment.

The test results of experiment 1 fit every well into the test results of experiment 3 as can be seen in figures 6.1 to 6.3, which show the reproducibility of the experimental set-up in the present study. This, however, is hardly to be expected with a practical contact joint from which the results are usually very scattered.

7.1.3 Correlation of test results with theoretical predictions

The calculated results of the thermal conductance were based on equation (4-8) derived from the simplified method and from equation (3-26) derived from the analytical method in which k_m is given by equation (4-7). The radius of the contact area is taken from figure 4.3 or 4.4 or 4.5 according to the experiment. The properties of the materials are given in the Appendix G. The results calculated from the simplified method and from the analytical method agree to within 3% of each other and therefore it would not seem necessary to make a distinction between them. The results plotted in figures 6.1 to 6.9 and 6.12 to 6.15 are simply designated as calculated values.

The test results under the first increase of loads in vacuo of experiments 3, 4 and 5 follow the calculated curve fairly well. In experiment 3 (see figure 6.1), however, the calculated values seem to be too low by about 15% compared with the test results. First it was thought that the thermal conductivity of the ball material quoted by the supplier (and used in the

present calculations) as equal to 0.081 cal cm^{-1} sec^{-1} $^{o}C^{-1}$ at 100°C was somewhat too low. The average value given in reference (32) for steels possessing similar compositions is about 0.092 cal cm^{-1} sec^{-1} $^{o}C^{-1}$. Yet the results of experiment 5, shown in figure 6.7, give an indication that the calculated values may be too high for the applied loads below 1.2 kg. The results of experiment 4 give no support to either case. It is true that one has to allow for a large margin of error in the properties values quoted by a commercial firm. The deviation of 0.081 cal cm^{-1} sec^{-1} $^{o}C^{-1}$ from its true value could well be the amount which compensates for the errors involved in the experiment to give the present results. What can not be compensated by a change in the properties of the balls is the slope of the tendency of the test results which in all three experiments is steeper than the calculated curves. We reason that an increase of the thermal conductance with increasing load can only come about as a result of the increase of the contact areas and the reduction of the contact gap distance. The reduction of metal hardness with time at elevated temperatures fits into the explanation. The same trend appears in the argon gas experiments, but not in the helium gas experiments. This is because the increase of the thermal conductance due to the presence of the helium gas out-weighs any increase due to the hardness reduction of the specimens.

In obtaining the thermal conductance represented by curve A for the gas conditions the fluid gap distance was calculated according to equation (4-6). A comparison of the results shows clearly that the values given by curve A are unreasonably low. In the experiments with helium gas the calculated values are as much as 30% below the test results. Any errors involved in taking too low a thermal conductivity value for the gas and for the steel balls would never amount to such a high percentage. There is a possibility that convection

might have taken place at the contact interface in the cavities formed by the balls and the contact surfaces. According to the present experimental conditions we obtain the Grashof number to be equal to 1 per 8.7°C of temperature drop for argon gas and per 670°C temperature drop for helium gas. Even with the maximum temperature drop of 200°C in our experiments, there is still no justification for the existence of free convection. Heat transfer by convection may occur in gas pockets which are large enough to support circulation currents. But this process was considered by Wiebbe (33) to be insignificant for cavity size less than 0.25 inch in diameter. One possibility, however, is in the interpretation of the fluid gap distance for the transmission of heat through the fluid medium. This we shall discuss in the next section.

7.1.4 Fluid gap distance.

In the theory presented in Chapter 3, the thermal resistance along the fluid path is taken to be proportional to the fluid gap distance across which heat is transferred through the fluid from one contact surface to the other without any lateral heat transfer taking place. This is reasonable for cases where the contact junctions can be assumed to be circular cylinders of small heights compared with the radius of the contact model. Under such circumstances, the gap distance between the contact surfaces can be used as the fluid gap distance . If the contact junctions are not circular cylinders, two points need be considered. First, heat transfer at the solid-fluid interface along the junctions' surfaces must inevitably occur. The process is very difficult to analyse. Provided that these protruding junctions in contact are small compared with the overall dimensions of the contact surfaces, the neglecting of such a local heat transfer process may not cause any appreciable error in the prediction. Secondly, the fluid gap distance can no longer be represented by the physical distance separating the contact

surfaces. Strictly speaking, surfaces are covered with irregularities and when two surfaces are brought into contact, contact surfaces become only a fictitious term in conformation only with the definition given to a contact model for mathematical treatment. We can appreciate that the fluid gap distance varies from point to point over the interface and an effective fluid gap distance δ_e is a dimensional parameter in length which when divided by the effective thermal conductivity of the fluid (including radiation etc.) gives the overall thermal resistance per unit area in the fluid path. We see, therefore, that the effective fluid gap distance must be necessarily connected with the fluid volume filling the contact interface.

When steel balls are inserted at the contact interface the fluid volume is greatly reduced, while the conducting surface of metals is greatly increased, an arrangement similar to that of a heat exchanger. It follows therefore that by taking the contact gap distance as the effective fluid gap distance, the values of the contact conductance become grossly underestimated. With these considerations, we modify the effective fluid gap distance according to the following expression

$$\delta_e = \frac{\pi R^2 \delta - \frac{4}{3}\pi R_b^3}{\pi (R^2 - a^2) + 2\pi R_b^2}$$

$$= 2 R_b \frac{\left(\sqrt{1 - N^2} - \frac{2}{3} L^2 \right)}{2L^2 + 1 - x^2} \qquad (7\text{-}1)$$

where $L = \frac{R_b}{R}$. Equation (7-1) is based on the assumption that the effective fluid gap distance is equivalent to the fluid volume divided by the total contact surface on one side of the contact plane, and on the assumption that

ball material has a conducting capability comparable to that of the specimens. If the inserted objects were of insulating material, blockage to the heat transfer would be likely to result.

Curve B in figures 6.2, 6.3, 6.5, 6.6, 6.8 and 6. is obtained from equation (4-8) with δ replaced by δ_e given by equation (7-1). It can be seen that the agreements between the test results and the calculated values are much more reasonable. The effect of δ_e on the overall thermal conductance is very marked with the helium experiments.

7.1.5 Hysteresis phenomenon

When a contact joint is loaded progressively and then unloaded, the thermal conductance upon increasing load is not reproducible upon decreasing load. The values of conductance during unloading are always higher than those during loading. This phenomenon has been reported by many investigators. Holm [5] found that the same phenomenon occurs in electric contacts and considered that the cause was due to cold welding. As the load is increased, the surface films at the contact points will gradually be broken down to allow for intimate contact to be established. The adherence of these points, as the result of cold welding will remain in firm contact even when the load is being reduced, giving rise to a relatively larger area of contact hence a higher conductance. Fenech and Roshenow[13], on the other hand, suggested that this was due to the elastic deformation of the bulk of material in the sublayers and thus bringing the two surfaces closer together.

In the present study, increasing load runs followed by decreasing load runs were conducted in the same experiment in order to observe this phenomenon. In experiment 3, a second increase of load runs was carried out whereas in experiment 5 two complete load cycles were accomplished. In all three experiments namely 3, 4 and 5, the hysteresis effect is very marked and can be seen in

figures 6.1 to 6.9. In experiment 3 the second increase of load runs was carried out when the applied load was decreased to 0.753 kg. per contact model. In this case the contact junctions, if welded, had not been broken completely. We see that the conductance values during the second increase of load runs repeat very closely those during the first decrease of load runs. There is no hysteresis loop and the nature of material deformation is recoverable. In experiment 5, however, the contact junctions were broken at the end of the first decrease of load runs when the applied load was reduced to zero. Hence during the second load cycle a hysteresis loop was formed following more or less the one formed by the first load cycle. This is rather surprising as one would expect that the material after the first load cycle would have been, to some extent, work-hardened, unless the amount of work-hardening had been removed by prolonged heating. The result during the third increase of load run follows fairly well the path marked by the results obtained during the previous two decreasing load runs.

The hysteresis phenomenon was explained by Wong[1] as due to two different natures of deformation. When the load is reduced, recovery of deformation will take place only in the elastic domain so that the variation of the contact area is proportional to $W^{\frac{2}{3}}$ whereas during increasing loads the deformation is plastic and the variation of the contact area is proportional to W. The thermal conductance values for decreasing loads were calculated according to the conditions of experiment 3, but assuming deformations to be elastic. The results plotted in figures 6.1, 6.2 and 6.3, are represented by the returning curves joining the curve B at the maximum applied load point. But they fall a long way below the test results. An examination of the test results indicates that the thermal conductance values remain practically unchanged over a substantial range of load reduction from the maximum load

level. The cause is believed to be the seizure of the junctions as described in section 6.3.2. Thus Holm's cold welding explanation is confirmed. When the seizure of the junctions is gradually broken down by a greater relief of load, recovery of deformation is essentially elastic. As can be seen that the slope of the tendency marked by the test results during the decreasing load runs at lower load levels follows very well the slope of the calculated curves based on elastic deformation.

7.2 Discussion of the experimental results with the insertion of aluminium discs

Experiments 6 and 7 were conducted with aluminium discs. The object was to obtain one set of test results from each experiment in which the aluminium discs were considered to be in full contact with the contact surfaces. It was thought that this condition could have been revealed as soon as the temperature readings remained substantially unchanged for a small increase of applied load. In actual fact, this was not the case. The thermal conductance of the contact increased steadily as load was increased and it was not possible to judge whether full contact conditions had been reached or surpassed. The bearing yield stress of the aluminium material is quoted to be 127 kg. per cm^2. The equivalent load is 1.415 kg. for the 0.0436 cm diameter discs and 2.5 kg. for the 0.086 cm discs. It is quite possible that the bearing strength of the material had been reduced considerably by heating. If this is the case, lateral deformation of the discs could have started at load levels much lower than the above figures. A number of test runs were carried out in each experiment; the results of only a few runs are given in tables 6.7 and 6.8. The calculated values are based on full contact conditions and there is no allowance made for the presence of

surface films. These values are compared with the test results of the nearest magnitudes. It is hard to justify such a method of correlating results as out of so many test runs there is always one set of results which agree well with the calculated values. We must be content, therefore, only with the order of magnitudes. In this case the conclusion is not altogether unsatisfactory. In both experiments the yielding of the material seems to start at an applied load much lower than expected. In experiment 7 the initial applied load was obviously too high. Materials with a higher bearing strength would have been a better proposition but then they could have caused a problem in production.

7.3 Discussion of the electric conductance measurements

Under bare metal contact condition, we expect there to be a definite relationship between the thermal conductance and electric conductance. This condition prevails provided that the surfaces are free from any surface films. The test results show that it is impossible for such a relationship to be established under the present experimental conditions. At low load levels the electric readings never became stable and they were very sensitive to any small disturbances. Separate investigations showed that the amount of current passing through the contact caused negligible heating to the parts, nor did the heating cause a great deal of difference to the potential measurements. Although the applied load was considered as the primary factor in governing the contact areas and hence the conductance of the contact, yet it was found that electrical readings were very much affected by local conditions at the contact points. For example, a small disturbance caused to the apparatus during the re-fitting of a thermocouple in experiment 3 did not affect the

temperature readings very much but did cause the electrical measurements to behave in a most disorderly manner. After the contact junctions were broken at the ends of the first decrease load runs in experiment 5, the electrical measurements during the second load cycle runs yielded totally different conductance values as compared with those during the first load cycle runs. Although it was thought that the use of steel balls might create a favourable condition for the surface films to be penetrated when the contact pressure became high enough. According to Hertz, the contact pressure is highest at the centre of the contact when a plane is deformed elastically by a spherical indenter and falls to zero at the edge of the contact area. If deformation is plastic, the contact pressure at the edge is somewhat higher according to Ishlinsky (see reference (3)). There is a possibility that surface films may be broken at the centre of the contact but may remain compressed away from the centre. Anderson in his experiments with metal balls[7] found that electrical resistance at the contact could drop by a decade if the contact was subjected to a small vibration by means of a tuning fork and by several 10^3 if subjected to a shearing action by means of twisting. We have every reason to believe that it was the surface films which caused the readings to be so unpredictable. A separate experiment conducted in atmosphere outside the chamber gave the same evidence of readings sensitive to any small disturbances.

The surface films cannot have been entirely removed under the present experimental conditions. Their presence at the contact junctions between the balls and the specimens apparently has very little effects on heat transfer because they are thin. The electric conductance results show that the contact resistance is exceedingly high. We suspect that this must have arisen from the presence of surface films. Normally we expect that electrons would still pass through the thin films by the tunnel effect so that a contact even covered

with surface films could become a good conductor. This is possible, however, if the gap potential difference is above a certain value (for a film of 20 Å thick, it is considered that the potential difference must be at least 10 volts (5)). The gap potential difference in the present set up is far below this value. Consequently the effective contact area for electric current flow becomes much smaller than that for heat flow. The contact area derived from the electric conductance result was only one thousandth of that from the thermal conductance result in some cases. We conclude therefore that it is unreliable to determine a thermal contact conductance from electric measurements.

7.4 Fluid thermal conductance

A comparison is made between the test fluid thermal conductance and the calculated values for the gas conditions under various applied loads. This is shown in figures 6.12 to 6.15. The test results were taken as the difference between the total conductance values for the vacuum condition and for the specific gas condition under the same applied load. The calculated values were computed according to equation (3-29). The results with helium gas show a better agreement with the calculated values than do those with argon gas. This can be explained as being largely due to experimental errors. Argon has a much smaller thermal conductivity than helium and therefore plays only a small part in the transmission of heat through the interstitial gap of the contact. This means that any small error in the measurements of the total thermal conductance magnifies the error in the part played by the fluid when it is shown as a percentage of the total conductance value. Judging only by the helium results, we see that the maximum deviation is about 15% which can be regarded as satisfactory.

7.5 Conclusions

From both the theoretical and experimental studies the following conclusions can now be drawn.

1. The analytical method and the simplified method agree with each other to within 3% based on the present experimental conditions. On the whole they give reasonably satisfactory predictions when compared with the test results, so long as the fluid gap distance is properly interpreted.

2. An effective fluid gap distance should be defined as a length which, when divided by the effective thermal conductivity of the fluid, gives the overall thermal resistance per unit area in the fluid path. Without an accurate means of determing this value, an approximation can be obtained by dividing the fluid volume at the interface by the conducting surface area of the solid on one side of the contact plane.

3. In formulating a theory on a thermal contact problem it is essential that the thermal resistance of the contact junctions be included. In the present experimental study, the resistance due to the inserted objects is almost twice as high as the constriction resistance in the main specimens. We would expect a considerable discrepancy between the calculated values and the test results, had the resistance of the junctions been ignored.

4. The present theories can be conveniently extended to cover contact models other than the idealised case with circular cylindrical junctions provided that heat transfer at the solid-fluid interface along the contact junctions is small. In this case the resistance of the junctions can be represented as δ/k_m which includes the secondary constriction resistance as well as the material resistance.

5. Since the shape of a surface irregularity resembles a cone more than a circular cylinder, it is more realistic to assume the metallic contact junctions

to be formed by a pair of conic frusta. The equivalent thermal conductivity k_m, in this case, can be obtained from equation (3-35).

6. The amount of heat transferred through the fluid path and through the solid path is governed by the fluid contact parameter K_f, the solid contact parameter K_s and the contact area parameter X. By specifying the magnitudes of these parameters, it is possible to estimate the heat transfer rate through each path across the contact. By altering their values, it may also be possible to control the thermal contact conductance for a given purpose.

7. The increase of a contact thermal conductance with load is very rapid under very low load levels. It tends to be proportional to the applied load as the magnitude of the applied load is increased. In the present experiments the fluid conductance values are not greatly affected by the applied load. This is because the change of the fluid gap distance due to load is small compared with the initial gap distance. For contacts with a very small initial gap distance, however, we expect the fluid conductance to be increased with load.

8. If the thermal conductivity of the interstitial fluid is small compared with that of the contact material, the thermal conductance becomes very sensitive to the size of the contact areas during an initial stage when two metallic surfaces are brought into contact. Thus any attempt to determine the conductance value at zero load condition by means of extrapolation of results under load may not be reliable.

9. The determination of the contact areas or the thermal conductance by means of electrical measurements is unreliable owing to the presence of surface films. Surface films may be broken by high contact pressure but may not necessarily be removed from the contact points. Thus they can still offer a substantial resistance to the flow of electric current unless the contact

potential difference is high enough to establish a tunnel effect. The adverse effect is additional heating at the contact junctions.

10. The hysteresis phenomenon concerning the thermal conductance of a contact observed under increasing and decreasing loads can be explained as being due to the seizure of the contact junctions as well as to the irreversible deformation of the material.

11. If the irregularities on the contact surfaces are not engaged in firm contact the cyclic contraction and expansion of these junctions may set up a thermal switch effect.

12. Surface properties of the materials at the contact interface are liable to change after prolonged heating, resulting in a change of the heat transfer characteristics of the contact.

APPENDIX A

Analysis of an idealised contact model

In the problem stated in section 3.1, the contact spot of height h_1 on solid 1 is in contact with the contact spot of height h_2 on solid 2. The void is filled by a fluid of thermal conductivity k_f, and the fluid gap $\delta = h_1 + h_2$ is divided by an isothermal contact plane the position of which is chosen so that

$$\delta_1 = \frac{k_{s2}}{k_{s1}+k_{s2}}\delta \quad \text{and}$$

$$\delta_2 = \frac{k_{s1}}{k_{s1}+k_{s2}}\delta$$

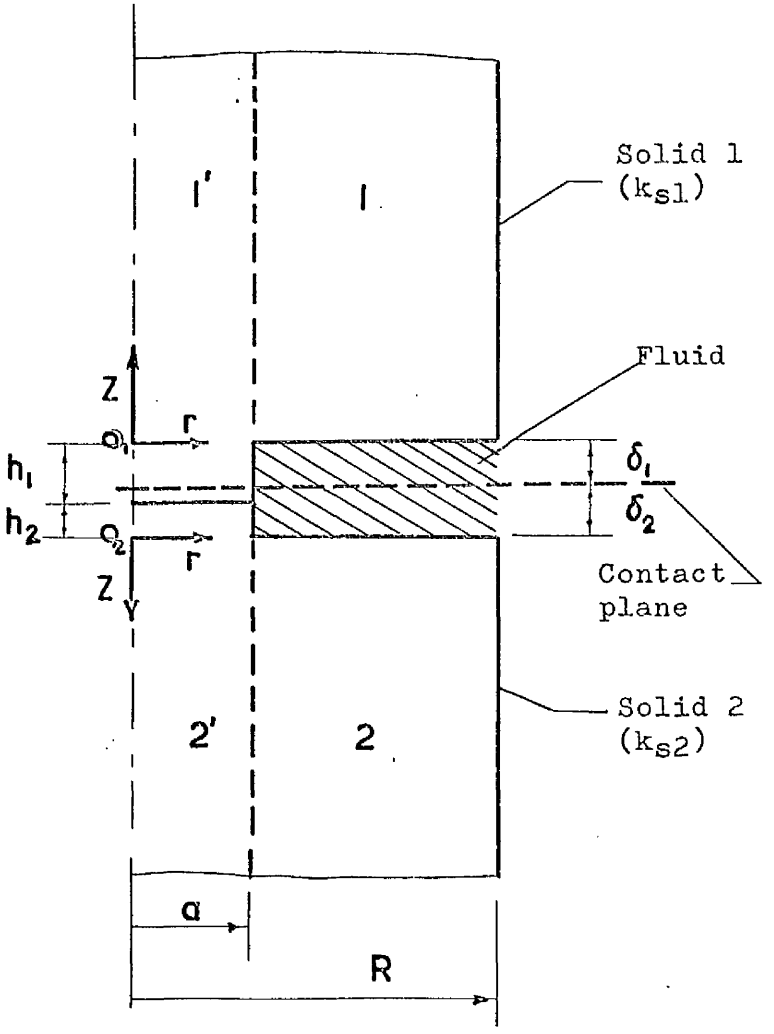

Fig. A.1 Idealised contact model

We consider first solid 1 which is divided into region 1 and 1'. At Z = 0, the fluid is assumed to be replaced by a medium with a heat transfer coefficient of $\frac{k_f}{\delta_1}$ and the solid spot by a medium with a heat transfer coefficient of $\frac{k_m}{\delta_1}$ where

$$k_m = \frac{k_{s1}\, k_{s2}}{h_1\, k_{s2} + h_2\, k_{s1}}\,\delta \qquad \text{(A-1)}$$

The temperature distribution in region 1 and 1' must satisfy the Laplace equations, i.e.

$$\frac{\partial^2 T_1'}{\partial r^2} + \frac{1}{r}\frac{\partial T_1'}{\partial r} + \frac{\partial^2 T_1'}{\partial Z^2} = 0 \qquad \text{(A-2)}$$

$$\frac{\partial^2 T_1}{\partial r^2} + \frac{1}{r}\frac{\partial T_1}{\partial r} + \frac{\partial^2 T_1}{\partial Z^2} = 0 \qquad \text{(A-3)}$$

The solutions to these two equations are so chosen that they satisfy the gereral considerations of the problem. They appear as

$$T_1' = T_o + \Delta T_1 + H_1 \frac{Z}{R} - A_1 e^{-\alpha \frac{Z}{R}} J_o(\alpha \frac{r}{R}) \qquad \text{(A-4)}$$

$$T_1 = T_o + \Delta T_1 + H_1 \frac{Z}{R} - B_1 e^{-\lambda \frac{Z}{R}} J_o(\lambda \frac{r}{R}) - D_1 e^{-\beta \frac{Z}{R}} Y_o(\beta \frac{r}{R}) \qquad \text{(A-5)}$$

where J_o and Y_o are the Bessel functions of the first and second kind[15], and A_1, B_1, D_1, H_1, α, λ, β are constants to be determined from the following boundary conditions.

$$T_1 = T_1' \propto Z \quad \text{as} \quad Z \longrightarrow \infty \qquad \text{(A-6)}$$

$$\frac{\partial T_1'}{\partial r} = 0 \quad \text{at} \quad r = 0, \quad 0 < Z < \infty \qquad \text{(A-7)}$$

$$\frac{\partial T_1}{\partial r} = 0 \quad \text{at } r = R, \quad 0 < Z < \infty \qquad \text{(A-8)}$$

$$\int_0^\infty T_1'\, dZ = \int_0^\infty T_1\, dZ \quad \text{at } r = a, \quad 0 < Z < \infty \qquad \text{(A-9)}$$

$$\int_0^{\infty} \frac{\partial T_1'}{\partial r}\, d \;=\; \int_0^{\infty} \frac{\partial T_1}{\partial r}\, d \qquad \text{at} \quad r = a, \quad 0 < Z < \infty \tag{A-10}$$

$$\int_0^{a} k_{s1} \frac{\partial T_1'}{\partial Z}\, rdr = \int_0^{a} k_m \frac{T_1' - T_o}{\delta_1}\, rdr \quad \text{at} \quad 0 < r < a, \quad Z = 0 \tag{A-11}$$

$$\int_a^{R} k_{s1} \frac{\partial T_1}{\partial Z}\, rdr = \int_a^{R} k_f \frac{T_1 - T_o}{\delta 1}\, rdr \quad \text{at} \quad a < r < R, \quad Z = 0 \tag{A-12}$$

Equation (A-6) is automatically satisfied when Z tends to infinity while (A-7) is satisfied because $J_1(0) = 0$. From equation (A-8), we obtain

$$B_1 \frac{\lambda}{R} e^{-\lambda \frac{Z}{R}} J_1(\lambda) \;+\; C_1 \frac{\beta}{R} e^{-\beta \frac{Z}{R}} Y_1(\beta) = 0 \tag{A-13}$$

This equation can be satisfied if we put

$$J_1(\lambda) = 0 \quad , \quad Y_1(\beta) = 0 \tag{A-14}$$

which determine the values of λ and β. The first positive zero of J_1 gives $\lambda = 3.832$ and of Y_1 gives $\beta = 2.197$. From equations (A-9) and (A-10) we obtain the following respective results.

$$A_1 \frac{R}{a} J_o(a\frac{a}{R}) - B_1 \frac{R}{\lambda} J_o(\lambda \frac{a}{R}) - D_1 \frac{R}{\beta} Y_o(\beta \frac{a}{R}) = 0 \tag{A-15}$$

$$A_1 J_1(a\frac{a}{R}) - B_1 J_1(\lambda \frac{a}{R}) - D_1 Y_1(\beta \frac{a}{R}) = 0 \tag{A-16}$$

The value of a is arbitrary and it is to be determined later. We now solve A_1 and B_1 in terms of D_1.

$$A_1 = D_1 \left[\frac{\frac{Y_o(\beta x)}{\beta} - \frac{J_o(\lambda x)}{\lambda} \frac{Y_1(\beta x)}{J_1(\lambda x)}}{\frac{J_o(\alpha x)}{\alpha} - \frac{J_o(\lambda x)}{\lambda} \frac{J_1(\alpha x)}{J_1(\lambda x)}} \right] = D_1 G_1 \qquad \text{(A-17)}$$

$$B_1 = D_1 \left[\frac{\frac{Y_o(\beta x)}{\beta} - \frac{J_o(\alpha x)}{\alpha} \frac{Y_1(\beta x)}{J_1(\alpha x)}}{\frac{J_o(\alpha x)}{\alpha} \frac{J_1(\lambda x)}{J_1(\alpha x)} - \frac{J_o(\lambda x)}{\lambda}} \right] = D_1 G_2 \qquad \text{(A-18)}$$

where G_1 and G_2 are self-evident and $x = \frac{a}{R}$.

Substituting (A-4) into (A-11) and making use of (A-17), we obtain

$$\left(\frac{H_1}{R} - \frac{k_m}{k_{s1}\delta_1}\Delta T_1\right)\frac{a}{2} = - D_1 G_1 J_1(\alpha x)\left(1 + \frac{R}{\alpha\delta_1}\frac{k_m}{k_{s1}}\right) \qquad \text{(A-19)}$$

The substitution of (A-5) into (A-12) together with (A-17) and (A-18) yields

$$\left(\frac{H_1}{R} - \frac{\Delta T_1}{\delta_1}\frac{k_f}{k_{s1}}\right)\frac{R^2 - a^2}{2} = a D_1 \left[G_1 J_1(\alpha x) + G_2 \frac{R}{\delta_1 \lambda}\frac{k_f}{k_{s1}} J_1(\lambda x) + \frac{R}{\delta_1 \beta}\frac{k_f}{k_{s1}} Y_1(\beta x)\right] \qquad \text{(A-20)}$$

With (A-19) and (A-20) we eliminate D_1, and by rearranging the results we obtain

$$\frac{\Delta T_1}{H_1} = \frac{(1-x^2)\left(1 + \frac{1}{\alpha y_1}\frac{k_m}{k_{s1}}\right) + x^2\left(1 + \frac{k_f}{y_1 k_{s1}} F(x)\right)}{(1-x^2)\left(1 + \frac{1}{\alpha y_1}\frac{k_m}{k_{s1}}\right)\frac{k_f}{y_1 k_{s1}} + x^2 \frac{k_m}{y_1 k_{s1}}\left(1 + \frac{k_f}{y_1 k_{s1}} F(x)\right)} \qquad \text{(A-21)}$$

where $y_1 = \frac{1}{R}$ and $F(x)$ is a function of x and is equal to

$$F(x) = \left(\frac{G_2 J_1(\lambda x)}{G_1 \lambda J_1(\alpha x)} + \frac{Y_1(\beta x)}{G_1 \beta J_1(\alpha x)}\right) \qquad \text{(A-22)}$$

The total heat flux is obtained from

$$Q = \pi R^2 k_{s1} \frac{\partial T}{\partial Z} = \pi R k_{s1} H_1 \quad \text{when} \quad Z \to \infty \qquad \text{(A-23)}$$

But the total contact resistance between solid 1 and the contact plane is

$$R_1 = \frac{\Delta T_1}{Q} = \frac{\frac{\Delta T_1}{H_1}}{\pi R k_{s1}} \qquad \text{(A-24)}$$

Thus from the result of (A-21), we obtain

$$R_1 = \frac{1}{\pi R k_{s1}} \left[\frac{(1-x^2)\left(1 + \frac{1}{\alpha y_1} \frac{k_m}{k_{s1}}\right) + x^2 \left(1 + \frac{k_f}{y_1 k_{s1}} F(x)\right)}{(1-x^2)\left(1 + \frac{1}{\alpha y_1} \frac{k_m}{k_{s1}}\right) \frac{k_f}{y_1 k_{s1}} + x^2 \frac{k_m}{y_1 k_{s1}} \left(1 + \frac{k_f}{y_1 k_{s1}} F(x)\right)} \right]$$

$$\text{(A-25)}$$

If we choose the following temperature distributions in region 2' and 2 of solid 2 with the origin of the r, z coordinates placed at O_2, such as

$$T_2' = T_o - \Delta T_2 - H_2 \frac{z}{R} + A_2 e^{-\alpha \frac{Z}{R}} J_o\left(\alpha \frac{r}{R}\right) \qquad \text{(A-26)}$$

$$T_2 = T_o - \Delta T_2 - H_2 \frac{Z}{R} + B_2 e^{-\lambda \frac{Z}{R}} J_o\left(\lambda \frac{r}{R}\right) + D_2 e^{-\beta \frac{Z}{R}} Y_o\left(\beta \frac{r}{R}\right) \qquad \text{(A-27)}$$

we use the similar approach as on solid 1 and find the contact resistance between solid 2 and the contact plane to be equal to

$$R_2 = \frac{1}{\pi R k_{s2}} \left[\frac{(1-x^2)(1+\frac{1}{\alpha y_2}\frac{k_m}{k_{s2}}) + x^2(1+\frac{k_f}{y_2 k_{s2}}F(x))}{(1-x^2)(1+\frac{1}{\alpha y_2}\frac{k_m}{k_{s2}})\frac{k_f}{y_2 k_{s2}} + x^2\frac{k_m}{y_2 k_{s2}}(1+\frac{k_f}{y_2 k_{s2}}F(x))} \right] \quad \text{(A-28)}$$

where $y_2 = \frac{\delta_2}{R}$

The total contact resistance is

$$R_t = R_1 + R_2$$

$$= \frac{1}{\pi R}\left[\frac{1}{k_{s1}}\left[\frac{(1-x^2)(1+\frac{1}{\alpha y_1}\frac{k_m}{k_{s1}}) + x^2(1+\frac{k_f}{y_1 k_{s1}}F(x))}{(1-x^2)(1+\frac{1}{\alpha y_1}\frac{k_m}{k_{s1}})\frac{k_f}{y_1 k_{s1}} + x^2\frac{k_m}{y_1 k_{s1}}(1+\frac{k_f}{y_1 k_{s1}}F(x))}\right]\right.$$

$$\left. + \frac{1}{k_{s2}}\left[\frac{(1-x^2)(1+\frac{1}{\alpha y_2}\frac{k_m}{k_{s2}}) + x^2(1+\frac{k_f}{y_2 k_{s2}}F(x))}{(1-x^2)(1+\frac{1}{\alpha y_2}\frac{k_m}{k_{s2}})\frac{k_f}{y_2 k_{s2}} + x^2\frac{k_m}{y_2 k_{s2}}(1+\frac{k_f}{y_2 k_{s2}}F(x))}\right]\right] \quad \text{(A-29)}$$

We now consider the case where $k_f = 0$, $k_{s1} = k_{s2} = k_s$ and $x \ll 1$. In this particular case we are dealing with a mathematical problem similar to those investigated by Jean in his treaties on Electricity and Magnetism[14], by Hohm on Electric Contact[5] and by Bowden and Tabor[6] on Friction and Lubrication of solids. From their conclusions the constriction resistance of the lines of flow through a circular junction is equal to $\frac{1}{2a\,k_s}$. This is used here as the limiting value for the determination of the value of α. With $k_f = 0$ and $k_{s1} = k_{s2} = k_s$, equation (A-29) reduces to

$$R_t = \frac{\delta}{\pi a^2 k_s} + \frac{2}{\pi a\, k_s\,(\alpha x)}(1-x^2) \quad \text{(A-30)}$$

The constriction resistance becomes

$$R_c = R_t - \frac{\delta}{\pi a^2 k_s} = \frac{2}{\pi a k_s (ax)} (1-x^2) \qquad (A-30)$$

If we set R_c to be equal to $\frac{1}{2ak_s}$ when x becomes very small, we obtain

$$(ax) = \frac{4}{\pi} \qquad (A-31)$$

We see that a is inversely proportional to x.

Since $y_1 k_{s1} = y_2 k_{s2}$, we introduce a solid contact parameter K_s and a fluid contact parameter K_f such that

$$K_s = \frac{k_m}{y_1 k_{s1}} = \frac{k_m}{y_2 k_{s2}} \quad \text{and} \quad K_f = \frac{k_f}{y_1 k_{s1}} = \frac{k_f}{y_2 k_{s2}}$$

It is now possible to rewrite equation (A-29) in the form

$$R_t = \frac{1}{\pi R} \left[\frac{(1 + \frac{\pi x}{4} K_s - x^2 \frac{\pi x}{4} K_s) + (x^2 K_f F(x))}{(1-x^2)(1+\frac{\pi x}{4} K_s)K_f + x^2 K_s (1 + K_f F(x))} \right] \left(\frac{k_{s1} + k_{s2}}{k_{s1} k_{s2}} \right) \qquad (A-36)$$

The total contact conductance is

$$C_t = \frac{1}{R_t} = \pi R \left(\frac{k_{s1} k_{s2}}{k_{s1}+k_{s2}} \right) \left(\frac{(1-x^2)(1+\frac{\pi x}{4} K_s)K_f + x^2 K_s (1 + K_f F(x))}{(1 + \frac{\pi x}{4} K_s - x^2 \frac{\pi x}{4} K_s) + (x^2 K_f F(x))} \right) \qquad (A-37)$$

Our next attempt is to find the solid contact conductance C_s and the fluid contact conductance C_f bearing in mind that

$$C_t = C_s + C_f \qquad (A-38)$$

The amount of heat flux passing through the solid contact spot can be obtained from

$$Q_s = 2\pi \int_0^a k_{s1} \frac{\partial T_1'}{\partial Z} \, rdr = 2\pi a k_{s1} \left(\frac{H_1}{R} \frac{a}{2} + A_1 J_1(ax)\right) \qquad (A-39)$$

The ratio of the heat flux passing through the solid spot to the total heat flux is obtained from equations (A-23) and (A-39)

$$\frac{Q_s}{Q} = \left(x^2 + A_1 \frac{2x}{H_1} J_1(ax)\right) \qquad (A-40)$$

Using equations (A-17) and (A-20) to eliminate A_1 and adopting the contact parameters, we obtain

$$\frac{Q_s}{Q} = x^2 K_s \left[\frac{\left(1 + \frac{\pi x}{4} K_s - x^2 \frac{\pi x}{4} K_s\right) + \left(x^2 K_f F(x)\right)}{(1-x^2)\left(1 + \frac{\pi x}{4} K_s\right) K_f + x^2 K_s (1 + K_f F(x))}\right] \qquad (A-41)$$

By definition the contact conductances can be written as

$$C_t = \frac{Q}{\Delta T_1 + \Delta T_2} \quad \text{and} \quad C_s = \frac{Q_s}{\Delta T_1 + \Delta T_2}$$

Hence

$$C_s = \frac{Q_s}{Q} C_t \qquad (A-42)$$

Substituting (A-37) and (A-41) into (A-42), we obtain

$$C_s = \pi R K_s x^2 \left(\frac{k_{s1} k_{s2}}{k_{s1} + k_{s2}}\right)\left[\frac{\left(1 + \frac{\pi x}{4} K_f - x^2 \frac{\pi x}{4} K_f\right) + x^2 K_f F(x)}{\left(1 + \frac{\pi x}{4} K_s - x^2 \frac{\pi x}{4} K_s\right) + \left(x^2 K_f F(x)\right)}\right] \qquad (A-43)$$

Since $C_f = C_t - C_s$, we find also

$$C_f = \pi R K_s (1-x^2)\left(\frac{k_{s1} k_{s2}}{k_{s1}+k_{s2}}\right)\left[\frac{\left(\frac{K_f}{K_s} + \frac{\pi x}{4} K_f - x^2 \frac{\pi x}{4} K_f\right) + x^2 K_f F(x)}{\left(1 + \frac{\pi x}{4} K_s - x^2 \frac{\pi x}{4} K_s\right) + x^2 K_f F(x)}\right]$$

(A-44)

APPENDIX B

Constriction and material resistance of a conic frustum

Let the radii of the base and tip of a conic frustum be a and a_o respectively. Let h be the height and k_s be the thermal conductivity of the material. The flow lines converge towards the point O and are perpendicular to a isothermal surface e-e which is part of the surface of a sphere of radius and a subtended angle $2\theta_o$ where $\theta_o = \tan^{-1}(\frac{a-a_o}{h})$. Such an arrangement also satisfies the Laplace equation of steadily axi-symmetrical heat flow in a solid. Consider the elementary ring generated

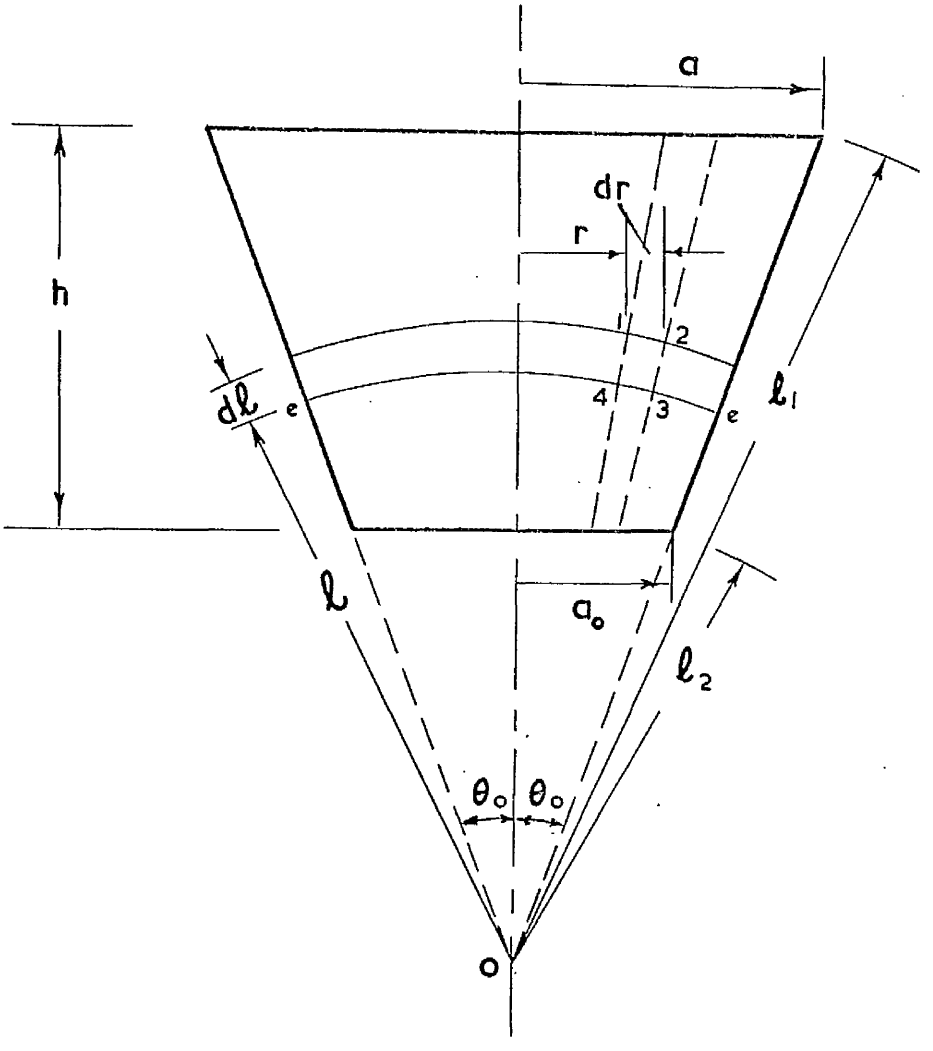

Fig. B.1 An asperity as a conic frustum

by the revolution of 1 2 3 4 about the axis of symmetry, where 1 2 3 4 is formed by the interception of two adjacent flow lines with two adjacent circular arcs. The resistance of the elementary ring is

$$\Delta R_{cf} = \frac{d\ell}{k_s \; 2\pi r \, \ell \, d\theta} \tag{B-1}$$

The total constriction resistance is

$$R_{cf} = \int_{\ell_2}^{\ell_1} \frac{d\ell}{2k_s \int_0^{\theta_0} 2\pi r \, \ell \, d\theta} \tag{B-2}$$

Let $\beta = \frac{a-a_o}{h}$ so that

$$\ell_1 = a \sqrt{1 + \left(\frac{h}{a-a_o}\right)^2} = a \sqrt{1 + \frac{1}{\beta^2}} \tag{B-3}$$

and

$$\ell_2 = a_o \sqrt{1 + \left(\frac{h}{a-a_o}\right)^2} = a_o \sqrt{1 + \frac{1}{\beta^2}} \tag{B-4}$$

Using $r = \ell \sin \theta$ and performing the integration, we obtain

$$R_{cf} = \frac{\frac{a}{a_o} - 1}{4\pi a \, k_s} \; \frac{\beta}{\sqrt{1+\beta^2} - \beta} \tag{B-5}$$

The material resistance of the conic frustum is now to be determined.

The resistance of the elementary disc of radius **d** and thickness dZ is

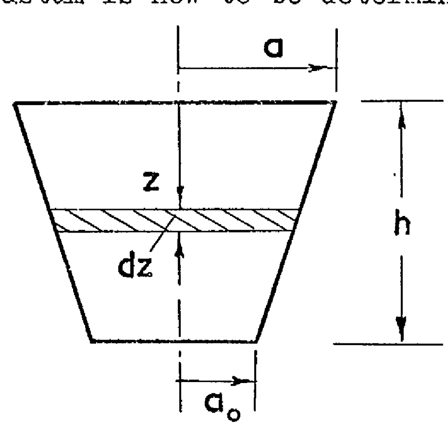

$$dR_{mf} = \frac{dZ}{k_s \pi d^2} \tag{B-6}$$

The radius d is given by

$$d = a - \frac{a-a_o}{h} Z = a - \beta Z \tag{B-7}$$

The material resistance of the whole conic frustum is then equal to

$$R_{mf} = \int_0^h \frac{dZ}{k_s \pi (a - \beta Z)^2} = \frac{h}{\pi k_s a a_o} \tag{B-8}$$

APPENDIX C

Constriction resistance between the sphere and a plane surface

When a sphere is brought into contact with a plane, the area of contact is usually very small compared with the size of the sphere. Under the maximum applied load in the present investigation, the radius of the contact area is of the order of 0.14 mm for the ball radius of 0.86 mm. As a first approximation the contact is assumed to form between two semi-infinite solids.

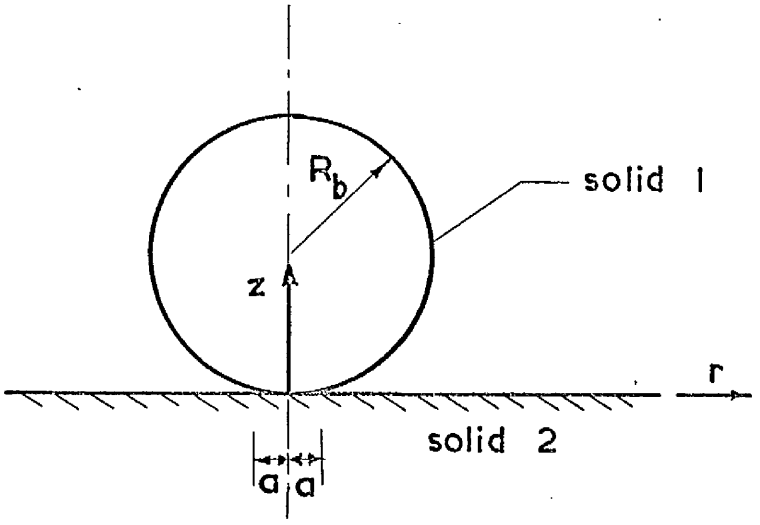

Fig. C.1 Contact between a sphere and a flat surface.

Let the centre of the contact area of radius a be at the origin of the coordinates r, Z. We assume that at a large distance from the contact area the sphere is maintained at a constant temperature T_{o1} while the plane is maintained at T_{o2}. Owing to the constriction resistance the temperature of the sphere and the plane in the contact region are represented by

$$T_1 = T_{o1} - T_1' \qquad (C\text{-}1)$$

$$T_2 = T_{o2} + T_2' \qquad (C\text{-}2)$$

respectively. Since T_1 and T_2 (hence T_1' and T_2') must satisfy the Laplace equation, we have

$$\frac{\partial^2 T_1'}{\partial r^2} + \frac{1}{r}\frac{\partial T_1'}{\partial r} + \frac{\partial^2 T_1'}{\partial Z^2} = 0 \qquad \text{(C-3)}$$

$$\frac{\partial^2 T_2'}{\partial r^2} + \frac{1}{r}\frac{\partial T_2'}{\partial r} + \frac{\partial^2 T_2'}{\partial Z^2} = 0 \qquad \text{(C-4)}$$

The solutions of these equations must satisfy the following boundary conditions:

$$\left.\begin{aligned} T_1' &= 0 \quad \text{at} \quad Z = \infty \\ T_2' &= 0 \quad \text{at} \quad Z = -\infty \end{aligned}\right\} \qquad \text{(C-5)}$$

$$\left.\begin{aligned} \frac{\partial T_1}{\partial Z} &= 0 \\ \frac{\partial T_2}{\partial Z} &= 0 \end{aligned}\right\} \quad \text{at} \quad Z = 0, \quad r > a \qquad \text{(C-6)}$$

$$k_1 \frac{\partial T_1}{\partial Z} = k_2 \frac{\partial T_2}{\partial Z} \quad \text{at} \quad Z = 0, \quad r < a \qquad \text{(C-7)}$$

$$T_1 = T_2 \quad \text{at} \quad Z = 0, \quad r < a \qquad \text{(C-8)}$$

Equation (C-3) may be solved by the use of the Hankel Transform[22], i.e. by multiplying both sides of the equation by $r\,J_o(\lambda r)$, where J_o is the Bessel function of the first kind and λ is a constant, and by integrating with respect to r from 0 to ∞.

$$\frac{\partial^2 \bar{T}_1'}{\partial Z^2} = \lambda^2 \bar{T}_1' \qquad \text{(C-9)}$$

where $$\bar{T}_1' = \int_0^\infty T_1' \, r \, J_o(\lambda r) dr \qquad (C\text{-}10)$$

We then find

$$\bar{T}_1' = B_1 e^{-\lambda Z} + B_2 e^{+\lambda Z} \qquad (C\text{-}11)$$

and the inversion formula is

$$T_1' = \int_0^\infty (B_1 e^{-\lambda Z} + B_2 e^{\lambda Z}) \, \lambda \, J_o(\lambda r) d\lambda$$

which can be written as

$$T_1' = \int_0^\infty (C_1 e^{-\lambda Z} + C_2 e^{\lambda Z}) \, J_o(\lambda r) d\lambda \qquad (C\text{-}12)$$

where C_1 and C_2 are arbitrary functions of λ. Since T_1' must vanish as Z tends to infinity, equation (C-12) reduces to

$$T_1' = \int_0^\infty C_1 e^{-\lambda Z} \, J_o(\lambda r) d\lambda \qquad (C\text{-}13)$$

Hence $$T_1 = T_{o1} - \int_0^\infty C_1 e^{-\lambda Z} \, J_o(\lambda r) d\lambda \qquad (C\text{-}14)$$

By similar approach, we find

$$T_2 = T_{o2} + \int_0^\infty D_1 e^{\lambda Z} \, J_o(\lambda r) d\lambda \qquad (C\text{-}15)$$

where D_1 is an arbitrary function of λ.

The boundary conditions by equation (C-6) yield

$$\frac{\partial T_1}{\partial Z} = \int_0^\infty C_1 \lambda \, J_o(\lambda r) d\lambda = 0 \qquad \text{at } Z = 0, \; r > a \qquad (C\text{-}16)$$

$$\frac{\partial T_2}{\partial Z} = \int_0^\infty D_1 \lambda \, J_o(\lambda r) d\lambda = 0 \qquad \text{at } Z = 0, \; r > a \qquad (C\text{-}17)$$

By the substitution of T_1 and T_2, equations (C-7) and (C-8) become

$$k_1 \int_0^\infty C_1 \lambda J_o(\lambda r) d\lambda = k_2 \int_0^\infty D_1 \lambda J_o(\lambda r) d\lambda \quad \text{at } Z = 0,\ r < a \tag{C-18}$$

$$T_{o1} - \int_0^\infty C_1 J_o(\lambda r) d\lambda = T_{o2} + \int_0^\infty D_1 J_o(\lambda r) d\lambda \quad \text{at } Z = 0,\ r < a \tag{C-19}$$

From (C-18) and (C-19) we obtain

$$T_{o1} - T_{o2} = \frac{k_1 + k_2}{k_2} \int_0^\infty C_1 J_o(\lambda r) d\lambda \quad \text{for } r < a \tag{C-20}$$

Use the well known results (22) such as

$$\left.\begin{aligned} \int_0^\infty \frac{J_o(ax)}{x} \sin\beta x\, dx &= \sin^{-1}\frac{\beta}{a} && \beta < a \\ &= \frac{\pi}{2} && \beta > a \end{aligned}\right\}$$

$$\left.\begin{aligned} \int_0^\infty J_o(ax) \sin\beta x\, dx &= 0 && \beta < a \\ &= \frac{1}{\sqrt{\beta^2 - a^2}} && \beta > a \end{aligned}\right\} \tag{C-21}$$

We see that if

$$C_1 = \frac{2(T_{o1} - T_{o2})k_2}{\pi (k_1 + k_2)} \frac{\sin\lambda a}{\lambda} \tag{C-22}$$

then both equations (C-16) and (C-20) are satisfied.

Hence a combination of (C-14), (C-15), (C-16), (C-20) and (C-22) yields

$$T_1 = \frac{k_1 T_{o1} + k_2 T_{o2}}{k_1 + k_2} = T_2 \qquad Z = 0,\ r < a \tag{C-23}$$

From equation (C-23), we see that the contact temperature is uniform and is independent of the size of the contact.

The constriction resistance, by definition, is given by

$$R_c = \frac{T_{o1} - T_{o2}}{Q} \qquad (C-24)$$

where Q is the heat flux through the contact area. Using equations (C-14) (C-21) and (C-22), we find

$$Q = \int_0^a 2\pi r\, k_1 \left(\frac{\partial T_1}{\partial Z}\right)_{Z=0} dr$$

$$= 2\, k_m'\, a\, (T_{o1} - T_{o2}) \qquad (C-25)$$

where

$k_m' = \frac{2k_1 k_2}{k_1 + k_2}$ which is the harmonic mean value of the thermal conductivities k_1 and k_2.

The constriction resistance is therefore equal to

$$R_c = \frac{1}{2k_m' a} \qquad (C-26)$$

The result obtained in equation (C-26) will give rise to a more severe prediction if the size of the contact area is not too small to warrant the use of the assumption in which the sphere is being treated as a semi-infinite body. Since, however, the problem of heat flow is similar to the electrostatic problem of capacitance (see Jeans (14) page 352) the result in equation (C-26)

may be modified to take the following form which gives only the constriction resistance of the sphere

$$R_{cb} = \frac{1}{4 k_b} \left(\frac{1}{a} - \frac{1}{R_b}\right) \qquad \text{(C-27)}$$

The total constriction resistance of the sphere is twice the above value, i.e.

$$R_{cb} = \frac{1}{2 k_b} \left(\frac{1}{a} - \frac{1}{R_b}\right) \qquad \text{(C-28)}$$

where k_b is the thermal conductivity of the sphere.

APPENDIX D

Material resistance to heat flow through a spherical body

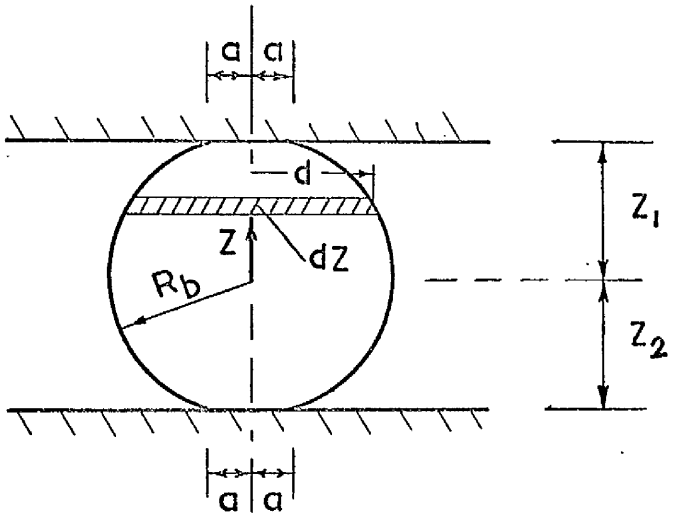

Fig. D.1 A sphere inserted between two flat surfaces.

Let the radius of the circular contact area between the sphere and the plane be a. Heat is considered to flow from one contact area to the other in the Z-direction. The resistance across an elementary disc of dZ thickness is

$$d\,R_{mb} = \frac{dZ}{k_b \pi\, d^2} \qquad (D\text{-}1)$$

where k_b is the thermal conductivity of the ball and $d = (R_b^2 - Z^2)^{\frac{1}{2}}$. Taking the integration from $Z = Z_1$ to $Z = -Z$, we find

$$R_{mb} = \int_{Z_2}^{Z_1} \frac{dZ}{k_b \pi (R_b^2 - Z^2)} \qquad (D\text{-}2)$$

But $Z_1 = (R_b^2 - a^2)^{\frac{1}{2}}$, therefore

$$R_{mb} = \frac{1}{k_b \pi R_b} \log \left(\frac{1 + \sqrt{1 - \left(\frac{a}{R_b}\right)^2}}{1 - \sqrt{1 - \left(\frac{a}{R_b}\right)^2}} \right) \qquad (D\text{-}3)$$

APPENDIX E

Mean fluid gap distance between two flat surfaces with the insertion of a spherical body.

The model to be considered is shown in figure E.1. Let R_b be the radius of the steel ball and a be the radius of the contact area. In the present investigation small steel balls are inserted between cylindrical blocks with flat contacting surfaces. The radius of the blocks is 2.54 cm. With n balls inserted between them we now find the effective radius of the cylinder used in the contact model according to

$$R = \frac{2.54}{\sqrt{n}} \text{ cm} \qquad \text{(E-1)}$$

When the specimen blocks are compressed against the inserted balls, deformations take place in the contact region as well as in the surrounding material. The two contacting surfaces are now brought nearer to each other by the amount

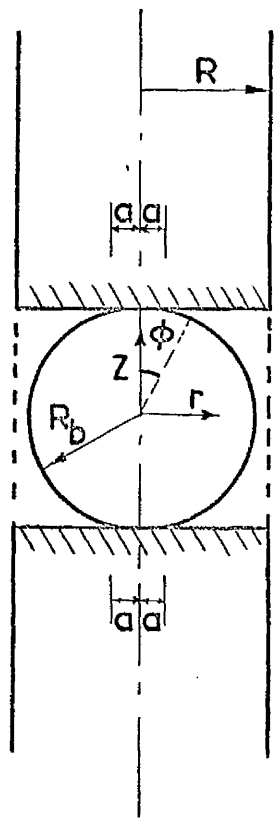

Fig. E.1 Steel ball compressed between two cylindrical specimens

$$\Delta\delta = 2(R_b - R_b\cos\phi) = 2R_b\left(1 - \sqrt{1 - \frac{a^2}{R_b^2}}\right) \qquad \text{(E-2)}$$

If a is small compared with R_b, we have

$$\Delta\delta \simeq \frac{a^2}{R_b} \qquad \text{(E-3)}$$

Owing to the pressure acting over the contact area, there will be local deformation of the contact surfaces outside the contact area in the Z-direction. We consider the deformation to be elastic and assume the distribution of pressure to be hemispherical which can be expressed as

$$\omega = \omega_o \sqrt{1 - (\frac{r^1}{a})^2} \qquad \text{(E-4)}$$

where ω_o is the maximum pressure at the centre of the contact area and is equal to $\frac{3W}{2\pi a^2}$ which is obtained by integrating the pressure over the contact area and then by setting it to be equal to the applied load W. r^1 is a radius within the contact area. According to reference (23), the local deformation can be obtained from

$$\Delta_r = (\frac{1-\nu^2}{\pi E}) \iint \omega \; ds \, d\psi \qquad \text{(E-5)}$$

where E is the Young's modulus and ν the Poisson's ratio of the material of the specimen and S and ψ are defined according to figure E.2.

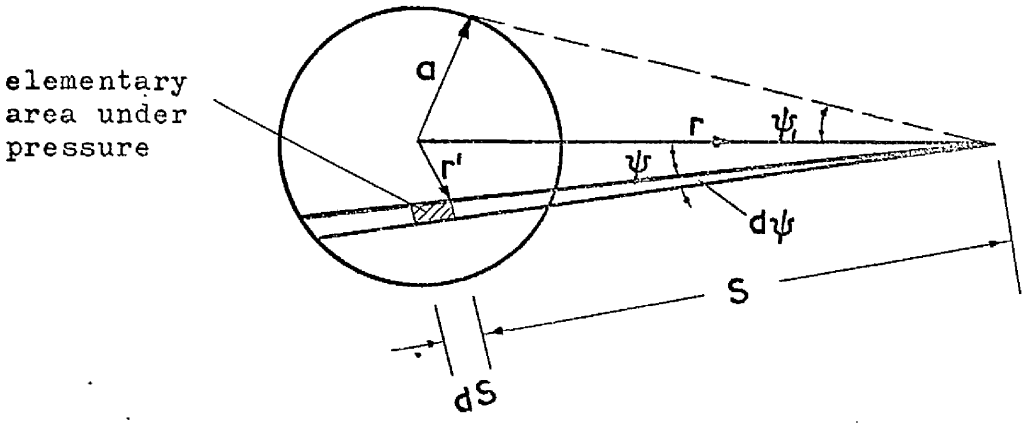

Fig. E.2 Diagram for determining deformation due to contact pressure

Since $r_1^2 = r^2 + s^2 - 2rs\cos\psi$, we find

$$\int_{\text{chord}} \omega\, ds = \frac{\omega_o \pi}{a\,2}\,(a^2 - r^2 \sin^2\psi) \qquad \text{(E-6)}$$

Substituting (E-6) into (E-5) and taking $\psi_1 = \sin^{-1}\frac{a}{r}$, we obtain

$$\Delta_r = \left(\frac{1-\nu^2}{\pi E}\right)\int_{-\psi_1}^{\psi_1} \frac{\omega_o \pi}{2a}\,(a^2 - r^2\sin^2\psi)\,d\psi$$

$$= \left(\frac{1-\nu^2}{E\pi}\right)\frac{3W}{4a}\left(2-\frac{r^2}{a^2}\right)\sin^{-1}\frac{a}{r} + \sqrt{\frac{r^2}{a^2}-1} \qquad \text{(E-7)}$$

The total separation of the two surfaces at a point r is

$$\delta_r = 2R_b - \Delta\delta + \Delta r \cdot 2$$

$$= 2R_b\sqrt{1-\frac{a^2}{R_b^2}} + \left(\frac{1-\nu^2}{E\pi}\right)\frac{3W}{2a}\left[\left(2-\frac{r^2}{a^2}\right)\sin^{-1}\frac{a}{r} + \sqrt{\frac{r^2}{a^2}-1}\right] \qquad \text{(E-8)}$$

The mean fluid gap can now be obtained from

$$\delta = \frac{2\int_a^R \delta_r \cdot r\,dr}{(R^2 - a^2)} \qquad \text{(E-9)}$$

Since the amount due to the elastic deformation of the material as the result of the contact pressure is usually very small and can be neglected, we may simply use

$$\delta = 2R_b\sqrt{1-\frac{a^2}{R_b^2}} \qquad \text{(E-10)}$$

or

$$\delta = 2R_b - \frac{a^2}{R_b}$$

if a is small compared with R_b.

APPENDIX.F

Radial heat loss correction

Because of the sudden temperature drop and a change of temperature gradient at the junction between the heat flux meter and specimen 1 and again at the junction between the specimens, it is rather difficult to expect the temperature distribution along the guard tubes to match correctly that along the central column of specimens especially when the applied load is small. Under this condition a certain amount of heat leak in the radial direction becomes inevitable. A correction is therefore required.

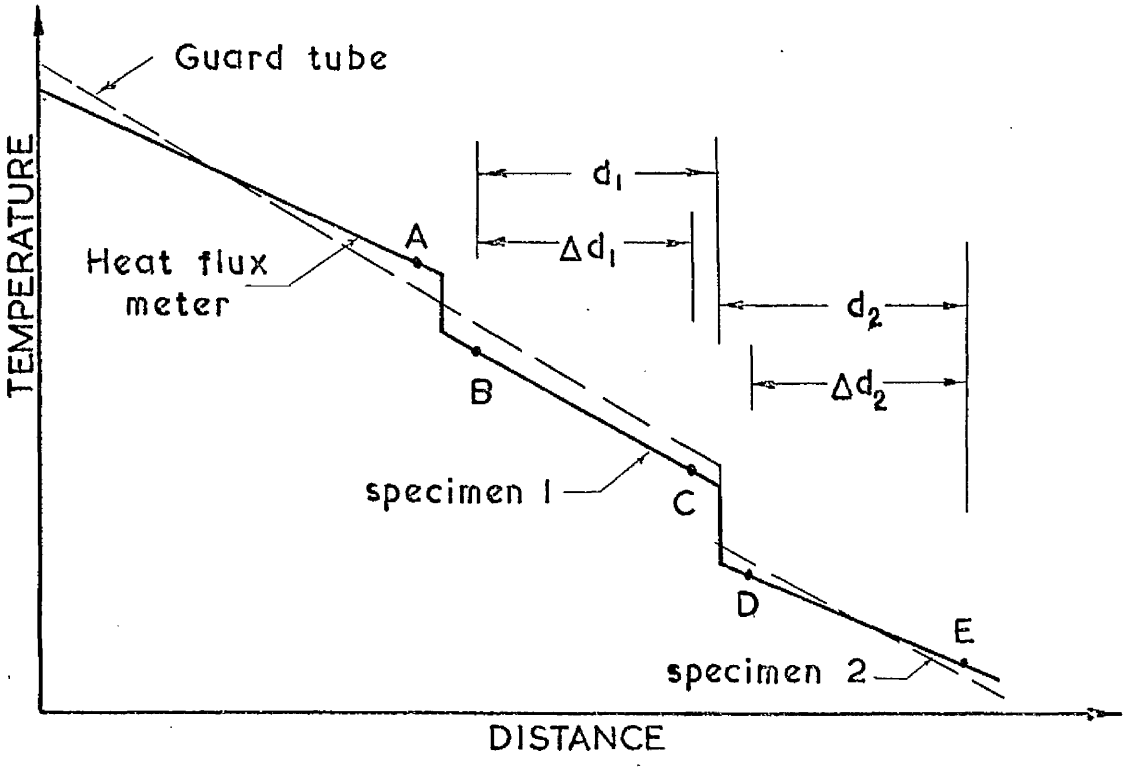

Fig. F.1 Temperature distribution along specimens and guard tubes.

Figure F.1 shows the general distribution of temperature along the guard tubes and along the central column of specimens. A, B, C, D and E denote the thermocouple positions near the ends of each specimen block. Let q_A

be the heat flux per unit area at A and q_c be that at C. Let k_A be the thermal conductivity of the material at A. We can now write

$$q_A = k_A \frac{dT_A}{dZ} \qquad (F\text{-}1)$$

The heat flux per unit area at C is given by

$$q_c = q_A + \Sigma \Delta q_1 \qquad (F\text{-}2)$$

where Δq_1 is the heat gained or lost in the radial direction over a section between any two adjacent thermocouple positions and the summation is to cover the whole length from A to C. The temperature at the contact surface of specimen 1 is obtained by extrapolation and it is equivalent to using the following computation.

$$T_1 = T_B - \frac{T_B - T_c}{\Delta d_1} d_1 \qquad (F\text{-}3)$$

Since the fluid gap distance is small we assume that the same amount of heat will flow across the contact interface. Thus

$$q_D = q_C \qquad (F\text{-}4)$$

At E, we have

$$q_E = q_C + \Sigma \Delta q_2 \qquad (F\text{-}5)$$

where Δq_2 represents the heat gained or lost radially along specimen 2. Although it does not influence the temperature at D to any appreciable amount, it does nevertheless affect the temperature gradient by $\frac{\Sigma \Delta q_2}{k_2}$

where k_2 is taken as the mean thermal conductivity of specimen 2. The temperature at the contact surface of specimen 2 can be determined from

$$T_2 = T_D + \left(\frac{T_D - T_E}{\Delta d_2} - \frac{\Sigma \Delta q_2}{k_2}\right)(d_2 - \Delta d_2) \qquad \text{(F-6)}$$

Approximate values of Δq can be obtained by means of equations for radial heat flow in the absence of any longitudinal temperature gradients, i.e.

$$\Delta q = \frac{2\pi (T_s - T_g) k_i \Delta \ell}{\ell n \left(\frac{r_g}{r_s}\right)} \qquad \text{(F-7)}$$

where k_i = thermal conductivity of the insulating powder

$(T_s - T_g)$ = mean temperature difference between the specimen (or heat flux meter) and the guard tube over the length .

r_s, r_g = radii of specimen and guard tube respectively.

The corrected experimental value of the thermal conductance of the contact is given by

$$C_e = \frac{\pi R^2 q_c}{T_1 - T_2}$$

$$= \frac{\pi R^2 \left(k_A \frac{dT_A}{dZ} + \Delta q_1\right)}{\left(T_B - \frac{T_B - T_C}{\Delta d_1} d_1\right) - \left(T_D + \frac{T_D - T_E}{\Delta d_2} - \frac{\Sigma \Delta q_2}{k_2}\right)(d_2 - \Delta d_2)} \qquad \text{(F-8)}$$

APPENDIX G.

Data of properties of materials

G.1. Gases

The thermal conductivity value is calculated according to equation (2-23) in which the constant C is determined from some specific values at a higher temperature taken from reference (16) Thus

$$(k_f)_{air} = 0.616 \frac{\sqrt{T}}{1+\frac{223}{T}} \times 10^{-5} \quad \text{cal cm}^{-1} \text{ sec}^{-1} \text{ o}_c^{-1}$$

$$(k_f)_{helium} = 0.224 \frac{\sqrt{T}}{1+\frac{13.7}{T}} \times 10^{-4} \quad \text{cal cm}^{-1} \text{ sec}^{-1} \text{ o}_c^{-1}$$

$$(k_f)_{argon} = 0.365 \frac{\sqrt{T}}{1+\frac{142}{T}} \times 10^{-5} \quad \text{cal cm}^{-1} \text{ sec}^{-1} \text{ o}_c^{-1}$$

where T is the absolution temperature in degrees Kelvin. The results of these gases are plotted in figure G.1.

We use the same expression by Sutherland (12) to obtain the viscosity formulae which are

$$\mu_{air} = 1.5 \frac{\sqrt{T}}{1+\frac{134}{T}} \times 10^{-5} \quad \text{gm cm}^{-1} \text{ sec}^{-1}$$

$$\mu_{helium} = 1.52 \frac{\sqrt{T}}{1+\frac{101}{T}} \times 10^{-5} \quad \text{gm cm}^{-1} \text{ sec}^{-1}$$

$$\mu_{argon} = 1.9 \frac{\sqrt{T}}{1+\frac{137}{T}} \times 10^{-5} \quad \text{gm cm}^{-1} \text{ sec}^{-1}$$

The values of C_v are obtained from reference (12)

$$(C_v)_{air} = 0.171 \text{ cal gm}^{-1} \text{ o}_c^{-1}$$

$$(C_v)_{helium} = 0.75 \text{ cal gm}^{-1} \text{ o}_c^{-1}$$

$$(C_v)_{argon} = 0.075 \text{ cal gm}^{-1} \text{ o}_c^{-1}$$

We determine the mean free path of a gas from the kinetic theory of gases and obtain

$$\lambda_{air} = 1.685 \frac{T}{p} \times 10^{-5} \text{ cm}$$

$$\lambda_{helium} = 4.9 \frac{T}{p} \times 10^{-5} \text{ cm}$$

$$\lambda_{argon} = 1.755 \frac{T}{p} \times 10^{-5} \text{ cm}$$

where p is the gas pressure in torrs.

There is very little information available concerning the accommodation coefficient of a gas with a metal surface. An average value is taken from references (26) and (27)

$$\alpha_{air} = 0.9$$

$$\alpha_{helium} = 0.61$$

$$\alpha_{argon} = 0.68$$

G.2. Specimens

En 8 normalised steel. see references (28) and (29)

deg C	20	100	200	300	400	500	600	700	800
k_s cal cm^{-1} sec^{-1} $^oc^{-1}$	.1073	.1069	.1055	.1026	.098	.092	.084	.0752	.068
ρ $\mu\Omega$ - cm	21.1	25.9	33.5	42.6	53.0	64.5	78.2	92.6	106.5

$E = 2.11 \times 10^6$ Kg cm^{-2}

$\nu = 0.272$

ultimate tensile stress = 5540 Kg. cm^{-2}

yield stress = 2850 Kg. cm^{-2}

Meyer hardness value, see reference (24) and figure 4.6.

ϵ = 0.06 (average value for polished steel)

Armco iron. see references (30) and (31)

deg. C.	0	100	200	300	400	500	600	700	800
k_s cal cm^{-1} sec^{-1} $^oc^{-1}$	.179	.164	.148	.132	.117	.105	.095	.085	.075
ρ $\mu\Omega$ - cm	9.4	14.8	22.2	31.0	42.4	54	67.5	83.3	100

$E = 2.11 \times 10^6$ Kg. cm^{-2}

$\nu = .3$

yield stress = 1900 Kg. cm^{-2}

Meyer hardness value, see figure 4.7.

ϵ = 0.1 (average value for polished iron).

The thermal conductivities and the electric resistivities of En 8 steel and Armco iron plotted against temperatures are given in figure G.2 and figure G.3 respectively.

G.3. Silocel insulating powder (supplied by Messrs. John Manville Ltd.)

deg. C	100	200	300	400	500	600
k_i cal cm^{-1} sec^{-1} $^oc^{-1}$	0.00013	0.000157	0.000184	0.000211	0.000238	0.000265

G.4. Steel ball

The steel balls (through-hardened 1% chrome carbon steel) were supplied by Messrs Miniature bearings Limited.

deg. C.	0	50	100	200	300
k_b cal cm^{-1} sec^{-1} $^oc^{-1}$	0.076	0.079	0.081	0.084	0.087
				extra-polated values	
'Rockwell' C hardness value	64	63	61.9	58.2	53.4

G.5. Aluminium disc.

Unalloyed aluminium with the minimum purity of 99.8% Al. This material was supplied by the Alcan Industries Limited with a specification number 2S$\frac{1}{2}$H.

reference (32)

deg. C.	0	50	100	200	300
Thermal conductivity cal cm^{-1} sec^{-1} $^{o}_{c}{}^{-1}$	0.542	0.531	0.52	0.499	0.476
electric resistivity $\mu\Omega$ - cm	2.4	2.96	3.5	4.66	5.87
surface emissivity	0.078	0.082	0.087	.10	.13

Brinell hardness value = 36

ultimate tensile stress = 127 Kg. cm^{-2}

bearing yield stress = 127 Kg. cm^{-2}

E = 7.05×10^{5} Kg. cm^{-2}

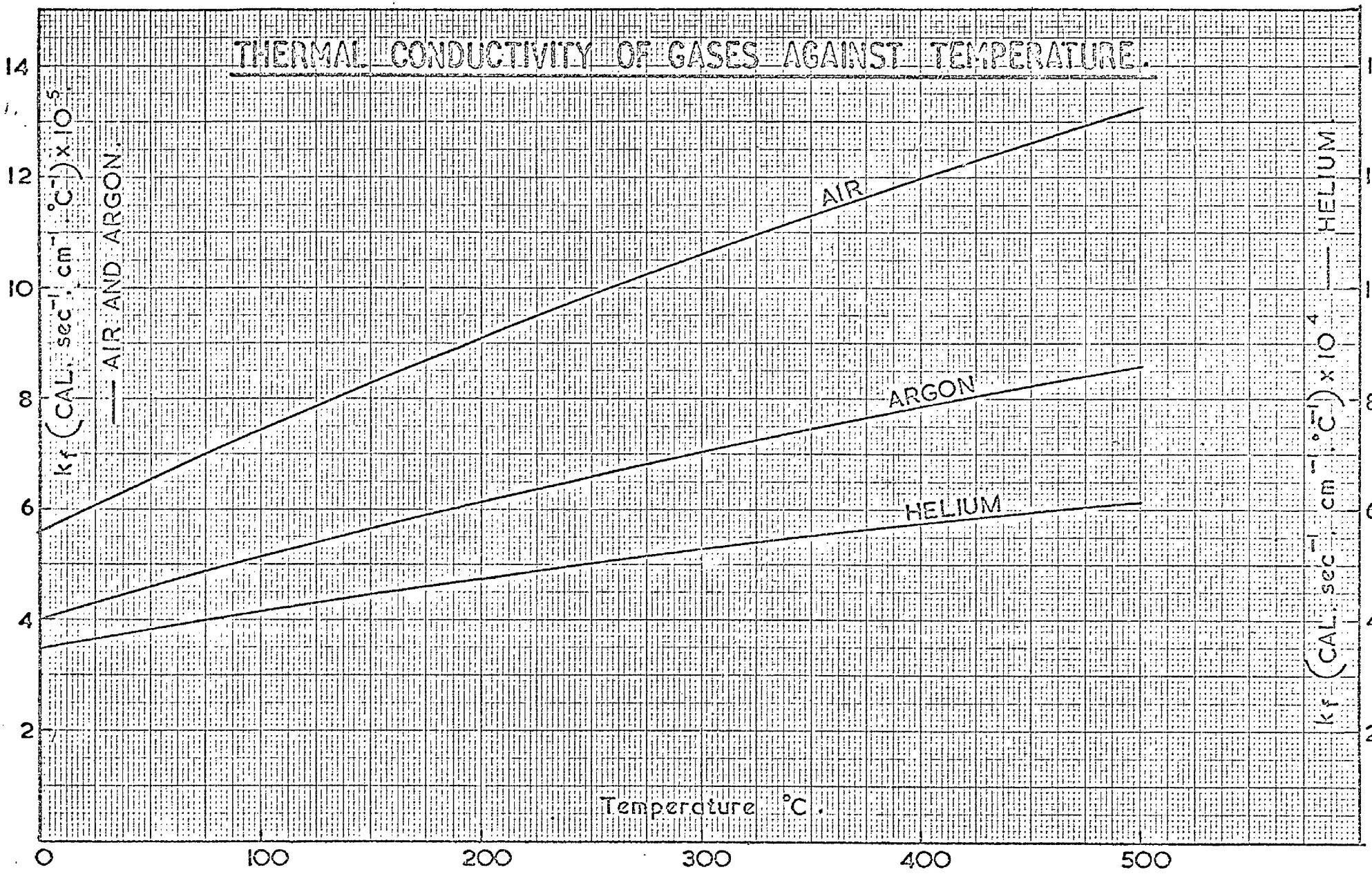
THERMAL CONDUCTIVITY OF GASES AGAINST TEMPERATURE.
AIR
ARGON
HELIUM
Kf (CAL. sec⁻¹. cm⁻¹ °C⁻¹) x 10⁻⁵
— AIR AND ARGON.
Kf (CAL. sec⁻¹. cm⁻¹ °C⁻¹) x 10⁻⁴
— HELIUM
Temperature °C.
0
100
200
300
400
500
2
4
6
8
10
12
14

FIG. G·1

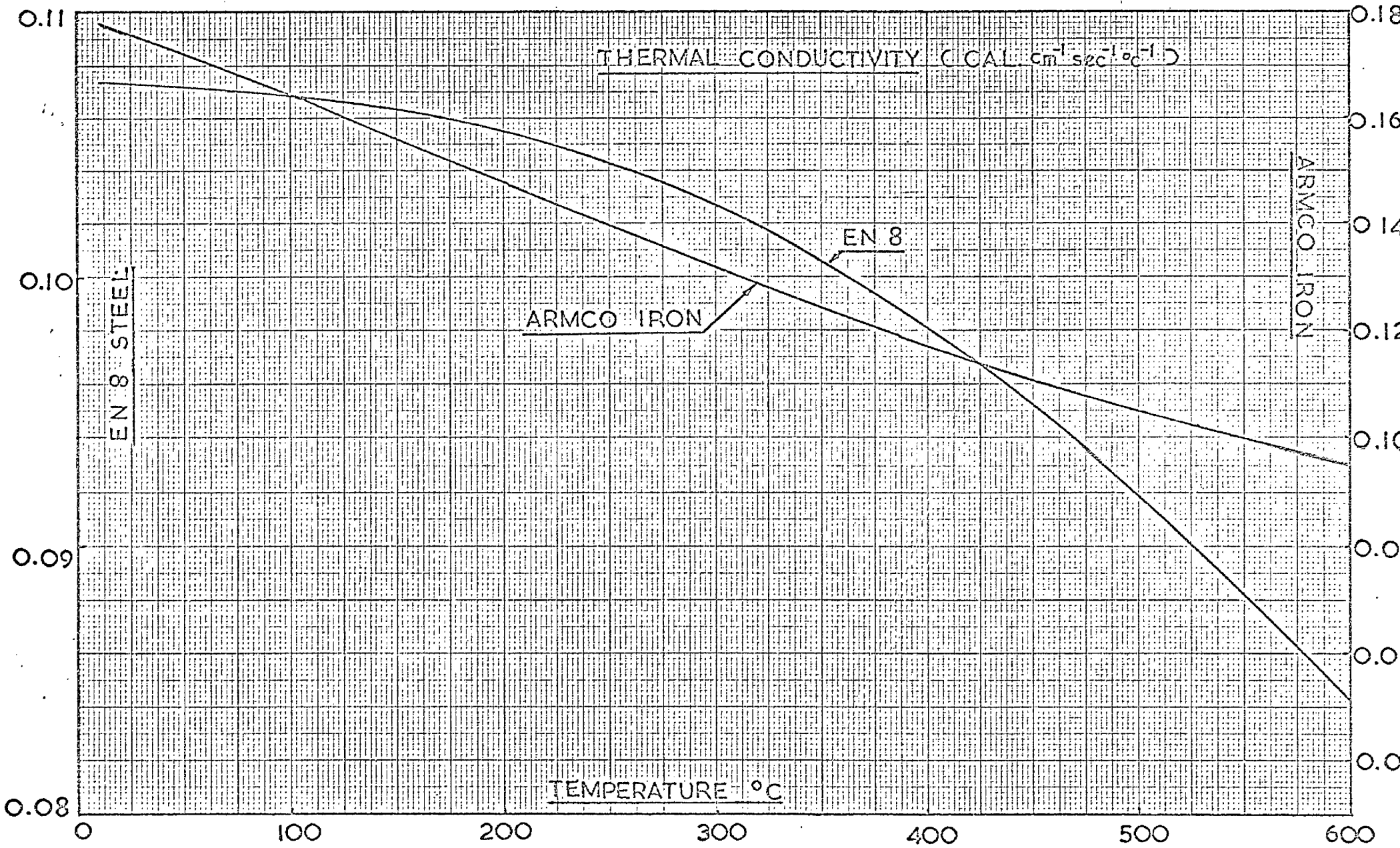
THERMAL CONDUCTIVITY (CAL cm⁻¹ sec⁻¹ °C⁻¹)
EN 8
ARMCO IRON
EN 8 STEEL
ARMCO IRON
TEMPERATURE °C
0.11
0.10
0.09
0.08
0.18
0.16
0.14
0.12
0.10
0.0
0.0
0.0
0
100
200
300
400
500
600

FIG. G.2

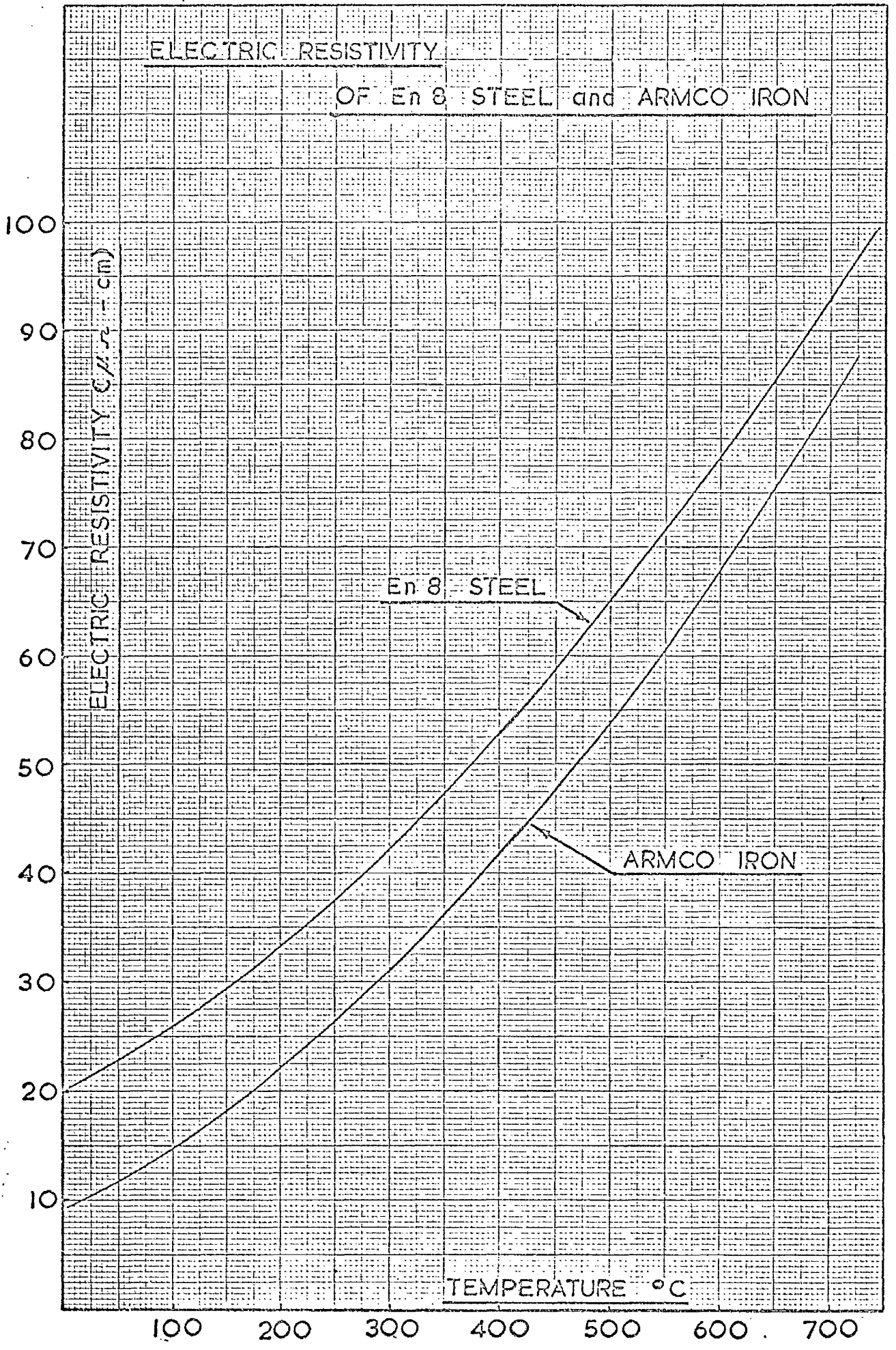
ELECTRIC RESISTIVITY
OF En 8 STEEL and ARMCO IRON
ELECTRIC RESISTIVITY (μΩ - cm)
100
90
80
70
60
50
40
30
20
10
En 8 STEEL
ARMCO IRON
TEMPERATURE °C
100
200
300
400
500
600
700

FIG. G. 3

LIST OF REFERENCES

1. Wong, H.Y., A survey of the thermal conductance of metallic contacts. Aeronautical Research Council, CP 972, 1967.

2. Hertz, H., J. reine angew. Math. 92, 156. 1881, translated in Miscellaneous Paper (1896), London.

3. Tabor, D., Hardness of metals, Oxford Clarenden Press, 1951.

4. Tabor, D., Private communication, 1965.

5. Holm, R., Electric contacts handbook, Springer-Verlag, 1958.

6. Bowden, F.P., and Tabor, D., The friction and lubrication of solids, Oxford Clarenden Press, 1950.

7. Anderson, O.L., The role of surface shear strains in the adhesion of metals, Part I, Wear, 3, 253-273, 1960.

8. Anonymous, Surface texture, B.S. 1134, 1961

9. Anonymous, Surface roughness, waviness and lag, ASA 1346, 1, 1955.

10. Olsen, K.V., On the standardization of surface roughness measurements, B. and K Technical Review 3, 1961.

11. Jakob, M., Heat transfer, Chapman & Hall, 1949.

12. Kennard, E.H., Kinetic theory of gases, McGraw-Hill, 1938.

13. Fenech, H. and Rohsenow, W.M., Thermal conductance of metallic surfaces in contact, U.S. Atomic Energy Commission, NYO - 2136, 1959.

14. Jeans, J.H., Electricity and magnetism, Cambridge University Press, 1911.

15. McLachlan, N.W., Bessel functions for engineers, Oxford Clarenden Press, 1955.

16. Eckert, E.R.G. and Drake, R.H., Heat and mass transfer, McGraw-Hill, 1959.

17. Goldsmith, A., Waterman, T.E. and Hirschborn, H.J., Handbook of thermophysical properties of solid materials, Vol. 1, Macmillan, 1961.

18. Cetinkale, T.N. and Fishenden, M., Thermal conductance of metal surfaces in contact, Proc. Int. Conf. on Heat Transfer, Inst. Mech. Eng., 1951.

19. Laming, L.C., Thermal conductance of machined metal contacts, International developments of heat transfer, London, 1962.

20. Greenwood, J.A. and Williamson, J.B.P., Contact of nominally flat surfaces, Proc. Roy, Soc., A 295, 300-314, 1966.

21. Archard, J.E., Elastic deformation and the law of friction, Proc. Roy. Soc., A 243, 190, 1957.

22. Sneddon, I.N., Fourier transforms, McGraw-Hill, 1951.

23. Timoshenko, S. and Goodier, J.N., Theory of elasticity, McGraw-Hill, 1951.

24. Wong, H.Y., Hardness testing at elevated temperatures, Lab. Practice, Vol. 16, No. 8, 1967.

25. Wong, H.Y., Multi-wire vacuum seal, Vacuum. 17, 11, 1967. (letter)

26. Hartnett, J.P., A survey of accommodation coefficients, Advances in Applied Mechanics, Supplement 1, 1961.

27. Sanderson, P.D., Heat transfer from the Uranium fuel to the Magnox can in a gas cooled reactor, an English Electric Co. Ltd. internal report, 1962.

28. Woolman, J. and Mottram, R.A., The mechanical and physical properties of British standard En steels, Vol. 1, 1964.

29. Powell, R.W. and Tye, R.P., Physical constants of some commercial steels at elevated temperatures, J. Iron Steel Inst., Vol. 184, 1956.

30. Powell, R.W., Thermal and electrical conductivities of metals and alloys - Part I, Iron from 0° - 800°C, Proc. Phy. Soc., 46, 659, 1934.

31. Powell, R.W., Further measurements of the thermal and electrical conductivity of iron of high temperatures, Proc. Phy. Soc., 51, 407, 1939.

32. Goldsmith, A., Waterman, T.E. and Hirschborn, H.J., Handbook of thermophysical properties of solid materials, Vol.1, 1961.

33. Wiebe, W., Some aspects of the behaviour and applications of high temperature materials in high speed flight vehicles, National Research Council of Canada, DME/NAE, 1961.